The Dissertation Committee for Julio Leva Lopez Certifies that this is the approved version of the following dissertation:

Fluvial, shoreline, and clastic wedge responses to foreland basin and Laramide style subsidence: Examples from experimental studies and the Greater Green River Basin, southern Wyoming

Committee:

Ronald J. Steel, Co-Supervisor

Wonsuck Kim, Co-Supervisor

Brian K. Horton

Cornel Olariu

Jeff P. Crabaugh

Fluvial, shoreline, and clastic wedge responses to foreland basin and Laramide style subsidence: Examples from experimental studies and the Greater Green River Basin, southern Wyoming

by

Julio Leva Lopez, Lic.

Dissertation

Presented to the Faculty of the Graduate School of

The University of Texas at Austin

in Partial Fulfillment

of the Requirements

for the Degree of

Doctor of Philosophy

The University of Texas at Austin
August, 2014

Dedication

To the rocks without which this dissertation would not have been possible.

"And so castles made of sand, fall in the sea, eventually." – Jimmy Hendrix

To Valentina and my friends without whom I would have given up long ago.

"It's not easy love, but you've got friends you can trust,

Friends will be friends,

When you're in need of love they give you care and attention,

Friends will be friends,

When you're through with life and all hope is lost,

Hold out your hand cos friends will be friends right till the end." – Queen

Acknowledgements

I wish to acknowledge and thank everyone involved in making this research possible. Ron Steel, my co-advisor, for his help during this study. Wonsuck Kim, my second co-advisor, for helping me transforming a class project into a great research experience and let me inaugurate the STEP basin which was a lot of fun. Brian Horton, Cornel Olariu and Jeff Crabaugh, my committee members, for some great feedback and encouragement both in the field and in the classroom.

I want to thank those companies and institutions that have supported my research. First and more importantly the members of the RioMAR consortium: BP, BHPBilliton, Shell, Statoil, PDVSA, Devon, Woodside, Eni, Petrobras and BG Group for the most of the funding that has made this research possible. I also want to thank the support from the Ronald K. DeFord Field Scholarship Fund, the John and Elizabeth M. Teagle Scholarship, the ConocoPhilips fellowship and the Chevron fellowship. And the land access and field support from the Twentymile Coal Company (Peabody Energy) and especially “Rocky” Thompson who gave me all the information, encouragement, advice, maps and support that he could.

Finally I also extend my gratitude to Valentina Rossi for field assistance, feedback, tidal education and much more; Tom Lovitz for his “support”; Anastasia Piliouras for plenty of geological discussions about real and “unreal” deltas; Mauricio Perillo for field assistance, meat and sedimentary structures; Manasij Santra for the

philosophical, literature and geological discussions; Edgardo Pujols for good feedback and good questions; Mark Helper for all his help, continued faith in me and a lot of fun in the field; Josh Dixon for field work experiences, beers and geology; Carolina Gomez for helping me start of this research; Esti Ukar for encouragement and many garagardo; Belen López for not caring how far I am; Travis Kloss for his mad Matlab skills; to the people in my research groups that have made my time in Austin more fun and helped my research Eric Swanson, Alison Ned, Ozge Karaman, Ashley Siks, Safiya Hassan, Brandee Carlson, Woong Mo Koo, Greg Kline, Eugen Tudor, Yu Ye, Si Chen, Shunli Li, Xiaojie Wei, Carlos Uroza and Rene Winter; people in the department like David Mohrig, Randy Marret, Lesli Wood, Philip Guerrero, Tricia Alvarez, Lindsay Olinde, Ale Bande, and Pat Bobeck who have helped me and from whom I have learned a lot; and to my family for supporting me no matter what or where.

Fluvial, shoreline, and clastic wedge responses to foreland basin and Laramide style subsidence: Examples from experimental studies and the Greater Green River Basin, southern Wyoming

Julio Leva Lopez, PhD

The University of Texas at Austin, 2014

Supervisors: Ronald J. Steel & Wonsuck Kim

Subsidence is one of the main factors controlling the stratigraphy and overall stratal architecture in tectonically active basins. This was particularly important in the Western US Cordilleran foreland and Laramide basins when some other controls were minor, e.g. reduced eustatic fluctuations in the late Cretaceous greenhouse period.

The first part of the dissertation examines the upper Campanian Williams Fork Clastic Wedge (WFCW) in southern Wyoming and northern Colorado, through an outcrop and subsurface database. The WFCW built out from the Sevier orogenic belt like earlier clastic wedges, but its large-scale geometry changed as basement involved Laramide structures partitioned it. At the center of the WFCW there is an extensive fluvial sandstone sheet, the Canyon Creek Member of the Ericson Formation. From its proximal to distal reaches (~200 km) there is a first order trend of stratigraphic thickening and net-to-gross reduction, and a change from braided to meandering depositional style. These trends are caused by isostatic rebound of the foreland basin during periods of relative quiescence in the Sevier orogenic belt and by the eastward migration of dynamic

subsidence. However, this long spatial trend was markedly modified by differential subsidence across Laramide-style structures. The Campanian age initiation of the Laramide structures appears to be earlier than the Maastrichtian to Paleogene age commonly attributed to the initiation of this orogeny.

The second part of this research focuses on the transgressive limb of the WFCW, particularly on two sandstone bodies isolated in marine mudstones in the uppermost Almond Formation. The sandstone bodies previously interpreted as lowstand shoreline deposits are re-interpreted as transgressive shelf ridges generated by tidal currents and storm waves. There are limited examples of ancient tidal shelf ridges published and no facies model was described. Using Almond Fm. outcrops and examples from the literature, the diagnostic characteristics of storm and tidal shelf ridges are presented.

The third part of the dissertation investigates the effects of differential subsidence on the large scale stratigraphic infill of a foreland basin through a geometric model and a series of flume experiments. The mathematical model and flume experiments show that despite constant allogenic forcing, three distinct autogenic responses in stratal architecture, associated with the imposed tectonic and sediment supply conditions are possible. The first response was “autoretreat”, where shoreline migration switched from initial progradation to retrogradation. The second response was progradation followed by constant aggradation. The third response was maintained progradation with a markedly accelerating rate, a new autogenic behavior termed “shoreline autoacceleration”.

Table of Contents

List of Tables

List of Figures

Figure 3.4: Photographs showing the characteristics of the facies. (A) Heterolithic alternation of sandstone (cm to dm thick) with mudstone (cm thick) beds (Facies F3). (B) Symmetrical ripple marks in 5-10 cm thick fine to very fine sandstone beds (Facies F3). (c) Dm thick very fine and fine sandstone beds with hummock-cross-stratification (HCS). Note the thin (cm) muddy beds between sandstone beds (Facies 4). (D) Swaley-cross-stratification (SCS) in dm thick very fine and fine sandstone beds (Facies 4). (E) Amalgamated fine sandstone beds with low angle cross-stratification devoid of bioturbation (Facies F5). (F) Contorted bedding with soft deformation increasing upward (Facies F6). (G) Several intervals of low angle cross-lamination and SCS with intense bioturbation at the top (Facies F7). (H) Low angle laminations and storm erosional surfaces (Facies F7). Some planar cross bedding in the bottom. (I) 10-20 cm thick fine sandstone beds *Rosselia socialis* showing multiple levels of equilibrichnia behavior and an erosional surface decapitating the specimens (Facies F8). (J) Crowded *Rosselia socialis* bioturbation destroying completely previous sedimentary structures (Facies F8). (K) 15cm (laterally variable) thick heterolithic layer with shells marking the contact between packages (Facies F9). (L) 10-20 cm Sandy shell layer marking the bottom of the sandstone body (Facies F9). (M) Dm thick fine sandstone beds with planar and through cross lamination. Notice

Chapter One: Introduction

The main focus of this research is investigating the architecture and evolution of parts of the stratigraphic fill of the Sevier foreland basin, including (1) the effect that spatial and temporal variability in subsidence had over the stratal architecture at a late stage of the fill, (2) the predicted (modelled) characteristics of shorelines building from the main foreland onto the forebulge at an early stage of the fill, and (3) the character of some unusual sandstone bodies (shelf sand ridges) that developed during the final major transgression in this basin. To achieve these goals this work uses a combination of outcrop observations, subsurface well-log analysis, mathematical modelling and flume tank experiments.

Foreland basins are important hydrocarbon provinces, such as in the Colville Basin in Alaska, the Mesopotamian foreland basin in Iraq and Saudi Arabia, the offshore province of Sakhalin, or the North-American Western Interior Basin. For oil and gas exploration it is of paramount interest to have a thorough understanding of how foreland basins are in-filled and the relationship between the stratigraphy and the structures that generate the basin.

The Williams Fork Clastic Wedge, an Upper Campanian regressive-transgressive interval of about 4 Myr duration, with 30 to 500m thick sedimentary succession that accumulated in the Western Interior Seaway, provides a study unit that improves our understanding of the late stages of development of the Sevier foreland. Its analysis unravels how the large Cretaceous foreland basin that dominated central North America transitioned to the small basins generated by the Laramide compartmentalization of the region. Although the William Fork clastic wedge, like the older Campanian wedges, has

both a fluvial proximal system and a fringing marine shoreline system, this study focuses mainly on the architecture of its fluvial deposits, and the relationship between this architecture and the growing local structures in the foreland basin.

Mathematical modeling and physical flume experiments are used to examine the early evolution of foreland basin in-fill under 'steady' forcing (i.e., forcing that does not vary though time) of sediment supply and basin subsidence. Sedimentary systems with steady allogenic conditions (i.e., sediment supply, subsidence, base level, and climate) will evolve in a predictable fashion, according to the geometry of the basin and of the deposits. This predictable evolution will result in characteristic stratal patterns which is the 'base-line' basin fill. This 'base-line' stratal patterns will be modified in natural systems by the unavoidable variations in allogenic forcing, in occasions to almost completely eradicate that response. However to properly unravel the magnitude, relative importance and timing of stratigraphic responses to those allogenic perturbations, it is still of paramount importance to understand more about the 'base-line' behavior. Autostratigraphy (Muto *et al.*, 2007) highlights these 'base-line' behaviors and their stratal signatures from the fundamental aspects. So far, autostratigraphic studies have been conducted with spatially uniform subsidence patterns and therefore are not applicable to foreland basins that present changes in subsidence across the basin. The mathematical model and flume tank experiments used in this study aim to discover this 'base-line' behavior in foreland basins and this is the first attempt to study spatially varying subsidence from an autostratigraphic view-point.

WESTERN INTERIOR SEAWAY BASIN

The Cretaceous Western Interior Seaway was an elongate epicontinental seaway that stretched from the Gulf of Mexico to the Arctic Ocean across the interior of the North American Plate (Fig. 1.1). The seaway was created due to a combination of high eustatic levels (Haq *et al.*, 1987), generated by the strong greenhouse conditions of the Late Cretaceous; flexural subsidence (Jordan, 1981), which was created by loading of the thin-skinned thrusting of the Sevier Orogen; and dynamic subsidence (Gurnis, 1993), a result of the subduction of the Farallon and Kulla plates under the North American plate.

Flexural subsidence is considered the main source of subsidence during the Cretaceous (Jordan, 1981; Flemings & Jordan, 1989), but it has been suggested that during the deposition of the Williams Fork Clastic Wedge the orogenic belt was in a period of reduced shortening and decreasing tectonic loading (Devlin *et al.*, 1993; DeCelles, 1994; DeCelles & Mitra, 1995) or at least during its progradational segment of the clastic wedge (Liu *et al.*, 2005). If this is correct, decreasing tectonic loading would have eliminated the flexural subsidence and dynamic subsidence would have become dominant (Pang & Nummendal, 1995; Liu & Nummedal, 2004). Additionally the denudation of the orogen removed the tectonic loading which would have caused an inversion of the subsidence patterns due to isostatic compensation; the area of maximum subsidence, the foredeep, would have been uplifted and the areas away from it would see some subsidence.

The Western Interior Seaway as a large continuous basin disappeared by latest Maastrichtian, replaced by a number of smaller asymmetric basins separated by small uplifts. The basin compartmentalization of the north-American Western Interior Seaway

was the key signature that characterized the switch from the Sevier orogeny with its large foreland basin, to the Laramide orogeny with the smaller intermontane foreland basins (Cross, 1986). This Laramide orogeny developed thick-skinned basement-cored uplifts with a strong asymmetry, where one of the flanks was most of the time much steeper than the other. Therefore the intermontane basins between these uplifts are also strongly asymmetric.

Figure 1.1: Paleogeographic reconstruction of present day North-America during the Late Cretaceous, showing the Western Interior Seaway basin. Modified from (Blakey, 2011).

CLASTIC WEDGES

Clastic wedge are basin-ward thinning packages of thick, relatively coarse-grained, non-marine to marine coastal deposits that pinch out into fine-grained marine sediments. These wedges result from major progradational-retrogradational episodes of the river-fed coastline into the basin, and occur on a range of thickness and time scales. Clastic wedges are a common feature in the stratigraphic fill of foreland basins.

Originally called exogeosyncline-infill (Marshall, 1951; King, 1959) or molasse tectonofacies (Van Houten, 1974), clastic wedges were defined to denote the synorogenic sedimentary products of mountain building. This synorogenic timing, already contested by the classical work of Davis (1898), was seriously questioned by the work of several authors (Blair & Bilodeau, 1988; Heller *et al.*, 1988). Some, like Steel (1988), suggested some delay between the orogenic pulse and the main progradation of the clastic wedge, while others like Blair and Bilodeau (1988) proposed a complete phase reversal, implying that the progradation pulses would happen during orogenic quiescence and the main tectonic events of mountain building would create major flooding surfaces. In the same vein, Heller *et al.* (1988) presented what became the most accepted idea, with the main progradation occurring after the end of the orogenic pulse. This became known as the "anti-tectonic hypothesis". The full circle of ideas was attained when more recently it has been suggested that when the sediment supply is initially large enough the progradation of the clastic wedge can be synchronous with the main thrusting events after all (Burbank *et al.*, 1992; Marzo & Steel, 2000; Horton *et al.*, 2004).

The gross shape of these wedges and their internal architectures reflect a suite of allogenic and autogenic responses to unsteady and steady forcing of the external controls such as regional climate, eustasy, regional tectonics and sediment supply. These controls create a complicated web of interactions with positive and negative feedbacks that vary along the basin.

WILLIAMS FORK CLASTIC WEDGE

The Williams Fork Clastic Wedge, part of the Mesaverde Group in northwestern Colorado and southern Wyoming, constitutes one of the last and most spectacular progradations of the western shorelines of the Cretaceous Western Interior Seaway. This sediment wedge is composed of two lesser order clastic wedges, the Twentymile sub-wedge and the Trout Creek sub-wedge. Overall this wedge built out a distance of some 500 km, from the Sevier Orogen, in the area of Kemmerer WY out to Middle Park Basin in northwestern Colorado, if not prograding right out to Denver Basin (Fig. 1.2) at a rate of more than 200 km/Myr. The wedge is of Upper Campanian age, spanning the ammonite zones *Exiteloceras jenneyi* to *Baculites baculus* about 4 Myr (Izzet *et al.*, 1971; Cobban *et al.*, 2006), and was previously studied by Crabaugh (2001) and by Liu *et al.* (2005).

Stratigraphy

At the center of this Williams Fork Clastic Wedge there is the Canyon Creek Member of the Ericson Formation. The Canyon Creek Member is a regionally continuous fluvial unit with locally variable style from braided to meandering. Inside the Canyon

Creek Mb., several high-relief composite erosional surfaces exist, which are possibly correlated with the multiple pulses of progradation at the marine end of the wedge.

The Williams Fork Clastic Wedge is bounded at its base by a strong erosional surface, which represents a slightly angular unconformity (Fig. 1.2). This composite surface represents a bypass and erosional episode, likely to be correlative down dip with the rapid progradation of the basal Trout Creek Sandstone (Roehler, 1990).

The Trout Creek Sandstone is a shallow marine deltaic unit that is mainly storm-wave dominated (Bullimore *et al.*, 2008), which indicates the regressive tract of the Trout Creek sub-wedge. The Trout Creek Sandstone has an initial very strong progradational character with an almost horizontally prograding shoreline trajectory (see Tongue 1 of Bullimore *et al.* (2008)), but progressively develops into the aggradational units (See Tongues 2, 3, 6 and 7 of the same authors). This aggradational interval is likely correlative with the lower part of the Canyon Creek Member.

The transgressive tract of the Trout Creek sub-wedge is the Mount Harris Member (Roehler, 1990; Bullimore *et al.*, 2008). This unit is composed of coastal plain, estuarine, tidal creek, distributary channel deposits, and abundant coals and leads to a marked marine transgression above it.

Further down dip the correlation becomes complicated due to the intervening presence of the Park Range Uplift, where the Williams Fork Clastic Wedge has been eroded away. The Trout Creek sub-wedge has been tentatively correlated with a silty to very fine-grained sandy Limestone Concretionary horizon in the Middle Park Basin based on ammonite zonation (Izzet *et al.*, 1971).

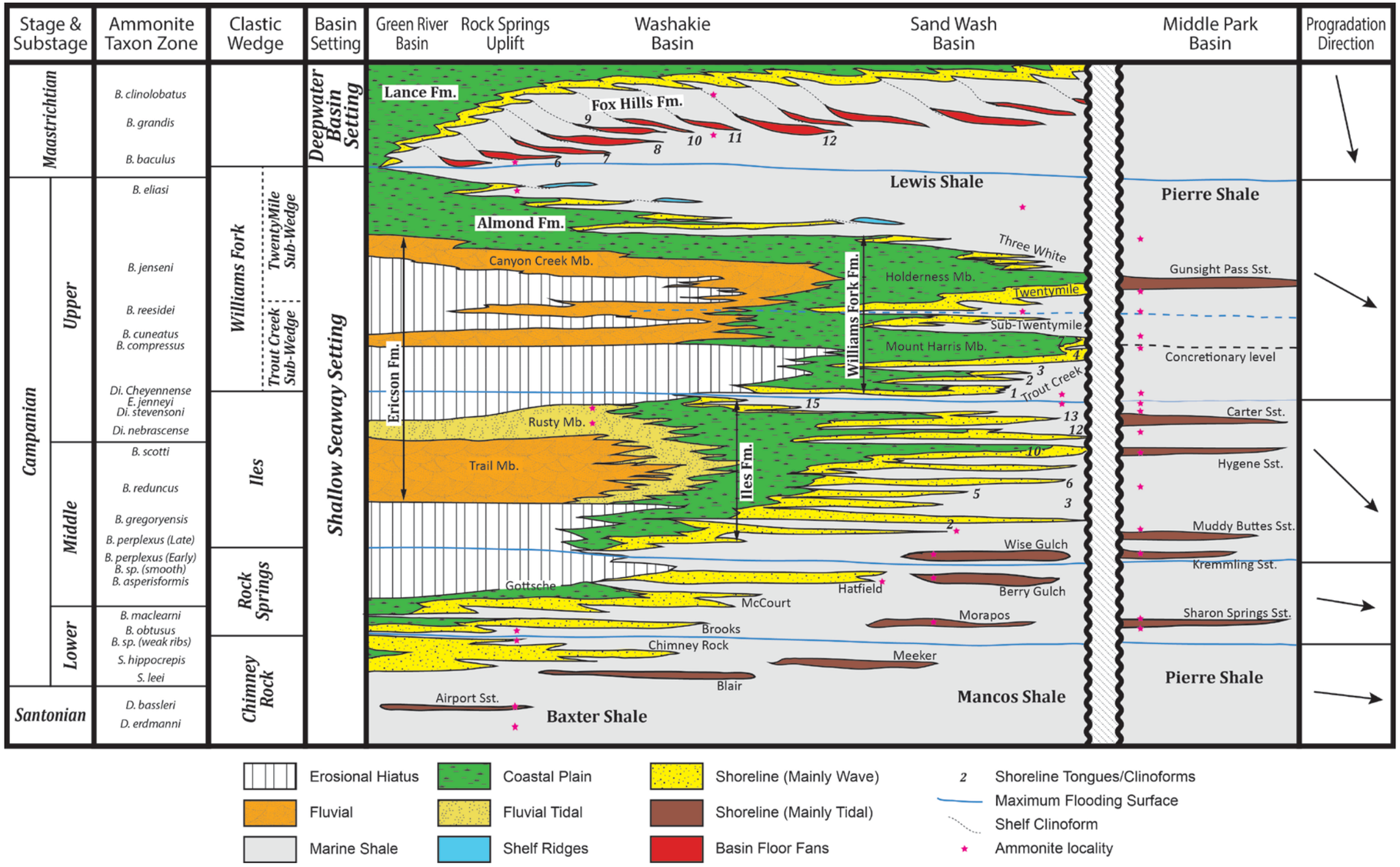

Figure 1.2: Stratigraphic reconstruction of the Campanian and early Maastrichtian from the Green River Basin in southwestern Wyoming to the Middle Park Basin in northwestern Colorado. All the clastic wedges of the Campanian are represented showing the main characteristics of their shoreline trajectories and their fluvial correlatives, along with the last shoreline progradation during the Maastrichtian before the disappearance of the seaway. *B – Baculites. Di – Didymoceras. E. – Exiteloceras. S. – Scaphites. D. – Desmoscaphites.* Modified after Carvajal and Steel (2009), Crabaugh (2001), Gomez-Veroiza and Steel (2010), (Izzet *et al.*, 1971) and Steel *et al.* (2012)

The Twentymile sub-wedge presents an even stronger aggradational character than the Trout Creek sub-wedge, even though it also progrades farther, fully reaching the Middle Park Basin. The regressive limb of this sub-wedge can be divided into an early thinner regressive unit, the Sub-Twentymile Sandstone, and the main regressive shallow marine body of the Twentymile Sandstone. These regressive shorelines are wave dominated, evidenced by the large number of wave ripples, swaley and hummocky cross-stratification, though there is also tidal influence, evidenced by stacked sets of planar cross-stratified sandstones, upper flow regime planar laminated intervals, and sigmoidal cross-laminated beds (Benda, 2000).

Above and up dip of the Twentymile Sandstone lies the Holderness Member. This unit corresponds to the paralic system landward of the shorelines of the Twentymile Sandstone. The Holderness Member is composed of coastal plain and estuarine deposits, as well as tidal creek, bay-head delta, lagoon, swamp, and distributary channel deposits; with strong fluvial and tidal influence.

The transgressive limb of the Williams Fork Clastic Wedge is the Almond Formation, usually divided into a lower and upper unit (Martinsen, 1995; Tobin *et al.*, 2010). The lower Almond consists of continental to paralic deposits, mainly fluvial and distributary channels with splay and overbank deposits, coaly swamps, and tidal flats, though there is also a significant marine transgressive-regressive marine shoreline occurring within its middle section. The upper Almond Formation is again dominated by paralic to shallow-marine deposits, consisting of repeated wave-dominated shorefaces or deltas with intervening back-barrier coaly deposits. The upper part of the upper Almond Formation is an overall major transgressive interval, though with repeated small punctuated regressive intervals. The punctuated characteristic of this final

Almond transgression is very different from the transgression that caps the Trout Creek sub-wedge, as it is still highly aggradational in character.

Tectonics

The topographic load of the growing Sevier fold-thurst belt was reputedly the main source of subsidence in the Western Interior Seaway Basin (Jordan, 1981) which resulted in an asymmetric basin with the foredeep along its western boundary, with subsidence rate decreasing eastward. Nevertheless, the Williams Fork Clastic Wedge shows a clear trend of thickening eastwards, away from the western edge of the basin. This is interpreted as a result of the Sevier orogenic belt being relatively inactive at the time of deposition of this clastic wedge. During this period of inactivity, the denudation of the orogen would have shifted the depocenter outward, with inversion of the former subsidence maximum. In addition, the effects of the easterly moving dynamic subsidence may have played a more important role (Liu & Nummedal, 2004; Liu *et al.*, 2011).

During the Late Cretaceous, the Farallon plate is known to have had its subduction angle reduced (Cross & Pilger, 1978); the shallower subduction then transferred the stress further into the North-American plate initiating the Laramide orogeny. The Laramide Orogeny developed a series of crustal rotated blocks with high-angle reverse faults that reached the crystalline basement, and created a complex pattern of subsidence and uplift. This is the origin of the Laramide uplifts and basins that compartmentalized the Western Interior Seaway (Dickinson *et al.*, 1988). It is still a matter of debate when these structures were initiated; some maintained that Laramide deformation did not start until the Maastrichtian-Paleocene (Cross & Pilger, 1978; Cross, 1986), while some argued that the Williams Fork Clastic Wedge already showed some indications of this deformation syn-depositionally (Devlin *et al.*, 1993).

Interaction between tectonics and sedimentation

The Williams Fork Clastic Wedge is the farthest eastward prograding clastic wedge of the four wedges in the Mesaverde Group. Only the Iles Clastic Wedge, directly underneath, shows a progradation distance of comparable magnitude. However, these two wedges show very contrasting architectures; the Iles Clastic Wedge is formed by 14 thin marine tongues that prograded and retrograded rapidly back and forth around 100 km across north-western Colorado (Gomez, 2009); the Williams Fork Clastic Wedge, on the other hand, is organized in two distinct thick progradational-retrogradational cycles. In further contrast, the Iles Clastic wedge has a very thick fluvial core at its proximal end compared to the Williams Fork Clastic Wedge.

The differences between the Williams Fork Clastic Wedge and the other wedges in the Mesaverde Group are caused by the interaction between the changing tectonic regime of the basin and the fluvio-deltaic systems being developed. It is generally accepted that both the Williams Fork Clastic Wedge and the Iles Clastic Wedge were developed in a period of relative quiescence in the Sevier fold and thrust belt (DeCelles, 1994; Pang & Nummendal, 1995; Liu *et al.*, 2005; DeCelles & Coogan, 2006). If the Sevier belt was inactive, also the flexural subsidence would have been negligible and the ensuing denudation of the orogen would have triggered isostatic uplift in those areas. Reduced subsidence in the proximal end of the system, but with continued sediment supply, would have forced the clastic wedge to prograde faster and farther, and if proximal uplift also occurred the fluvial system would have become erosive, and created unconformities. Both the Iles and Williams Fork clastic wedges and the unconformities at their bases in the proximal areas perfectly fit this scenario.

During the greenhouse condition of the late Cretaceous, sea-level changes of glacioeustatic origin were of small magnitude, probably no more than 20-40 m (Miller *et al.*,

2005). This sea-level change was not enough to be a major control in large-scale continental margins, but large enough to drive shorelines in shallow, gently dipping basins. Without flexural subsidence and only affected by the gentle dynamic subsidence, the Western Interior Seaway probably would be very shallow and would have extremely reduced gradients. Therefore glacioeustatic changes have been proposed as the most probable cause for the rapid back and forth transits of the Iles shorelines (Gomez, 2009).

The Williams Fork Clastic Wedge shows signs of a more complicated history. The base of the wedge in its proximal end, underneath the fluvial Canyon Creek Member, is a strong erosional surface that is slightly angular over Laramide structures like the Rock Springs uplift. The unconformity is correlative with the strong and fast progradation of the Trout-Creek shorelines. The unconformity is of uncertain age and probably time-transgressive, but it is probably post-*Didymoceras stevensoni*, which is found in the underlying Rusty Member (Gill *et al.*, 1970), and prior to *Baculites jenseni* which is found in overlying Almond Fm. equivalent. The Trout Creek age is well defined by *Baculites resideii* and *Exiteloceras jenneyi* in the marine tongues immediately above and below respectively (Bader *et al.*, 1983). The dating therefore allows for its correlation even if uncertain. The strong proximal unconformity with slight angularity indicates that the Sevier belt was relatively inactive, while the increased erosion over the Rock Springs Uplift indicates that the laramide structures were active. This out-of-phase structural regime, *sensu* Devlin *et al.* (1993), enhanced the progradational character of the Trout Creek shorelines by delivering more sediment supply to the distal end of the basin.

The transgressive part of the Trout Creek sub-wedge possibly along with the Sub-Twentymile sandstone of *Baculites Resideii* age likely represents a time of increased subsidence in the proximal reaches of the system, being correlative with the oldest part of the Canyon Creek

Mb. This retrogradation was probably also related to the enhanced subsidence in the southern Greater Green River Basin created by the early loading of the Uinta Mountains.

The renewed progradation of the Twentymile sandstone is dated between *Baculites resideii* and *Baculites eliasii* (Bader *et al.*, 1983) and probably its maximum during *Baculites jensei* as the Gunsight Pass sandstone (Izzet *et al.*, 1971). The Twentymile sandstone is probably correlative with an intra-Canyon Creek Mb. unconformity (Fig. 1.2) and was likely caused by increased Laramide activity.

The lower Almond Formation of *Baculites jenseni* age is a marked transgressive continuation of the coastal Holderness Member at the top of the Twentymile sandstone. However, this early transgression is culminated in the mid-Almond marine incursion that reaches as far west as mid Washakie Basin, and it reverses in a marked mid-Almond shoreline regression. Above this in upper Almond, there is further aggradation and several repeated regressive-transgressive shoreline. Finally the main Almond transgression continues with a huge westward sweep (albeit with several small regressions punctuating the overall retrogradation), probably caused by the reactivation of the Absaroka thrust sheet of the Sevier orogenic belt (DeCelles, 1994; 2004). This thrusting reactivated the flexural subsidence near the orogen, where sediments are trapped to form the Hams Fork Conglomerate of the Evanston Formation.

CHAPTER OVERVIEW

Chapter Two: Campanian Laramide signals and architecture of a widespread fluvial sand-sheet: Canyon Creek Member, southern Wyoming

The second chapter is a manuscript submitted for publication to Journal of Sedimentary Research. It explores the characteristics, architecture, and fluvial style of the Canyon Creek Member, as well as the subsidence pattern over which the stratigraphic infill developed. This chapter focuses to provide insight into the relationship between these depositional characteristics under the foreland-basin tectonics and possible local tectonic disruptions. This study generated several significant findings: 1) there is a general trend within the Canyon Creek Mb. of decreasing channel-belt amalgamation, increased total thickness and change from braided to meandering style away from the sediment source in the Sevier Orogen; 2) the Laramide structures were already active at the time of deposition of the Canyon Creek Member; 3) the Laramide structures locally distorted the general trends, increasing the amalgamation, decreasing thickness and favoring braided systems locally; and 4) the Laramide structures had no topographic expression, except slightly increased depositional slopes enough to induce fluvial style change, but not enough to concentrate the fluvial system in the subsiding areas.

Chapter Three: Architecture of storm to tidal shelf sandstone bodies; an example from Campanian Almond Formation in Hanna Basin, USA

The third chapter explores the sedimentological characteristics of mud-encased sandstone bodies at the very top of the Almond Formation. These bodies have been vaguely described previously as either sand waves, barrier bars, or simply grouped with the underlying wave-

dominated shorelines. The current study reinterpreted the sandstone bodies as shelf tidal sand ridges because of their basal ravinement, constituent stacked dunes, and overlying shelf mudstones. The chapter proposes a series of critical characteristics for recognizing these bodies in the geological record.

Chapter Four: Autoacceleration of clinoform progradation in foreland basins: Theory and experiments

The fourth chapter is an expanded version of a previously published manuscript (Leva López *et al.*, 2014). This chapter explores the autogenic behavior of deltaic and shelf clinoforms under the characteristic subsidence style of foreland basins, where the maximum accommodation is created right next to the sediment source. With this objective a mathematical model was developed and flume tank experiments were conducted. This study generated several important findings: 1) There are three possible modes of clinoform evolution: autoretreat, stationary shoreline, and autoacceleration. Autoacceleration has never been previously described. 2) The development of these evolutionary modes is controlled by a simple relationship between sediment supply and the maximum subsidence. 3) The use of this relationship allows for first order estimation of long-term "over-fill" and "under-fill" basin fill style.

REFERENCES

BADER, J.W., GILL, J.R., COBBAN, W.A. & LAW, B.E. (1983) Biostratigraphic Correlation Chart of Some Upper Cretaceous Rocks from the Lost Soldier Area, Wyoming to West of Craig, Colorado, U.S. Geological Survey. Denver, CO.

BENDA, T.L. (2000) Facies, Architecture, and Sequence Stratigraphy of a Fourth-Order Clastic Wedge: Upper Cretaceous Twentymile Sandstone, (Mesaverde Group) Northwest Colorado, University of Wyoming, Laramie.

BLAIR, T.C. & BILODEAU, W.L. (1988) Development of Tectonic Cyclothems in Rift, Pull-Apart, and Foreland Basins: Sedimentary Response to Episodic Tectonism. *Geology*, **16,** 517-520.

BLAKEY, R. (2011) Colorado Plateau Geosystems, Inc., from http://cpgeosystems.com/index.html.

BULLIMORE, S.A., HELLAND-HANSEN, W., HENRIKSEN, S. & STEEL, R.J. (2008) Shoreline Trajectory and Its Impact on Coastal Depositional Environments: An Example from the Upper Cretaceous Mesaverde Group, Northwestern Colorado, USA. In: *Recent Advances in Models of Siliciclastic Shallow-Marine Stratigraphy* (Ed. by G. J. Hampson, R. J. Steel & P. M. Burgess), *Sepm Special Publication*, **90**, 209-236. SEPM - Soc. Sedimentary Geology, Tulsa.

BURBANK, D.W., PUIGDEFABREGAS, C. & MUÑOZ, J.A. (1992) The Chronology of the Eocene Tectonic and Stratigraphic Development of the Eastern Pyrenean Foreland Basin, Northeast Spain. *Geological Society of America Bulletin*, **104,** 1101-1120.

CARVAJAL, C. & STEEL, R. (2009) Shelf-Edge Architecture and Bypass of Sand to Deep Water: Influence of Shelf-Edge Processes, Sea Level, and Sediment Supply. *Journal of Sedimentary Research*, **79,** 652-672.

COBBAN, W.A., WALASZCZYK, I., OBRADOVICH, J.D. & MCKINNEY, K.C. (2006) A Usgs Zonal Table for the Upper Cretaceous Middle Cenomanian--Maastrichtian of the Western Interior of the United States Based on Ammonites, Inoceramids, and Radiometric Ages. *USGS Open Report*, USGS. Denver**,** 45.

CRABAUGH, J.P. (2001) Nature and Growth of Nonmarine-to-Marine Clastic Wedges: Examples from the Upper Cretaceous Iles Formation, Western Interior (Colorado) and the Lower Paleogene Wilcox Group of the Gulf of Mexico Basin (Texas). Ph. D. Dissertation Thesis, University of Wyoming, Laramie.

CROSS, T.A. & PILGER, R.H. (1978) Tectonic Controls of Late Cretaceous Sedimentation, Western Interior, USA. *Nature*, **274,** 653-657.

CROSS, T.A. (1986) Tectonic Controls of Foreland Basin Subsidence and Laramide Style Deformation, Western United States. *Special Publications International Association of Sedimentologists*, **8,** 453.

DAVIS, W.M. (1898) *The Triassic Formations of Connecticut.* U.S.G.S. Annual report, No. 18, part 2.

DECELLES, P.G. (1994) Late Cretaceous-Paleocene Synorogenic Sedimentation and Kinematic History of the Sevier Thrust Belt, Northeast Utah and Southwest Wyoming. *Geological Society of America Bulletin*, **106,** 32-56.

DECELLES, P.G. & MITRA, G. (1995) History of the Sevier Orogenic Wedge in Terms of Critical Taper Models, Northeast Utah and Southwest Wyoming. *Geological Society of America Bulletin*, **107,** 454-462.

DECELLES, P.G. (2004) Late Jurassic to Eocene Evolution of the Cordilleran Thrust Belt and Foreland Basin System, Western USA. *American Journal of Science,* **304,** 105-168.

DECELLES, P.G. & COOGAN, J.C. (2006) Regional Structure and Kinematic History of the Sevier Fold-and-Thrust Belt, Central Utah. *Geological Society of America Bulletin,* **118,** 841-864.

DEVLIN, W.J., RUDOLPH, K.W., SHAW, C.A. & EHMAN, K.D. (1993) The Effect of Tectonic and Eustatic Cycles on Accommodation and Sequence-Stratigraphic Framework in the Upper Cretaceous Foreland Basin of Southwestern Wyoming. In: *Sequence Stratigraphy and Facies Associations* (Ed. by H. W. Posamentier, C. P. Summerhayes, B. U. Haq & G. P. Allen), *Spec. Publ. Int. Ass. Of Sediment.,* **18**, 501-520. Blackwell Publishing Ltd., Boston.

DICKINSON, W.R., KLUTE, M.A., HAYES, M.J., JANECKE, S.U., LUNDIN, E.R., MCKITTRICK, M.A. & OLIVARES, M.D. (1988) Paleogeographic and Paleotectonic Setting of the Laramide Sedimentary Basins in Central Rocky-Mountain Region. *Geological Society of America Bulletin*, **100,** 1023-1039.

FLEMINGS, P.B. & JORDAN, T.E. (1989) A Synthetic Stratigraphic Model of Foreland Basin Development. *Journal of Geophysical Research-Solid Earth and Planets,* **94,** 3851-3866.

GILL, J.R., MEREWETHER, E.A. & COBBAN, W.A. (1970) *Stratigraphy and Nomenclature of Some Upper Cretaceous and Lower Tertiary Rocks in South-Central Wyoming*. U.S. Geological Survey, Denver, CO.

GOMEZ-VEROIZA, C.A. & STEEL, R.J. (2010) Iles Clastic Wedge Development and Sediment Partitioning within a 300-Km Fluvial to Marine Campanian Transect (3 M.Y.), Western Interior Seaway, Southwestern Wyoming and Northern Colorado. *AAPG Bulletin,* **94,** 1349-1377.

GOMEZ, C.A. (2009) Clastic Wedge Development and Sediment Budget in a Source-to-Sink Transect (Late Campanian Western Interior Basin, Sw Wyoming and N Colorado). Ph.D. Dissertation Thesis, University of Texas at Austin, Austin.

GURNIS, M. (1993) Phanerozoic Marine Inundation of Continents Driven by Dynamic Topography above Subducting Slabs. *Nature,* **364,** 589-593.

HAQ, B.U., HARDENBOL, J. & VAIL, P.R. (1987) Chronology of Fluctuating Sea Levels since the Triassic. *Science*, **235,** 1156-1167.

HELLER, P.L., ANGEVINE, C.L., WINSLOW, N.S. & PAOLA, C. (1988) Two-Phase Stratigraphic Model of Foreland-Basin Sequences. *Geology*, **16,** 501-504.

HORTON, B.K., CONSTENIUS, K.N. & DECELLES, P.G. (2004) Tectonic Control on Coarse-Grained Foreland-Basin Sequences: An Example from the Cordilleran Foreland Basin, Utah. *Geology*, **32,** 637-640.

IZZET, G.A., COBBAN, W.A. & GILL, J.R. (1971) The Pierre Shale near Kremmling, Colorado, and Its Correlation to the East and the West. *Geological Survey Professional Paper*. U. S. G. Survey. **684-A**.

JORDAN, T.E. (1981) Thrust Loads and Foreland Basin Evolution, Cretaceous, Western United-States. *Aapg Bulletin-American Association of Petroleum Geologists*, **65,** 2506-2520.

KING, P.B. (1959) *The Evolution of North America*. Princeton University Press, Princeton.

LEVA LÓPEZ, J., KIM, W. & STEEL, R.J. (2014) Autoacceleration of Clinoform Progradation in Foreland Basins: Theory and Experiments. *Basin Research***,** 1365-2117.

LIU, S.F. & NUMMEDAL, D. (2004) Late Cretaceous Subsidence in Wyoming: Quantifying the Dynamic Component. *Geology*, **32,** 397-400.

LIU, S.F., NUMMEDAL, D., YIN, P.G. & LUO, H.J. (2005) Linkage of Sevier Thrusting Episodes and Late Cretaceous Foreland Basin Megasequences across Southern Wyoming (USA). *Basin Research*, **17,** 487-506.

LIU, S.F., NUMMEDAL, D. & LIU, L. (2011) Migration of Dynamic Subsidence across the Late Cretaceous United States Western Interior Basin in Response to Farallon Plate Subduction. *Geology*, **39,** 555-558.

MARSHALL, K. (1951) *North American Geosynclines*. The Geological Society of America, New York.

MARTINSEN, R.S. (1995) Stratigraphy and Lithofacies of the Almond Formation, Washakie and Great Divide Basins, Wyoming. *Guidebook - Wyoming Geological Association*. G. E. Christiansen, M. A. Olson & R. C. Surdam, Wyoming Geological Association : Casper, WY, United States. United States. **1995,** 297-310.

MARZO, M. & STEEL, R.J. (2000) Unusual Features of Sediment Supply-Dominated, Transgressive-Regressive Sequences: Paleogene Elastic Wedges, Se Pyrenean Foreland Basin, Spain. *Sedimentary Geology*, **138,** 3-15.

MILLER, K.G., WRIGHT, J.D. & BROWNING, J.V. (2005) Visions of Ice Sheets in a Greenhouse World. *Marine Geology*, **217,** 215-231.

MUTO, T., STEEL, R.J. & SWENSON, J.B. (2007) Autostratigraphy: A Framework Norm for Genetic Stratigraphy. *Journal of Sedimentary Research*, **77,** 2-12.

PANG, M. & NUMMENDAL, D. (1995) Flexural Subsidence and Basement Tectonics of the Cretaceous Western Interior Basin, United-States. *Geology*, **23,** 173-176.

ROEHLER, H.W. (1990) *Stratigraphy of the Mesaverde Group in the Central and Eastern Greater Green River Basin, Wyoming, Colorado and Utah* U.S. Geological Survey, Denver, CO.

STEEL, R.J. (1988) Coarsening-Upward and Skewed Fan Bodies: Symtoms of Strike-Slip and Transfer Fault Movement in Sedimentary Basins. In: *Fan Deltas: Sedimentology and Tectonic Settings* (Ed. by W. Nemec & R. J. Steel), 75-83. Blackie and Son Ltd., Glasgow.

STEEL, R.J., PLINK-BJORKLUND, P. & ASCHOFF, J. (2012) Tidal Deposits of the Campanian Western Interior Seaway, Wyoming, Utah and Colorado, USA. In: *Principles of Tidal Sedimentology* (Ed. by R. A. Davis Jr & R. W. Dalrymple), 437-471. Springer Netherlands.

TOBIN, R.C., MCCLAIN, T., LIEBER, R.B., OZKAN, A., BANFIELD, L.A., MARCHAND, A.M.E. & MCRAE, L.E. (2010) Reservoir Quality Modeling of Tight-Gas Sands in Wamsutter Field: Integration of Diagenesis, Petroleum Systems, and Production Data. *AAPG Bulletin*, **94,** 1229-1266.

VAN HOUTEN, F.B. (1974) Northern Alpine Molasse and Similar Cenozoic Sequences of Southern Europe. In: *Modern and Ancient Geosynclinal Sedimentation* (Ed. by R. H. Dott Jr. & R. H. Shaver), *Sepm Special Publication*, **No.19**, 14. SEPM, Tulsa.

Chapter Two: Campanian Laramide Signals and Architecture of a Widespread Fluvial Sand-sheet: Canyon Creek Member, Southern Wyoming

ABSTRACT

The Upper Campanian Canyon Creek Member of the Ericson Formation in the Greater Green River Basin of Southern Wyoming is a regionally extensive sandstone sheet of fluvial origin. A well-log and outcrop dataset allows this ancient fluvial system to be examined basin-wide, covering an area of approximately 45000 km^2. Changes in fluvial style and architecture occur both down-dip and along strike, across the whole fluvial system allowing insight on both local and regional structural styles in the basin.

From the proximal reaches of the system in the west and northwest to the distal areas in the east and south-east, the Canyon Creek Member (and its co-eval equivalents) shows a first order trend of thickening and of net-to-gross reduction, as well as a change of planform style from braided to meandering. The reason for these trends is an eastward increase of subsidence away from the orogenic belt, possibly resulting from a reduced activity in the fold-thrust belt that decreased the importance of the tectonic loading and flexural subsidence and enhanced the dynamic subsidence signal.

The Laramide orogeny is typically thought to have been initiated during the Maastrichtian or Paleocene. However, study of the Canyon Creek Member strongly suggests earlier initiation during the Campanian. The above general proximal-to-distal trends in the Canyon Creek are locally modified by early differential movement across the Rock Springs Uplift, the Uinta Mountains, the Rawlins Uplift, and the Sierra Madre Uplift, all of which are Laramide-style structures. This early movement is shown by reduced thickness and increased net-to-gross over the crest of these structures and by the opposite trend down-flank on the structure into the footwall of the adjacent structure. This asymmetric pattern of thickness and net-to-gross development within individual Canyon Creek 'sub-basins' is the typical and distinctive Laramide basin signature.

INTRODUCTION AND OBJECTIVES

A series of eastward to southeastward prograding clastic wedges, each a linked alluvial-coastal plain-shoreline-shelf system, filled the Campanian Western Interior Seaway (WIS). The main sediment source for these clastic wedges was the mountain range produced by the Sevier fold-thrust belt (Masters, 1966; Siepman, 1986; Roehler, 1990). At some point, late during the deposition of the clastic wedges (Early Campanian), the Wind River Range became a secondary but important sediment source (Carvajal, Cristian & Steel, 2012). This study focusses on the Campanian Canyon Creek Member of the Ericson Formation, which represents the fluvial system inside the Williams Fork Clastic Wedge (Roehler, 1990; Crabaugh, 2001), the last and the farthest prograding wedge that filled the Western Interior Seaway (Steel *et al.*, 2012).

The objectives of the present work are two-fold:

1. To demonstrate how this regionally widespread Canyon Creek sheet sandstone changes character from a thin, highly amalgamated, internally channelized fluvial sand-body to a thick succession of thinner sheets and increasingly isolated channels and channel belts as it tracks downslope across its alluvial and coastal plain towards the coeval Campanian shorelines.
2. To document the impact of growing Laramide structure on the Canyon Creek Member. Locally this is expressed as channel-belt merging, fairway directional changes, and local amalgamation with deep erosion adjacent to embryonic Laramide structures whereas sub-regionally the multi-directional thickness asymmetry (thickening into the Rock Springs, Rawlins and Uinta uplifting blocks), so typical of Laramide basins, can be seen.

GEOLOGICAL CONTEXT

The Western Interior Seaway (WIS) was a wide (at times up to 1500 km) epicontinental seaway that connected the Gulf of Mexico to the Arctic Ocean throughout most of the

Cretaceous; this seaway was created by a combination of high eustatic sea levels during the Campanian, flexural subsidence, and induced dynamic subsidence across this portion of the North American plate. The subduction of the Kula and Farallon plate (Fig. 2.1) under the western margin of the North American Plate during the Cretaceous generated long-wave dynamic subsidence (Liu, Lijun & Gurnis, 2010; Liu *et al.*, 2011) and thin-skinned compressive structures of the Sevier fold and thrust belt (DeCelles & Mitra, 1995; DeCelles & Coogan, 2006). The Sevier belt induced short-wave flexural subsidence on the western side of the WIS (Jordan, 1981; Flemings & Jordan, 1989; DeCelles & Giles, 1996). Towards the end of the Cretaceous, the subduction angle of the Farallon plate became very shallow (Cross & Pilger, 1978; Dickinson, W.R. & Snyder, 1978). This caused stresses to be transferred further into the North American plate and initiated a change in orogenic style from the thin-skinned structures characteristic of the Sevier orogeny to the thick-skinned structures of the Laramide orogeny (DeCelles, 2004; Jones *et al.*, 2011). This change in tectonic style triggered an initial and widespread shallowing and embaying of the shorelines in the WIS (Aschoff, J. & Steel, 2011a; Aschoff, Jennifer L & Steel, 2011b) and eventually led to the development of a series of Laramide tilted blocks and basins, producing a more complex pattern of subsidence (e.g. Sand Wash, Washakie, and Hanna basins) and uplifts (Moxa Arch, Rock Springs Uplift, and Sierra Madre Uplift) (Dickinson, W. R. *et al.*, 1988).

Within the Late Cretaceous WIS basin, the combined effect of eustatic variations, climatic changes, and spatially non-uniform uplift and subsidence generated a series of large-scale regressive to transgressive clastic wedges along the western margin of this ancient seaway (Crabaugh, 2001) (Fig. 2.2); the source of sediments was mainly from the nearby Sevier Orogenic belt (Fig. 2.3) (Devlin *et al.*, 1993; Gomez-Veroiza & Steel, 2010; Aschoff, J. & Steel, 2011a). The work described in this paper focuses on the fluvial portion of the youngest of these clastic wedges, likely sourced from the uplifting Wind River Range (Pryor, 1961) in addition to the Sevier orogenic belt.

Figure 2.1: Paleogeographic and tectonic reconstruction of present day North America during the Late Campanian. The map shows the approximate location and extent of the Sevier Orogenic Belt and the Western Interior Seaway Basin. The study area of this work is highlighted in a yellow rectangle. Modified from Blakey (2011).

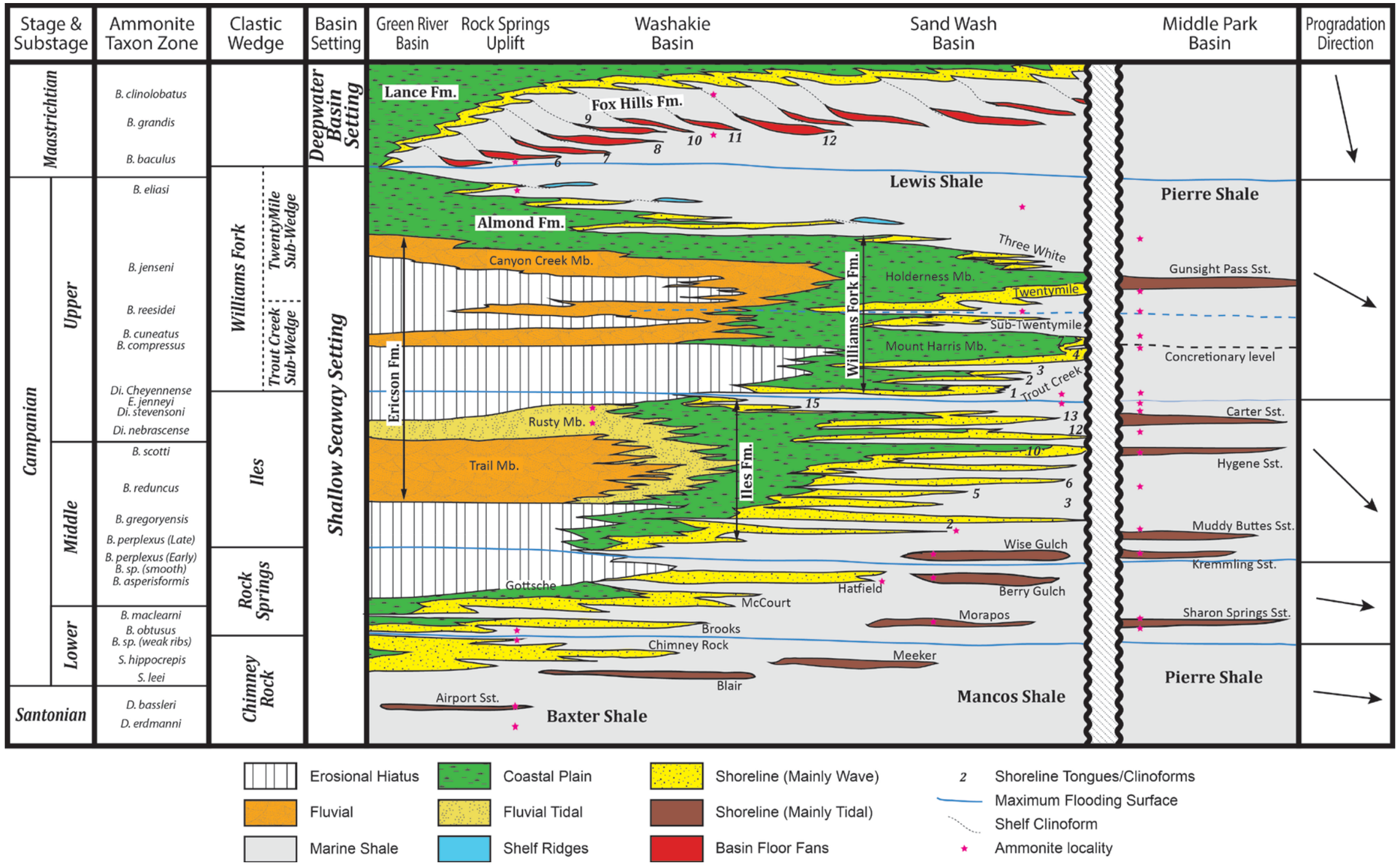

Figure 2.2: Stratigraphic reconstruction of Campanian and early Maastrichtian strata from the Green River Basin in south-western Wyoming to the Middle Park Basin in northwestern Colorado. All four clastic wedges of the Campanian as well as the final Lewis/Fox Hills Wedge are shown. Each wedge has a highly amalgamated fluvial core that passes downslope into coastal plain deposits and multiple marine shorelines, mainly wave dominated. Some of the shorelines eventually become tidally-influenced subaqueous deltas farther down-dip. *B – Baculites. Di – Didymoceras. E. – Exiteloceras. S. – Scaphites. D. – Desmoscaphites.* Modified after Carvajal, C. and Steel (2009), Crabaugh (2001), Gomez-Veroiza and Steel (2010), Izzet *et al.* (1971) and Steel *et al.* (2012).

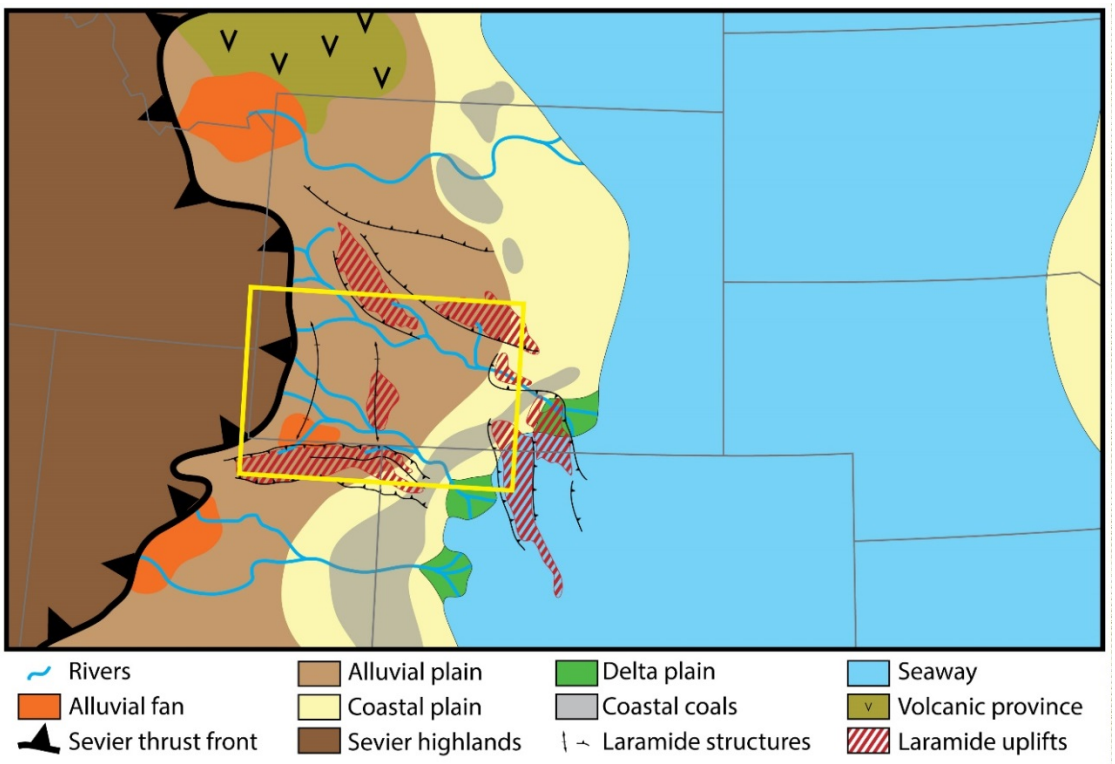

Figure 2.3: Depositional system reconstruction of the central United States during the Late Campanian. The map shows the approximate location of the Western Interior Seaway shoreline, the main river and deltaic systems around the study area (yellow rectangle), and the embryonic Laramide uplifts referred to in this work. Modified from Kirschbaum and Roberts (2005).

The Williams Fork Clastic Wedge

The Williams Fork Clastic Wedge (Steel *et al.*, 2012), part of the Mesaverde Group in northwestern Colorado and southern Wyoming, constitutes the last and most spectacular progradation of the western shorelines of the WIS (Fig. 2.1). In the distal reaches of the system in Colorado, the wedge can be subdivided into two lower rank clastic wedges, the younger Twentymile sub-wedge and the older Trout Creek sub-wedge (Fig. 2.2 & 2.4). The Twentymile and Trout Creek sandstones are the marine shoreline components of the wedge (Crabaugh, 2001).

This Williams Fork clastic wedge built out a distance of more than 500 km from the Sevier Orogen in the area of Kemmerer, Wyoming, and to the Denver Basin (Fig. 2.2) (Masters, 1966; Liu *et al.*, 2005; Gomez, 2009). The wedge extends across the present-day Green River, Great Divide, Washakie, Sand Wash, Hanna, Middle Park, and Denver/Laramie basins (Love, 1961). The wedge is Upper Campanian in age, spanning the ammonite zones *Exiteloceras jenneyi* to *Baculites baculus*, about 3-4 Myr (Obradovich, 1993; Cobban *et al.*, 2006).

Unlike older Cretaceous clastic wedges, the Williams Fork thickens into the basin, showing clearly that there was no longer any Sevier 'foredeep' at this time. This basin-ward thickening has been interpreted as Sevier tectonic relative quiescence and possible isostatic uplift at this time (DeCelles, 1994; Pang & Nummendal, 1995; Liu *et al.*, 2005; DeCelles & Coogan, 2006), although the Laramide syn-tectonic sediment flux to the system has generally been ignored or underestimated. Liu *et al.* (2011) recently suggested that this eastward thickening could reflect eastward migration of the dynamic subsidence component in the basin.

DATASET

For this study we used a combination of 17 outcrop-measured stratigraphic sections, 234 well logs, and a number of interpreted photo-mosaics (Fig. 2.5).

Most of the outcrop-measured sections were collected by J. Leva-Lopez, two by Bullimore *et al.* (2008) and one by Izzet *et al.* (1971). The stratigraphic sections measured by J. Leva-Lopez were measured with special emphasis on grain-size variations, sedimentary structures, and paleocurrent indicators; they are used in combination with interpreted photo-mosaics to determine the fluvial style and fluvial sub-environments at each location, as well as the paleohydrological characteristics of the system.

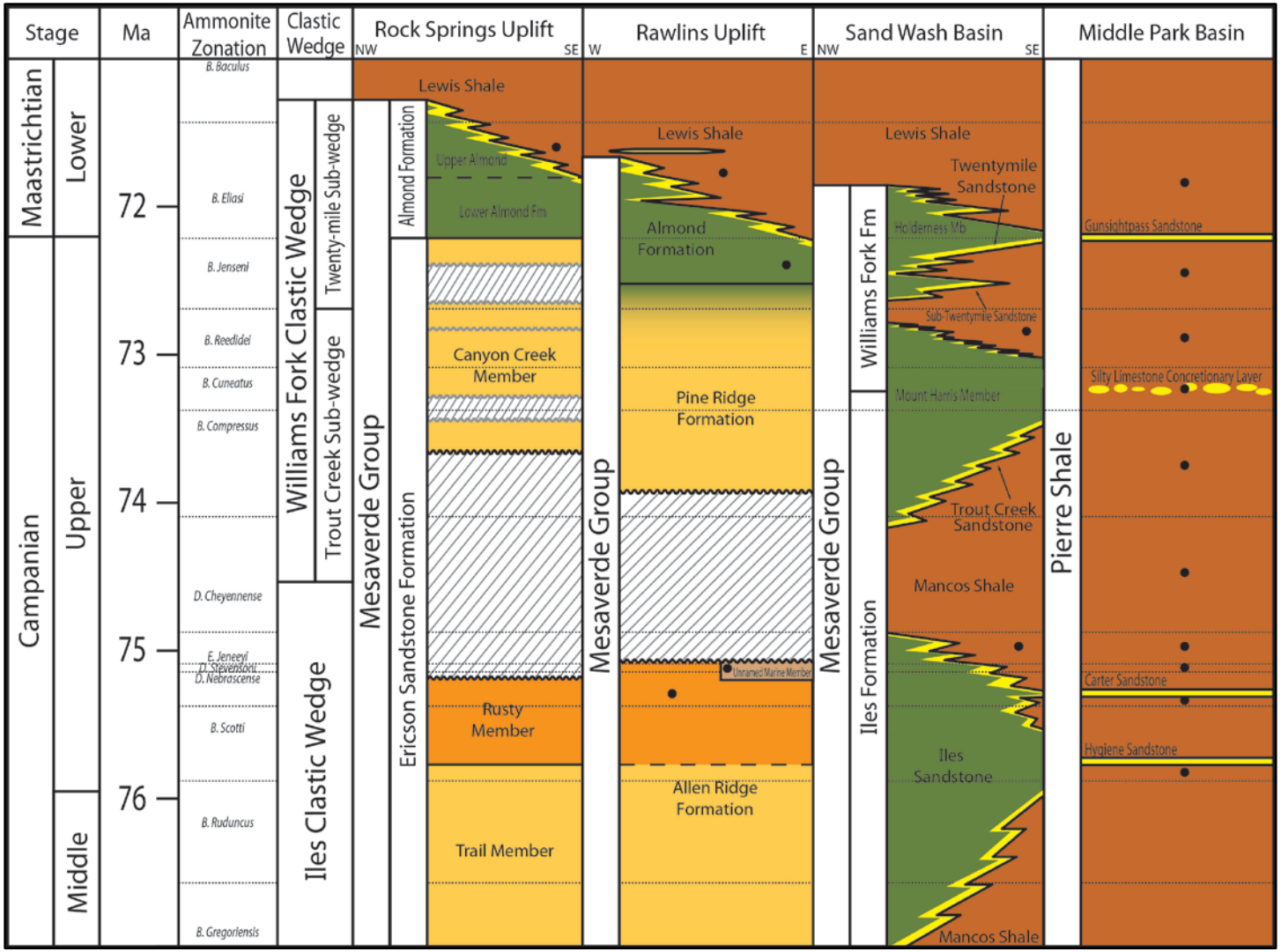
Stage
Ma
Ammonite Zonation
Clastic Wedge
Rock Springs Uplift
NW
SE
Rawlins Uplift
W
E
Sand Wash Basin
NW
SE
Middle Park Basin
Maastrichtian
Lower
Campanian
Upper
Middle
72
73
74
75
76
B. Baculus
B. Eliasi
B. Jenseni
B. Reedlidei
B. Cuneatus
B. Compressus
D. Cheyennense
E. Jeneeyi
D. Stevensoni
D. Nebrascense
B. Scotti
B. Ruduncus
B. Gregoriensis
Williams Fork Clastic Wedge
Twenty-mile Sub-wedge
Trout Creek Sub-wedge
Iles Clastic Wedge
Mesaverde Group
Ericson Sandstone Formation
Almond Formation
Lewis Shale
Upper Almond
Lower Almond Fm
Canyon Creek Member
Rusty Member
Trail Member
Lewis Shale
Almond Formation
Pine Ridge Formation
Unnamed Marine Member
Allen Ridge Formation
Mesaverde Group
Williams Fork Fm
Iles Formation
Lewis Shale
Twentymile Sandstone
Holderness Mb
Sub-Twentymile Sandstone
Mount Harris Member
Trout Creek Sandstone
Mancos Shale
Iles Sandstone
Mancos Shale
Pierre Shale
Gunsightpass Sandstone
Silty Limestone Concretionary Layer
Carter Sandstone
Hygiene Sandstone

Figure 2.4

Figure 2.4: Upper Campanian chronostratigraphic correlation of lithostratigraphic units across southern Wyoming and northern Colorado. It shows the fluvial Canyon Creek Member and Pine Ridge Formation, the main stratigraphic interval of this study, along with the correlative shorelines of the Trout Creek and Twentymile Sandstones, and the overlying Almond Formation. The erosional hiata within the Canyon Creek are not intended to be exact but rather an indication of the existence of internal unconformities. This chart is based on well-log correlations across the Greater Green River Basin, previous studies in the area (Masters, 1966; Roehler, 1990; Crabaugh, 2001; Gomez-Veroiza & Steel, 2010), paleontological data (Izzet *et al.*, 1971; Cobban *et al.*, 2006) and radiological data (Obradovich, 1993). *B – Baculites. D – Didymoceras. E. – Exiteloceras.*

The fluvial outcrop locations can be considered as “proximal locations” around the Rock Springs Uplift and in the Glades Ridge on the northern flank of the Uinta Mountains, and as “distal locations” in the Rawlins Uplift and Vermillion Creek on the eastern flank of the Uinta Mountains (Fig. 2.5).

The well-log dataset consists of gamma-ray logs where available, as well as conductivity and spontaneous potential records. The well logs were downloaded as image files from the Colorado Oil and Gas Commission and the Wyoming Oil and Gas Commission and subsequently digitized. A complete list of the wells used in this study can be found in Appendix A.

Some well logs were combined to create two, obliquely down-dip cross sections approximately 200 km long (Figs. 2.5, 2.6 & 2.18), and two shorter (~100 km) transects, one parallel and one perpendicular to the axis of the Moxa Arch (Figs. 2.5, 2.19 & 2.20). These transects identify (a) regional thickness changes of the Canyon Creek Member that reflect regional subsidence and (b) local thickness changes that signal growing Laramide local structures. Additionally, changes in well-log patterns indicate changes in channel-belt connectivity and fluvial style throughout the basin. From outcrops and wells we have extracted the net-to-gross ratio and the thickness of the Canyon Creek Member to create maps that allow interpretation of the lateral evolution of this system.

RESULTS

Regional fluvial style variation

Several stratigraphic changes can be readily observed in the fluvial Canyon Creek Member as it is followed from proximal (west and northwest) to distal (east and southeast) positions. The long west to east well-log correlation (Fig. 2.6) shows a trend of

increasing thickness and decreasing net-to-gross within the fluvial unit from the most proximal areas near the Sevier orogenic belt (Fig. 2.6) to the most distal areas in the Washakie Basin. This change occurs irregularly but fairly gradually over the approximately 250 to 350 km between the Sevier orogenic front and the Cretaceous shorelines in the Hanna/Laramie and the Sand Wash basins.

These general proximal-to-distal trends are, however, clearly modified in the proximity of the Rock Springs and Rawlins uplifts. There, the thickness decreases substantially and the net-to-gross ratio increases, abruptly reversing the thickening trend seen in the adjacent basins to the west.

Representative well logs of the proximal and distal reaches (Fig. 2.7) show that upward-increasing gamma counts, a signature for upward fining grain-size trends, also occur more frequently in the distal reaches of the Canyon Creek system, whereas blocky gamma-ray patterns are more common in proximal areas of the system. For example, well logs in the vicinity of the Pine Canyon outcrops (Fig 2.5) shows the amalgamated and condensed thickness, around 25 meters, an almost total lack of fine material, generally low gamma-ray values and a very blocky log pattern (Fig. 2.7A). On the other hand, a well log in the vicinity of the Seminoe Road (Fig 2.5) outcrop shows a much thicker package, about 100 meters, abundant fine material preserved and more organized fluvial deposits, with finning-upward patterns and high gamma-ray values (Fig. 2.7B).

Examples of fluvial style from proximal and distal locations are discussed in more detail below.

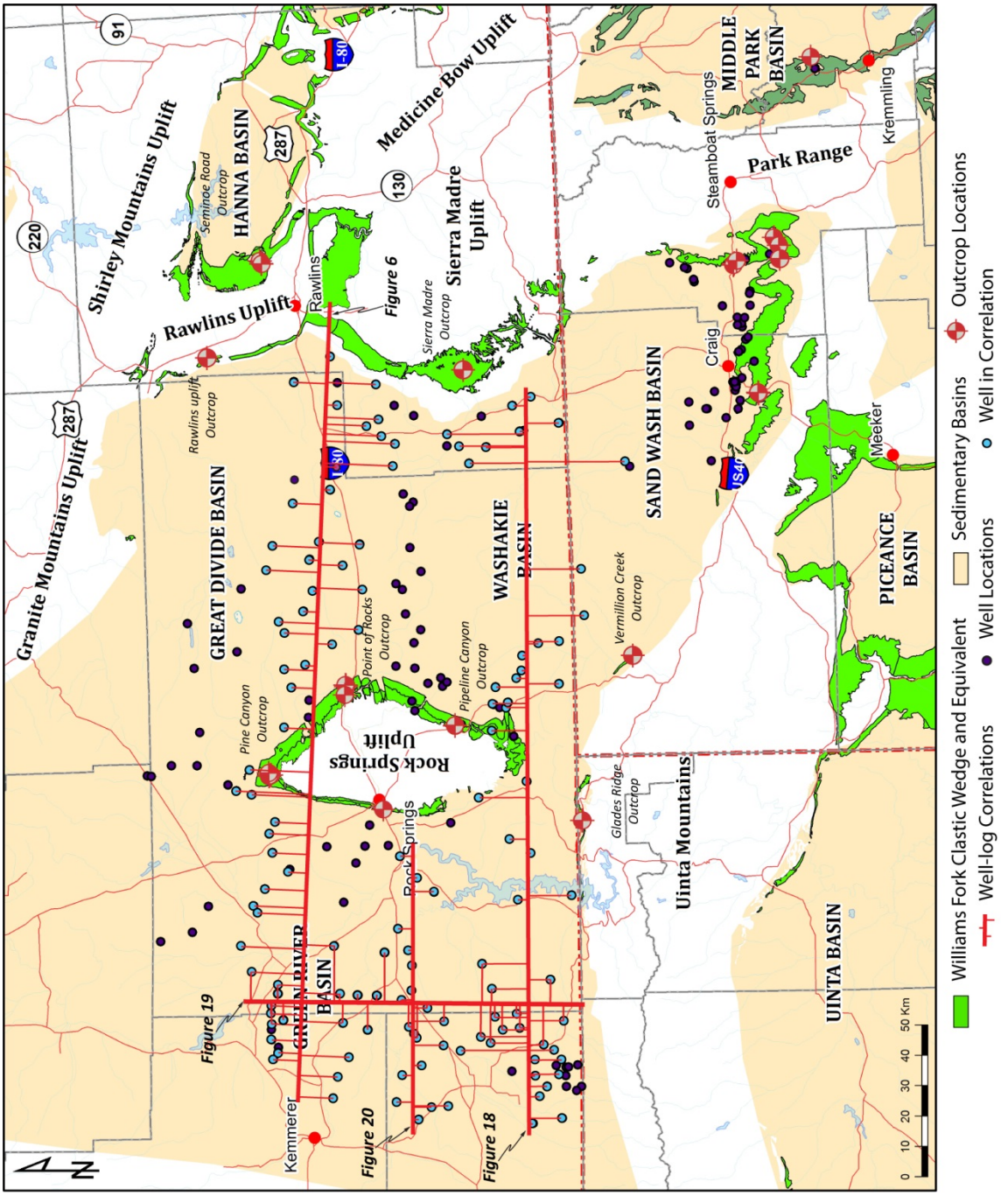

Figure 2.5: Map of the study area and the dataset used. The outcrop locations were selected to obtain a range of observations in representative areas across the Greater Green River Basin. The well-log correlations shown here are those in Figures 2.6, 2.18, 2.19 and 2.20. Outcrops of the Williams Fork Clastic wedge after Green (1992); Green and Drouillard (1994) and Hintze *et al.* (2000).

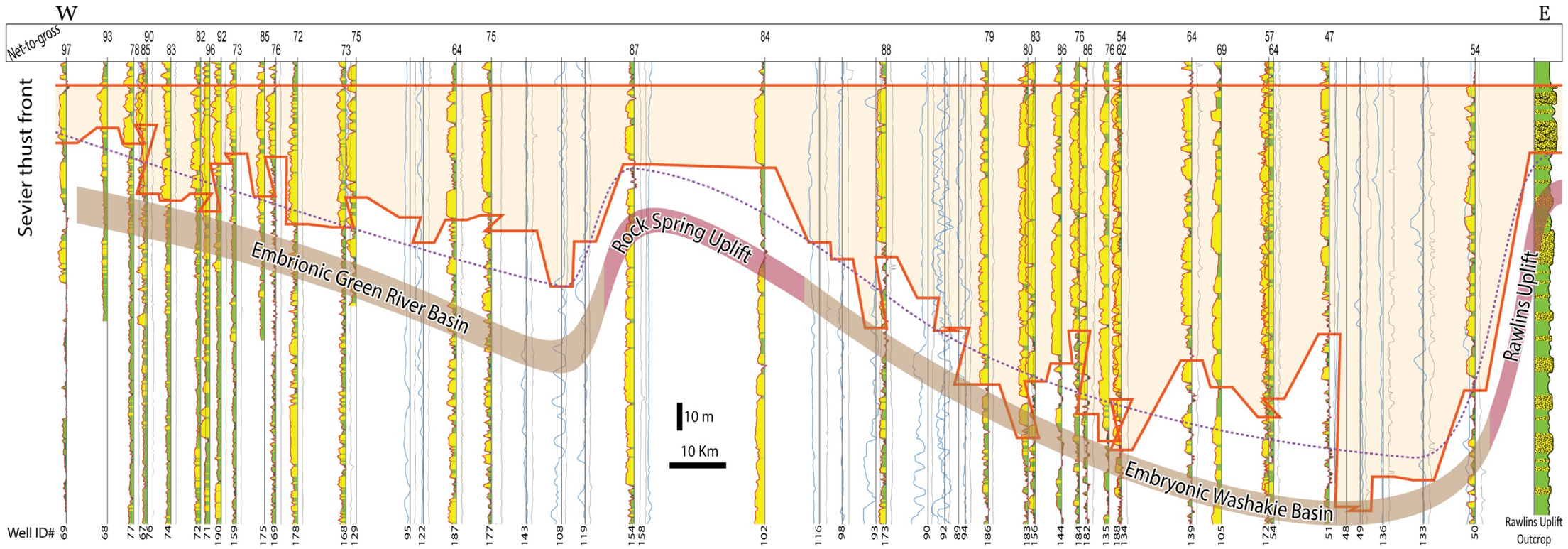

Figure 2.6: East-west well-log correlation across the northern part of the Greater Green River Basin (Location in Fig. 2.5). The orange shaded interval corresponds to the Canyon Creek Mb. The dashed purple line is the averaged bottom of the unit, showing the overall east-thickening trend, as well as the two sub-basin eastward thickening trends, broken by the Rock Springs Uplift. The numbers above each well are the Canyon Creek net-to-gross values of each well, which show an east-decreasing trend also broken in the area of the Rock Springs Uplift. Well ID# identifies each well in Appendix A. Well logs are vertically exaggerated ~400 times.

Proximal Canyon Creek: Pine Canyon outcrop

The Pine Canyon outcrops, the most northerly and most proximal in the Greater Green River Basin, are situated near the axis of the Rock Springs Uplift anticline (Fig. 2.5). In this area the Canyon Creek Mb. has a modest thickness of approximately 25 meters, and is primarily composed of highly incised and stacked sandstone bodies with very little or no fine material preserved between the sandstones packages. These outcrop were previously described by Martinsen *et al.* (1999) and Roehler (1990).

Grain size within the lower half of the Canyon Creek Mb. in this area ranges from granule to medium-grained sand with an almost total absence of shale material. Grain size in the upper half of the unit ranges from upper medium to fine-grained sand; although some overbank material is preserved, it is still infrequent, showing a net-to-gross value of around 90%. This upward trend represents a transition from the purely fluvial Canyon Creek facies to the overlying coastal plain facies of the Almond Formation.

The main lithofacies are amalgamated nested channel fills, dominated by planar and trough cross-stratified coarse-grained sandstones. The high energy of the fluvial environment, as evidenced by the large grain sizes, and the significant number of erosion surfaces associated with the amalgamated unit, strongly suggest that fine-grained overbank and flood plain deposits were prevented from being deposited or preserved (Fig. 2.8). Both the degree of amalgamation and the grain size show a slight decrease upward at most proximal locations. Figure 2.9 illustrates the multi-story, multi-lateral architecture of this proximal Canyon Creek interval, which contains almost no fine-grained deposits.

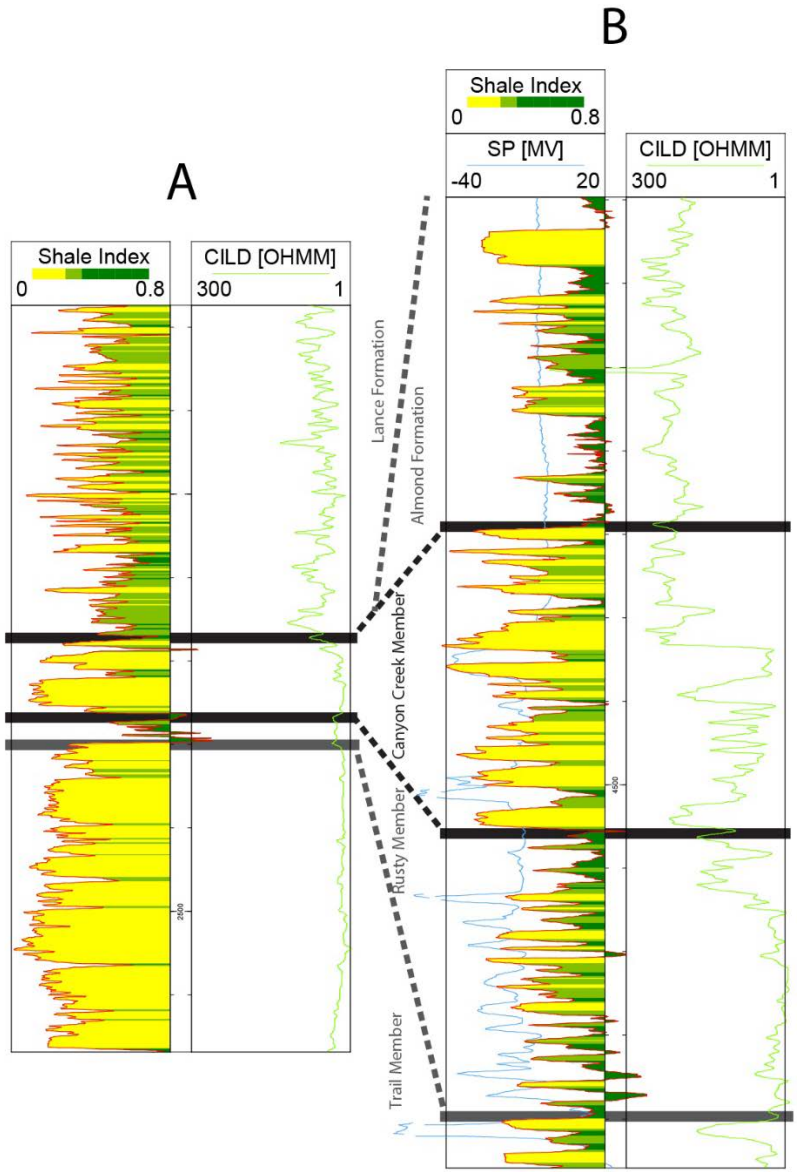

Figure 2.7: Typical thickness and net-to-gross changes in proximal vs distal located wells. A.- Well log, near the Pine Canyon outcrop at the axis of the Rock Springs Uplift, showing the very condensed thickness and high net-to-gross typical of the Canyon Creek Mb. in the proximal areas of the basin. B.- Well log, near the Seminoe Road outcrop just northeast of Rawlins, showing the increased thickness and low net-to-gross typical of the Canyon Creek Mb. in the distal reaches of the basin. Many of the sandstone units in this well log also show upward-fining grain-size trends that suggest point bars of a meandering fluvial system.

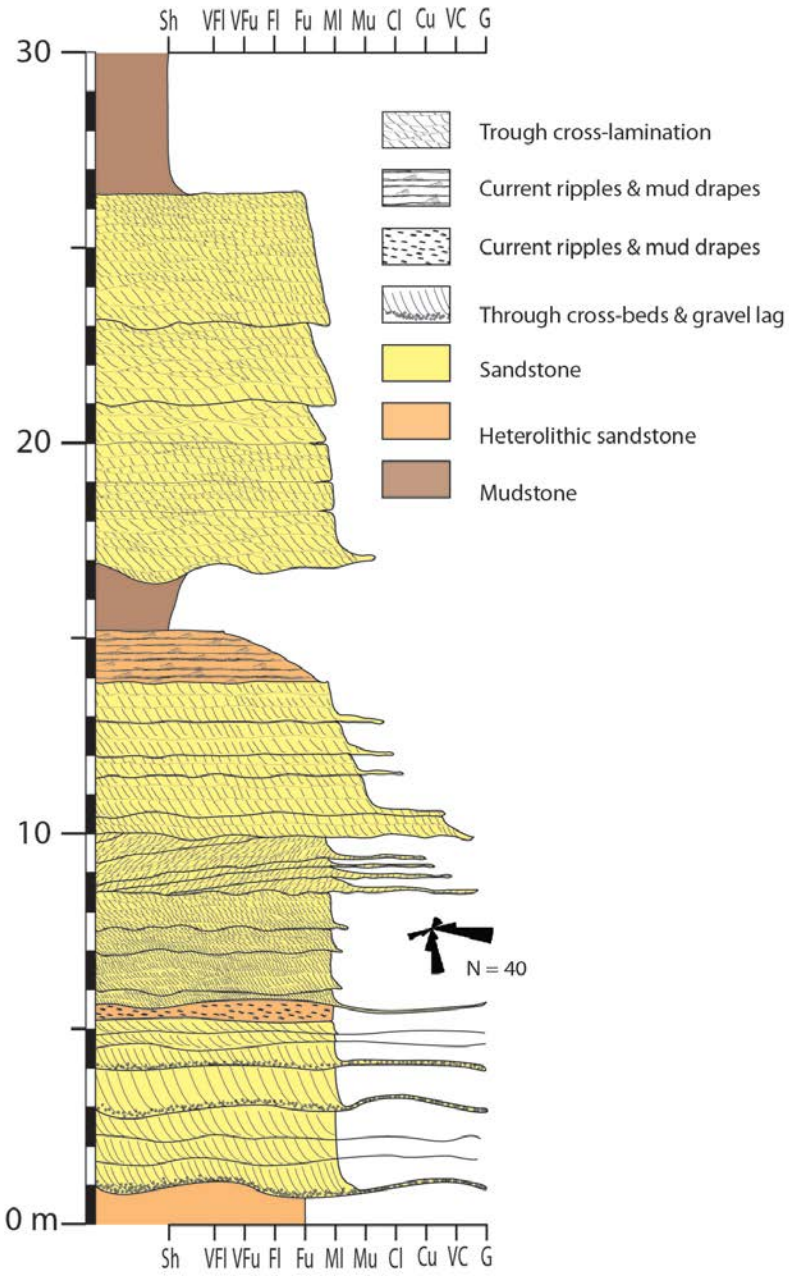

Figure 2.8: Representative measured section through the Canyon Creek Mb. in the proximal Pine Canyon outcrop area. The multiple erosional surfaces and the scarcity of fine-grained deposits indicate the high degree of channel amalgamation of the fluvial system in this area. Note also the coarse grain sizes as well as the relatively narrow spread of fluvial paleocurrents.

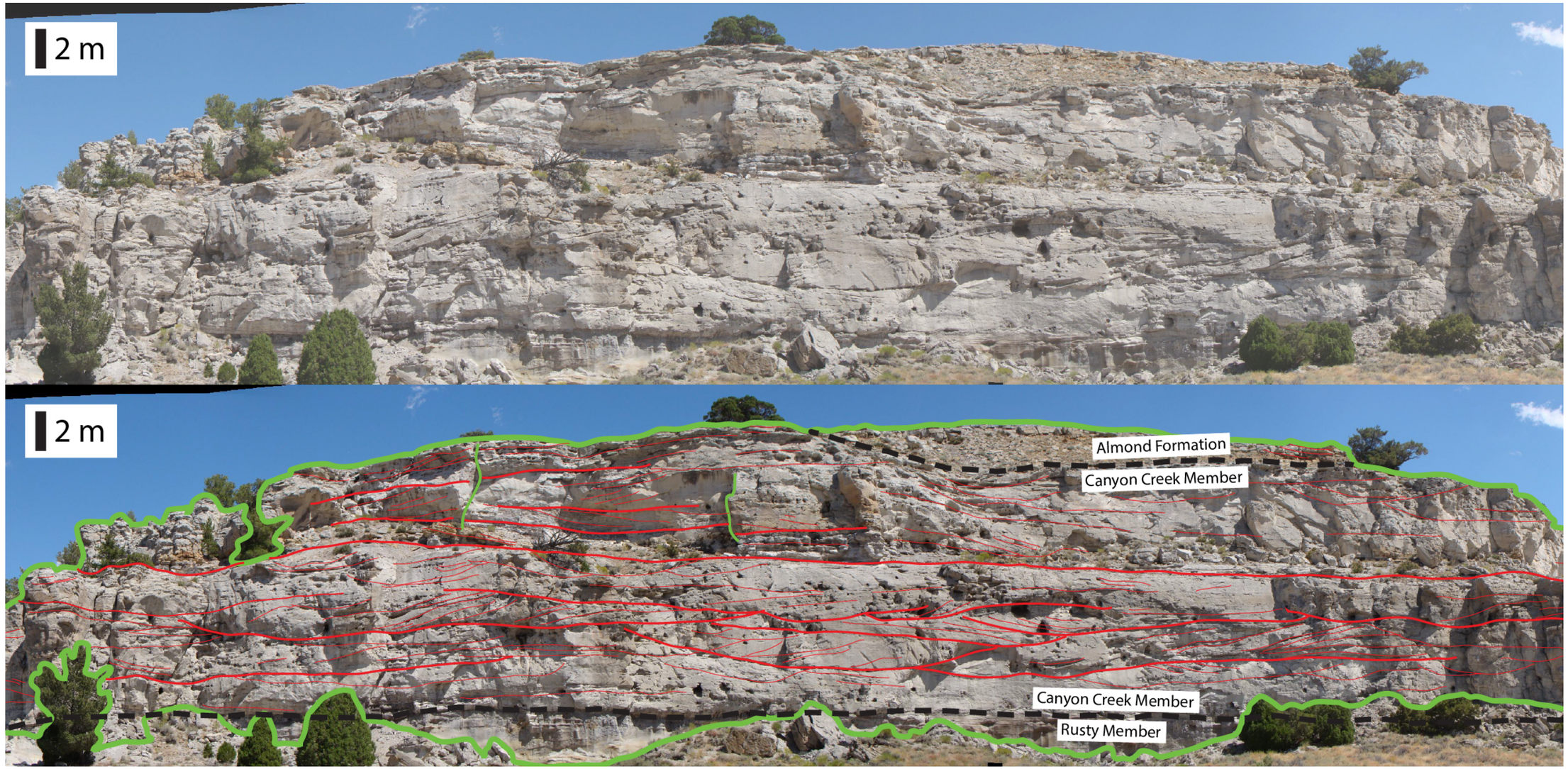

Figure 2.9: A representative outcrop of the Canyon Creek Mb. in the proximal Pine Canyon outcrop. The multi-story, multi-lateral and highly amalgamated characteristics of the fluvial deposits are readily observable in the line drawing. Trough cross-stratified sandstone generated from 3D dunes is the most frequent facies filling the river channels.

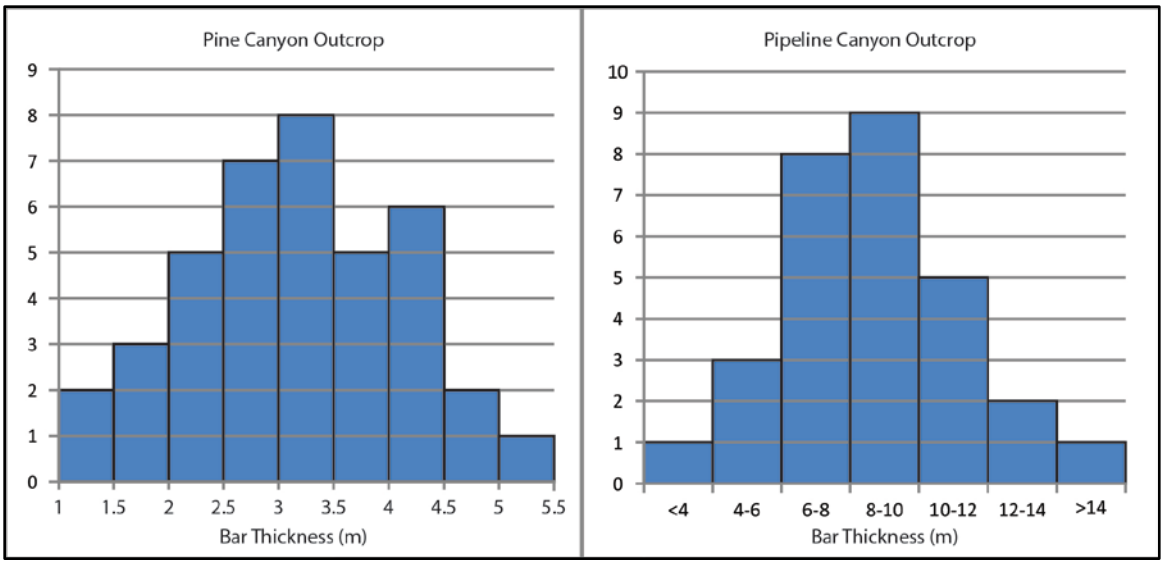

Figure 2.10: Histograms of channel-fill and bar thickness measured in outcrop and from photographs. Channels-fills in Pine Canyon are thinner (mode 3 to 4.5 meters thick) than the channels and bars of Pipeline Canyon (8 to 10 meters thick). Directly measured bar heights and flow depth calculations from preserved dune heights (Leclair & Bridge, 2001) also shows a trend of channel deepening basin-wards.

The channels within the proximal Canyon Creek Mb. have a characteristic width of 15 to 20 meters and range from 3 to 4 meters in depth (Fig. 2.10). The sets of cross-strata that fill the channels are on average 19.6 cm thick. Using these values and the Leclair and Bridge (2001) methodology, the fluvial channels that generated these deposits are estimated to have had flow depths of approximately 5.1 (±2.5) meters. The paleocurrents from this area indicate that channels flowed generally towards the east and south (Fig. 2.8).

Martinsen *et al.* (1999) interpreted this outcrop as representing a meandering fluvial system based on the identification of low-angle accretion surfaces at one location of the Pine Canyon outcrop (Fig. 3 in Martinsen *et al.*, 1999) and the similarity of this

outcrop to others in the Rock Springs Uplift. We suggest that the low-angle accretion surfaces are not necessarily the result of point-bars but could also have been generated by downstream-accreting bars. The relatively high aspect ratio of the channels, the lack of overbank material, the modest paleocurrent spread, the coarse grain sizes (which suggest high depositional gradients), and the relatively low abundance of low-angle inclined strata suggest that the rivers likely had low sinuosity planform, especially in the lower portion of the Canyon Creek Mb.

Canyon Creek in the middle reaches of the system: Pipeline Canyon (Cooper Ridge) outcrop

Outcrops in the Pipeline Canyon area of Rock Springs Uplift are approximately 60 kilometers away (Fig. 2.5), somewhat oblique to depositional dip relative to the outcrops of Pine Canyon. The Canyon Creek Mb. thickness has increased to about 75 meters. This location shows greater occurrence and preservation of overbank and floodplain deposits and the channels are better organized with internal barforms and less interconnected than in Pine Canyon. These outcrops were previously recorded by Martinsen *et al.* (1999) and Roehler (1990).

The main lithofacies are stacked sets of ripple-laminated and low-angle or trough cross laminated sandstones; occasionally separated by thin layers of soft-deformed over-bank deposits, and fine-grained channel plugs (Fig. 2.11). Although the channels still have a high degree of amalgamation, a significant volume of preserved fine-grained, over-bank material is present here, unlike the Pine Canyon outcrops; the common presence of large muddy intra-clasts and soft-sediment deformation is probably related to a higher degree of channel bank stability. However, the architecture here is still one of multi-story, multi-lateral stacked channels (Fig. 2.12).

The Canyon Creek Member in this area has a net-to-gross around 80% and grain size ranges from upper medium to lower fine-grained sand, with rare granule lag deposits in the bottom of some channels. Mudstones are present as channel plugs and as over-bank deposits. In Pipeline Canyon there is also a general upward fining grain-size trend related to the transition between the Canyon Creek Mb. and the overlying Almond Formation; this change possibly also records a maturation of the fluvial system with lower depositional gradients.

The cross strata sets within channels average a thickness of 24.1 cm (Fig. 2.10) Based on these values and using the Leclair and Bridge (2001) methodology, the fluvial channels that generated these deposits probably had flow depths on the order of 6.3 (±3.1) meters. The preserved thickness of the channels is 6-15 meters with widths of 20 to 30 meters, giving a lower aspect ratio than at Pine Canyon. Paleocurrents measured from the cross-strata show a general east to southeast trend but with a paleocurrent spread of around 120°.

Inside each channel fill there are frequently low angle accreting surfaces at high angles (40-110º) from the paleocurrent indicators measured inside each package. They usually down-lap into the erosive base of individual channels, sometimes are marked by a small (5-10cm thick) layer of mud and silt, and can show signs of minor slumping. These surfaces represent the accreting surfaces of bars, probably scroll bars. The thickness of these bars, and therefore the depth of the rivers that form them, ranges from 4 to 14 meters (Fig. 2.10).

The difference between the river depth estimated from the cross-bed sets and those estimated from the bar thickness, is likely caused by using cross-bed thicknesses that were not deposited in the thalweg of the river and therefore records slightly shallower waters. Both methods nonetheless show a consistent trend of channel deepening from the outcrops in Pine Canyon to those in Pipeline Canyon.

The lower aspect ratio of the channels, the increased preservation of overbank material and channel plugs, the increased paleocurrent spread, and the smaller grain sizes (consistent with lower depositional gradients) in addition to the relative abundance of low-angle accreting surfaces, together suggest that the rivers that deposited the Canyon Creek Mb. in this area were most likely meandering rivers.

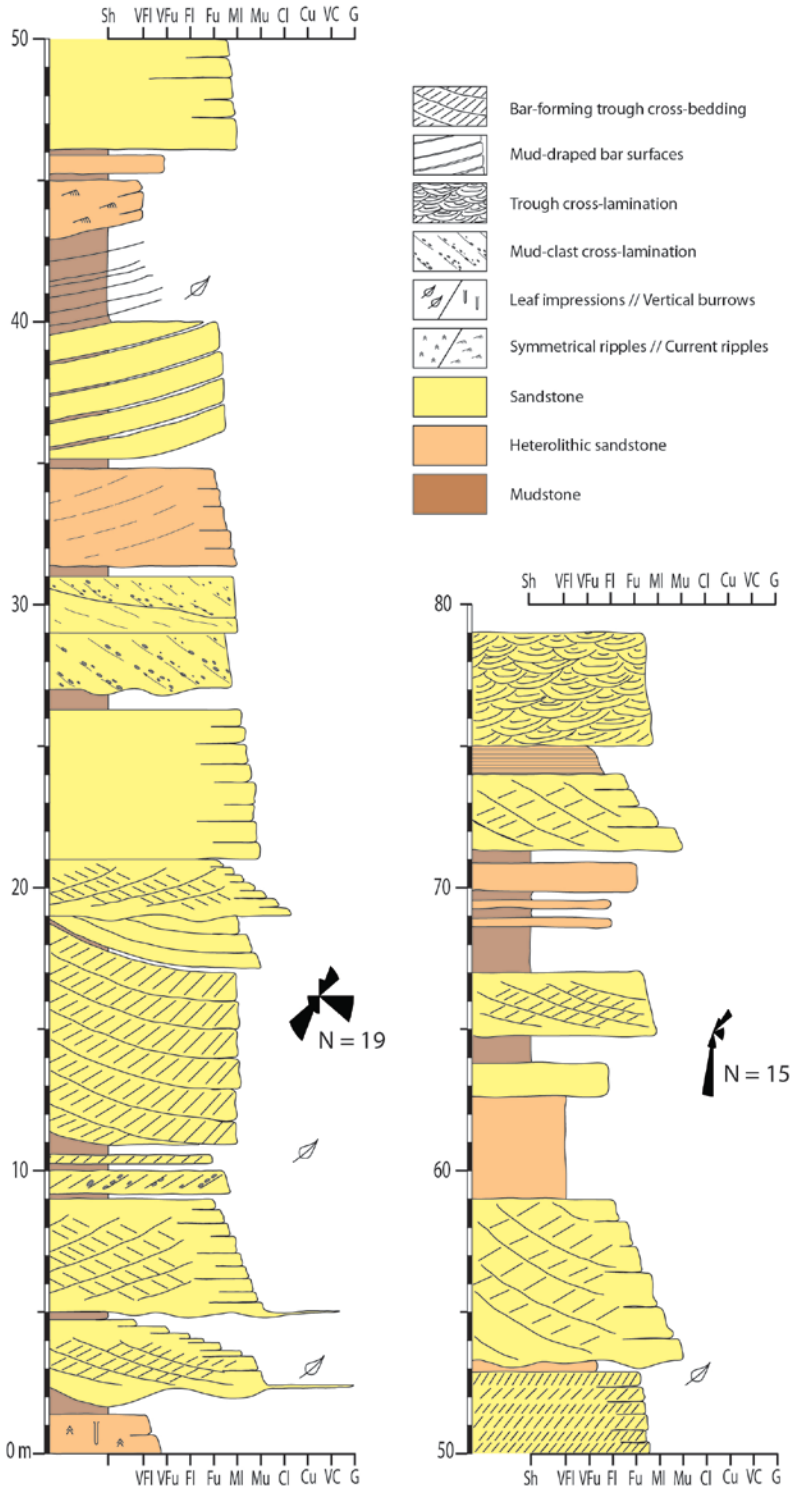
Sh VFl VFu Fl Fu Ml Mu Cl Cu VC G
50
40
30
20
10
0 m
N = 19
Bar-forming trough cross-bedding
Mud-draped bar surfaces
Trough cross-lamination
Mud-clast cross-lamination
Leaf impressions // Vertical burrows
Symmetrical ripples // Current ripples
Sandstone
Heterolithic sandstone
Mudstone
80
70
60
50
N = 15

Figure2.11

Figure 2.11: Representative measured section up through the Canyon Creek Mb. in the Pipeline Canyon outcrop area. This down-flank location presents sandstone bodies with a reduced frequency of erosional surfaces and some fine-grained sediment preservation between channels compared to Pine Canyon. This indicates only a moderate degree of channel amalgamation. The grain size in this area is very variable. The paleocurrents here have an almost 180 degree spread, suggesting increased channel sinuosity in the system here.

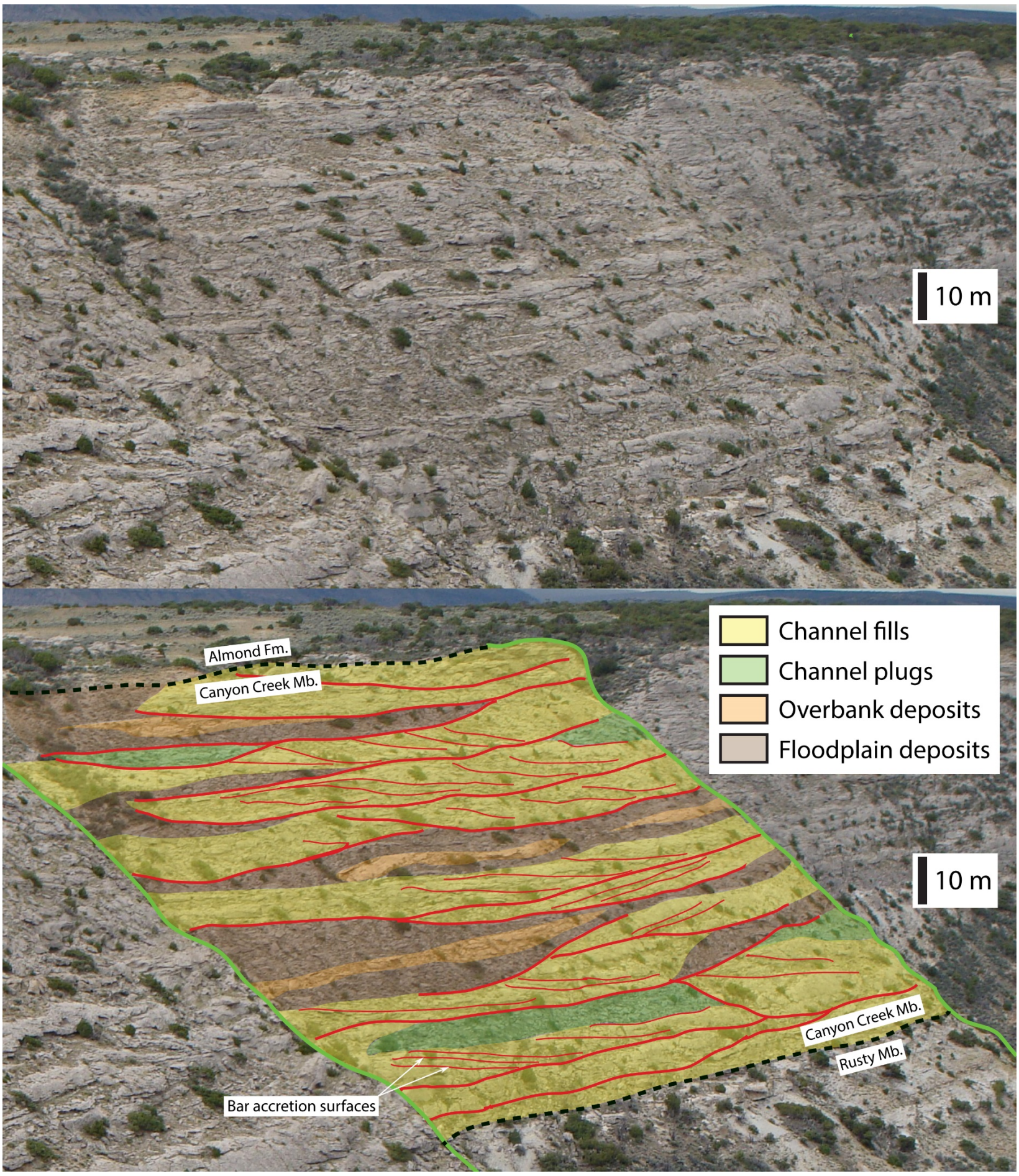

Figure 2.12: Photo interpretation of the Canyon Creek outcrops in the Pipeline Canyon. Moderate channel amalgamation and the multilateral, multi-story character of the fluvial system is visible in this outcrop. The common presence of fairly low-angle inclined strata indicates individual scroll bars, some laterally accreting.

Canyon Creek development in distal areas: Seminoe Road outcrop

East of the Rock Springs Uplift, the Canyon Creek Member is buried and does not crop out again for 130 km, before the Rawlins Uplift. Near Rawlins (Fig. 2.5) the outcrop characteristics are significantly different from the two areas described above. Around the Rawlins Uplift, the Canyon Creek Mb. is called the Pine Ridge Formation. The Seminoe Road outcrop is on the eastern flank of the Rawlins Uplift (Fig 2.5), where these fluvial deposits are approximately 120 meters thick. The section contains thick units of fine-grained strata containing lensoidal to sheet-like bodies of fine-grained sandstone (Martinsen *et al.*, 1993).

In the Seminoe Road outcrop the Pine Ridge is composed of three main facies (Fig. 2.13). The predominant facies is dark to black organic-rich shale, with thin layers (few cm) of coal and fine sand; this facies is interpreted as vegetated floodbasin and floodplain deposits, probably in a coastal-plain setting. The second facies consists of lens-shaped sandstone units, 5 to 15 meters thick, composed of upper fine to upper very fine-grained sandstones with common low-angle accretion surfaces, trough cross-strata and common soft-sediment deformation. These sandstone units are interpreted as bars that filled fluvial channels on the vegetated coastal plain. The third facies comprises thin (<1m), lower to upper very-fine grained sandstones with current and climbing ripple lamination and occasional symmetrical ripples; this facies is interpreted as crevasse-splay deposits or small mouth bars entering vegetated floodbasin areas. The combination of these facies resulted in a net-to-gross value of approximately 30%, with poorly-connected channel architectures (Fig. 2.14).

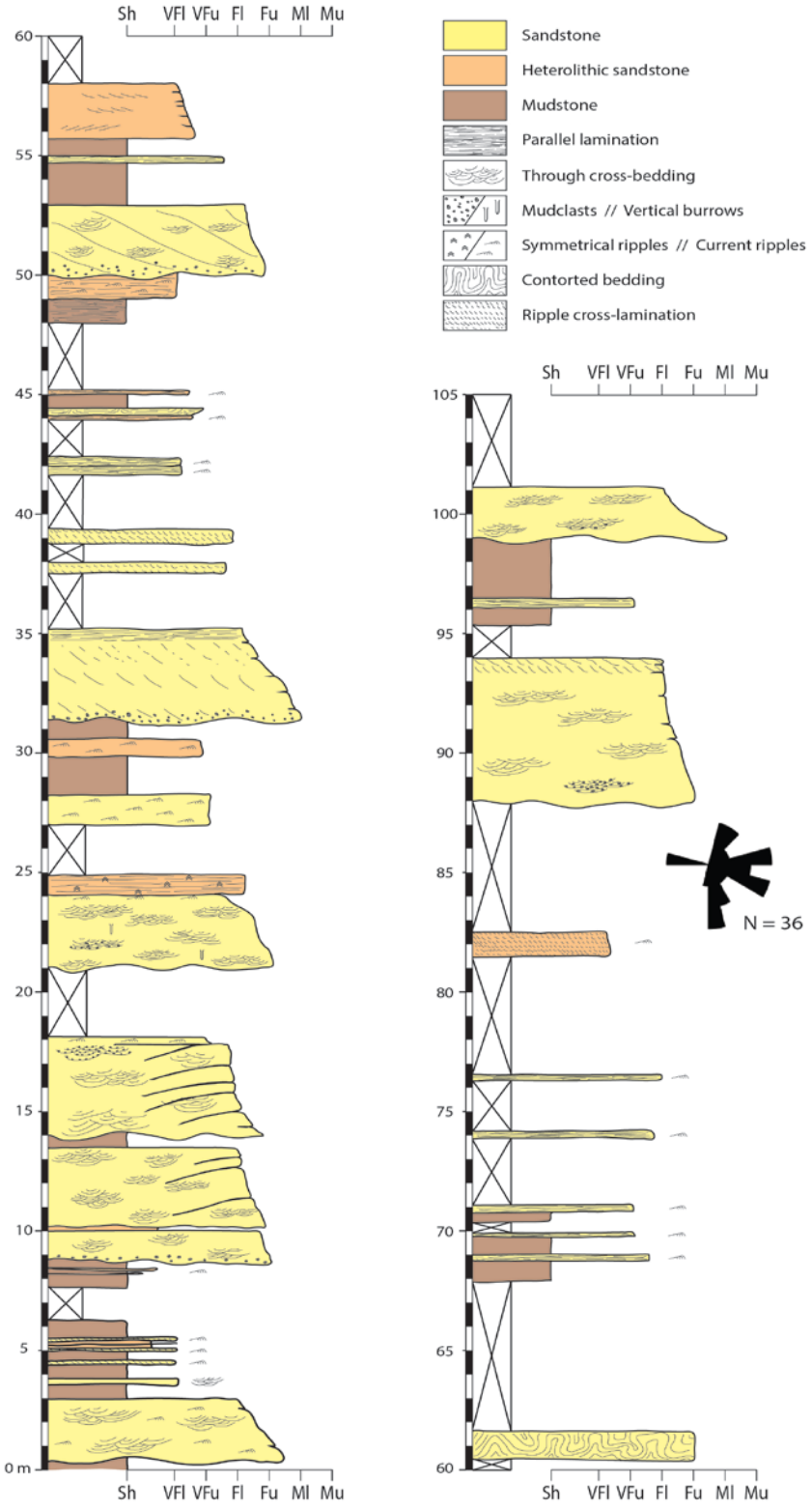
Sh VFl VFu Fl Fu Ml Mu
60
55
50
45
40
35
30
25
20
15
10
5
0 m
Sandstone
Heterolithic sandstone
Mudstone
Parallel lamination
Through cross-bedding
Mudclasts // Vertical burrows
Symmetrical ripples // Current ripples
Contorted bedding
Ripple cross-lamination
105
100
95
90
85
80
75
70
65
60
N = 36

Figure 2.13

Figure 2.13: Representative measured section of the Canyon Creek equivalent (Pine Ridge Formation) in the Seminoe Road outcrop area. The measured section shows the frequent muddy intervals present here. The sandstone units are generally fine grained and paleocurrents have a large (>180°) spread.

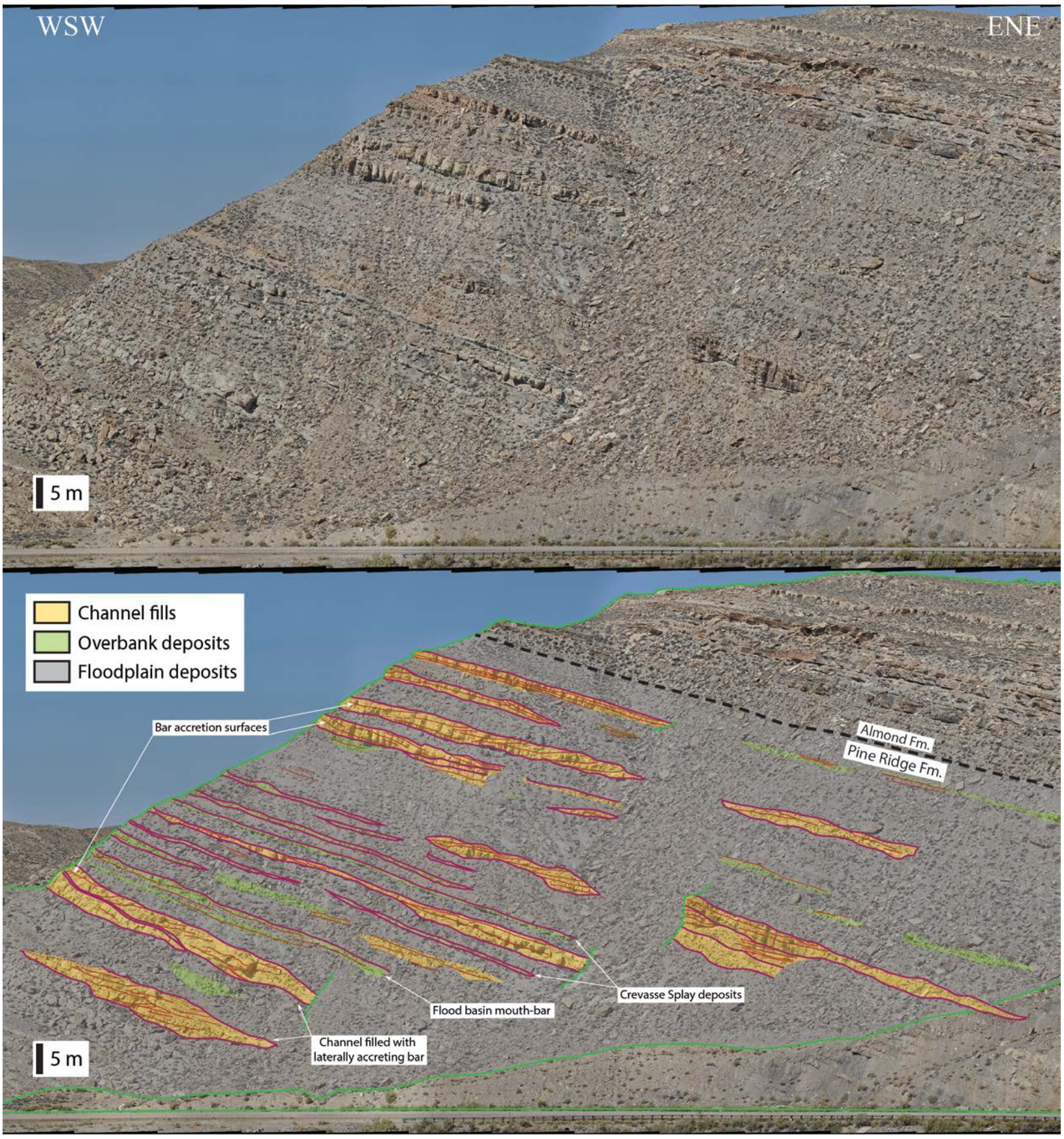

Figure 2.14: Photo interpretation of the Canyon Creek Mb (Pine Ridge Fm.) along the Seminoe Road. This figure shows the dis-connected character of the lensoidal channel-sandstone bodies in this outcrop, as well as the frequent low angle inclined strata inside them. Where the sand-bodies are thick, composed of cleaner sands, and have accretion surfaces and an erosive base, they are interpreted as bars filling channels (orange in the figure). Where the sands are dirtier and occur in thinner sheet-like bodies; they are interpreted as overbank deposits (levees and crevasse splays) (green in the figure). The Allen Ridge Formation lies below the Pine Ridge Formation immediately to the left of this photograph.

In this distal reach of the Canyon Creek the transition into the overlying Almond Formation can be recognized by the transition to the brackish marine character of the Almond Fm. (lower coastal plain and shoreline). The Almond Fm. presents brackish fauna (*Inoceramus*) and ichnofauna (*Ophiomorpha*), increased thickness and quality of coal layers, and predominance of wave ripple lamination in the sandstones.

The paleocurrents measured in the channels indicate a general easterly flow direction, but with a very large 80° spread (Fig. 2.13), and it is at 40-50° angle from the dip direction of the accretion surfaces.

The dimensions of the bars in this area suggest that the channels were approximately 10 to 15 meters deep. The average thickness of cross-strata in this area is 28.8 cm; using that value with the methodology of Leclair and Bridge (2001), a channel depth of 7.5 (±3.7) meters can be estimated.

The low aspect ratio of the channels, the preservation of abundant overbank and flood plain material including organic-rich mudstones, the small grain sizes, and the numerous low angle accreting surfaces perpendicular to the paleocurrent indicators, along with the large paleocurrent spread, indicate that in this area the Pine Ridge Formation (Canyon Creek Member equivalent) was deposited by meandering fluvial channels in a high accommodation coastal plain. Similar muddy coastal-plain deposits with coal beds, of about the same age and developed along depositional strike, have been described in the south of the region, up-dip of and associated with the Trout Creek shorelines in the Sand Wash Basin (Crabaugh, 2001; Bullimore *et al.*, 2008).

Summary of down-dip changes in fluvial style

Across the study region from proximal to distal, the Canyon Creek Member succession shows a gradual but clear change of increasing thickness, decreasing net-to-gross ratio and decreasing sand-body connectedness. The outcrop data show a transition from a sand-rich, highly amalgamated braided fluvial system in proximal positions to isolated meandering fluvial channels in mud-rich distal positions (Fig. 2.15). This fluvial style change can also be seen in gamma-ray logs as more frequent upward increasing gamma-counts in the more distal wells (Fig. 2.6). The size of the river channels also shows a change down-dip, showing a trend of deepening towards the distal areas. This changing Canyon Creek Member gradually leads out to and interfingers with co-eval shorelines (Fig. 2.16) to the east and southeast, in both the Rawlins and Hanna/Laramie basins area (Rock River Formation), and in the Sand Wash Basin of northern Colorado (Trout Creek and possibly Twentymile Sandstones).

Even though the Cretaceous Western Interior Seaway is generally a foreland basin caused by the growth of the Sevier Orogenic Belt, the patterns here described are not in accordance with patterns expected in a foreland basin. Instead of a foredeep near the orogenic belt, the Canyon Creek Mb is thin in proximal locations and thickens away from the orogen. This arrangement suggests that there was no longer a well-developed foredeep in this basin and that isostatic rebound of the earlier foredeep led to increased subsidence rates away from the orogeny. The absence of a foredeep suggests that the orogenic wedge had become relatively inactive and was being denuded during the deposition of the Canyon Creek Mb. This inversion to reduced subsidence in the proximal areas of the basin and enhanced subsidence in the distal part would have increased slopes in the proximal areas, in turn facilitating the braided fluvial systems.

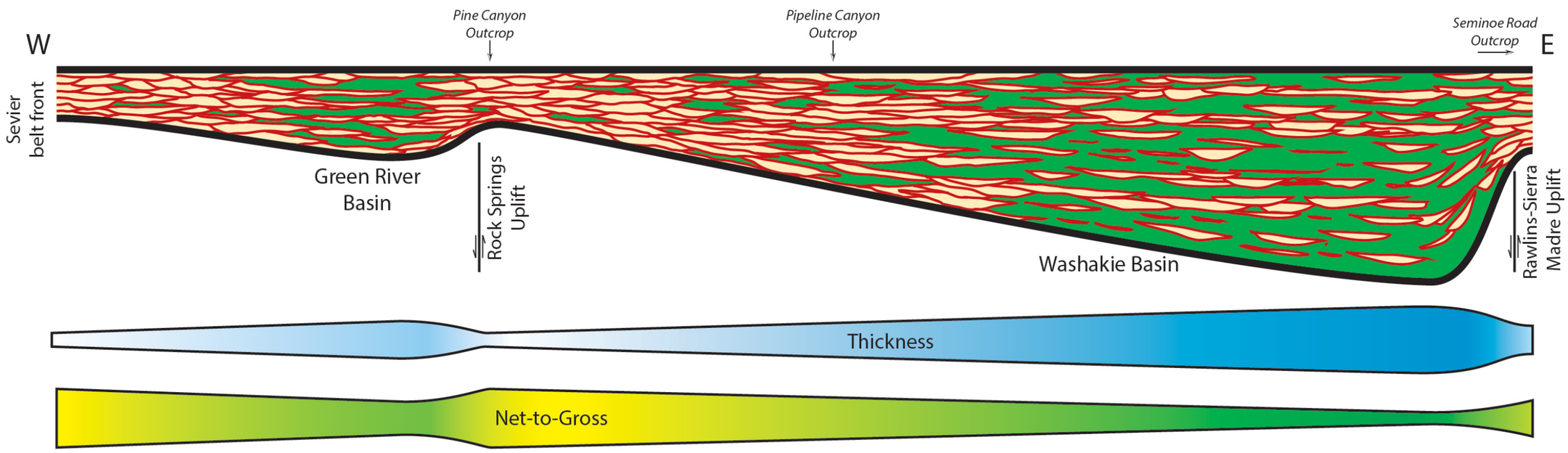

Figure 2.15: Schematic representation of the Canyon Creek Mb. along a 160 km W-E transect from Pine Canyon area to Rawlins area, highlighting the thickness and net-to-gross trends and the manner in which they are broken into two sub-basins (embryonic asymmetric Laramide basins) by the Rock Springs Uplift.

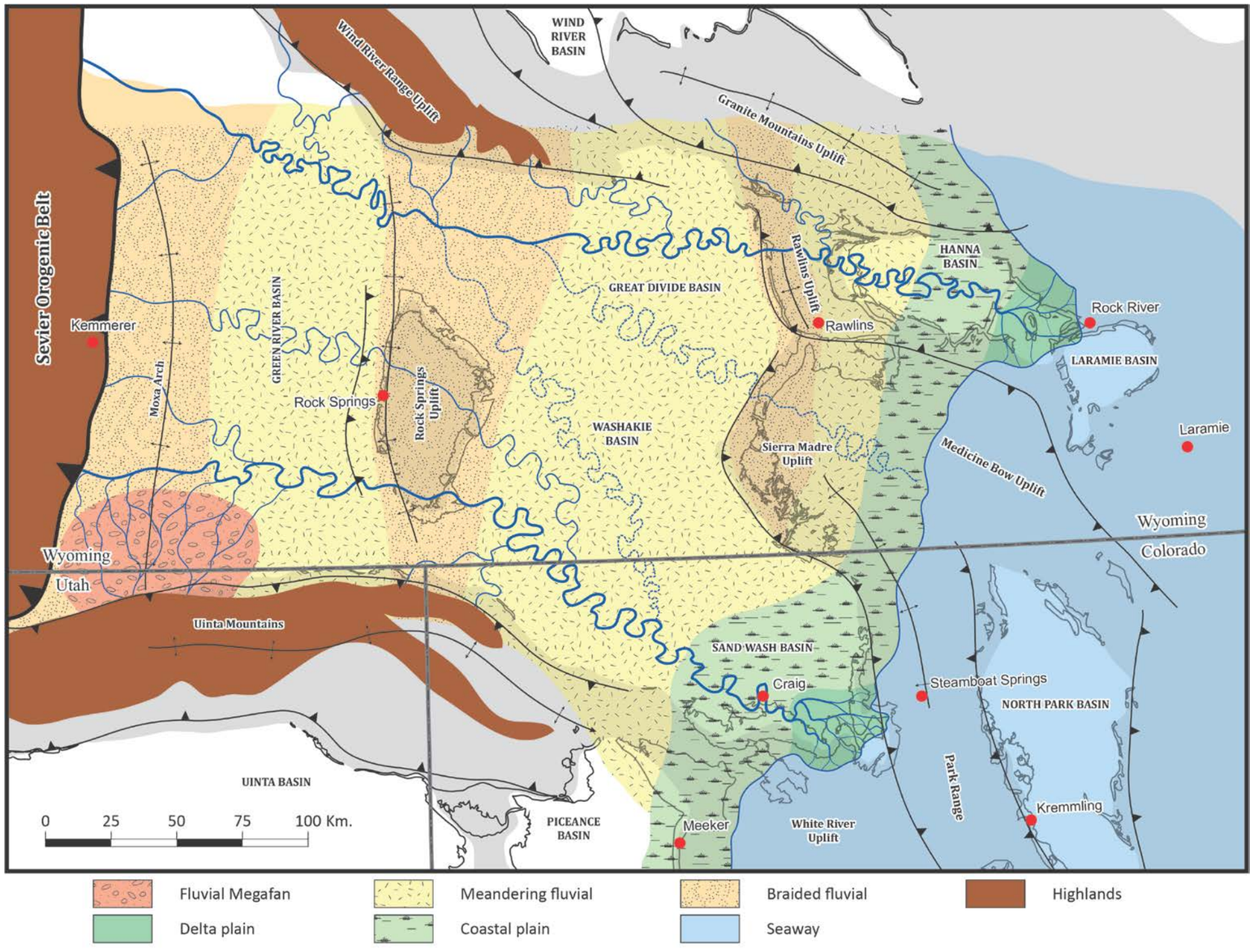

Figure 2.16: Paleogeographic reconstruction of the fluvial systems that deposited the Canyon Creek Member and the coeval shorelines in the Laramie and Sand Wash Basins. It shows the influence that the Laramide structures exercised on the fluvial style.

Foreland basin break-up as seen in the Canyon Creek Member

As already noted above, the thickness distribution of the Canyon Creek Member does not conform a typical foreland basin subsidence pattern, but rather quite the opposite. The isopach map (Fig. 2.17) of the entire study region shows a general but irregular thickening of Canyon Creek strata from northwest to southeast. However, detailed examination of both the thickness and the net-to-gross (Figs. 2.17 & 2.18) maps draws a picture of greater complexity within the Greater Green River Basin. This complexity takes the form of local but severe thickening and thinning of strata on either side of W-E and N-S tectonic lineaments that modified the depositional patterns of fluvial systems that evolved over those structures. The lineaments were structures that were later to bind the Uinta, Moxa Arch, Rock Springs, Sierra Madre and Rawlins uplifts and their adjacent basins. During Canyon Creek deposition the Western Interior foreland was already breaking up and a series of new sub-basins was being superimposed on the Western Interior Seaway.

Canyon Creek Member thickens into the W-E oriented Uinta Uplift

The Uinta uplift is an east-west oriented, east-plunging anticline bounded on the south and north by reverse faults (Marshak *et al.*, 2000; Ashby *et al.*, 2005). The uplift is usually considered Paleogene in age (Hansen, 1986), although other authors have suggested an earlier initiation as a result of studies of the Currant Creek Formation on the southern edge of the Uinta Mountains (Constenius *et al.*, 2003; Horton *et al.*, 2004) and the recent provenance study (Leary *et al.*, 2014).

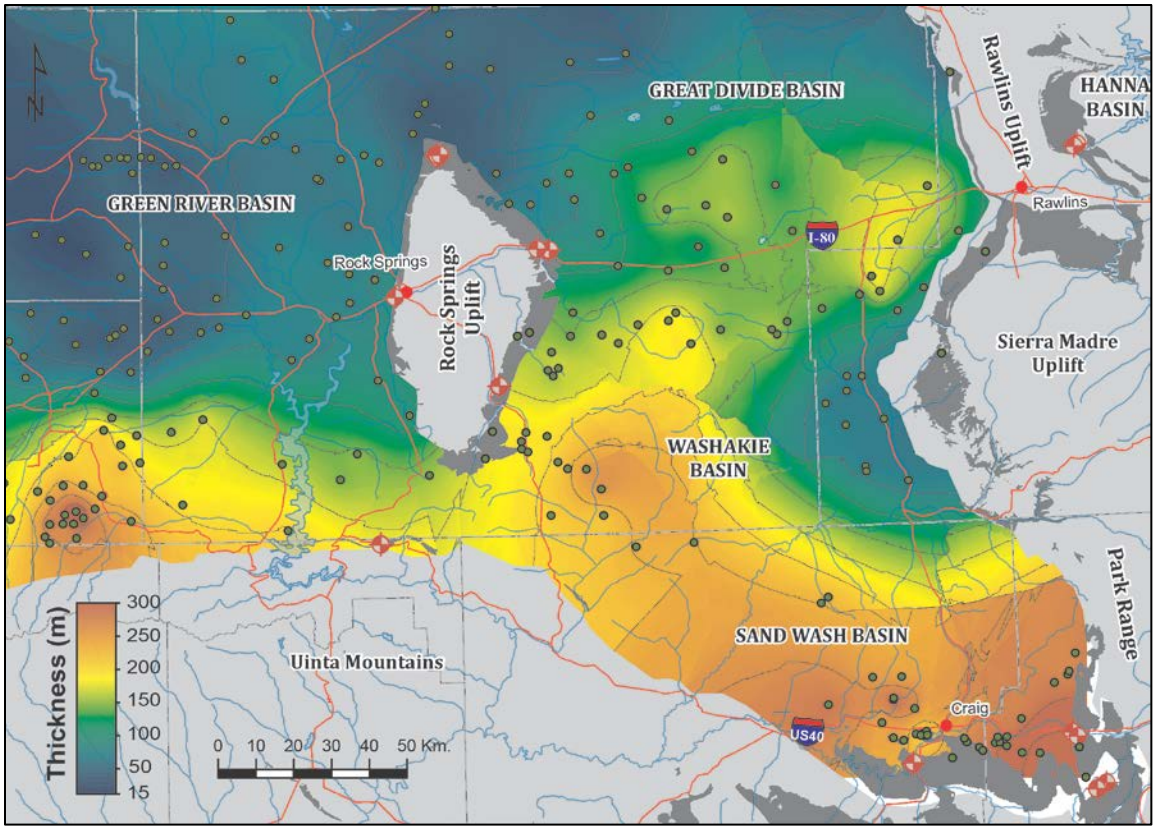

Figure 2.17: Isopach map of the Canyon Creek Member thickness across the Greater Green River Basin. Two domains of thickness can be identified, one in the northern part of the basin with very low values on the western side of the basin and a trend of increased thickness towards the east; and a southern domain with increased thicknesses towards the Uinta Fault. In the very southwestern corner of the basin a lobate area of increased thickness can also be observed against the Uinta Mountains. The very high thickness in the southeastern corner of the map, around the town of Craig, are related to the coeval shorelines of the Williams Fork clastic wedge.

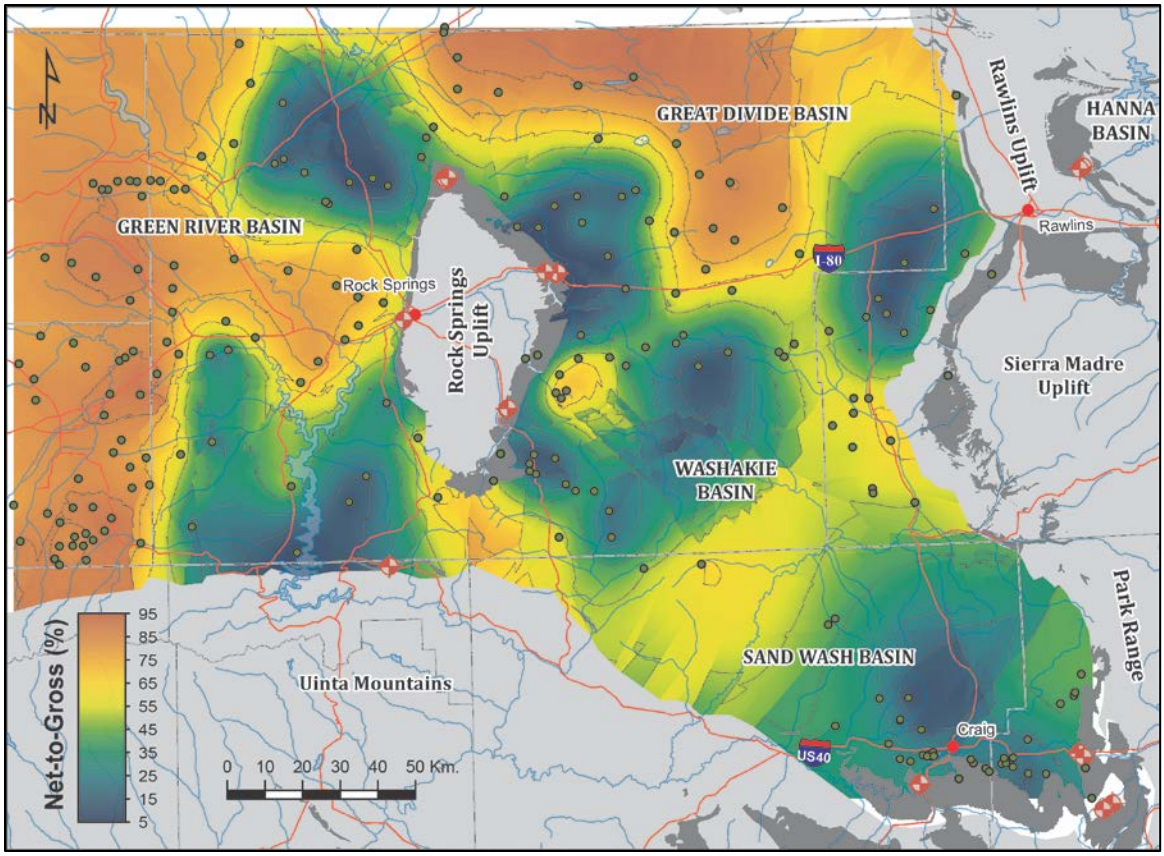

Figure 2.18: Net-to-gross map of the Canyon Creek interval across the Greater Green River Basin.

The proximal to distal trend of thickness and net-to-gross distribution shown in Figure 2.15 is not apparent in the southern part of the Greater Green River Basin; an east-west correlation in the south (Fig. 2.19) shows greatly increased thicknesses. This increase is especially notable in the western areas, where the unit reaches a thickness of 290 meters while net-to-gross values remain between 75 and 90%.

Increased Canyon Creek thicknesses south of Rock Springs are clearly visible on the isopach map (Fig. 2.17) indicating strongly enhanced subsidence along parts of the northern edge of the Uinta Uplift. The net-to-gross map (Fig. 2.18) shows extreme values in spite of the large accommodation, which indicates an adjacent and abundant sediment

source. These characteristics can be explained if the Uinta Mountains were becoming a positive topographical feature at the time of Canyon Creek Mb. deposition. This uplift created tectonic loading and increased subsidence along the southern edge of the Green River Basin. The young Uinta Mountains apparently shed large amounts of coarse material to form a fluvial megafan (Horton & DeCelles, 2001; Leier *et al.*, 2005); an interpretation supported by the approximately 2000 km^2 lobate feature located at the southeastern end of the isopach map (Fig. 2.17). This feature has net-to-gross values ranging from 75% to more than 90%. This net-to-gross variability, consistent with relatively low depositional slopes, is characteristic of this type of system (Horton & DeCelles, 2001). Alluvial fans are much smaller (no more than 100 km^2) and have high depositional slopes (Hartley *et al.*, 2010) than megafans, and usually present high net-to-gross values.

A deeper north-south transect in the area of this megafan (Fig. 2.20) shows the relationship between the Canyon Creek Mb. and older deeper strata down to the Turonian Frontier Formation (Kirschbaum & Roberts, 2005). Along this transect the extreme thickening of the Canyon Creek Mb. towards the south is visible.

Canyon Creek as evidence of early Rocks Springs Uplift

The Rock Springs Uplift is a doubly-plunging north-south anticline; its western limb dips steeply whereas the dip of the eastern limb is much gentler. The initiation of the Rock Springs Uplift is usually considered to be Maastrichtian or Paleogene (Roehler, 1990; Devlin *et al.*, 1993) although other studies suggest an earlier initiation (e.g. Martinsen *et al.*, 1999; Nicholson, 2010; Leary *et al.*, 2014).

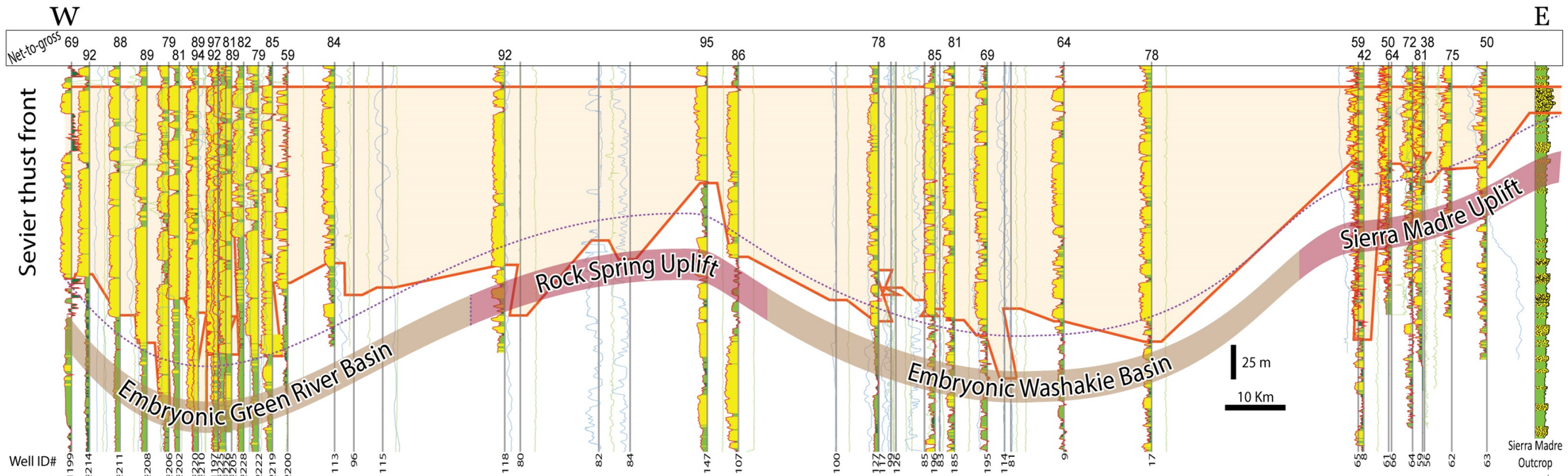

Figure 2.19: East-west well-log correlation across the southern part of the Greater Green River Basin. The orange shaded interval corresponds to the Canyon Creek Mb. The dashed purple line is the averaged base of the unit, showing a very different pattern than in the northern part of the basin (Fig. 2.15) with generally large thicknesses reduced only in the vicinity of the Rock Springs Uplift. The numbers above each well are the net-to-gross values. The difference in trend here in the south is due to the different orientation of the Laramide structure. Well ID# identifies each well in Appendix A.

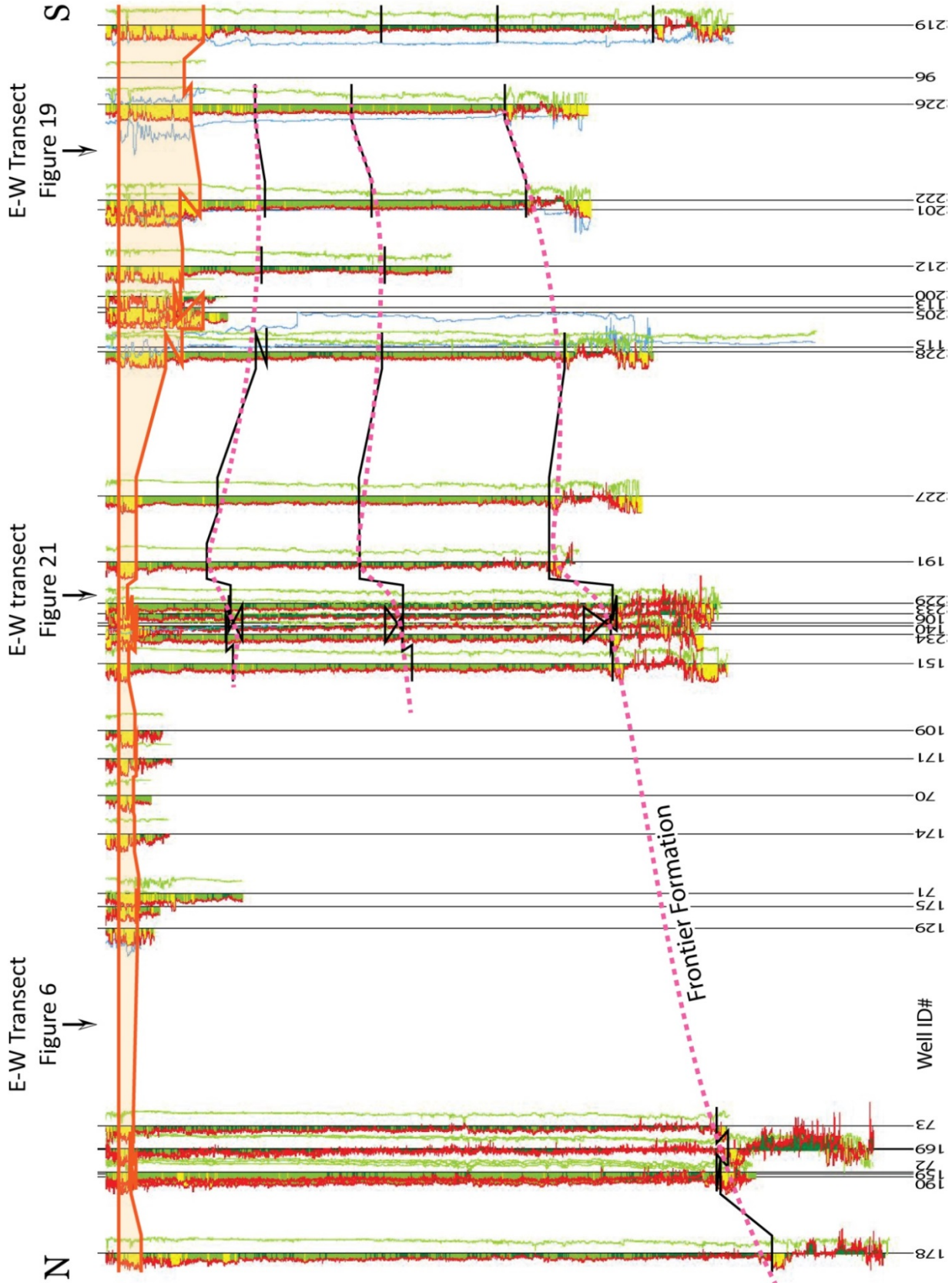
S
N
E-W Transect
Figure 19
E-W transect
Figure 21
E-W Transect
Figure 6
Frontier Formation
Well ID#
219
96
226
222
201
212
200
113
205
115
228
227
191
229
234
106
140
151
109
171
70
174
71
175
129
73
169
72
159
190
178

Figure 2.20

Figure 2.20: North-south well-log correlation across the Green River Basin along the axis of the Moxa Arch (Fig.2.15). The orange shaded interval at the top of the panel corresponds to the Canyon Creek Mb. The black lines correspond to three markers in the underlying strata, the deepest one being the top of the Frontier Formation. The correlation shows a southward Canyon Creek thickness increase against the Uinta Fault. Well ID# identifies each well in Appendix A.

As discussed in the previous section, the easterly trend of increased stratigraphic thickness, increased fine material preservation, and decreased net-to-gross is disrupted in the Rocks Springs Uplift area. The east-west well-log transect (Fig. 2.6) across the northern half of the study area clearly shows a stratal thickening and decreasing net-to-gross of the Canyon Creek Member toward the western boundary of the Rock Springs Uplift, as well as an abrupt reduced thickness and increased net-to-gross of the Canyon Creek Member on the crest of the Rock Springs Uplift. Along the axis of this structure, the thickness of the Canyon Creek Mb. is only 25 meters while the net-to-gross reaches 90%, as shown in the Pine Canyon Outcrops (Fig. 2.8). Down the gentler eastern flank of the tilted structure, the regional trend is re-established; at the Pipeline Canyon outcrop, the succession thickens to 75 meters, whereas the net- to-gross value decreases (Fig. 2.11).

The reduced thickness over the crest of Rock Springs uplift was most probably caused by a locally reduced subsidence rate as the Laramide-style Rock Springs Uplift was being initiated. An increased net-to-gross due to a higher degree of fluvial-channel amalgamation was developed on the more slowly subsiding crest of the tilted Laramide block, whereas stratal thickening and increased net-to-gross values occurred gradually down-flank to the east. The crest of the uplift is unlikely to have ever been a topographic feature because no evidence exists that the river flow pattern to the southeast was diverted or reversed. Similarly no evidence shows Canyon Creek strata onlapping the eastern flank of the uplift nor wholesale erosive removal of strata to cause the crestal thinning. The Rock Springs Uplift therefore was active during the Late Campanian, i.e., during deposition of the Canyon Creek Member.

Thickening of Canyon Creek strata into Rawlins and Sierra Madre uplifts

The Rawlins and Sierra Madre uplifts are two N-S trending Laramide asymmetric anticlines that bound the eastern side of the Greater Green River Basin. As with most

Laramide structures the western flank is steeper than the eastern flank in each case. This asymmetry, very marked along the Rawlins uplift is much gentler along the Sierra Madre uplift. The initiation of these uplifts was earlier considered to have occurred in late Paleogene or early Eocene (Barlow Jr, 1955), although an earlier *Rawlins platform* has been suggested as an "structural up-warp of the sea floor" possibly as an extension of the Wind River Range (Roehler, 1990).

The regional trend of easterly increasing Canyon Creek thickness reaches its maximum along the eastern side of the Great Divide Basin against the Rawlins Uplift, where it reaches 170 meters (Fig. 2.6). Farther south in the Washakie Basin the Canyon Creek reaches a maximum thickness of approximately 150 meters in the middle of the basin (Fig. 2.19). To the east of the N-S lineaments, on the crestal areas of the Rawlins and Sierra Madre tilted Laramide blocks, the Canyon Creek Member is sharply reduced in thickness to 35 and 25 meters respectively, on the western crestal areas of these uplifts (Roehler & Hansen, 1989).

As with the Rock Springs Uplift, the decreased thickness and the increased net-to-gross values of the Canyon Creek across the crestal area of the Sierra Madre and Rawlins Uplifts suggest that they too were already active during deposition of the late Campanian strata.

Embryonic Laramide Basins

The Western Interior Seaway is well known to have been compartmentalized into a series of smaller Laramide basins during the Maastrichtian and especially during the Paleocene (Dickinson *et al.*, 1988). The compartmentalization is the response to a series of basement-involved reverse faults, associated Laramide block tilting and the generation of asymmetric basinal sinks (Cross, 1986; Dickinson *et al.*, 1988; Weil & Yonkee, 2012). What

has been documented above in the late Campanian is the embryonic stage of these Laramide basins in southern Wyoming, played out by a series of asymmetric Canyon Creek depocenters in the northern and southern Green River basins, as well as in the Great Divide, Washakie and Hanna basins (Fig 2.5).

Moxa Arch: an Early Campanian Laramide uplift

The Moxa Arch, as described previously (Roehler, 1990; Devlin *et al.*, 1993; Leary *et al.*, 2014), is a north-south doubly-plunging anticline without present topographic expression buried in the Green River Basin.

A deep well-log transect over the Moxa Arch (Fig. 2.21) showing the Canyon Creek Mb. and older, deeper strata down to the Turonian Frontier Formation illustrates the deeper structure and thickness patterns in this area. In this anticlinal section across the Moxa Arch, stratigraphic units older than the Canyon Creek Mb. can be seen. The anticline has been spectacularly decapitated by an erosional surface at the base of the Canyon Creek Member that cuts down as deep as the Baxter Shale (Krystinik & DeJarnett, 1995). This erosive surface illustrates that deep-seated Laramide uplift activity as early as 80Ma. The Canyon Creek Mb. was deposited over this erosional surface without any evidence of continued Laramide activity.

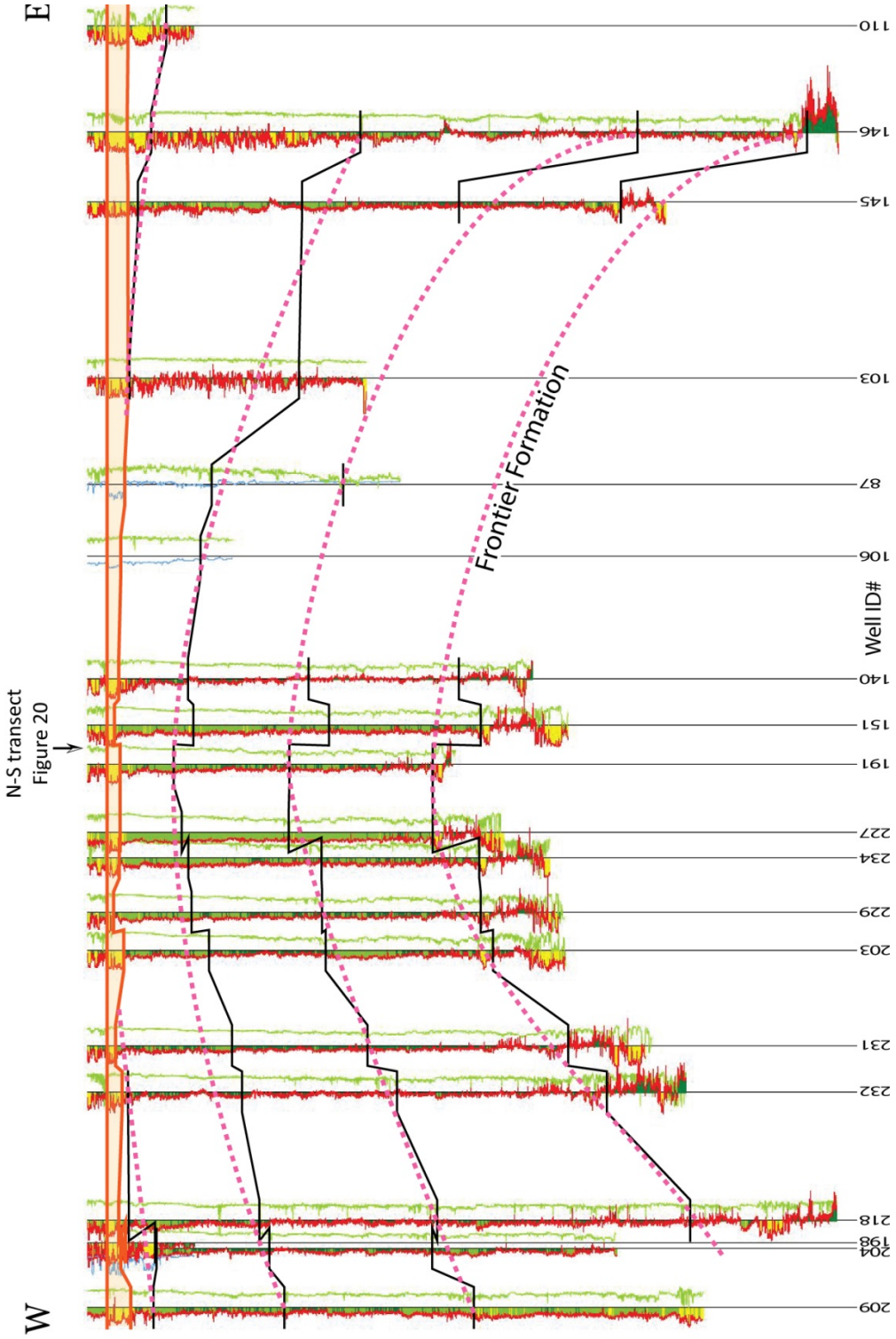

Figure 2.21: Well-log correlation across the axis of the Moxa Arch. The orange shaded interval corresponds to the Canyon Creek Mb. The black lines are two conductivity markers in the underlying strata and the deepest one is the top of the Frontier formation. The correlation shows constant thickness of the Canyon Creek interval overlying the decapitated Moxa Arch anticline. Well ID# identifies each well in Appendix A.

CONCLUSIONS

The Canyon Creek Member of the Ericson Formation, part of the Mesaverde Group, is a regionally extensive unit formed by fluvial deposits, which allows for the study of the regional and local behavior of these rivers in the basin.

The Western Interior Seaway was a foreland basin created by the growth of the Sevier Orogenic Belt, and as such during most of the Cretaceous Period most of the rapid subsidence occurred along its western edge. In contrast, the Canyon Creek Member fluvial system developed greater thickness at the most distal positions from the Sevier Orogenic Belt, and the member is thinnest next to the thrust front (Fig. 2.15). This pattern suggests a period of relative quiescence in the orogenic belt during which the subsidence pattern in the foreland basin was reversed by denudation of the orogen and eastward migration of the dynamic subsidence across the region.

The effects of the subsidence pattern are not only a change in the thickness of the Canyon Creek Member but it also drove a change in its fluvial style. The Canyon Creek Member evolves from a thin and highly amalgamated braided fluvial system at the proximal end of the Green River Basin to a thick mud-rich meandering fluvial system with isolated channels at the distal end of the basin. Isostatic rebound of the foreland basin likely increased the depositional slopes of the proximal reaches of the basin favoring the braided character of the rivers in this area. Meanwhile the increased subsidence in the distal reaches of the system favored the development of meandering systems by decreasing coastal-plain depositional slopes and allowed the deposition and preservation of fine sediments that would contribute to bank stability. From the distal coastal plain, the Canyon Creek system then interdigitates with a series of stacked shoreline systems in the east and southeast.

This general behavior of the Canyon Creek fluvial system, however, shows important local variations that reveal the occurrence of active structures of Laramide origin in the basin during deposition of the Canyon Creek Member (Fig. 2.16).

The Uinta Mountains were a topographic feature that probably shed abundant sediments northward into the adjacent Green River Basin. The anomalous thickness of the Canyon Creek Mb.

at the southern edge of the Greater Green River Basin represents the flexural foredeep of the Uinta Mountains, whereas the lobate feature observable in the net-to-gross map (with high but variable values) likely represents an alluvial megafan shedding off the Uinta Mountains.

The Rock Springs Uplift was active during the Upper Campanian as an area of reduced subsidence that probably lacked topographic expression. The early differential movement along the western edge of the Rock Springs Uplift with respect to the Canyon Creek Mb. is shown by the thinning of the Canyon Creek strata above the structure and by the increased net-to-gross values.

The Sierra Madre and Rawlins uplifts were similarly active as areas of reduced subsidence during Canyon Creek deposition, as shown by the reduction of stratal thickness and increase of net-to-gross of the Canyon Creek Mb. in the across the crestal areas of these structures. The reduction is rather gradual in the case of the Sierra Madre Uplift while it is much sharper near the Rawlins uplift. The subsidence reduction mimics the structural style of these uplifts.

The areas between these uplifts became asymmetric, embryonic Laramide basins (as the Western Interior Seaway broke up) during the Maastrichtian and especially during the Paleocene.

REFERENCES

ASCHOFF, J. & STEEL, R. (2011a) Anomalous Clastic Wedge Development During the Sevier-Laramide Transition, North American Cordilleran Foreland Basin, USA. *Geological Society of America Bulletin*, **123,** 1822-1835.

ASCHOFF, J.L. & STEEL, R.J. (2011b) Anatomy and Development of a Low-Accommodation Clastic Wedge, Upper Cretaceous, Cordilleran Foreland Basin, USA. *Sedimentary Geology*, **236,** 1-24.

ASHBY, J.M., GEISSMAN, J.W. & WEIL, A.B. (2005) Has the Eastern End of the Uinta Mountains Been Bent? Paleomagnetic and Fault Kinematic Assessment. In: *Uinta Mountain Geology* (Ed. by C. M. Dehler, J. L. Pederson, D. A. Sprinkel & B. J. Kowallis), **33**, 285-. Utah Geological Association, Salt Lake City, UT.

BARLOW JR, J.A. (1955) Structure of the Rawlins Uplift, Carbon County, Wyoming.

BLAKEY, R. (Accessed 2011) Colorado Plateau Geosystems, Inc., from http://cpgeosystems.com/index.html.

BULLIMORE, S.A., HELLAND-HANSEN, W., HENRIKSEN, S. & STEEL, R.J. (2008) Shoreline Trajectory and Its Impact on Coastal Depositional Environments: An Example from the Upper Cretaceous Mesaverde Group, Northwestern Colorado, USA. In: *Recent Advances in Models of Siliciclastic Shallow-Marine Stratigraphy* (Ed. by G. J. Hampson, R. J. Steel & P. M. Burgess), *Sepm Special Publication*, **90**, 209-236. SEPM - Soc. Sedimentary Geology, Tulsa.

CARVAJAL, C. & STEEL, R. (2009) Shelf-Edge Architecture and Bypass of Sand to Deep Water: Influence of Shelf-Edge Processes, Sea Level, and Sediment Supply. *Journal of Sedimentary Research*, **79,** 652-672.

CARVAJAL, C. & STEEL, R. (2012) Source-to-Sink Sediment Volumes within a Tectono-Stratigraphic Model for a Laramide Shelf-to-Deep-Water Basin: Methods and Results. *Tectonics of Sedimentary Basins: Recent Advances***,** 131-151.

COBBAN, W.A., WALASZCZYK, I., OBRADOVICH, J.D. & MCKINNEY, K.C. (2006) A Usgs Zonal Table for the Upper Cretaceous Middle Cenomanian--Maastrichtian of the Western Interior of the United States Based on Ammonites, Inoceramids, and Radiometric Ages. *USGS Open Report*, USGS. Denver**,** 45.

CONSTENIUS, K.N., ESSER, R.P. & LAYER, P.W. (2003) Extensional Collapse of the Charleston-Nebo Salient and Its Relationship to Space-Time Variations in Cordilleran Orogenic Belt Tectonism and Continental Stratigraphy. In: *Cenozoic Systems of the Rocky Mountain Region* (Ed. by R. G. Raynolds & R. M. Flores), 303-354. Rocky Mountain Section (SEPM), Denver, CO.

CRABAUGH, J.P. (2001) Nature and Growth of Nonmarine-to-Marine Clastic Wedges: Examples from the Upper Cretaceous Iles Formation, Western Interior (Colorado) and the Lower

Paleogene Wilcox Group of the Gulf of Mexico Basin (Texas). Ph. D. Dissertation Thesis, University of Wyoming, Laramie.

CROSS, T.A. & PILGER, R.H. (1978) Tectonic Controls of Late Cretaceous Sedimentation, Western Interior, USA. *Nature*, **274,** 653-657.

DECELLES, P.G. (1994) Late Cretaceous-Paleocene Synorogenic Sedimentation and Kinematic History of the Sevier Thrust Belt, Northeast Utah and Southwest Wyoming. *Geological Society of America Bulletin*, **106,** 32-56.

DECELLES, P.G. & MITRA, G. (1995) History of the Sevier Orogenic Wedge in Terms of Critical Taper Models, Northeast Utah and Southwest Wyoming. *Geological Society of America Bulletin*, **107,** 454-462.

DECELLES, P.G. & GILES, K.A. (1996) Foreland Basin Systems. *Basin Research*, **8,** 105-123.

DECELLES, P.G. (2004) Late Jurassic to Eocene Evolution of the Cordilleran Thrust Belt and Foreland Basin System, Western USA. *American Journal of Science*, **304,** 105-168.

DECELLES, P.G. & COOGAN, J.C. (2006) Regional Structure and Kinematic History of the Sevier Fold-and-Thrust Belt, Central Utah. *Geological Society of America Bulletin*, **118,** 841-864.

DEVLIN, W.J., RUDOLPH, K.W., SHAW, C.A. & EHMAN, K.D. (1993) The Effect of Tectonic and Eustatic Cycles on Accommodation and Sequence-Stratigraphic Framework in the Upper Cretaceous Foreland Basin of Southwestern Wyoming. In: *Sequence Stratigraphy and Facies Associations* (Ed. by H. W. Posamentier, C. P. Summerhayes, B. U. Haq & G. P. Allen), *Spec. Publ. Int. Ass. Of Sediment.*, **18**, 501-520. Blackwell Publishing Ltd., Boston.

DICKINSON, W.R. & SNYDER, W.S. (1978) Plate Tectonics of the Laramide Orogeny. In: *Laramide Folding Associated with Basement Block Faulting in the Western United States* (Ed. by V. Mattheus), **Memoir no.121**, 355-366. Geological Society of America, Boulder, CO.

DICKINSON, W.R., KLUTE, M.A., HAYES, M.J., JANECKE, S.U., LUNDIN, E.R., MCKITTRICK, M.A. & OLIVARES, M.D. (1988) Paleogeographic and Paleotectonic Setting of the Laramide Sedimentary Basins in Central Rocky-Mountain Region. *Geological Society of America Bulletin*, **100,** 1023-1039.

FLEMINGS, P.B. & JORDAN, T.E. (1989) A Synthetic Stratigraphic Model of Foreland Basin Development. *Journal of Geophysical Research-Solid Earth and Planets*, **94,** 3851-3866.

GOMEZ-VEROIZA, C.A. & STEEL, R.J. (2010) Iles Clastic Wedge Development and Sediment Partitioning within a 300-Km Fluvial to Marine Campanian Transect (3 M.Y.), Western Interior Seaway, Southwestern Wyoming and Northern Colorado. *AAPG Bulletin*, **94,** 1349-1377.

GOMEZ, C.A. (2009) Clastic Wedge Development and Sediment Budget in a Source-to-Sink Transect (Late Campanian Western Interior Basin, Sw Wyoming and N Colorado). Ph.D. Dissertation Thesis, University of Texas at Austin, Austin.

GREEN, G.N. (1992) The Digital Geologic Map of Colorado in Arc/Info Format: U.S. Geological Survey, Open-File Report of-92-507, Scale 1:500000.

GREEN, G.N. & DROUILLARD, P.H. (1994) The Digital Geologic Map of Wyoming in Arc/Info Format: U.S. Geological Survey, Open-File Report of-94-425, Scale 1:500000.

HARTLEY, A.J., WEISSMANN, G.S., NICHOLS, G.J. & WARWICK, G.L. (2010) Large Distributive Fluvial Systems: Characteristics, Distribution, and Controls on Development. *Journal of Sedimentary Research*, **80,** 167-183.

HANSEN, W.R. (1986) *Neogene Tectonics and Geomorphology of the Eastern Uinta Mountains in Utah, Colorado, and Wyoming*. U.S. Geological Survey, Denver, CO.

HINTZE, L.F., WILLIS, G.C., LAES, D.Y.M., SPRINKEL, D.A. & BROWN, K.D. (2000) Digital Geologic Map of Utah: Utah Geological Survey, Map 179dm, Scale 1:500000.

HORTON, B.K. & DECELLES, P.G. (2001) Modern and Ancient Fluvial Megafans in the Foreland Basin System of the Central Andes, Southern Bolivia: Implications for Drainage Network Evolution in Fold-Thrust Belts. *Basin Research*, **13,** 43-63.

HORTON, B.K., CONSTENIUS, K.N. & DECELLES, P.G. (2004) Tectonic Control on Coarse-Grained Foreland-Basin Sequences: An Example from the Cordilleran Foreland Basin, Utah. *Geology*, **32,** 637-640.

IZZET, G.A., COBBAN, W.A. & GILL, J.R. (1971) The Pierre Shale near Kremmling, Colorado, and Its Correlation to the East and the West. *Geological Survey Professional Paper*. U. S. G. Survey. **684-A**.

JONES, C.H., FARMER, G.L., SAGEMAN, B. & ZHONG, S. (2011) Hydrodynamic Mechanism for the Laramide Orogeny. *Geosphere*, **7,** 183-201.

JORDAN, T.E. (1981) Thrust Loads and Foreland Basin Evolution, Cretaceous, Western United-States. *Aapg Bulletin-American Association of Petroleum Geologists*, **65,** 2506-2520.

KIRSCHBAUM, M.A. & ROBERTS, L.N. (2005) Stratigraphic Framework of the Cretaceous Mowry Shale, Frontier Formation and Adjacent Units, Southwestern Wyoming Province, Wyoming, Colorado, and Utah. *US Geological Survey Southwestern Wyoming Province Assessment Team, Petroleum systems and geologic assessment of oil and gas in the southwestern Wyoming province, Wyoming, Colorado, and Utah: US Geological Survey digital data series DDS*, **69**.

KRYSTINIK, L. & DEJARNETT, B.B. (1995) Lateral Variability of Sequence Stratigraphic Framework in the Campanian and Lower Maastrichtian of the Western Interior Seaway. In: *Sequence Stratigraphy of Foreland Basin Deposits* (Ed. by J. C. Van Wagoner & G.

T. Bertram), *Aapg Memoir*, **64**, 11-26. The American Association of Petroleum Geologists, Tulsa, OK.

LEARY, R., DECELLES, P., GEHRELS, G. & MORRISS, M. (2014) Fluvial Deposition During Transition from Flexural to Dynamic Subsidence in the Cordilleran Foreland Basin: Ericson Formation, Western Wyoming, U.S.A. *Basin Research***,** n/a-n/a.

LECLAIR, S.F. & BRIDGE, J.S. (2001) Quantitative Interpretation of Sedimentary Structures Formed by River Dunes. *Journal of Sedimentary Research*, **71,** 713-716.

LEIER, A.L., DECELLES, P.G. & PELLETIER, J.D. (2005) Mountains, Monsoons, and Megafans. *Geology*, **33,** 289-292.

LIU, L. & GURNIS, M. (2010) Dynamic Subsidence and Uplift of the Colorado Plateau. *Geology*, **38,** 663-666.

LIU, S.F., NUMMEDAL, D., YIN, P.G. & LUO, H.J. (2005) Linkage of Sevier Thrusting Episodes and Late Cretaceous Foreland Basin Megasequences across Southern Wyoming (USA). *Basin Research*, **17,** 487-506.

LIU, S.F., NUMMEDAL, D. & LIU, L. (2011) Migration of Dynamic Subsidence across the Late Cretaceous United States Western Interior Basin in Response to Farallon Plate Subduction. *Geology*, **39,** 555-558.

LOVE, J.D. (1961) Definition of Green River, Great Divide, and Washakie Basins, Southwestern Wyoming. *AAPG Bulletin*, **45,** 1749-1755.

MARSHAK, S., KARLSTROM, K. & TIMMONS, J.M. (2000) Inversion of Proterozoic Extensional Faults: An Explanation for the Pattern of Laramide and Ancestral Rockies Intracratonic Deformation, United States. *Geology*, **28,** 735-738.

MARTINSEN, O.J., MARTINSEN, R.S. & STEIDTMANN, J.R. (1993) Mesaverde Group (Upper Cretaceous), Southeastern Wyoming - Allostratigraphy Versus Sequence Stratigraphy in a Tectonically Active Area. *Aapg Bulletin-American Association of Petroleum Geologists*, **77,** 1351-1373.

MARTINSEN, O.J., ALF RYSETH, A., HELLAND-HANSEN, W., FLESCHE, H., TORKILDSEN, G. & IDIL, S. (1999) Stratigraphic Base Level and Fluvial Architecture: Ericson Sandstone (Campanian), Rock Springs Uplift, Sw Wyoming, USA. *Sedimentology*, **46,** 235-263.

MASTERS, C.D. (1966) Sedimentology of the Mesaverde Group and of the Upper Part of the Mancos Formation, Northwestern Colorado, Yale University, New Haven.

NICHOLSON, A. (2010) Tectonic Control on Sedimentation: An Example from the Rock Springs Uplift, Sw Wyoming. *Undergraduate Senior Honors Thesis*, University of Texas at Austin. Austin**,** 29.

OBRADOVICH, J.D. (1993) A Cretaceous Time Scale. In: *Evolution of the Western Interior Basin* (Ed. by W. G. E. Caldwell & E. G. Kauffman), **Special Paper**, 379-396. Geological Association of Canada.

PANG, M. & NUMMENDAL, D. (1995) Flexural Subsidence and Basement Tectonics of the Cretaceous Western Interior Basin, United-States. *Geology*, **23,** 173-176.

PRYOR, W.A. (1961) Petrography of Mesaverde Sandstones in Wyoming.

ROEHLER, H.W. & HANSEN, D.E. (1989) Surface and Subsurface Correlations Showing Depositional Environments of Upper Cretaceous Mesaverde Group and Associated Formations, Lost Soldier Field to Cow Creek, Southwest Wyoming, U.S. Geological Survey. Denver, CO.

ROEHLER, H.W. (1990) *Stratigraphy of the Mesaverde Group in the Central and Eastern Greater Green River Basin, Wyoming, Colorado and Utah* U.S. Geological Survey, Denver, CO.

SIEPMAN, B.R. (1986) Facies Relationships in Campanian Wave-Dominated Coastal Deposits in Sand Wash Basin. In: *New Interpretations of Northwest Colorado Geology* (Ed. by D. S. Stone & K. S. Johnson), 157-164. Rocky Mountain Association of Geologists, Denver.

STEEL, R.J., PLINK-BJORKLUND, P. & ASCHOFF, J. (2012) Tidal Deposits of the Campanian Western Interior Seaway, Wyoming, Utah and Colorado, USA. In: *Principles of Tidal Sedimentology* (Ed. by R. A. Davis Jr & R. W. Dalrymple), 437-471. Springer Netherlands.

WEIL, A.B. & YONKEE, W.A. (2012) Layer-Parallel Shortening across the Sevier Fold-Thrust Belt and Laramide Foreland of Wyoming: Spatial and Temporal Evolution of a Complex Geodynamic System. *Earth and Planetary Science Letters*, **357–358,** 405-420.

Chapter Three: Architecture of Storm to Tidal Shelf Sandstone Bodies; an example from Campanian Almond Formation in Hanna Basin, USA

ABSTRACT

A facies and architectural model for shelf sandstone bodies is built using outcrop data and examples from previous literature. The model is based on the well-known Campanian Almond Formation which is overall a transgressive interval punctuated by short time regressions.

There is a continuous vertical transition between shoreface up to storm (wave) ridges and to tidal and storm ridges on the shelf. The main mechanism of generating such shelf sandstone bodies is by the reworking of sands from previous shorelines wave ravinement during transgression. Using three sandstone bodies from the outcrop it is shown that shoreline deposits, storm ridges and tidal ridges on the shelf can be adjacent and linked vertically or spatially or can be completely isolated. The connection or disconnection between the different sand-bodies is controlled by the relative rate of sea level change and the dominant processes during the transgression.

INTRODUCTION

Shelf sand ridges (storm or tide-dominated) are formed during transgressions, as a result of storm and tidal currents reworking lowstand (coarse-grained) deposits, and therefore they overlie a transgressive surface of erosion (Posamentier, 2002; Snedden *et al.*, 2011; Schwarz, 2012).Very few examples of transgressive shelf ridges have been identified in the geological record (Olariu *et al.*, 2012c; Schwarz, 2012) when compared to their abundance in modern shelf systems (Swift, Donald J. P. & Field, 1981; Thomas & Anderson, 1994; Reynaud *et al.*, 1999; Snedden & Dalrymple, 1999; Trentesaux *et al.*, 1999; van de Meene & van Rijn, 2000; Snedden *et al.*, 2011).

The lack of examples of ancient shelf sand ridges is partially due to the reinterpretation of some shelf sandstone deposits, e.g. Shannon Sandstone in the Cardium Formation (Tillman &

Martinsen, 1984) as lowstand shoreline deposits (Plint, 1988; Walker, Roger G. & Bergman, 1993a). The lowstand shoreline model (Plint, 1988) emphasize that the coarse-grained material is transported across the shelf during periods of falling and low sea level during the migration of the shoreline. The sandstone bodies (shoreline deposits) become isolated from the main shoreline deposits by an erosional sequence boundary below caused by the sea level drop and an erosional transgressive ravinement surface above.

The second reason for the scarcity of recognized ancient shelf ridge examples is the lack of a detailed facies model for transgressive shelf ridges, in part because most modern transgressive ridges are imaged with seismic, and there is a lack of detailed facies information (Reynaud *et al.*, 1999; Snedden *et al.*, 2011). Additionally, in some modern examples it is still unclear if the ridges formed as the result of a tidal reworking of relict sediments (tidal ridge s. s.) or if they represent flooded and only slightly reworked fluvial tidal mouth bars (lowstand shoreline), e.g. Yangtze River (ZhenXia *et al.*, 1998).

A tidal ridge facies model is proposed based on the architecture and facies associations of three sandstone units described in the uppermost Almond Formation outcrops in the Hanna Basin of Southern Wyoming and from previous examples found in the literature.

The Upper Almond Formation which outcrops in Laramie, Hanna and Greater Green River basins, is considered a wave and storm dominated transgressive succession (Flores, 1978; Roehler, 1990; Martinsen, R. S. & Christiansen, 1992; Martinsen, R. S., 1998; Tobin *et al.*, 2010), characterized by relatively short lived and thick (15-30 meters) shoreface deposits alternating with thinner (4-25 meters) bay and estuary deposits. At the top of the Almond Fm., the Lewis Shale Fm. represents a major regional transgression.

The depositional environments of the uppermost sandstone bodies of the Almond Formation in outcrops along the southern edge of the Hanna Basin are re-evaluated here. The uppermost sandstone units of Almond Fm. were previously interpreted as isolated forced regressive strand-plains (Tobin *et al.*, 2010) or as transgressive sand shoals (Martinsen, O. J. *et al.*, 1993). This study advocates for a new interpretation of some of these bodies as transgressive shelf

ridges; it also proposes a facies model linked to the inception-evolution-abandonment cycle of shelf sand ridges.

GEOLOGICAL SETTING OF THE ALMOND FORMATION

The Campanian Almond Formation is some of the youngest deposits that filled the Western Interior Seaway (WIS). The Western Interior Seaway was a north-south elongated epicontinental basin created by a combination of the high eustatic sea-level of the late Cretaceous (Haq *et al.*, 1987), the flexural subsidence imposed by the tectonic loading of the Sevier fold and thrust belt (Jordan, 1981; Pang & Nummendal, 1995), and by dynamic subsidence related to the subduction of the Farallon plate under the western edge of the North American plate (Liu *et al.*, 2011).

The WIS was in-filled mainly from its western shores with sediment shed from the Sevier Orogenic Belt, creating a series of clastic wedges that prograded eastward into the WIS Basin (Crabaugh, 2001). In southern Wyoming the last clastic wedge before the Laramide break-up of the WIS during the Maastrichtian is the Williams Fork clastic wedge, which prograded more than 200km in an east-south-east direction (Roehler, 1990; Steel *et al.*, 2012).

The transgressive limb of the Williams Fork clastic wedge contains the basal alluvial deposits of the Canyon Creek Sandstone and Pine Ridge Fm., the coastal-plain to marine Almond Fm., and (Fig. 3.1) and is capped by the Lewis Shale Fm. The Pine Ridge Fm. is composed of cross-bedded sandy channels with low angle accretion surfaces, interpreted as channel-fills of a distal meandering fluvial system (Martinsen, O. J. *et al.*, 1993; Leva López & Steel, In preparation). Conformably above the Pine Ridge Fm. sits the Almond Fm. subdivided into two members (Fig. 3.1). The lower Almond Fm. is dominated by dark carbonaceous mudstones with frequent coal intervals, and some marine influence in the form of small coarsening upward cycles with wave and combined flow ripples as well as some restricted marine ichnofauna (Martinsen, O. J. *et al.*, 1993; Martinsen, R.S., 1995). Rare lensoidal

sandstone bodies are interpreted as delta distributary channels, and the lower Almond member is interpreted as lower coastal-plain deposits (Roehler, 1990; Martinsen, R.S., 1995).

The upper Almond Fm. has a series of repeated upward coarsening cycles of wave and storm dominated shoreface origin (Roehler, 1990; Martinsen, R.S., 1995; Kieft *et al.*, 2011). The shoreface deposits have been interpreted as small progradational pulses (Fig. 3.2) that punctuate the general transgression of the Almond system (Roehler & Hansen, 1989).

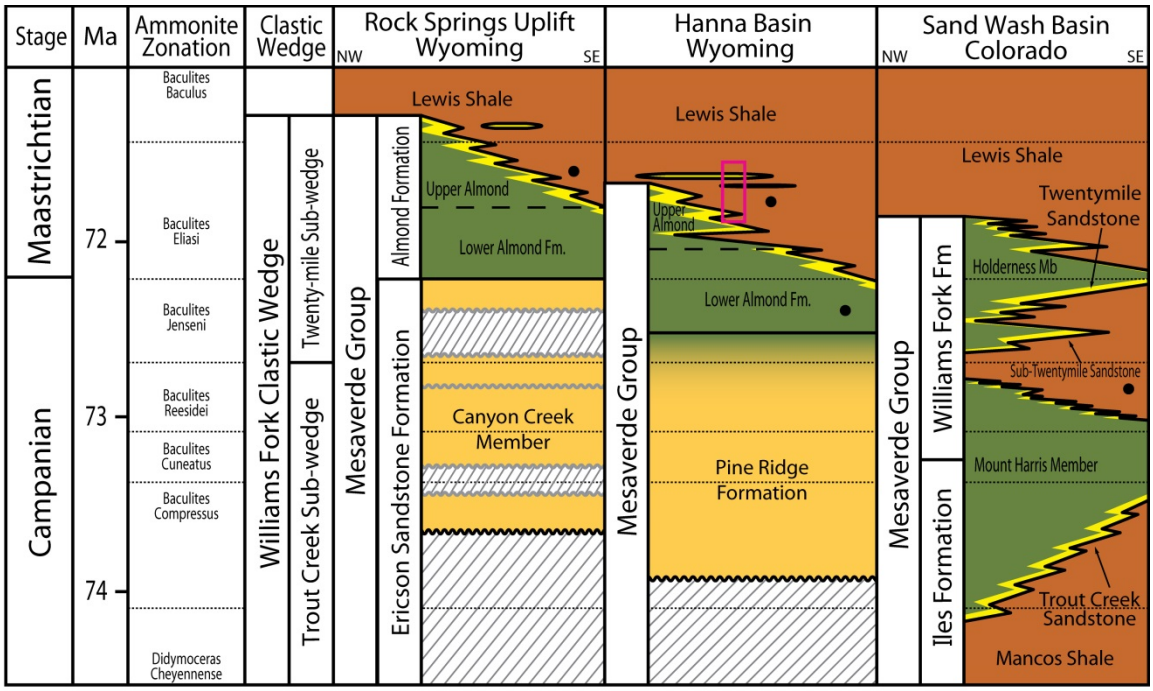

Figure 3.1: Upper Campanian chronostratigraphic correlation of the Williams Fork Clastic Wedge lithostratigraphic units across southern Wyoming and northern Colorado. It shows the sandstone bodies encased in Lewis shale the main object of this study, along with the Almond Formation, underlying fluvial strata, and correlative shorelines in Colorado. This chart is based in well-log correlations across the Greater Green River Basin, previous studies in the area (Masters, 1966; Roehler, 1990; Martinsen, O. J. *et al.*, 1993; Crabaugh, 2001), paleontological data (Cobban et al. 2006; Izzet et al. 1971(Gill *et al.*, 1970; Izzet *et al.*, 1971; Bader *et al.*, 1983; Cobban *et al.*, 2006) and radiological data (Obradovich, 1993).

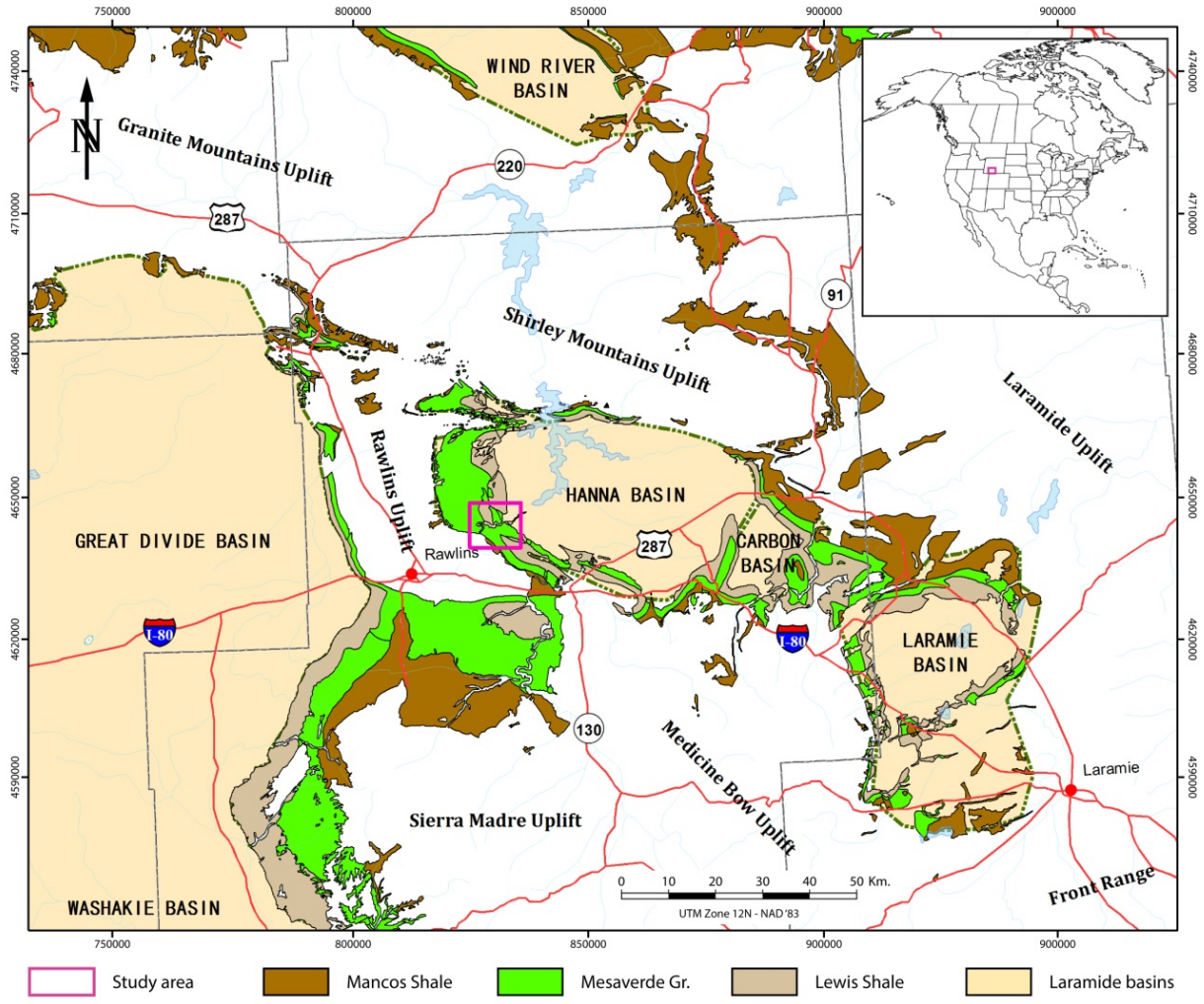

Figure 3.2: Location map of the area of study (pink rectangle), showing the Laramide sedimentary basins, the Laramide uplifts in the area and the outcrops of related strata. Geology after Green and Drouillard (1994).

The Hanna Basin where the studied Almond Fm. outcrops are located is a small (2600km^3) Laramide basin with a very thick (13.6km) sedimentary succession from the Cambrian to the Eocene. Hanna Basin lies flanked by Laramide uplifts, the Rawlins Uplift in the west, the Shirley Mountains on the north, and the Medicine Bow Uplift in the south and east (Fig. 3.2). The subsidence in this basin was similar to other basins in the region during the main phase of the WIS foreland basin, although with a slightly accelerated subsidence during the

Cenomanian-Turonian (LeFebre, 1988). During the Maastrichtian the Hanna basin became an individualized basin due to the initiation of Laramide down-warping against the adjacent uplifts, at which time the subsidence had been greatly accelerated (240 m/ My) (Martinsen, O. J. *et al.*, 1993).

DATASET AND METHODOLOGY

The oldest study sandstone body, Body A (Fig. 3.3), is one of the regressive shorefaces of the Upper Almond Fm. and it is used as a point of comparison with the other two younger sandstone bodies. One stratigraphic section through this body has been measured to characterize its facies and depositional environment. One section is judged sufficient since inspection along the body shows no important lateral changes in this sandstone body and also is in concordance with previous regional interpretations (Martinsen, O. J. *et al.*, 1993; Martinsen, R.S., 1995; Kieft *et al.*, 2011).

The middle sandstone body, Body B (Fig. 3.3), is a thin (about 7m) sandstone body with relatively simple architecture. Five detailed stratigraphic sections and five additional thickness sections were measured along the 300m extent of the sand-body and a high resolution photomosaic and LiDAR data were interpreted.

The uppermost body, Body C (Fig. 3.3), is a thicker (about 20m) sandstone body with a more complex internal architecture. Four detailed stratigraphic sections were measured, and a high resolution photomosaic and LiDAR data were collected and interpreted.

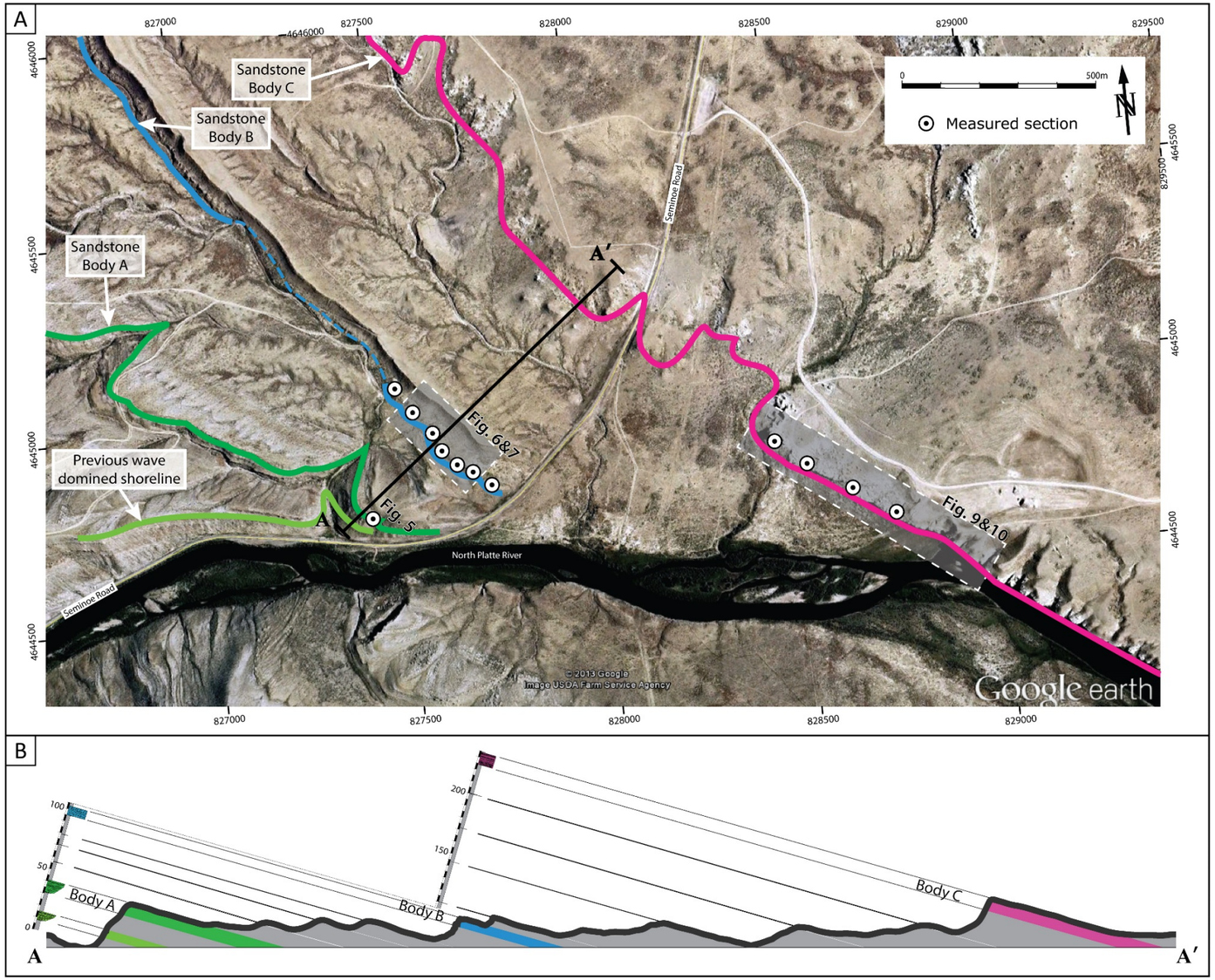

Figure 3.3: (A) Google earth image of the area of study with the sandstone ridges object of study and stratigraphic measured sections marked in the photography. (B) Cross-section showing the structural dip (40°/11°) and the stratigraphic position of each sandstone ridge.

FACIES AND FACIES ASSOCIATIONS

Facies Descriptions

Twelve facies have been distinguished based on sedimentary and biogenic features, grain size, grain-size trends, sorting and lithology. Some facies are present in one or more of the bodies of this study while some appear in the areas between sandstone-bodies.

Laminated mudstone facies, F1

F1 facies is dominated by laminated green to black mudstones with thin, few millimeters thick, layers of siltstone and rare symmetrical ripples. Small horizontal (*Planolites* and *Terebellina*) and rare vertical (*Skolithos*) trace fossils are present and can be locally pervasive; obliterating completely the sedimentary structures. F1 facies outcrops very poorly and usually is covered by debris, soil or vegetation; recessive covered areas are generally attributed to F1 facies. F1 facies is the predominant facies in the study area.

Facies F1 is interpreted to be formed in a very low energy marine setting. The low energy environment is suggested by the overall fine grain-size and the presence of parallel lamination. The rare symmetrical ripples indicate that at times the substrate was reworked by oscillatory flows (waves) (Harms *et al.*, 1975). The trace fossils presence suggests the marine setting (Pemberton & MacEachern, 1995) and the local intense bioturbation suggests low depositional rates. The sedimentary structures, grain size and, ichnofossil assemblage suggest that facies F1 was deposited in a marine offshore setting (Boggs Jr., 2012).

Highly bioturbated interbedded mudstones, siltstones and very fine sandstones, F2

F2 facies consists of thinly laminated interbedded mudstones, siltstones and lower very fine grained sandstones with planar lamination and symmetrical ripples, and pervasive bioturbation. Facies F2 has a coarsening upward trend at the outcrop scale and the sandstone beds thicken upwards. This facies appears inside or at the top of the laminated mudstone facies (F1) with gradual contacts.

Facies F2 is interpreted as deposited in a similar environment to facies F1 but with slightly higher energy in an offshore transition or lower shoreface setting (Plint, 2010). The difference in the grain size and the abundance of symmetrical ripples support the increased energy interpretation with oscillatory flows frequently reworking the deposits (Harms *et al.*, 1975).

Muddy heterolithic strata and very fine grained rippled sandstones facies, F3

F3 facies is dominated by siltstone to very fine-grained sandstone beds (cm to dm thick) separated by cm-thick heterolithic mudstones (Fig. 3.4A). Sandstone bed thickness increases upward as individual beds (few cm thick) become amalgamated into thicker sandstone bedsets (0.5 meter thick). Siltstones and sandstones contain frequent symmetrical wave (Fig. 3.4B) and combined flow ripples, and rare thin sets of hummocky cross-stratification. Common *Skolithos, Planolites, Ophiomorpha,* and other unidentified vertical and horizontal ichnofossils are present.

The frequent symmetrical and combined flow ripples, and sets of HCS indicates that the sediments were frequently reworked by oscillatory flows and occasional storms (Harms *et al.*, 1975). The sedimentary structures and the trace fossil assemblage suggests that facies F3 was deposited in the lower shoreface (Hampson & Storms, 2003)

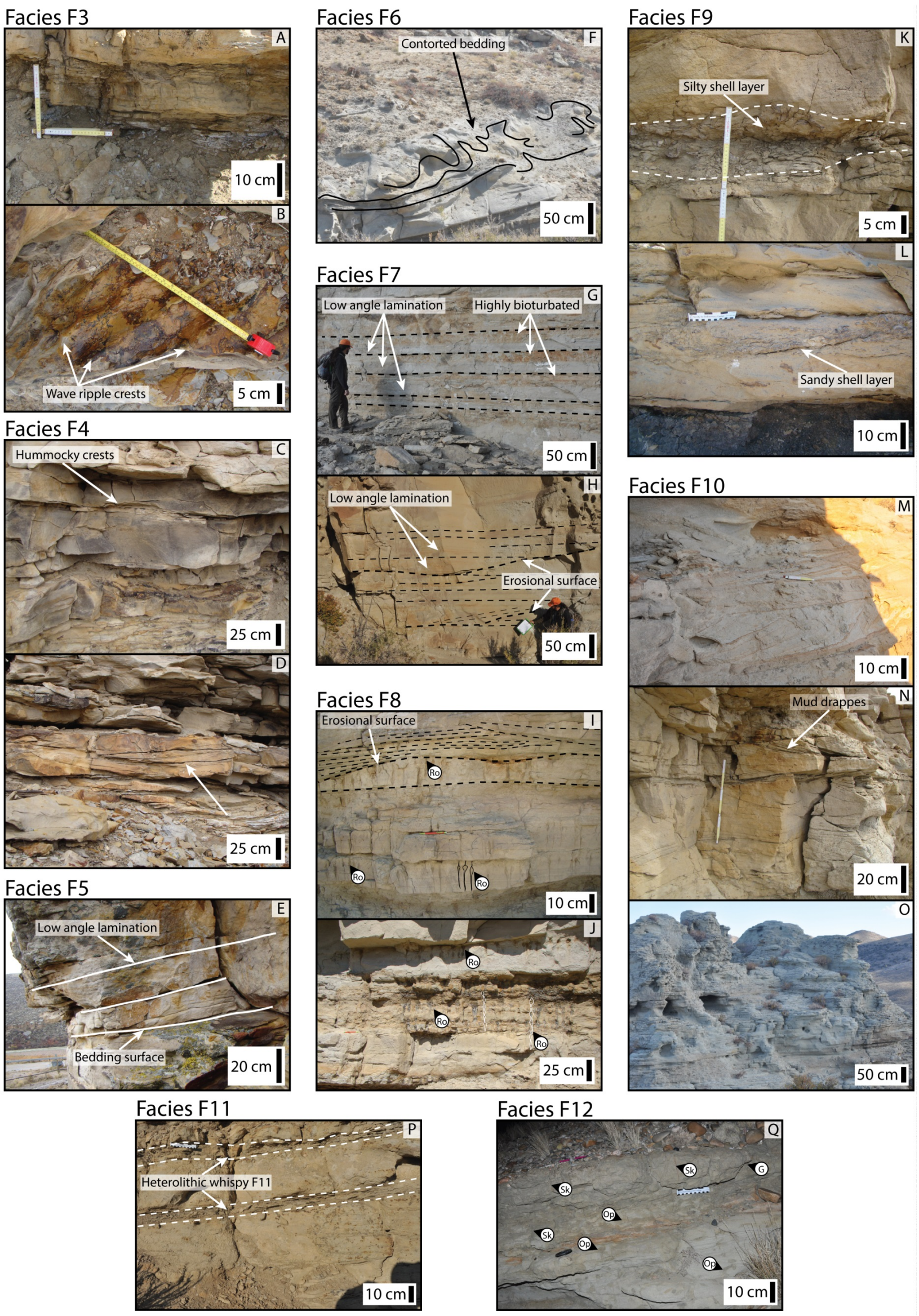
Facies F3
A
10 cm
B
Wave ripple crests
5 cm
Facies F4
C
Hummocky crests
25 cm
D
25 cm
Facies F5
E
Low angle lamination
Bedding surface
20 cm
Facies F6
F
Contorted bedding
50 cm
Facies F7
G
Low angle lamination
Highly bioturbated
50 cm
H
Low angle lamination
Erosional surface
50 cm
Facies F8
I
Erosional surface
Ro
Ro
Ro
10 cm
J
Ro
Ro
Ro
25 cm
Facies F9
K
Silty shell layer
5 cm
L
Sandy shell layer
10 cm
Facies F10
M
10 cm
N
Mud drappes
20 cm
O
50 cm
Facies F11
P
Heterolithic whispy F11
10 cm
Facies F12
Q
Sk
G
Sk
Op
Sk
Op
Op
10 cm

Figure 3.4

Figure 3.4: Photographs showing the characteristics of the facies. (A) Heterolithic alternation of sandstone (cm to dm thick) with mudstone (cm thick) beds (Facies F3). (B) Symmetrical ripple marks in 5-10 cm thick fine to very fine sandstone beds (Facies F3). (c) Dm thick very fine and fine sandstone beds with hummock-cross-stratification (HCS). Note the thin (cm) muddy beds between sandstone beds (Facies 4). (D) Swaley-cross-stratification (SCS) in dm thick very fine and fine sandstone beds (Facies 4). (E) Amalgamated fine sandstone beds with low angle cross-stratification devoid of bioturbation (Facies F5). (F) Contorted bedding with soft deformation increasing upward (Facies F6). (G) Several intervals of low angle cross-lamination and SCS with intense bioturbation at the top (Facies F7). (H) Low angle laminations and storm erosional surfaces (Facies F7). Some planar cross bedding in the bottom. (I) 10-20 cm thick fine sandstone beds *Rosselia socialis* showing multiple levels of equilibrichnia behavior and an erosional surface decapitating the specimens (Facies F8). (J) Crowded *Rosselia socialis* bioturbation destroying completely previous sedimentary structures (Facies F8). (K) 15cm (laterally variable) thick heterolithic layer with shells marking the contact between packages (Facies F9). (L) 10-20 cm Sandy shell layer marking the bottom of the sandstone body (Facies F9). (M) Dm thick fine sandstone beds with planar and through cross lamination. Notice the absence of mud and the grain size rhythmicity accentuated by the red coloration (Facies F10). (N) Dm thick fine sandstone beds with planar cross-bedding and minor mud-draping (Facies F10). (O) 0.5-1 m thick fine sandstone cross-bed sets showing the larger scale architecture (Facies F10). (P) 5-10 cm thick silty sandstone beds with wispy lamination (Facies F11). (Q) Highly bioturbated sandstone indicating fully marine low energy environment.

Hummocky and swaley cross-stratified sandstones facies, F4

F4 facies is characterized by very fine to upper fine grained sandstones with dominant hummocky (HCS) (Fig. 3.4C) and swaley (SCS) (Fig. 3.4D) cross-stratification, and frequent wave and combined flow ripples . There are common thin (<10cm) mudstone beds that separate meter thick amalgamated sandstone beds. F4 facies shows a general upward coarsening trend and it is commonly found overlying the heterolithics and fine grained rippled sandstone (F3 facies) with a gradational contact. *Skolithos* and *Ophiomorpha* burrows are common in Facies F4.

The dominance of HCS and SCS indicate that F4 facies was deposited with constant reworking of the sediments by storm waves (Harms *et al.*, 1975; Dott & Bourgeois, 1982), which indicates deposition at the middle to upper shoreface (Leckie & Walker, 1982).

Low angle laminated sandstone facies, F5

F5 facies have upper fine grained sandstone beds without visible vertical trend in grain size, rare indistinct trace fossils and very low angle lamination (Fig. 3.4E). The bedsets containing F5 facies have a sharp lower boundary which caps the underlying hummocky and swaley cross-stratified sandstone (facies F4).

The very low angle lamination and its stratigraphic position above F4 facies suggest that F5 facies was deposited in the foreshore area with its sediments affected and reworked by the swash of breaking waves (Plint, 2010).

Deformed laminated sandstones facies, F6

F6 facies has thick (up to 2m) highly deformed fine to medium grained sandstones with convolute bedding (Fig. 3.4F). The base of the bed is slightly erosive and contains some remnants of parallel to low angle cross lamination. F6 facies is likely

result of the very fast deposition of sediment forming low angle or cross-strata sedimentary structures which later were deformed by high pore water pressure migrating upward (water escape structures) (Allen, 1982).

Flat or low angle laminated to structureless sandstones facies, F7

F7 facies is characterized by thick (dm) beds of fine grained, low angle to planar laminated, sandstone (Fig. 3.4H) with common bioturbation of *Skolithos*, *Cylindrichnus*, *Arenicolites* and *Rosselia*. The bioturbation is locally intense and obliterates sedimentary structures toward the top of some beds (Fig. 3.4G). The bed laminations are frequently faint and some beds look structureless. The bases of the beds are sharp or slightly erosive and the tops are sharp and contain rare symmetrical ripples. On rare occasions mudclasts formed of the eroded and resedimented *Rosselia* mud "bulbs" are present.

Facies F7 was deposited in a marine environment with a high energy setting. The ichnofauna suggest a fully marine environment (Pemberton & MacEachern, 1995). The flat laminations are probably upper flow regime, the erosional base and the capacity to rework mudclasts indicate a highly energetic depositional environment (Harms *et al.*, 1975). The deposition of this facies can be attributed to wave supported density flows (Dott & Bourgeois, 1982) or more likely to storm reworking of the shelf sand-bodies (Snedden *et al.*, 2011).

Crowded Rosselia sandstone facies, F8

F8 facies is characterized by stacked sandstone beds intensely bioturbated by *Rosselia socialis* trace fossils (Fig. 3.4J). The sandstone beds are upper fine grained sandstones originally planar and low angle laminated (Fig. 3.4I). A single *Rosselia* burrow can be traced upward for more than a meter through several beds, showing equilibrichnia behavior (Nara, 1995; 1997). Several levels of re-establishment at the

substrate-water interface indicate extremely high (dm per year) local sedimentation rates since the burrowers, likely a terebellid polychaete (Nara, 1995), live for only a few decades. If the upper surface of the facies is erosive, the muddy bulbs of *Rosselia* burrows can be eroded (Fig. 3.4I) and resedimented at the base of the overlying bed.

Facies F8 was deposited in a moderate energy marine environment subject to frequent pulses of strong sedimentation due to the storm driven erosion of a retreating shoreline. The monospecific ichnofossil assemblage reflects a stressful environment, probably due to periodic and very strong pulses of sedimentation as indicated by the equilibrichnia behavior of the *Rosselia,* probably due to transgressive coastal erosion (Nara, 2002).

Shell bearing silty sandstone facies, F9

F9 facies has upper fine to medium grained silty sandstone beds with common oyster shells and shell fragments (Figs. 3.4K & 3.4L). The oyster shells are dominantly in hydrodynamic position (concave side upward and arranged in the same orientation to offer least resistance to flow) and sometimes articulated. The largest observed shell was 15 cm in length. This facies usually appears as a single bed up to 30 cm thick with erosive to sharp base, and sometimes showing an upward finning trend reflected in shell size and also an upward decrease in shell content.

Facies F9 is interpreted as deposited by very strong erosive currents that have sorted the oyster shells over relative short distances. Facies F9 likely represents shell-lag deposits above erosional ravinement surfaces during transgression or generated by storms or strong shelf currents.

Cross bedded sandstone facies, F10

F10 facies consists of stacked sets of fine to medium grained sandstone with trough or planar cross strata (Figs. 3.4M & 3.4N). Bioturbation intensity is low with recognized trace fossils including *Skolithos*, *Arenicolites*, *Ophiomorpha*, *Cylindrichnus* and *Rosselia*. Beds show a fining upward trend and current ripples in the bed tops are common. The bottomsets of the cross strata can contain asymmetrical (unidirectional) ripples in rare cases. The beds of F10 facies have a sharp erosional contact with underlying shelly sandstone (facies F9) at some locations, in which case shell fragments also became worked into the cross-strata. Some cross-strata show rhythmic foresets, possibly tidal bundles, and in some cases the foresets are marked by mud drapes (Fig. 3.4N).

Facies F10 is likely to have been deposited under strong unidirectional currents in an open marine environment. The presence of stacked 2D and 3D dunes, foreset rhythmicity, fully marine ichnofauna assemblage and dominantly unidirectional currents suggests strong offshore tidal currents (Dalrymple, 1984) with current strength asymmetry.

Flaser to wispy laminated heterolithic sandstone facies, F11

F11 facies have flaser to wispy lamination with unidirectional (current) ripples in very fine to fine sandstones. Small shell fragments may be present, and usually contain no bioturbation (Fig. 3.4P). Facies F11 is found in thin intervals (few dm thick) between cross stratified sandstone (facies F10) possibly as the toe sets of larger dunes.

Facies F11 is interpreted to represent periods of weaker flow in the general high energy environment in which facies F10 is deposited. The lower energy, heterolithic deposits can also represent the inter-dune areas where currents were weaker and finer sediments accumulated (Olariu *et al.*, 2012a).

Skolithos highly-bioturbated sandstone facies, F12

This facies consists of fine grained grey to green sandstone pervasively bioturbated by *Skolithos* and other un-identified burrowers, no sedimentary structures are preserved (Fig. 3.4Q). The facies F12 is overlying the stacked cross-strata (Facies F10) and is overlain by offshore muds.

F12 facies is interpreted to represent a deepening of the water and drowning of previous deposits into marine environment with change into very low energy conditions where the burrowers colonized the substrate.

Facies Associations

Genetically related lithofacies are grouped into facies associations to identify environments of deposition.

Offshore and offshore transition facies association, FA1

Formed by the *laminated mudstone* (F1 facies) and *highly bioturbated interbedded mudstones, siltstones and very fine sandstones* (F2 facies), the FA1 facies association records a very low energy setting in a fully marine environment. The beds are formed by settling of suspended mud from weak currents, a setting only interrupted by thin siltstone and sandstone beds introduced to the environment by storms reworking. The trace fossil assemblage (*Planolites, Skolithos, and Rhizocorallium*) indicates a fully marine environment.

The F1 facies represents the offshore, open shelf, deposits. Alternating with F1 facies beds there are interspersed F2 facies beds which represent the offshore transition environment with slightly higher energy. FA1 facies association gradually changes upward to the wave and storm dominated shoreface facies association FA2.

Wave and storm dominated shoreface/deltaic facies association, FA2

FA2 facies association contains *heterolithic and very fine grained rippled sandstones* (facies F3), *hummocky and swaley cross-stratified sandstones* (F4 facies), and *low angle laminated sandstones* (F5 facies), with minor occurrence of *deformed laminated sandstones* (F6 facies), *flat or low angle laminated to structureless sandstones* (F7 facies). Facies association FA2 represents shoreface deposits that have been extensively reworked by storm and wave processes. This is supported by the predominance of HCS, SCS and symmetrical ripples; the gradual contact with the offshore and offshore transition facies association (Fig. 3.5); the coarsening upward trend; and the *Skolithos* ichnofacies.

FA2 facies association shows a common upward-coarsening succession of F3, F4, and F5 facies. This represents a common shoreface to foreshore succession in the Almond Fm. (Martinsen, R.S., 1995), with shallowing and increased energy upward trend indicating progradation of the shoreline.

Transgressive storm shelf facies association, FA3

Hummocky and swaley cross-stratified sandstones (F4 facies), *flat or low angle laminated to structureless sandstones* (F7 facies), and *crowded Rosselia sandstones* (F8 facies) make up the FA3 facies association. FA3 is interpreted to be formed by erosion and wave reworking (based on the abundance of storm beds and erosion surfaces) during transgression of a previous shoreline. The appearance of vertically stacked crowded *Rosselia socialis* beds similar to those described by Nara (2002) indicates high sedimentation rates, high energy and high amounts of organic matter available for the benthic organisms. These conditions are met when transgressive coastal erosion delivers sediment and organic matter into the shelf.

Tidal ridge facies association, FA4

The FA4 facies association contains *shell bearing silty sandstones* (F9 facies), *cross-bedded sandstones* (F10 facies), *flaser to wispy laminated heterolithic sandstones* (F11 facies), and *Skolithos highly bioturbated* sandstones (F12 facies). The FA4 association is dominated by the vertically stacked sets of planar and trough cross-laminated beds of facies F10, with sparse ichnofauna (*Skolithos, Cylindrichnus, Rosselia*, and *Ophiomorpha*) and locally abundant shell fragments. Facies 9 (shell lag) is usually concentrated above erosional surfaces internal to the sandstone-bodies or at their basal surfaces. FA4 association represents deposition in the marine setting under strong tidal-current reworking of previous shoreline or shelf deposits.

RESULTS

There are three sandstone bodies described in this section (Fig. 3.3), each with its own depositional characteristics. The first sandstone body is about 10 meters thick and laterally continuous for tens of kilometers. The second sandstone body is about 7 m thick and outcrops for about 2 km laterally. The third sandstone body is about 15 m thick and extends laterally for about 4 km.

Sandstone Body A

This sandstone-body (Fig. 3.3) shows a marked upward coarsening and upward thickening trends of facies association FA2 (Fig. 5). The facies gradually changes from *heterolithics and very fine grained sandstones facies* (F3) to *hummocky and swaley cross-stratified sandstones facies* (F4), and then to *low angle laminated sandstone facies* (F5) as part of the shallowing upward trend typical of regressive shorefaces. The sandstone of FA2 lies conformably on top of facies association FA1 with which has a gradual contact.

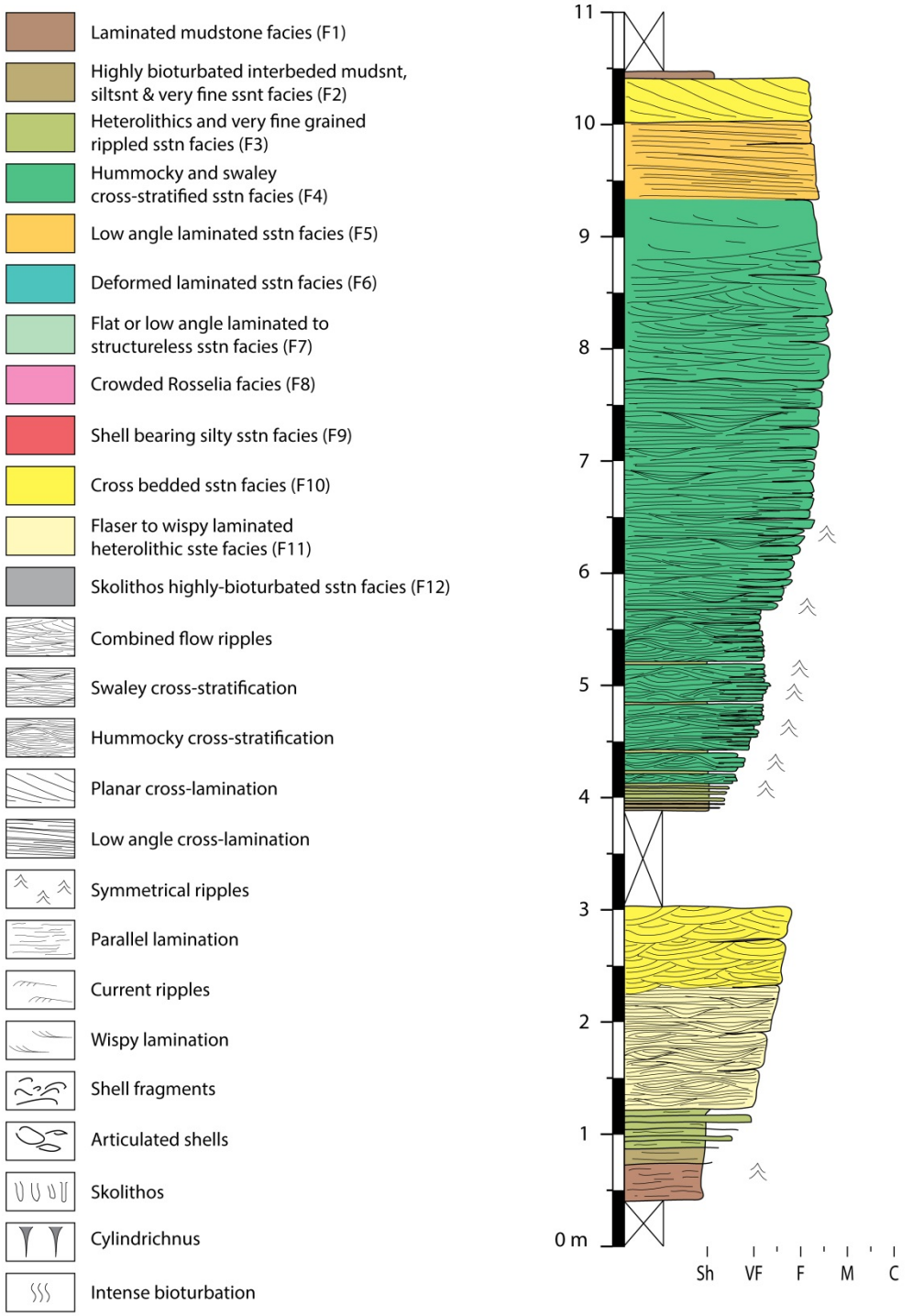

Figure 3.5: Measured section of Body A showing a clear coarsening upward pattern and dominated by storm and wave structures.

Sandstone body A is capped occasionally by thin but erosional *cross-bedded sandstones* (F10 facies) (Fig. 3.5). This sandstone-body is laterally extensive for long distances, outcropping with similar characteristics for tens of kilometers, and with a thickness of around 10 meters. Internally there are no visible large accretion surfaces at the scale of the sandstone body.

Interpretation

Sandstone Body A is interpreted as a wave and storm dominated shoreline that represents one of the short regressive pulses that punctuate the overall transgressive Upper Almond Fm. (Fig. 3.1).

Sandstone body A has the characteristics of a normal wave and storm dominated coastal wedge with the classical divisions of foreshore, shoreface and offshore-transition (Boggs Jr., 2012). Foreshore is the sandy area between the low and high tide levels, dominated by the swash and backwash of breaking waves (Plint, 2010), where the main sedimentary structures are planar and low angle laminations (Fig. 3.4E). The shoreface, between the low tide level and the fair-weather wave base, is sandy to heterolithic dominated by the oscillatory movements of waves and storms (Hampson & Storms, 2003). The main sedimentary structures are swaley cross-stratification (SCS) and hummocky cross-stratification (HCS) with some wave and combined flow ripples (Fig. 3.4C&D) Facies F4 represents the upper and middle shoreface in Body A, while facies F3 is the lower shoreface (Fig. 3.4A&B). The offshore-transition zone, between the fair-weather and the storm wave base, is dominated by muddy sedimentation with minor wave rework in the form of small wave and combined flow ripples. Facies F2 is the offshore transition or lower shoreface in Sandstone Body A. Beside the facies, another

argument for a shoreface deposits is the lateral extent of sandstone body A for tens of kilometers with little thickness change (of about 10m).

All the sandstone-bodies in the upper part of the Almond Formation have been usually presented as wave and storm dominated shoreline deposits with some tidal influence (Martinsen, R. S. & Christiansen, 1992; Tobin *et al.*, 2010; Kieft *et al.*, 2011).

Sandstone Body B

Sandstone body B (Fig. 3.3) is 6-7 meters thick, formed by facies association FA4 and sits atop deposits of facies association FA1 with a very sharp and erosional contact marked by shell fragments (Fig. 3.6 & 3.7). Immediately above the erosional surface there is *shell bearing silty sandstones* (F9 facies) with oyster shells in hydrodynamic position. The dominant facies of the sandstone body B is stacked sets of *cross bedded sandstone facies* (F10) (Figs. 3.7 and 3.8).

The deposits underlying the sandstone body B show a coarsening upward trend that would probably have culminated in a wave dominated shoreline, not unlike those of the sandstone body A. But this inferred shoreline became eroded during transgression of the shoreline and the erosional surface at the bottom of sandstone body B is the record of that erosion, being therefore a wave-generated transgressive ravinement surface.

Sandstone body B can be broadly divided into three distinct units (Figs. 3.7 and 3.8). The lowest unit, Unit 1, is bounded at its base by the transgressive ravinement surface and it is dominated by facies F9 and F10. The second unit, Unit 2, is bounded at the base by a surface extremely rich in articulated oyster shells, dispersed in heterolithic sandstone of facies F9 (Fig. 3.6 & 3.7). Unit 2 is dominated by facies F10 with some thin intervals of

facies F11 (Fig. 3.8). In both the units 1 and 2 are mainly planar cross-laminated and the beds are between 20 and 50 cm thick. The top unit, Unit3, is separated from the second unit by a very thin recessive interval, and it is dominated by facies F10 with thicker cross-stratified beds (0.5 to 1 meter thick), mainly trough cross-laminated (Figs. 3.6 & 3.7). Unit 3 is overlain by highly bioturbated thin bedded deposits of FA1 without an erosive surface.

The extensive surfaces that separate the three units mark a pause in sedimentation, with muddier sediments and the presence of articulated, in living position, shells. These surfaces are interpreted as accretion surfaces. The LiDAR data allowed identification of a bounding surface between the lower and middle units that dips gently (~3°) to the north-east (Fig. 3.6) after the correction of the structural dip of about 11 degrees towards N40°E.

Paleocurrent indicators (cross-strata foresets) point mainly towards the south, aligning with the dip direction of the master surfaces (cross-strata set surfaces) (Fig. 3.6 rose diagrams on the left). In contrast the dip direction of the large scale accreting surfaces of the sandstone body is towards the east-northeast. Therefore we have a superposition of forward accreting elements (compound dunes of cross-strata foresets and cross-strata sets) on this laterally accreting body (cross-strata sets and large accreting surfaces).

Interpretation

Sandstone Body B is interpreted as a tidal shelf ridge formed by the sediments eroded and reworked from a previous shoreline by tidal currents during transgression (Fig. 3.8).

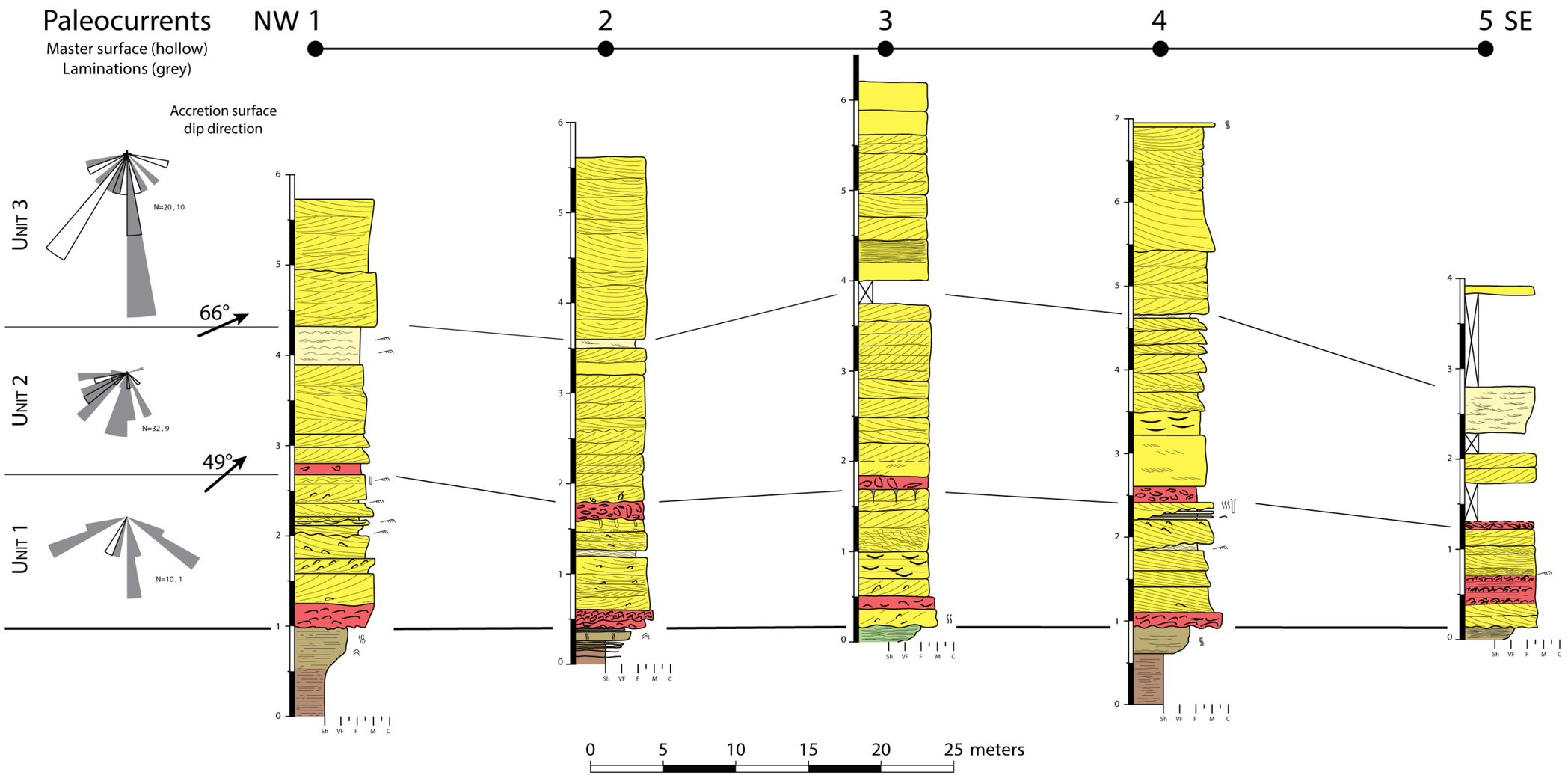

Figure 3.6: Measured section correlation for sandstone body B. The correlation shows the three packages in which Body B is divided, and the paleocurrents in each package (black outline are the dip direction of the cross-bedding and grey sector are the dip direction of the cross-lamination) showing the forward accreting architecture inside each package. For the color and the sedimentary structure key see figure 3.5.

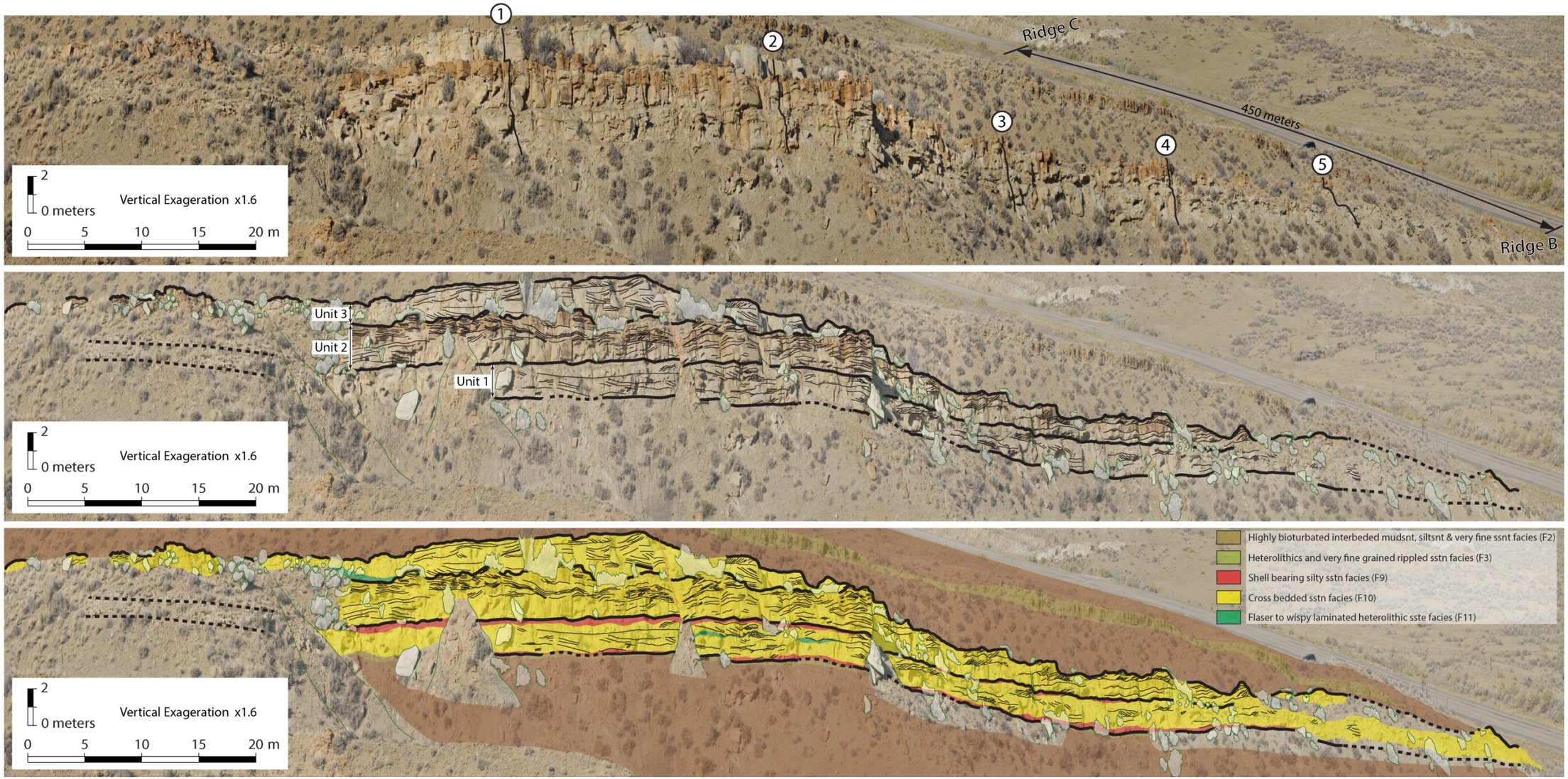

Figure 3.7: Above, high resolution photomosaic (Gigapan©) of the Body B with the locations of the measured sections marked. Middle, interpreted photomosaic with main cross-strata highlighted. Below, facies map over the interpreted photomosaic. The scale in the three images is the same with a vertical exaggeration of 1.6

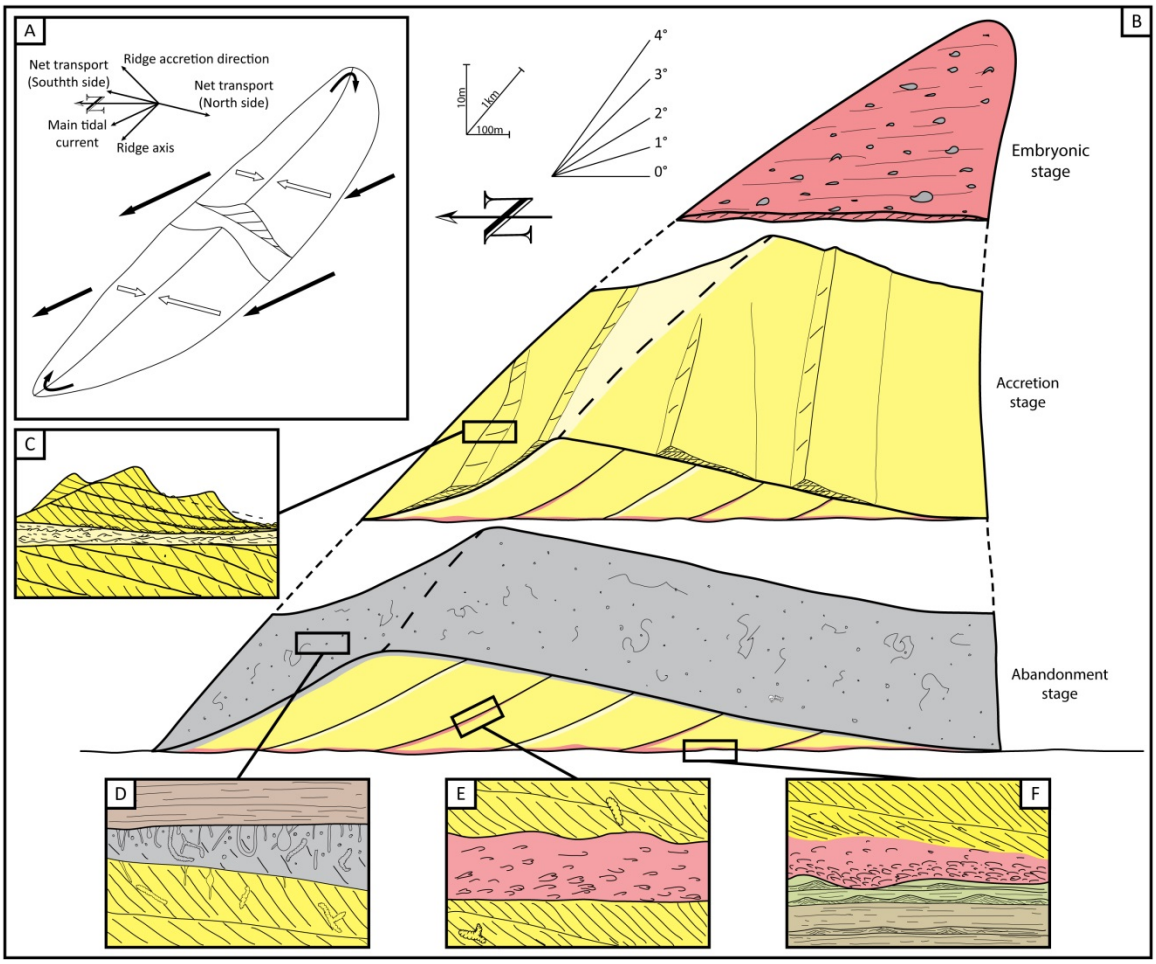

Figure 3.8: Facies model and reconstruction of the transgressive tidal shelf ridge that formed sandstone body B. (A) Reconstruction of the main tidal currents and the resultant net sediment transport based on Reynaud and Dalrymple (2012). (B) Evolutionary stages of the tidal ridge. The embryonic stage represents the basal erosional surface with a thin veneer of shell rich sandstone. The accretion stage shows compound dunes accreting in the north side of the ridge, while dunes with net erosion migrate in the south side of the ridge. The abandonment stage is characterized by hemipelagic deposition and intense bioturbation. (C) Detail of the compound dune accretion. (D) Abandonment facies and highly bioturbated upper boundary of the ridge. (E) Detail of the accretion surfaces with shell rich sandstones. (F) Detail of the bottom surface eroding into previous offshore and offshore transition deposits. For color key see figure 3.5.

The 7 meters thick Sandstone body B is encased in fully marine mudstones and thin sandstone beds with marine bioturbation. The basal surface of the sandstone body is highly erosive and it is interpreted as a wave or tidal transgressive erosional surface. The erosional surface was probably formed by shelf tidal currents; the shell lag at some locations change gradually into the overlying cross-strata, indicating that the later tidal currents reworked the transgressive lag. The basal surface eroded underlying shelf deposits, a possible lowstand shoreline that served as sediment source for the later tidal ridge. The ridge is interpreted to be tidally dominated based on the abundance (90%) of the cross-strata (Fig. 3.6). The upper surface, although sharp, is not found to be erosive; probably indicating the abandonment and drowning phase of the tidal ridge as the transgression deepened the environment.

Abundance of cross bedded sandstone facies with occurrences of mud-drapes and dominant unidirectional net sediment transport direction is the expected signature of tidal currents on the shelf (Reynaud & Dalrymple, 2012). These simple cross-strata are organized in forward accreting compound dunes (Olariu *et al.*, 2012a), which in turn accrete laterally to form the sandstone-body (Fig. 3.8), a common feature in transgressive tidal shelf ridges as was recognized in modern environments (Houbolt, 1968; Reynaud *et al.*, 1999; Trentesaux *et al.*, 1999; Dalrymple, 2012) and ancient tidal bars (Olariu *et al.*, 2012c; Schwarz, 2012).

Sandstone Body C

The sandstone Body C (Fig. 3.3) has a more complex architecture than the previous two and can be divided into three units according to their main facies associations and architecture (Fig. 3.9).

The lower unit, formed dominantly by facies association FA2, is only exposed on southern end of the outcrop belt (Fig. 3.9C) and has been measured only in one stratigraphic section (Fig. 3.9D). The lower part of the sandstone body C is dominated by *flat or low angle laminated to structureless sandstones* (F7 facies) and *heterolithic and very fine grained rippled sandstones* (F3 facies), capped by an erosional surface and a thick bed of *deformed laminated sandstone* (F6 facies). The contact between the lower unit and the overlying middle unit is mainly covered.

The middle unit of sandstone body C is dominated by facies association FA3, with little grain size variability (mostly fine and very fine sandstone) and numerous low angle erosional surfaces (Figs. 3.4I & 3.9C). The low angle erosional surfaces represent the bottom-sets of the low angle cross-strata of facies F7 (Fig. 3.4H). The erosional surfaces can be internal to F7 facies or they can erode into underlying *crowded Rosselia sandstone* (F8 facies); when the latter occurs, the mud bulbs of *Rosselia* are eroded and can be found resedimented laterally. The basal surface of this unit is covered. The middle unit is interpreted to have been generated by wave and storm reworking of sediments from the lower unit.

The upper unit of sandstone Body C is dominated by facies association FA 4, i.e., by *cross-bedded sandstones* (F10 facies) with sets between 0.5 and 1 meter thick, with south-easterly oriented paleocurrent directions (Fig. 3.10). The upper unit is interpreted to

have been deposited by tidal currents which are dominantly unidirectional. There are some intervals with *flaser to wispy laminated heterolithic sandstones* (F11 facies) and *crowded Rosselia sandstones* (F8 facies) representing inter-dunes areas or periods of decreased tidal influence due to the migration of the dunes into deeper water (Olariu *et al.*, 2012a). At the top of the sandstone body C there is a layer of *Skolithos highly bioturbated sandstones* (F12 facies) that represents the disappearance of the tidal currents probably due to increasing water depth, which brought about the drowning and abandonment of the sandstone body. There seems to be a gradual contact between the middle and upper unit, probably indicating a progressive change in the depositional processes from storm-wave to tidal currents. The upper boundary of the sandstone body is slightly gradational with cross-strata passing into the thin-bedded heterolithics of facies association FA1.

Paleocurrents and accretion surface dips are highly variable in Unit 2, showing generally north-easterly directions but also northwesterly and westerly directions. This can be expected in a storm dominated deposit which will present relatively chaotic orientation, non-withstanding a general major direction towards the north to northeast. Paleocurrents and accretion surfaces in Unit 3 are more consistent. Accretion surfaces are generally towards the northeast, while the paleocurrent indicators are oriented towards the north-west at high angle from the accretion surfaces.

Interpretation

Sandstone body C shows a more variable facies and architecture than the other bodies, reflecting a more complex evolution. Unit 1 (Figs. 3.9 & 3.10) is interpreted as the remnant of a shoreline, which during transgression was partially eroded by storm and fair-weather waves (Fig. 3.11). The sandstone was initially reworked mainly by wave and storm processes (Fig. 3.11); as reflected in the presence of HCS, SCS, abundant *Rosselia* (partially eroded) and low angle cross-stratification of Unit 2 (Figs. 3.9 & 3.10). The storm-dominated Unit 2 is overlain by the deposits of Unit 3 dominated by cross-strata (Figs. 3.9 & 3.10), suggesting a change in the dominant process from storm to tidal currents (Fig. 3.11).

The upper unit shows very similar facies with sandstone Body B i.e., a predominance of cross bedded sandstone facies. The cross-strata indicate predominant dune paleo-flow directions toward the north-west while the dominant master surfaces (surfaces between the cross-strata) dip toward the north-east, again indicating lateral accretion of the sand body. The top bounding surface of the sandstone body C represents the abandonment and drowning event of the tidal shelf ridge marked by the thin (dm thick) *Skolithos highly-bioturbated sandstone facies* (Facies F12).

The stacked and laterally connected environments (shoreface, storm-dominated and tidal-dominated bodies) of the sandstone body C suggest a more complex evolution of the sand body with changes between dominant processes, as discussed below.

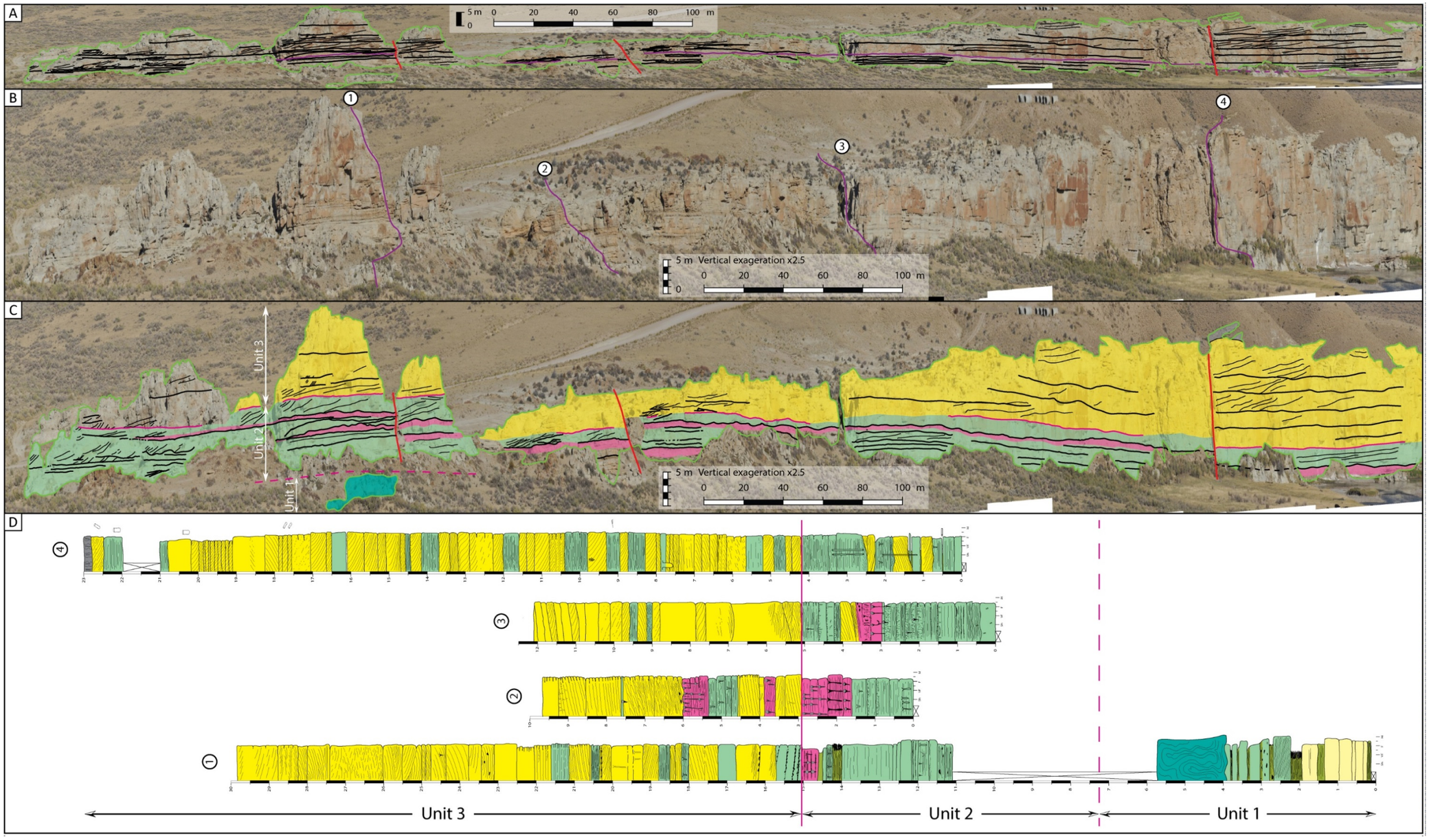
A
5 m
0
0
20
40
60
80
100 m
B
1
2
3
4
5 m Vertical exageration x2.5
0
0
20
40
60
80
100 m
C
Unit 3
Unit 2
Unit 1
5 m Vertical exageration x2.5
0
20
40
60
80
100 m
D
4
3
2
1
Unit 3
Unit 2
Unit 1

Figure 3.9

Figure 3.9: Outcrop study of sandstone body C. (A) Photomosaic of the north-western end of sandstone body C, with interpreted surfaces and no vertical exaggeration. (B) Same photomosaic as panel A with 2.5x vertical exaggeration and with the position of the measured sections. (C) Photomosaic of sandstone body C with surfaces and facies interpreted. (D) Measured sections of sandstone body C, showing the characteristics of the three described units. For color key see figure 3.5

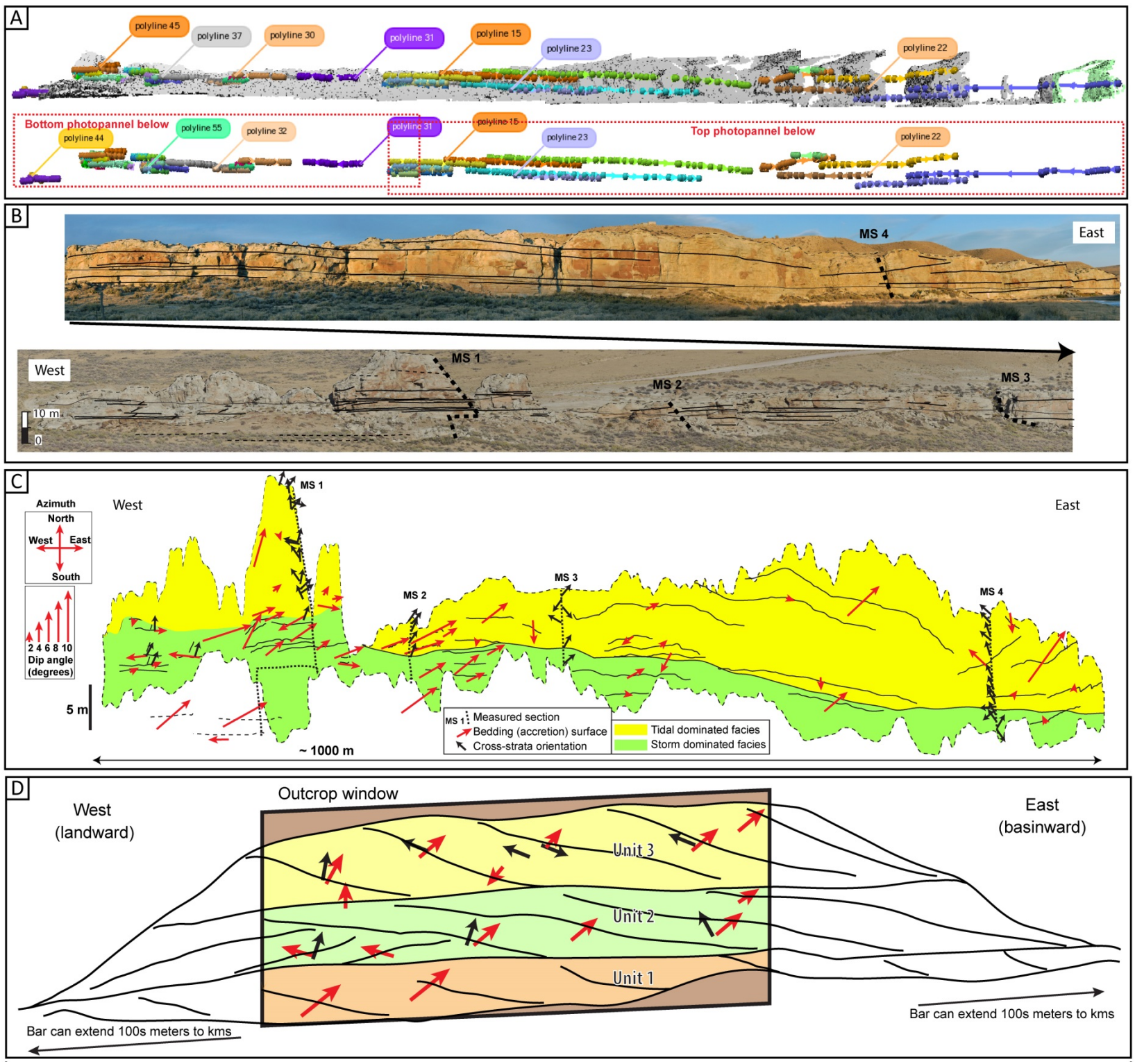

Fig. 3.10: Architecture of sandstone body C. (A) LiDAR images. In the top, point cloud with interpreted surfaces. In the bottom, extracted surfaces and photopanel location. (B) Photopanel with the surfaces extracted from the LiDAR data and the location of the measured sections. (C) Orientation of the bedding (accreting) surfaces (red arrows) extracted from LiDAR data and cross-strata foresets (paleocurrents) measured on the outcrop and on the LiDAR data (black arrows). Note the orientation of the arrow represents the azimuth of the surface and the length of the arrow its dip. (D) Summary interpretation of the bedding architecture.

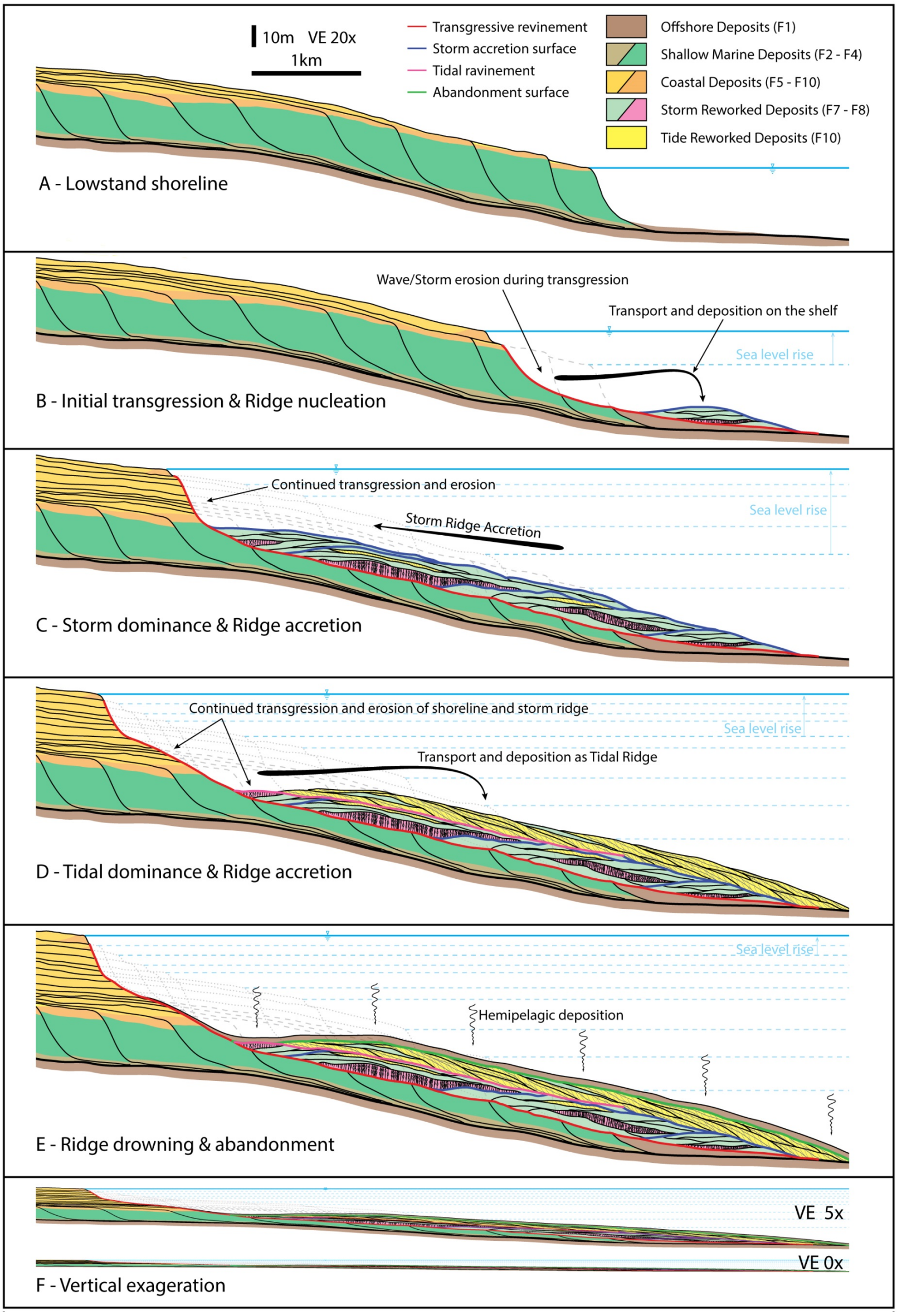

Fig. 3.11: Evolution of the transgressive shelf ridge sandstone body C. (A) Initial lowstand position of the coastal wedge. (B) Relative sea level raises causing erosion of the previous shallow marine deposits, which are deposited on the shelf. (C) Continued sea level raise and erosion of the coastal wedge, the sediments are reworked into storm deposits on the shelf that accrete to form a shelf storm ridge. (D) Tidal current become dominant over the storms which causes rework of the previous storm deposits and of the initial coastal wedge. The shelf ridge continues to accrete but as a tidal dominated ridge. (E) Continued sea level raise causes drowning and abandonment of the shelf ridge which gets covered by marine hemipelagic sediments. (E) Vertical exaggeration removed from panel E to better show the disconnection of the ridge from the contemporary shoreline and the architecture of the body.

DISCUSSION

The three sand-bodies presented above appear completely (Sandstone body B) or partially (Sandstone body C) encased in marine mudstones in a transgressive formation. The absence of basal erosional surface, heterolithic character and coarsening upward trend, sets sandstone body A apart from the two overlying bodies and together with the presence of HCS, SCS and symmetrical ripples characterize it as a wave and storm dominated shoreline.

Sandstone bodies B and C have some common key characteristics: 1) they are encased in very thick marine mud intervals above and below, 2) have a basal unconformity that erodes into marine muds or into the remnant of a previous shoreline, 2) their upper boundary is non-erosional and transitions into marine muds, 3) are formed by very clean and well-sorted sandstone, 4) contain fully marine ichnofauna, and 5) present complicated compounded architectures with large accretion surfaces and lesser order structures inside. These characteristics suggest that these sandstone bodies were deposited as shelf ridges with sediments reworked from previously transgressed shorelines.

Sandstone body B shows a simpler architecture than sandstone body C. The heterolithic lower unit in sandstone body C is interpreted as the remnants of an older lowstand shoreline that was eroded during transgression. The presence of this lower unit indicates that the ridge was in a relatively immature stage where the transgressive shelf ridge is still attached to the original shoreline, class 2 in Snedden and Dalrymple (1999). In contrast, sandstone body B does not preserve such a heterolithic unit, and therefore indicates a more evolved transgressive shelf ridge, class 3 in Snedden and Dalrymple (1999).

A striking characteristic of sandstone body C is the change in sedimentary processes from unit 1 and 2, dominated by storm currents with some subordinate tidal currents, to unit 3 where tidal currents became dominant and very few storm signals remaining. This process regime is likely caused by an increase of the tidal resonance of the basin, brought about by the sea level rise, and particularly by the significant widening of the shelf. This change in process regime is very common in the Western Interior Seaway where it has been observed how many regressive shorelines have variable process dominance (Plink-Bjorklund, 2008; Li *et al.*, 2011; Olariu *et al.*, 2012b; Olariu, 2014) and there is a significant change between wave and tidal processes between highstand and lowstand (Steel *et al.*, 2012).

The fact that sandstone body B does not present a change in process domination may be a result of its maturity; having completely reworked not only the original shoreline but also any storm reworked deposits. Or simply in this case the whole transgression may have been tidally dominated. Single process domination during the whole transgression is common in modern shelves; the New Jersey (Snedden *et al.*, 2011) shore has only been dominated by storms and has generated purely shelf storm ridges, while the strong tidal currents in the modern North Sea (Berne *et al.*, 1998; Trentesaux *et al.*, 1999) and China Sea (ZhenXia *et al.*, 1998) have produced tidal ridges with minimal storm deposit preservation.

The origin of sandstone bodies encased in offshore-mudstone

The origin of sharp-based, sandstone bodies encased in offshore mudstone can be a combination of structural and stratigraphic control (Martinsen, R. S., 2003a; b), or just stratigraphic controlled (Swift, D. J. P. *et al.*, 1995). Many sharp-based sand-

bodies, originally interpreted as shelf ridges (Tillman & Martinsen, 1984), have been later reinterpreted as falling-stage shorelines (Plint, 1988; Walker, R. G. & Bergman, 1993b). Recently, new emphasis has been put on the role of current (tides and waves) enhancement during transgression (Reynaud & Dalrymple, 2012), and a revived interest in shelf sandstone ridges is driven by new data on modern shelf ridges.

Three possible depositional environments for sandstone bodies encased in offshore mudstone have been recognized: forced regressive lowstand shorelines (Plint, 1988; Mellere & Steel, 1995; 2000; Steel *et al.*, 2012), transgressive storm shelf ridges (Snedden & Dalrymple, 1999; Bassetti *et al.*, 2006) and transgressive tidal shelf ridges (Davis & Balson, 1992; Davis *et al.*, 1993; Berne *et al.*, 1998; Reynaud *et al.*, 1999; Trentesaux *et al.*, 1999; Posamentier, 2002; Olariu *et al.*, 2012c; Schwarz, 2012). The characteristics of these three types of bodies, as recorded in the outcrops here presented and in previous examples in the literature, are explained below and summarized in Table 3.1. However, despite the differences between lowstand shorelines, storm ridges and tidal ridges presented in Table 1, this study emphasizes the possible transition and connections between those three end members.

During transgression the main controls on the preservation potential of the lowstand shorelines and the intensity of the transgressive reworking, that can lead to transgressive ridges, are the rate of sea level rise, the angle of shoreline transgression and the sediment supply (Cattaneo & Steel, 2003; and references therein)

Mud encased lowstand shorelines (Plint, 1988; Mellere & Steel, 1995; Steel *et al.*, 2012) would preserve shoreline characteristics such as coarsening and thickening upward trends, heterolithic character, and facies succession typical of wave or tide

dominated shorelines (Table 3.1 and of sandstone body A), while the isolated shelf ridges will present a sharp base and contain offshore ichnofauna and bedforms (Table 3.1 and sandstone body B).

The different units of sandstone body C (Figure 3.9 & 3.10) suggest a transition from shoreline to transgressive shelf ridge indicating a relatively immature stage of development of this ridge (Snedden & Dalrymple, 1999) but it also records a change in process domination during the shelf ridge development. In fact, even though most emphasis is placed in the end members descried in Table 1, most of these sandstone bodies will record some mixture of lowstand shoreline and of storm or tidal reworked deposits (Fig. 3.12) as shown in sandstone body C. This is so because the sand-sized material that forms the storm or tidal shelf ridges are sourced from older shorelines and it is very possible for a developing sand ridge to change its dominant process as sea level changed the oceanographic conditions or the morphology of the basin.

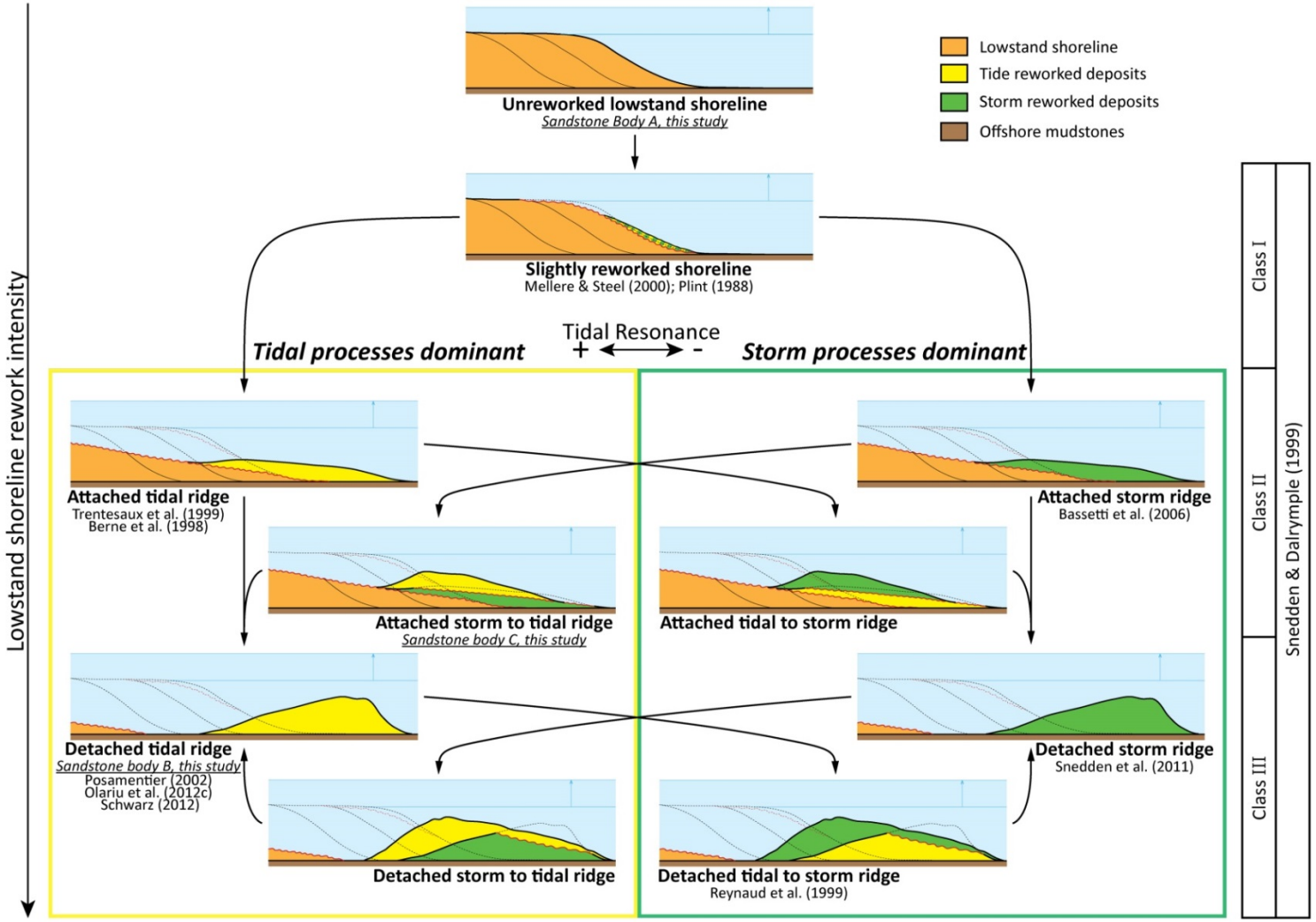

Fig. 3.12: Diagram showing the possible evolutionary paths of transgressive shelf ridges and their outcomes; emphasis is given to changes in process domination.

Table 3.1: Most important identification characteristics of lowstand shorelines, storm and wave transgressive shelf ridges and tidal transgressive shelf ridges as described in this work and from literature review (Houbolt, 1968; Swift, Donald J. P. & Field, 1981; Thomas & Anderson, 1994; Berne *et al.*, 1998; ZhenXia *et al.*, 1998; Reynaud *et al.*, 1999; Snedden & Dalrymple, 1999; Trentesaux *et al.*, 1999; van de Meene & van Rijn, 2000; Posamentier, 2002; Wood, 2004; Snedden *et al.*, 2011; Dalrymple, 2012; Olariu *et al.*, 2012a; Olariu *et al.*, 2012c; Reynaud & Dalrymple, 2012; Schwarz, 2012).

Characteristic criteria	Lowstand Shoreline	Storm-Wave Ridge	Tidal Ridge
Lower boundary	Gradational to erosional	Ravinement surface	Ravinement surface
Upper boundary	Abrupt (erosional) Ravinement deposits	Abrupt or gradual (recording the abandonment of the ridge)	Abrupt or gradual (recording the abandonment of the ridge)
Facies	Depends by the dominant processes at the shoreline	Dominated by HCS, SCS, wave ripples, graded beds Subordinate cross-strata	Dominated by cross-stratification (Compound dunes) Uncommon mud-drapes and flaser bedding
Internal surfaces	No internal surfaces No inclined accretion surfaces	Multiple internal erosion surfaces (storm generated) Possible inclined accretion surfaces.	Inclined laterally accreting surfaces. Possible presence of swatchway channels
Grain size trends	Coarsening upward	Any trend Commonly with no grain size trend	Any trend Commonly finning upward
Orientation	Parallel to paleocoast	Usually parallel or low angle to paleocoast	< 20º angle to predominant tidal current Any orientation to the paleocoast
Fauna	Shallow marine	Shallow marine macrofauna Fully marine microfauna	Shallow marine macrofauna Fully marine microfauna
Ichofauna	Shallow marine to brackish ichnofauna	Fully marine ichnofauna Possible crowded *Rosselia*	Fully marine ichnofauna
Connection to highstand shoreline	Possible	No	No
Source of the sand sediments	From a coeval delta (river fed sediment)	Reworked by storms from previous shoreline	Reworked by tidal currents from previous shoreline
Dimensions	Meters to tens of meters thick Laterally continuous for tens of kms	Meters to tens of meters thick Laterally continuous for kms?	Meters to tens of meters thick Laterally continuous for kms?
Water depth range	< 20 meters	40 – 110 meters	40 – 200 meters
Duration	10s Kyrs	Few Kyrs	Few Kyrs

CONCLUSIONS

The uppermost sandstone bodies in the Almond Formation are interpreted as shelf tidal ridges, being most likely formed from the reworking of sandstone from an earlier shoreline. Ancient shelf tidal ridges are recognized based on the pervasive presence of the tidal sand dune and compound-dune facies (Figs. 3.7 & 3.9), presence of obliquely-accreting internal accretion surfaces and the presence of a sharp to erosional base (Fig. 3.8 & 3.10). In the case of sandstone Body C, there was an interplay of wave-storm and tidal currents which is reflected in the preserved facies. In a basin with a change in tidal regime during transgression the transgressive shelf ridges will have a mixed storm-wave and tidal facies.

The lower and upper surfaces, large architectural geometry and the overall dimensions (meters to tens of meters thick) kms wide or long of the tidal- or storm-wave ridges are similar. However, the internal facies will be distinct with storm beds, structureless beds, HCS and SCS in the case of storm-wave ridge and cross-strata in the case of tidal ridge. Internal accretion surfaces are more obvious in the case of tidal ridges, while storm ridges present more internal erosive surfaces, as summarized in Table 3.1.

In previous studies much emphasis have been given to end members of the "transgressive shelf ridge" spectrum, while shelf ridges are likely to show a mixture of process domination and preservation of the previous lowstand shoreline that records the evolution of these bodies and the processes that dominated the shelf (Fig. 3.12).

REFERENCES

ALLEN, J.R.L. (1982) *Sedimentary Structures, Their Character and Physical Basis, Volume 2*. Elsevier, Amsterdam, Netherlands.

BADER, J.W., GILL, J.R., COBBAN, W.A. & LAW, B.E. (1983) Biostratigraphic Correlation Chart of Some Upper Cretaceous Rocks from the Lost Soldier Area, Wyoming to West of Craig, Colorado, U.S. Geological Survey. Denver, CO.

BASSETTI, M.A., JOUET, G., DUFOIS, F., BERNÉ, S., RABINEAU, M. & TAVIANI, M. (2006) Sand Bodies at the Shelf Edge in the Gulf of Lions (Western Mediterranean): Deglacial History and Modern Processes. *Marine Geology,* **234,** 93-109.

BERNE, S., LERICOLAIS, G., MARSSET, T., BOURILLET, J.F. & DE BATIST, M. (1998) Erosional Offshore Sand Ridges and Lowstand Shorefaces; Examples from Tide- and Wave-Dominated Environments of France. *Journal of Sedimentary Research*, **68,** 540-555.

BOGGS JR., S. (2012) Marginal Marine Environments. In: *Principles of Sedimentology and Stratigraphy* (Ed. by S. Boggs Jr.), 246-227. Pearson Education, Upper Saddle River, NJ.

CATTANEO, A. & STEEL, R.J. (2003) Transgressive Deposits: A Review of Their Variability. *Earth-Science Reviews*, **62,** 187-228.

COBBAN, W.A., WALASZCZYK, I., OBRADOVICH, J.D. & MCKINNEY, K.C. (2006) A Usgs Zonal Table for the Upper Cretaceous Middle Cenomanian--Maastrichtian of the Western Interior of the United States Based on Ammonites, Inoceramids, and Radiometric Ages. *USGS Open Report*, USGS. Denver**,** 45.

CRABAUGH, J.P. (2001) Nature and Growth of Nonmarine-to-Marine Clastic Wedges: Examples from the Upper Cretaceous Iles Formation, Western Interior (Colorado) and the Lower Paleogene Wilcox Group of the Gulf of Mexico Basin (Texas). Ph. D. Dissertation Thesis, University of Wyoming, Laramie.

DALRYMPLE, R.W. (1984) Morphology and Internal Structure of Sandwaves in the Bay of Fundy. *Sedimentology*, **31,** 365-382.

DALRYMPLE, R.W. (2012) Tidal Depositional Systems. In: *Facies Model 4* (Ed. by N. P. James & R. W. Dalrymple), 201-231. Geological Association of Canada, St. John's, Canada.

DAVIS, R.A. & BALSON, P.S. (1992) Stratigraphy of a North Sea Tidal Sand Ridge. *Journal of Sedimentary Research,* **62,** 116-121.

DAVIS, R.A., KLAY, J. & JEWELL, P. (1993) Sedimentology and Stratigraphy of Tidal Sand Ridges Southwest Florida Inner Shelf. *Journal of Sedimentary Research*, **63,** 91-104.

DOTT, R.H. & BOURGEOIS, J. (1982) Hummocky Stratification - Significance of Its Variable Bedding Sequences. *Geological Society of America Bulletin*, **93,** 663-680.

FLORES, R.M. (1978) Barrier and Back-Barrier Environments of Deposition of the Upper Cretaceous Almond Formation, Rock Springs Uplift, Wyoming. *Mountain Geologist*, **15,** 57-65.

GILL, J.R., MEREWETHER, E.A. & COBBAN, W.A. (1970) *Stratigraphy and Nomenclature of Some Upper Cretaceous and Lower Tertiary Rocks in South-Central Wyoming*. U.S. Geological Survey, Denver, CO.

GREEN, G.N. & DROUILLARD, P.H. (1994) The Digital Geologic Map of Wyoming in Arc/Info Format: U.S. Geological Survey, Open-File Report of-94-425, Scale 1:500000.

HAMPSON, G.J. & STORMS, J.E.A. (2003) Geomorphological and Sequence Stratigraphic Variability in Wave-Dominated, Shoreface-Shelf Parasequences. *Sedimentology*, **50,** 667-701.

HAQ, B.U., HARDENBOL, J. & VAIL, P.R. (1987) Chronology of Fluctuating Sea Levels since the Triassic. *Science*, **235,** 1156-1167.

HARMS, J.C., SOUTHARD, J.B., SPEARING, D.R. & WALKER, R.G. (1975) Stratification Produced by Migrating Bed Forms. In: *Depositional Environments as Interpreted from Primary Sedimentary and Stratigraphic Sequences* (Ed. by J. C. Harms, J. B. Southard, D. R. Spearing & R. G. Walker), *Sepm Short Course Notes*, **2**, 45-61. SEPM (Society for Sedimentary Geology).

HOUBOLT, J.J.H.C. (1968) Recent Sediments in the Southern Bight of the North Sea. *Geologie en Mijnbouw*, **47,** 245-273.

IZZET, G.A., COBBAN, W.A. & GILL, J.R. (1971) The Pierre Shale near Kremmling, Colorado, and Its Correlation to the East and the West. *Geological Survey Professional Paper*. U. S. G. Survey. **684-A**.

JORDAN, T.E. (1981) Thrust Loads and Foreland Basin Evolution, Cretaceous, Western United-States. *Aapg Bulletin-American Association of Petroleum Geologists*, **65,** 2506-2520.

KIEFT, R.L., HAMPSON, G.J., JACKSON, C.A.-L. & LARSEN, E. (2011) Stratigraphic Architecture of a Net-Transgressive Marginal- to Shallow-Marine Succession: Upper Almond Formation, Rock Springs Uplift, Wyoming, U.S.A. *Journal of Sedimentary Research*, **81,** 513-533.

LECKIE, D.A. & WALKER, R.G. (1982) Storm- and Tide-Dominated Shorelines in Cretaceous Moosebar-Lower Gates Interval; Outcrop Equivalents of Deep Basin Gas Trap in Western Canada. *AAPG Bulletin*, **66,** 138-157.

LEFEBRE, G.B. (1988) Tectonic Evolution of Hanna Basin, Wyoming: Laramide Block Rotation in the Rocky Mountain Foreland. Ph.D. Dissertation Thesis, University of Wyoming, Laramie, WY.

LEVA LÓPEZ, J. & STEEL, R.J. (In preparation) Campanian Laramide Signals and Architecture of a Widespread Fluvial Sheetsand: Canyon Creek Sandstone, Southern Wyoming.

LI, W.G., BHATTACHARYA, J. & ZHU, Y.J. (2011) Architecture of a Forced Regressive Systems Tract in the Turonian Ferron "Notom Delta", Southern Utah, USA. *Marine and Petroleum Geology*, **28,** 1517-1529.

LIU, S.F., NUMMEDAL, D. & LIU, L. (2011) Migration of Dynamic Subsidence across the Late Cretaceous United States Western Interior Basin in Response to Farallon Plate Subduction. *Geology*, **39,** 555-558.

MARTINSEN, O.J., MARTINSEN, R.S. & STEIDTMANN, J.R. (1993) Mesaverde Group (Upper Cretaceous), Southeastern Wyoming - Allostratigraphy Versus Sequence Stratigraphy in a Tectonically Active Area. *Aapg Bulletin-American Association of Petroleum Geologists*, **77,** 1351-1373.

MARTINSEN, R.S. & CHRISTIANSEN, G.E. (1992) A Stratigraphic and Environmental Study of the Almond Formation, Mesaverde Group, Greater Green River Basin, Wyoming. In: *Rediscover the Rockies; 43rd Annual Field Conference Guidebook* (Ed. by C. E. Mullen), 171-190. Wyoming Geological Association, Casper, WY.

MARTINSEN, R.S. (1995) Stratigraphy and Lithofacies of the Almond Formation, Washakie and Great Divide Basins, Wyoming. *Guidebook - Wyoming Geological Association*. G. E. Christiansen, M. A. Olson & R. C. Surdam, Wyoming Geological Association : Casper, WY, United States. United States. **1995,** 297-310.

MARTINSEN, R.S. (1998) Compartmentalization of Sandstone Reservoirs Due to Syndepositional Faulting, Almond Formation, Washakie Basin, Wyoming. In: *Compartmentalized Reservoirs in Rocky Mountain Basins* (Ed. by R. M. Slatt),

Rmag Symposium, 71-98. The Rocky Mountain Association of Geologists, Denver, CO.

MARTINSEN, R.S. (2003a) Depositional Remnants, Part 2: Examples from the Western Interior Cretaceous Basin of North America. *Aapg Bulletin*, **87,** 1883-1909.

MARTINSEN, R.S. (2003b) Depositional Remnants, Part 1: Common Components of the Stratigraphic Record with Important Implications for Hydrocarbon Exploration and Production. *Aapg Bulletin*, **87,** 1869-1882.

MASTERS, C.D. (1966) Sedimentology of the Mesaverde Group and of the Upper Part of the Mancos Formation, Northwestern Colorado, Yale University, New Haven.

MELLERE, D. & STEEL, R.J. (1995) Variability of Lowstand Wedges and Their Distinction from Forced-Regressive Wedges in the Mesaverde Group, Southeast Wyoming. *Geology*, **23,** 803-806.

MELLERE, D. & STEEL, R.J. (2000) Style Contrast between Forced Regressive and Lowstand/Transgressive Wedges in the Campanian of South-Central Wyoming (Hatfield Member of the Haystack Mountains Formation). *Geological Society, London, Special Publications*, **172,** 141-162.

NARA, M. (1995) Rosselia Socialis - a Dwelling Structure of a Probably Terebellid Polychaete. *Lethaia*, **28,** 171-178.

NARA, M. (1997) High-Resolution Analytical Method for Event Sedimentation Using Rosselia Socialis. *Palaios*, **12,** 489-494.

NARA, M. (2002) Crowded Rosselia Socialis in Pleistocene Inner Shelf Deposits: Benthic Paleoecology During Rapid Sea-Level Rise. *Palaios*, **17,** 268-276.

OBRADOVICH, J.D. (1993) A Cretaceous Time Scale. In: *Evolution of the Western Interior Basin* (Ed. by W. G. E. Caldwell & E. G. Kauffman), **Special Paper**, 379-396. Geological Association of Canada.

OLARIU, C., STEEL, R.J., DALRYMPLE, R.W. & GINGRAS, M.K. (2012a) Tidal Dunes Versus Tidal Bars: The Sedimentological and Architectural Characteristics of Compound Dunes in a Tidal Seaway, the Lower Baronia Sandstone (Lower Eocene), Ager Basin, Spain. *Sedimentary Geology*, **279,** 134-155.

OLARIU, C. (2014) Autogenic Process Change Modern Deltas: Lessons for the Ancient. In: *From Depositional Systems to Sedimentary Successions on the Norwegian Continental Shelf* (Ed. by A. W. Martinius, R. Ravnås, J. A. Howell, R. Steel, . J. & J. P. Wonham), *Int. Assoc. Sedimentol. Spec. Publ.*, **46**, 149-166. John Wiley & Sons, Inc.

OLARIU, M.I., CARVAJAL, C.R., OLARIU, C. & STEEL, R.J. (2012b) Deltaic Process and Architectural Evolution During Cross-Shelf Transits, Maastrichtian Fox Hills Formation, Washakie Basin, Wyoming. *AAPG Bulletin*, **96,** 1931-1956.

OLARIU, M.I., OLARIU, C., STEEL, R.J., DALRYMPLE, R.W. & MARTINIUS, A.W. (2012c) Anatomy of a Laterally Migrating Tidal Bar in Front of a Delta System: Esdolomada Member, Roda Formation, Tremp-Graus Basin, Spain. *Sedimentology*, **59,** 356-378.

PANG, M. & NUMMENDAL, D. (1995) Flexural Subsidence and Basement Tectonics of the Cretaceous Western Interior Basin, United-States. *Geology*, **23,** 173-176.

PEMBERTON, S.G. & MACEACHERN, J.A. (1995) The Sequence Stratigraphic Significance of Trace Fossils: Examples from the Cretaceous Foreland Basin of Alberta, Canada. In: *Sequence Stratigraphy of Foreland Basin Deposits* (Ed. by J. C. Van Wagoner & G. T. Bertram), *Memoirs*, **64**, 429-475. American Association of Petroleum Geologists, Tulsa, OK.

PLINK-BJORKLUND, P. (2008) *Wave-to-Tide Facies Change in a Campanian Shoreline Complex, Chimney Rock Tongue, Wyoming-Utah, USA*. SEPM - Soc Sedimentary Geology, Tulsa.

PLINT, A.G. (1988) Sharp-Based Shoreface Sequences and "Offshore Bars" in the Cardium Formation of Alberta: Their Relationship to Relative Changes in Sea Level. In: *Sea Level Changes: An Integrated Aproach* (Ed. by C. K. Wilgus, B. S. Hastings, H. W. Posamentier, J. C. Van Wagoner, A. C. Ross & C. G. S. C. Kendall), *Sepm Special Publication*, **42**, 357-370. SEPM, Tulsa, OK.

PLINT, A.G. (2010) Wave- and Storm-Dominated Shorelines and Shallow-Marine Systems. In: *Facies Models 4* (Ed. by N. P. James & R. W. Dalrymple), 167-201. Geological Association of Canada, St.John's, Newfoundland & Labrador.

POSAMENTIER, H.W. (2002) Ancient Shelf Ridges—a Potentially Significant Component of the Transgressive Systems Tract: Case Study from Offshore Northwest Java. *AAPG Bulletin*, **86,** 75-106.

REYNAUD, J.-Y., TESSIER, B., PROUST, J.-N., DALRYMPLE, R., MARSSET, T., DE BATIST, M., BOURILLET, J.-F. & LERICOLAIS, G. (1999) Eustatic and Hydrodynamic Controls on the Architecture of a Deep Shelf Sand Bank (Celtic Sea). *Sedimentology*, **46,** 703-721.

REYNAUD, J.-Y. & DALRYMPLE, R.W. (2012) Shallow-Marine Tidal Deposits. In: *Principles of Tidal Sedimentology* (Ed. by R. A. Davis Jr & R. W. Dalrymple), 335-369. Springer, Dordrecht.

ROEHLER, H.W. & HANSEN, D.E. (1989) Surface and Subsurface Correlations Showing Depositional Environments of Upper Cretaceous Mesaverde Group and Associated Formations, Lost Soldier Field to Cow Creek, Southwest Wyoming, U.S. Geological Survey. Denver, CO.

ROEHLER, H.W. (1990) *Stratigraphy of the Mesaverde Group in the Central and Eastern Greater Green River Basin, Wyoming, Colorado and Utah* U.S. Geological Survey, Denver, CO.

SCHWARZ, E. (2012) Sharp-Based Marine Sandstone Bodies in the Mulichinco Formation (Lower Cretaceous), Neuquen Basin, Argentina: Remnants of Transgressive Offshore Sand Ridges. *Sedimentology*, **59**.

SNEDDEN, J.W. & DALRYMPLE, R.W. (1999) Modern Shelf Sand Ridges: From Historical Perspective to a Unified Hydrodynamic and Evolutionary Model. In: *Isolated Shallow Marine Sand Bodies : Sequence Stratigraphic Analysis and Sedimentologic Interpretation* (Ed. by K. M. Bergman & J. W. Snedden), *Sepm Special Publication No.64*, **64**, 13-28. SEPM (Society for Sedimentary Geology), Tulsa, OK.

SNEDDEN, J.W., TILLMAN, R.W. & CULVER, S.J. (2011) Genesis and Evolution of a Mid-Shelf, Storm-Built Sand Ridge, New Jersey Continental Shelf, U.S.A. *Journal of Sedimentary Research*, **81,** 534-552.

STEEL, R.J., PLINK-BJORKLUND, P. & ASCHOFF, J. (2012) Tidal Deposits of the Campanian Western Interior Seaway, Wyoming, Utah and Colorado, USA. In: *Principles of Tidal Sedimentology* (Ed. by R. A. Davis Jr & R. W. Dalrymple), 437-471. Springer Netherlands.

SWIFT, D.J.P. & FIELD, M.E. (1981) Evolution of a Classic Sand Ridge Field: Maryland Sector, North American Inner Shelf. *Sedimentology*, **28,** 461-482.

SWIFT, D.J.P., SNEDDEN, J.W. & PLINT, A.G. (1995) Tongues, Ridges and Wedges: Highstand Versus Lowstand Architecture in Shallow Marine Basins. *SEPM Field Research Conference*, SEPM. Casper and Thermopolis, Wyoming. **June 24-29, 1995**.

THOMAS, M.A. & ANDERSON, J.B. (1994) Sea-Level Controls on the Facies Architecture of the Trinity/Sabine Incised-Valley System, Texas Continental Shelf. In: *Incised-Valley Systems* (Ed. by R. W. Dalrymple, R. Boyd & B. A. Zaitlin), *Sepm Special Publication*, **51**, 63-82. SEPM (Society for Sedimentary Geology), Tulsa, OK.

TILLMAN, R.W. & MARTINSEN, R.S. (1984) The Shannon Shelf-Ridge Sandstone Complex, Salt Creek Anticline Area, Powder River Basin, Wyoming. In:

Siliciclastic Shelf Sediments (Ed. by R. W. Tillman & C. T. Siemers), *Special Publication*, **34**, 85-142. SEPM (Society for Sedimentary Geology), Tulsa, OK.

TOBIN, R.C., MCCLAIN, T., LIEBER, R.B., OZKAN, A., BANFIELD, L.A., MARCHAND, A.M.E. & MCRAE, L.E. (2010) Reservoir Quality Modeling of Tight-Gas Sands in Wamsutter Field: Integration of Diagenesis, Petroleum Systems, and Production Data. *AAPG Bulletin*, **94,** 1229-1266.

TRENTESAUX, A., STOLK, A. & BERNÉ, S. (1999) Sedimentology and Stratigraphy of a Tidal Sand Bank in the Southern North Sea. *Marine Geology*, **159,** 253-272.

VAN DE MEENE, J.W.H. & VAN RIJN, L.C. (2000) The Shoreface-Connected Ridges Along the Central Dutch Coast — Part 1: Field Observations. *Continental Shelf Research*, **20,** 2295-2323.

WALKER, R.G. & BERGMAN, K.M. (1993a) Shannon Sandstone in Wyoming; a Shelf-Ridge Complex Reinterpreted as Lowstand Shoreface Deposits. *Journal of Sedimentary Research*, **63,** 839-851.

WALKER, R.G. & BERGMAN, K.M. (1993b) Shannon Sandstone in Wyoming: A Shelf-Ridge Complex Reinterpreted as Lowstand Shoreface Deposits. *Journal of Sedimentary Petrology*, **63,** 839-851.

WOOD, L.J. (2004) Predicting Tidal Sand Reservoir Architecture Using Data from Modern and Ancient Depositional Systems. In: *Integration of Outcrop and Modern Analogs in Reservoir Modeling* (Ed. by G. M. Grammer, P. M. Harris & G. P. Eberli), *Aapg Memoir*, **80**, 45-66. The American Association of Petroleum Geologists, Tulsa, OK.

ZHENXIA, L., DONGXING, X., BERNE, S., KUIYANG, W., MARSSET, T., YUXIANG, T. & BOURILLET, J.F. (1998) Tidal Deposition Systems of China's Continental Shelf, with Special Reference to the Eastern Bohai Sea. *Marine Geologyv*, **145,** 225-253.

Chapter Four: Autoacceleration of clinoform progradation in foreland basins: Theory and experiments[1]

ABSTRACT

Understanding the relationship between sedimentation and tectonics is critical to the analysis of stratigraphic evolution in foreland basins. Previous models of foreland basins have explained stratal development, but were done generally under the assumption that steady allogenic forcing produces a steady stratigraphic response. They did not consider autogenic shoreline behavior during the development of the subsidence pattern characteristic of foreland basins.

We present a mathematical model and flume experiments that explore how subsidence and sediment-supply rates control the shoreline trajectory and the stratal patterns that fill foreland basins. Through these models, we found differing autogenic responses in the rate and direction of shoreline migration, and these generated three distinct styles of stratal architecture, despite the constant external forcing (i.e., constant sediment discharge and basin substrate tilting).

The first response was "autoretreat", where shoreline migration switched from initial progradation to retrogradation. The second response was progradation followed by constant aggradation of the shoreline. The third response was maintained progradation with a markedly accelerating rate. We termed this latter, newly observed autogenic behavior "shoreline autoacceleration".

[1] LEVA LÓPEZ, J., KIM, W. & STEEL, R.J. (2014) Autoacceleration of Clinoform Progradation in Foreland Basins: Theory and Experiments. *Basin Research*, **26,** 489-504.
Kim,W. and Steel, R.J. supervised the research contained in this article.

These three modes of shoreline behavior and their accompanying stratal architecture provide a basic framework for the relationship between sedimentation and tectonic activity in foreland basins under the simplified conditions presented here.

INTRODUCTION

Foreland basins are depressions on continental crust caused by the downward flexure of the lithosphere under the weight of a growing orogenic thrust wedge, which can appear on both sides of the mountain belt. If the orogen is created through the subduction of oceanic lithosphere under continental lithosphere, the basin created on the continental side of the orogen is termed a *retro-arc* foreland basin (Dickinson, 1974; Jordan, 1995). If the orogen is created through collision of continental lithosphere, one basin will form on the underthrusted plate, the *pro*-foreland basin, whereas another basin will form on the overthrusted plate, the *retro*-foreland basin (Naylor & Sinclair, 2008).

The growing orogen sheds large volumes of sediment creating clastic wedges that prograde into the basin, at times reaching the peripheral bulge or beyond (Jordan, 1981; Ingersoll, 1988; Jordan, 1995; DeCelles & Giles, 1996; Catuneanu, 2004; Naylor & Sinclair, 2008). Pro-foreland basins generally see an accelerated tectonic subsidence created by the movement of the basin fill towards the orogenic wedge (Naylor & Sinclair, 2008).

Types of foreland basin-fill modeling

There are several ways to model foreland-basin infill; the choice of model depends primarily on the focus of the study. Mass-balance geometrical models are ideal for large-scale, long-term modeling and especially for tracking moving boundaries such as the shoreline or the shelf-edge (Blair & Bilodeau, 1988; Heller *et al.*, 1988). These models are deterministic, in as much as the geometry of the sediment fill is predetermined and the

volume (or area in 2D studies) of the sediment pile balances with the volume of sediment introduced into the system. Geometrical models do not account for the response-time present in natural systems; the adjustment of the sediment-pile geometry in response to allogenic forcing; or for any feedback between tectonics, subsidence, and sedimentation that may develop in natural systems. However, due to these simplifications, the relationship between external forcing and stratal pattern can be clearly visualized.

Another school of modeling uses diffusive sediment transport and an elastic response for the lithospheric loading (Flemings, P.B. & Jordan, 1989; Flemings, P. B. & Jordan, 1990; Sinclair *et al.*, 1991). The models assume that sediment transport is a function of downstream sediment surface slope. The advantage of this approach is that it can capture stratal geometries produced under a wide range of initial and boundary conditions (Flemings, Peter B & Grotzinger, 1996).

There are also more recent, three-dimensional forward numerical models (Garcia-Castellanos, 2002; Clevis *et al.*, 2003; Garcia-Castellanos *et al.*, 2003; Clevis *et al.*, 2004) that allow river network development and investigation of interactions between the dynamics of the orogenic belt, the subsidence style of the basin, and the sedimentation and erosional processes. The strength of these models is their ability to incorporate feedback between allogenic drivers and fluvial evolution. However, extracting the signature of each forcing mechanism in the resulting stratigraphy is not straightforward, if even possible.

The objective of this paper is to further understand the fundamental stratigraphic responses, particularly the shoreline or shelf-edge trajectory responses, to the particular subsidence style of the foreland basin. A mass-balance geometrical model is most appropriate for examining these trajectories under steady allogenic forcing and for building a better understanding of the relationship between rate of back-tilting subsidence and the resultant stratigraphy.

Clastic-wedge migration and tectonics

The timing of clastic-wedge migration in retro-arc foreland basins relative to the onset of crustal thickening in the adjacent orogen has been intensely debated for several decades (Blair & Bilodeau, 1988; Heller *et al.*, 1988; Steel, 1988; Flemings, P.B. & Jordan, 1989; Burbank *et al.*, 1992; Devlin *et al.*, 1993; DeCelles *et al.*, 1995; Catuneanu *et al.*, 1998; Marzo & Steel, 2000; Crabaugh, 2001; Yang & Miall, 2010; Aschoff & Steel, 2011; Yang, 2011). Knowledge of the relative timing of tectonic events and clastic wedge growth into the basin, as well as the absolute ages of both, is crucial for understanding the drivers of clastic wedge evolution in foreland basins (Cross & Pilger, 1978; Heller *et al.*, 1986; Pang & Nummendal, 1995; Horton *et al.*, 2004).

Before the 1980s, conceptual models described progradation of coarse-grained clastic wedges as syntectonic (e.g. Marshall (1951), King (1959), Van Houten (1974)). However, subsidence in a retro-arc foreland basin is now known to be mostly associated with the flexural response of the lithosphere to tectonic loading of the orogen. Since the late 1980s, it has also been generally accepted that the orogenic pulse coincides with the maximum subsidence rate in the foreland basin, at which time sediments are trapped in the proximal region of the foredeep depositional zone, adjacent to the orogen (Fig. 4.1A). This conceptual model was first mooted by Blair and Bilodeau (1988), Steel (1988) and Heller *et al.* (1988). The latter authors put this in the context of a "two-phase" model, suggesting that there are some poorly defined time lags between the thrust pulse, basin subsidence, and the main pulse of coarse-grained sediment out into the basin. Heller *et al.* (1988) advocated entrapment of the coarsest sediments next to the growing orogen during the main thrust pulse.

Recently, field evidence has suggested that if the sediment flux into the basin is large enough, it can overwhelm the subsidence of the foredeep such that more extensive clastic wedge progradation becomes synchronous with the main thrusting events

(Burbank *et al.*, 1992; Marzo & Steel, 2000; Horton *et al.*, 2004) (Fig. 4.1B). This is consistent with more comprehensive conceptual studies (Heller & Paola, 1992; Paola *et al.*, 1992) showing how forcing of sediment flux, basin subsidence or other factors produces different responses in basin stratigraphy.

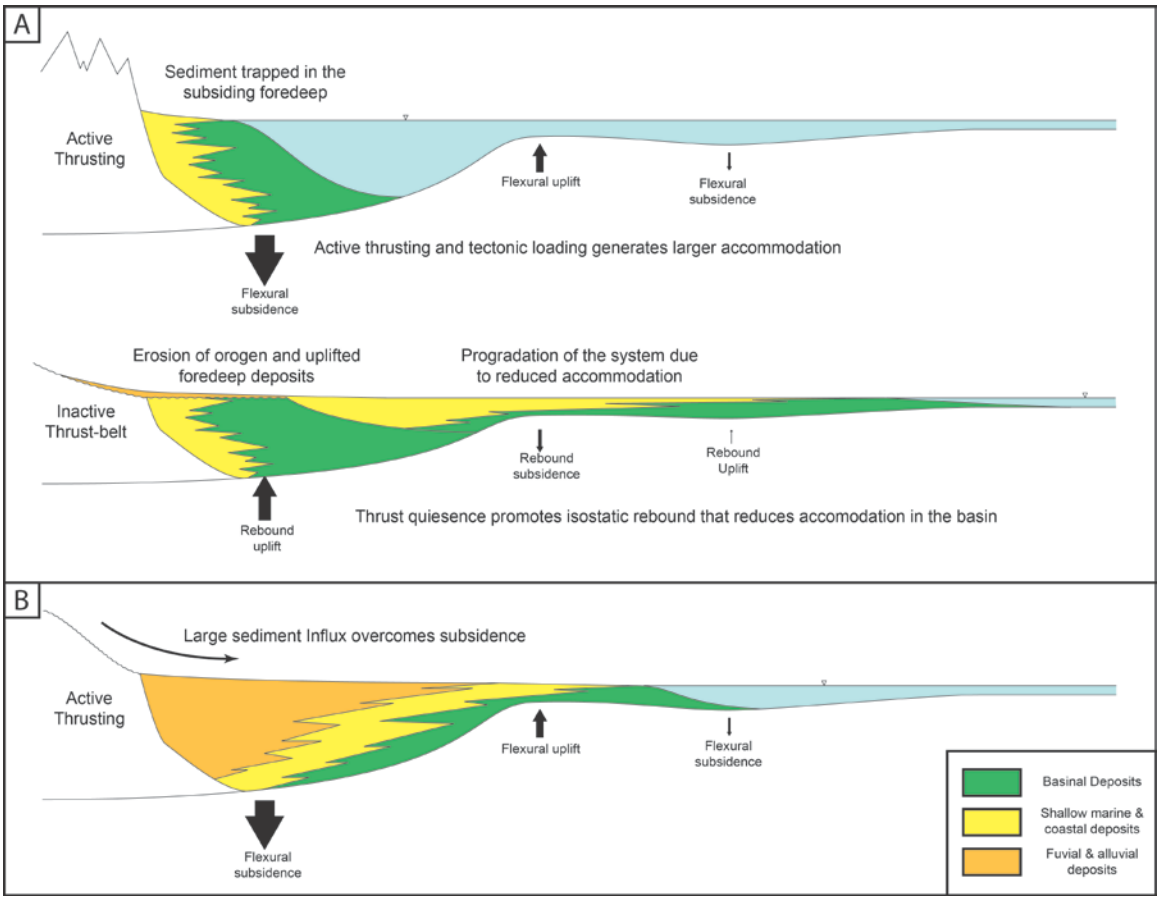

Figure 4.1: Depositional models for foreland basins in relation to the tectonic activity of the orogen. This figure is highly schematic and the vertical scales vary laterally, the peripheral bulge and the back-bulge basin are exaggerated compared to the foredeep. A: Post-orogenic progradation of clastic wedges in response to variations in the subsidence-uplift of the basin (Blair & Bilodeau, 1988; Heller *et al.*, 1988). B: Synorogenic progradation of clastic wedges due to large sediment influx (Burbank *et al.*, 1992; Marzo & Steel, 2000; Horton *et al.*, 2004).

Despite the abundance of hypotheses on the timing of sediment wedge progradation relative to the orogenic pulse and its flexural response, a fundamental piece of understanding is missing from earlier proposals, namely the response of a prograding wedge or the deltaic shoreline (at the tip of the wedge) to constant back-tilting subsidence.

Autostratigraphy and shoreline studies

Conventional stratigraphy generally assumes an equilibrium response of depositional systems to external forcing, whereby the shoreline, or shelf-edge, trajectory is in a constant state of progradation, retrogradation or aggradation under a given balance between sediment supply and accommodation. This equilibrium response is also one of the underlying assumptions in sequence stratigraphy (Jervey, 1988; Posamentier & Vail, 1988; Galloway, 1989; Schlager, 1993; Gawthorpe *et al.*, 1994). The models presented previously are based on this assumption.

Physical and numerical studies of shoreline response to steady forcing of the external variables, have recently demonstrated that non-equilibrium responses of shoreline movement are equally or more common than equilibrium responses (Tomer *et al.*, 2011). Such non-equilibrium responses were exemplified by experiments showing the development of shoreline autoretreat or of multiple cycles of terrace development and valley incision despite constant forcing of sediment supply and base level change (Muto & Steel, 1997; 2004), and have been formalized into the concept of *autostratigraphy* (Muto *et al.*, 2007). These concepts have been included in modern studies of shoreline and shelf-edge trajectories (Henriksen *et al.*, 2009; Ryan *et al.*, 2009), which better define and unravel the stratigraphic signatures of allogenic forcing.

The present study uses a combination of geometrical modeling and flume experiments to explore the autostratigraphic response of sedimentary systems to tectonic forcing in foreland basins. We conducted experiments in a two-dimensional flume and examined the control exerted by differential rates of back-tilting subsidence on shoreline (or shelf-edge) migration and the accompanying stratigraphic patterns. The geometrical model was developed to predict a two-dimensional evolution of the shoreline position during sediment wedge progradation, and was tested with physical experiments. Both mathematical and experimental investigations were conducted under steady allogenic forcing, using a constant rate of basement tilting and constant sediment flux, which isolated the control of foreland basin-type subsidence on the shoreline (or self-edge) migration.

Although this paper discusses mainly the implications for *retro-arc* and *retro*-foreland basins, the mathematical model is applicable to any basin undergoing back-tilted hinge type subsidence that has a sediment source next to the main locus of subsidence e.g. some rift and pull-apart basins.

MATHEMATICAL SHORELINE MODEL

Consider a laterally averaged, two dimensional (x being the down-basin coordinate and z the vertical coordinate) coastal prism that progrades across a back-tilting, subsiding basin (Fig. 4.2). The model assumes that 1) the coastal prism advances into a standing body of water, 2) the fluvial topset and delta foreset slopes are linear and do not change through time, 3) there is no sediment dispersal out onto the basin floor beyond the coastal prism and therefore there is no bottomset, and 4) allogenic controls (i.e., sediment supply and basin tilting rate) are constant through time.

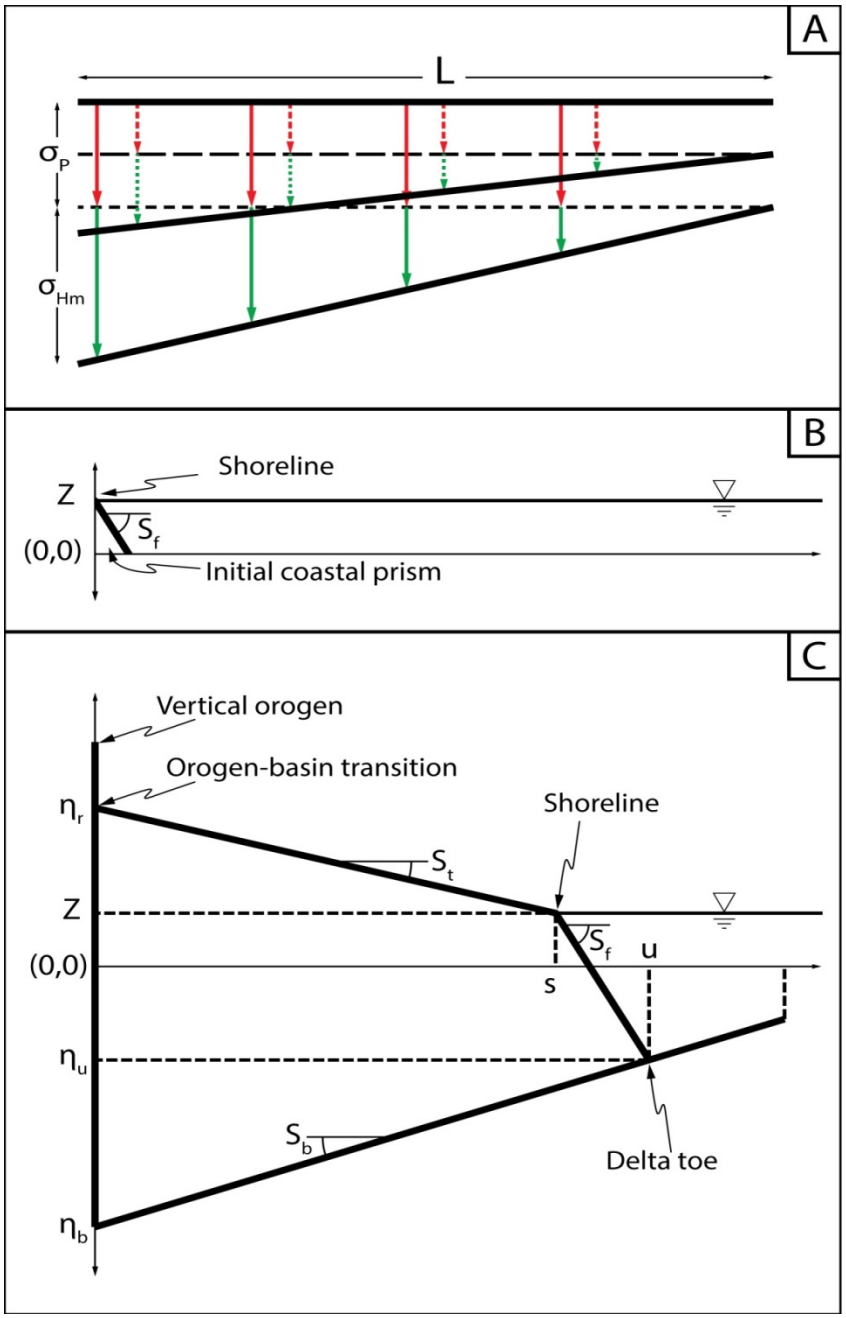

Figure 4.2: A: Three time stages of the subsidence pattern applied to the model. The initial step with horizontal basement and two incremental steps (dashed arrows second step and bold arrows third step) showing the piston-like (red arrows) and hinge-like (green arrows) subsidence. B: Initial configuration of the modeled coastal prism prior to the introduction of any subsidence or sediment. C: Geometry of the modeled deltaic body and the main variables.

The coastal prism is two-dimensional such that the topography is averaged laterally across the basin width. The foreset and topset slopes, S_f and S_t respectively, are assumed to be constant across the basin length. Sediment flux (q_s) is assumed constant through time (t) and is supplied to the upstream orogen-basin transition at $x = 0$ and $z = \eta_r(t)$. The orogen-basin transition is fixed in the x direction, but it is able to vertically aggrade against the upstream vertical orogen slope (Fig 4.2C).

The coastal prism has a subaerial topset bounded downstream by the shoreline at $x = s(t)$; $z = Z(t)$. The topset is coupled with a subaqueous foreset that terminates downstream at the delta toe at $x = u(t)$; $z = \eta_u(t)$ (Fig. 4.2C). The base level of the delta front is defined as $Z = Z_i + (dZ/dt) \cdot t$, where Zi denotes the initial base level and dZ/dt denotes the rate of base-level change. This base-level equation allows for testing of steady base-level rise and fall on the basin evolution by using a constant value for dZ/dt. The subsidence is composed of both a spatially uniform "piston-type" component at a rate of σ_P and a "hinge-type" component $\sigma_H(x) = (x/L)\ \sigma_{Hmax}$, where σ_{Hmax} is the rate at the orogen-basin transition (Fig. 4.2A). The hinge-type subsidence rate decreases linearly away from the transition and becomes zero at the downbasin end ($x = L$). The slope of the basement (S_b) increases with time due to the hinge-type subsidence (Fig. 4.2C). As a simplification, neither base-level change nor piston-type subsidence were applied to the model runs described below and thus $dZ/dt = 0$ and $\sigma_P = 0$. However the model is applicable to a basin that experiences base-level fluctuations or that has a complex subsidence pattern.

Prior to the onset of sedimentation the model considers a triangular initial coastal prism with no topset, of area A_i. In this way, we avoid the modeling artifact of a shoreline position with a negative sign in the initial part of run (Fig. 4.2B).

Sediment mass balance of the coastal-deltaic prism takes the following form:

$$q_s t + A_i = \left[\frac{1}{2}(\eta_r - Z)s + \frac{1}{2}(Z - \eta_u)s + \frac{1}{2}(Z - \eta_b)u\right](1 - \varphi) \quad (1)$$

where φ is the porosity of the deposits.

Equation (1) can be rearranged to solve for the shoreline position:

$$0 = \left(S_f - \alpha S_f^2 - S_t\right)s^2 + 2\alpha S_f(Z - \eta_b)s - \alpha(Z - \eta_b)^2 - \frac{2(q_s t + A_i)}{1-\varphi} \quad (2)$$

where

$$\alpha = \left(S_f - S_b\right)^{-1} \quad (3a)$$

$$Z = Z_i + \frac{\partial Z}{\partial t}t \quad (3b)$$

$$\eta_b = (\sigma_P + \sigma_{Hmax})t \quad (3c)$$

$$s_b = \frac{\sigma_{Hmax} t}{L} \quad (3d)$$

Solving for the downstream shoreline position using a quadratic formula yields the following relation:

$$s = \frac{-2\alpha S_f(Z-\eta_b) + \sqrt{\left[2\alpha S_f(Z-\eta_b)\right]^2 + 4\left(S_f - \alpha S_f^2 - S_t\right)\left[\alpha(Z-\eta_b)^2 + \frac{2(q_s t + A_i)}{1-\varphi}\right]}}{2\left(S_f - \alpha S_f^2 - S_t\right)} \quad (4)$$

and the other moving boundaries can then be written as:

$$u = \alpha\left(S_f s - Z + \eta_b\right) \quad (5a)$$

$$\eta_u = u S_b + \eta_b \quad (5b)$$

$$\eta_r = Z - S_t s \quad (5c)$$

The evolution of the coastal prism is largely dependent on the subsidence rate applied to the total basin length and the sediment influx in the basin. Here we use the characteristic length scale (Λ) and the characteristic time scale (τ), as follows:

$$\Lambda = L \quad (6a)$$

$$\tau = \Lambda({\sigma_H}^{-1}) \quad (6b)$$

to present the modeling results in dimensionless form. The tectonic length of the basin is used for the length scale, while the accommodation creation time scale is chosen for the characteristic basin time scale. The results of the shoreline migration in dimensionless form facilitate scaling of the modeling and experimental results to field conditions.

A list of all the variables can be found in Table 4.1.

MODEL TEST RUNS

To help visualize the results of this model, we have created synthetic plots that represent the stratigraphy generated by the model (Fig. 4.3), analogous to a series of reflectors in a seismic dataset. The model creates surfaces by connecting the position of the moving boundaries (i.e. toe-of-slope, shoreline and alluvium-orogen transition) for discrete time steps. The position of each time step is then corrected for the final subsidence to create the final strata.

A key result of the model is the shoreline trajectory, defined as the shoreline migration path through time in a dip-oriented cross-section of the stratal unit (Helland-Hansen & Gjelberg, 1994; Muto & Steel, 1997). The shoreline trajectory reflects the progradational or retrogradational history of the coastal depositional system.

Table 4.1: List of variable names in the model

x	Horizontal coordinate axis
z	Vertical coordinate axis
t	Time
L	Length of the basin
q_s	Sediment flux
A_i	Initial area of sediment pile
σ_P	Piston-like subsidence rate
σ_H	Hinge-like subsidence rate
σ_{Hmax}	Maximum hinge-like subsidence rate (at x=0)
s	Shoreline position x coordinate
Z	Base level (z coordinate)
Z_i	Initial base level
u	Delta toe position in x coordinate
η_u	Delta toe elevation in z coordinate
η_r	Orogen-basin surface boundary z coordinate
η_b	Orogen-basin basement boundary z coordinate
S_t	Topset slope
S_f	Foreset slope
S_b	Basement Slope
φ	Deposit porosity
Λ	Characteristic length scale
T	Characteristic time scale

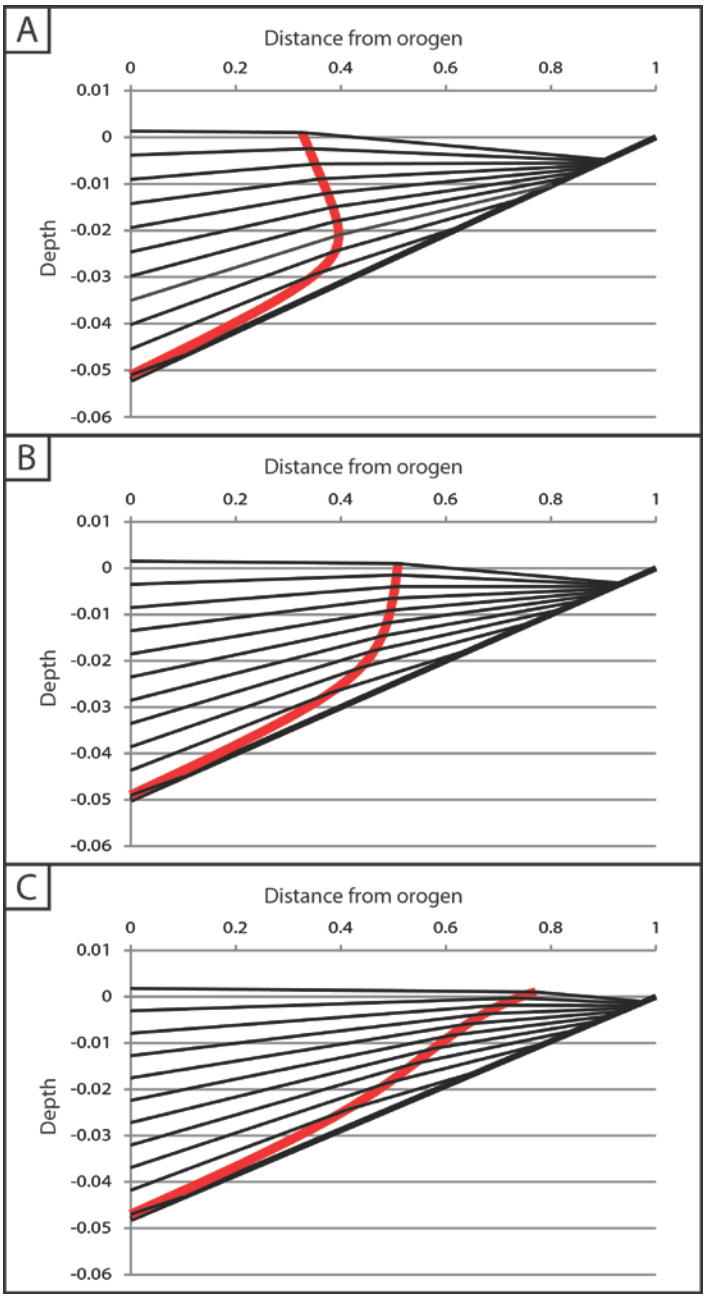

Figure 4.3: Synthetic stratigraphy produced by the geometrical model showing the three different types of shoreline behavior predicted by the model. The red line is the shoreline position through the stratigraphy. The run time is extremely long in these plots to better show the final behavior of each test run. A) Autoretreat shoreline trajectory, where $2q_s/L\sigma_{Hmax}$ = 0.96. B) Stationary shoreline trajectory, where $2q_s/L\sigma_{Hmax}$ = 1. C) Autoaccelerated shoreline trajectory, where $2q_s/L\sigma_{Hmax}$ = 1.47.

Figures 4.3 and 4.4 show three distinct types of shoreline behavior that correspond to different subsidence rates (Table 4.2). The three model runs start with very high shoreline progradation rates, but these rapidly decrease, resulting in the three divergent behaviors described below, depending on differing input parameters. The first case (hereafter Test-A, Fig. 4.3A and Fig. 4. 4A) results in an autoretreat trajectory (*sensu* Muto and Steel (1992)) whereby the initial regression switches rapidly to transgression. This behavior is a result of the constant sediment flux not being sufficient to maintain shoreline progradation as the length of foreset and topset progressively increases, and is similar to the autoretreat trajectories found in studies of basins with spatially uniform subsidence (Muto & Steel, 1992). However, because of the back-tilting subsidence pattern, the initial progradational stage is shorter lived than it would be with uniform subsidence across the length of the basin.

The second case (Test-B, Fig. 4.3B and Fig. 4.4B) produces a stationary shoreline and results in an aggradational stacking of shoreline strata. The stationary shoreline represents a pseudo-equilibrium balance between subsidence and sediment supply, and as a result, the size of the delta plain remains constant. In this second model, the balance between accommodation-creation and sediment flux results in a constant distance from the orogen-basin transition to the shoreline and from the shoreline to the toe-of-slope, as the shoreline position converges to a fixed location with time (Fig. 4.4B).

In the final scenario (Test-C, Fig. 4.3C and Fig. 4.4C), the shoreline regression is initially similar to Test-B, but eventually the progradation rate increases significantly. We term this response shoreline “autoacceleration”. The sustained increase in the shoreline progradation rate is driven by the shortening of the foreset as it progrades into shallower water downstream (Fig. 4.4C). The lengthening of the topset as the shoreline progrades

acts to diminish the sediment flux at the shoreline, but the shortening of the foreset has an even greater impact and causes the increase in rate of shoreline regression.

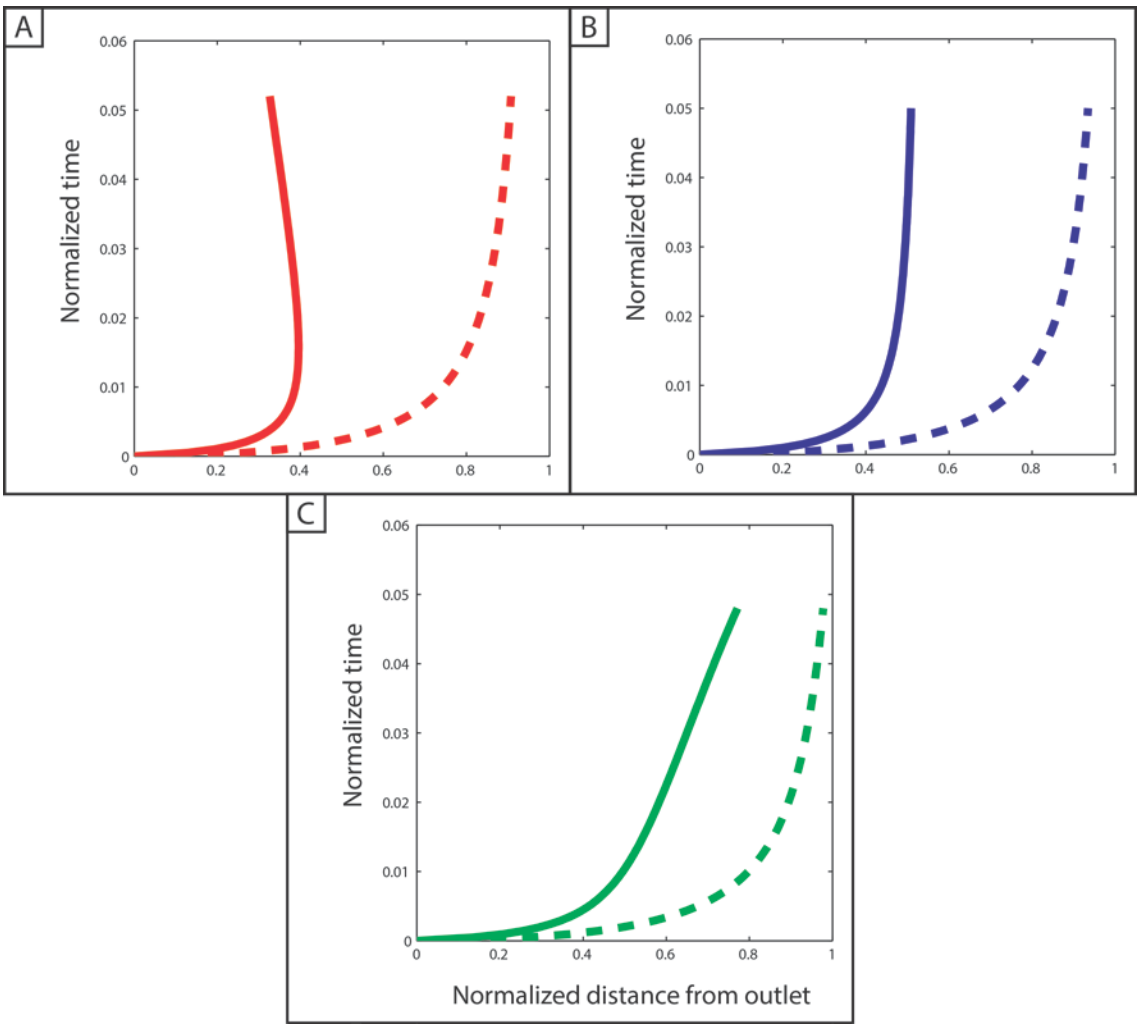

Figure 4.4: Plots of shoreline and toe-of-slope position through time for the three test runs of the geometrical model. A: Test 1 shows an autoretreat shoreline trajectory. B: Test 2 develops a stationary shoreline trajectory with a purely aggradational stratal pattern. C: Test 3 shows an autoaccelerated shoreline trajectory.

Table 4.2: Parameters used in each geometrical model run

	q_s (km^2/kyr)	q_s*	σ_H (km/kyr)	σ_H*	σ_P (km/kyr)	Z (km)	dZ (km/kyr)	L (km)	T (Myr)	T*	S_f	S_t
Test A	0.025	2.5e-6	5.2e-4	5.2e-6	0	0.1	0	100	10	0.052	0.01	0.001
Test B	0.025	2.5e-6	5e-4	5e-6	0	0.1	0	100	10	0.05	0.01	0.001
Test C	0.025	2.5e-6	4.8e-4	4.8e-6	0	0.1	0	100	10	0.048	0.01	0.001

FLUME EXPERIMENTS

To validate the mathematical modeling results, a set of flume experiments in the new Sediment Transport and Earth-surface Processes (STEP) basin at The University of Texas at Austin was conducted.

The STEP basin facility

The STEP basin is 5 m long, 4 m wide and 1.5 m deep. Half of the basin is covered with a rigid table (4 m long and 2.5 m wide) that allows for basement motion. The table can reproduce hinge-type rotation of a basin. The short edge of the table is attached to the tank wall so as to form a hinge axis. The other short edge is attached to two sets of transmission chains connecting to an electric motor, which vertically move the table at a maximum speed of 0.3 mm/s. The hinge axis can be attached at 1250 mm or 500 mm down from the top of the tank wall, and the table can be either lifted or dropped from the other side. The subsiding table is made of a number of 10.16cm wide aluminum beams allowing for the total width of the table to be changeable and for compartmentalization of the table surface into sections.

The water level in the tank is independently controlled at sub-millimeter precision using a motorized weir located outside of the basin. A hydraulic pump attached to a constant head tank controls the input water discharge and can provide a maximum discharge of 2,500 cm^3/s. The sediment is supplied by a dry material feeder, which has a range of sediment-supply rates between ~1 and ~10 cm^3 /s.

A computer program controls the functions of the subsiding table, base-level weir, hydraulic pump, and sediment feeder and monitors their operations.

Experimental design

The subsiding table was compartmentalized with Plexiglas sheets to make an inner flume to explore the foreland basin evolution in two dimensions. This inner flume was 3 m long, 0.5 m high and 0.1016 m wide with the downstream end open to the rest of the basin.

Instead of lowering the subsiding table on the proximal side close to the sediment input, we opted to use the lower hinge-axis elevation in the tank and raise the distal end of the table while raising the water level to maintain a constant base level (Fig. 4.5). This more complex set-up was used because it was not possible to place the sediment feeder on the subsiding end of the flume.

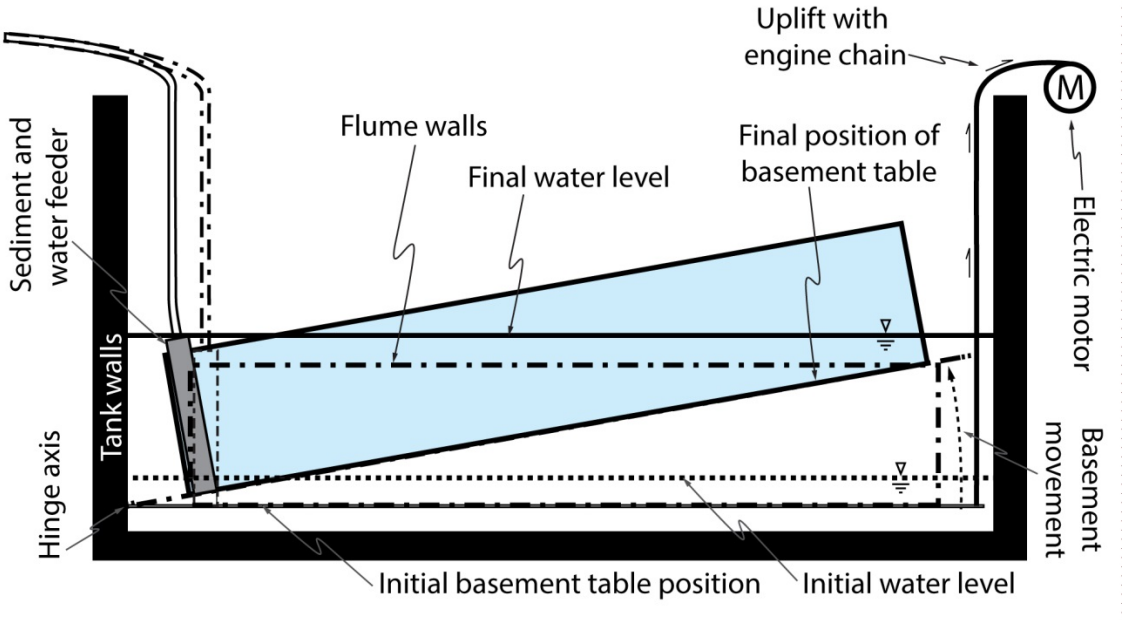

Figure 4.5: Schematic diagram of the initial and final positions of the subsiding table and the sediment and water inlet.

We conducted two sets of experiments with differing sediment flux, each was composed of three runs with different subsidence rates. A mathematical model was used to design the experiments so as to obtain three sets of input parameters that provided the cases of shoreline autoretreat, stationary shoreline, and shoreline autoacceleration. The parameters of these experiments are summarized in Table 4.3. We named the experiments according to their sediment flux (q), with H for high and L for low and their subsidence (σ), with H for high, M for medium, and L for low.

Table 4.3: Parameters used in each of the experimental runs.

	q_s (m^2/s)	σ_H (m/s)	σ_P (m/s)	Z (m)	dZ (m/s)	T (hr)	q_w (m^2/s)	L(m)
qHσH	$5.38\cdot10^{-5}$	$7.5\cdot10^{-5}$	0	0.05	0	1.5	$2.68\cdot10^{-3}$	3.048
qHσM	$5.38\cdot10^{-5}$	$3.5\cdot10^{-5}$	0	0.05	0	2.75	$2.68\cdot10^{-3}$	3.048
qHσL	$5.38\cdot10^{-5}$	$1.7\cdot10^{-5}$	0	0.05	0	1.83	$2.68\cdot10^{-3}$	3.048
qLσH	$1.78\cdot10^{-5}$	$2.5\cdot10^{-5}$	0	0.05	0	4.5	$9.2\cdot10^{-4}$	3.048
qLσM	$1.78.\cdot10^{-5}$	$1.17\cdot10^{-5}$	0	0.05	0	8	$9.2\cdot10^{-4}$	3.048
qLσL	$1.78\cdot10^{-5}$	$4\cdot10^{-6}$	0	0.05	0	6	$9.2\cdot10^{-4}$	3.048

The sediment is a two-to-one volume mixture of fine and coarse quartz grains of 100- and 200-μm diameter, respectively. The water to sediment-volume discharge ratio is kept constant at 0.8. This ratio is extremely low compared to natural systems, and it causes higher depositional slopes in the experiments than in natural systems. However, this accentuated slope allows for an easier visual evaluation of the behavior of the system. The difference in the overall shoreline migration rate due to higher topset slopes can be corrected geometrically, so as to reproduce the conditions observed in natural systems.

The back-wall of this flume at the upstream end was fixed perpendicular to the subsiding substrate and rotated at the same rate as the table, instead of the fixed vertical wall assumed in the mathematical model. This geometry caused slight offsets between the experimental shoreline migration and the modeling results, and these were larger for runs with higher subsidence rates. We will discuss the errors arising from this different configuration in a later section.

Data collection

Time-lapse photographs were taken through a side window and from the top of the tank, in order to monitor and analyze the evolution of the system. The overhead photographs were processed to obtain time series of the average shoreline position.

At the end of each experiment, after draining the tank, an elevation profile of the resulting deposit was recorded with a laser altimeter. The topographic data have a horizontal resolution of 1 mm and a vertical resolution of 0.1 mm. This accuracy allowed for calibration of the modeling results by optimizing both the porosity in the final deposit and the slopes of the clinoform topset and foreset. The slopes were similar due to the constant q_w/q_s in all the experiments (Table 4.4). The topset slope ranged from 0.022 to 0.033, whereas the foreset slope ranged between 0.6 and 0.65. The foreset slopes in the qMσL and qLσL experiments, however, were lower than the others. The final shorelines in these runs were located further downstream than other runs and the flow over the distal part of the delta surface could not fully cover the entire flume width, which caused irregular shorelines in plan-view. The angle measured in the downstream direction over the oblique foreset is smaller than the real foreset slope in these two experiments.

Table 4.4: Foreset and topset slopes of each experimental run

	qHσH	qHσM	qHσL	qLσH	qLσM	qLσL
S_t	0.057	0.0221	0.025	0.0301	0.0325	0.033
S_f	0.6019	0.6216	0.6536	0.601	0.4652	0.3115

Experimental results

In high subsidence runs, i.e. qHσH and qLσH, the shoreline autoretreated (Fig. 4.6) as the mathematical model predicted in Test-A (Figs. 4.3A, 4.4A). Runs qHσL and qLσL resulted in a clear autoacceleration of the shoreline regression (Fig. 4.7) as also shown in the Test-C results (Figs. 4.3C, 4.4C). The results from runs qHσM and qLσM (Fig. 4.8) were comparable to Test-B, producing a shoreline that migrated to a fixed downstream location with time (Figs. 4.3B, 4.4B). Although a fully stationary shoreline could not be achieved in the flume experiments (a much longer run time would be required); the experimental results reproduced the shoreline behavior predicted in the early stages of Test-B.

Figure 4.6 features the qHσH case, illustrating the evolution of an autoretreating system. The low sediment supply relative to subsidence ratio that was applied in this run created a large amount of unfilled accommodation, leading to an under-filled basin. The shoreline between the start of the run (Fig. 4. 6A) and run time t = 15 min (Fig. 4.6B) was strongly progradational, covering about 75% of the length of the system in merely 15% of the run time. Between t = 15 min and t = 30 min (Fig. 4.6C), the shoreline prograded at a highly reduced rate and this continued until t = 45 min (Fig. 4.6D). From t = 45 min through t = 90 min (Fig. 4.6G) the shoreline retreated. In contrast to the shoreline turnaround at t = 45 min, the toe-of-slope advance was maintained, albeit at a decelerating rate throughout the experiment.

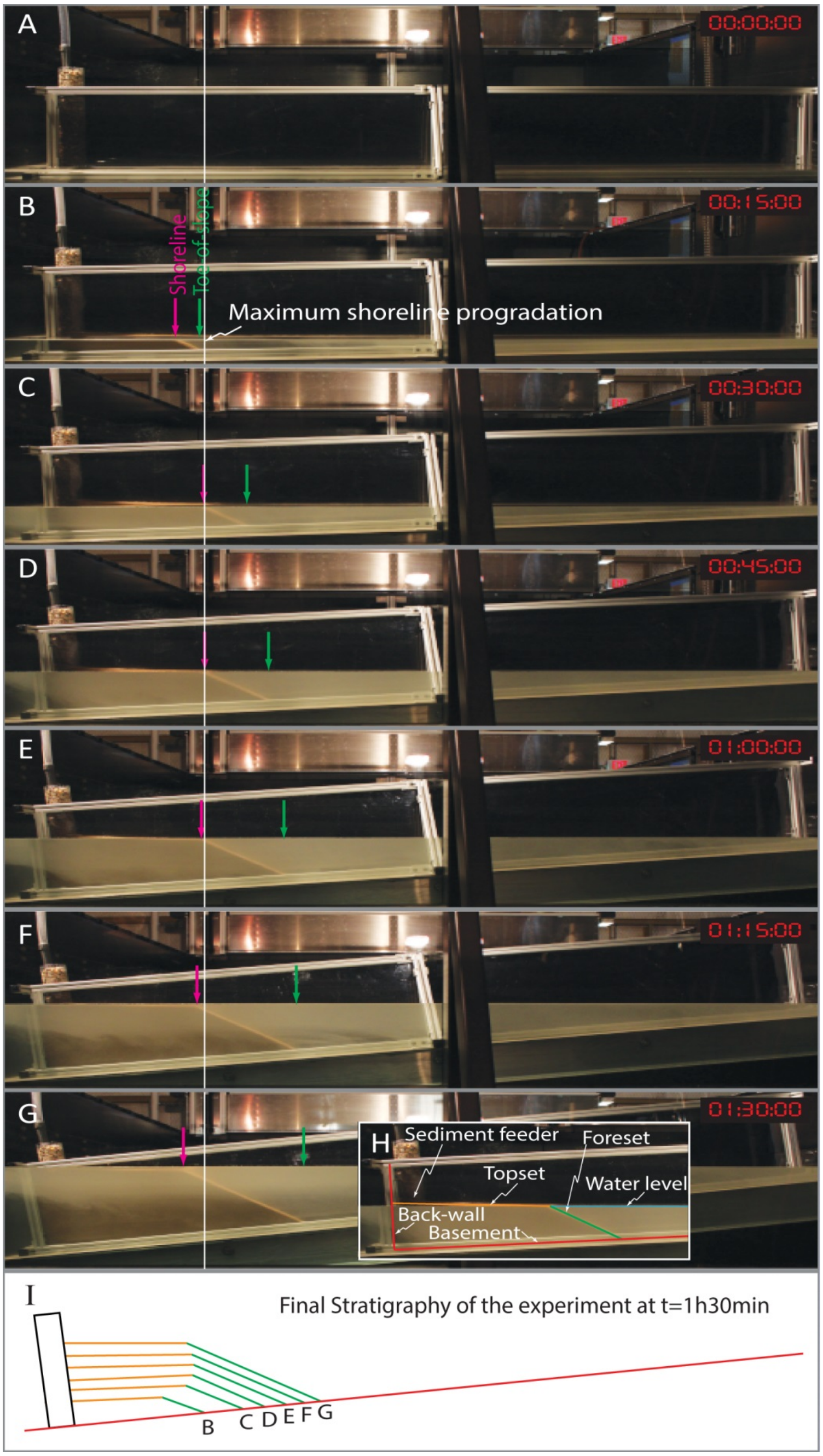
A
00:00:00
B
00:15:00
Shoreline
Toe of slope
Maximum shoreline progradation
C
00:30:00
D
00:45:00
E
01:00:00
F
01:15:00
G
01:30:00
H
Sediment feeder
Foreset
Topset
Water level
Back-wall
Basement
I
Final Stratigraphy of the experiment at t=1h30min
B C D E F G

Fig. 4.6

Figure 4.6: Panels A through G show a series of time-lapse photographs taken during run qHσH. In this experiment, due to the low q_s to σ_H ratio, the system cannot maintain progradation during the whole experimental run and so the shoreline rapidly exhibits retrogradation. Panel H is a sketch of panel D showing the geometry of the sediment pile and of the basin. Panel I is a line drawing of the internal architecture of the sediment pile, featuring, as labeled, the same intervals shown in panels A through G. The pink arrow points to the position of the shoreline at each step, whereas the green arrow points to the position of the toe-of-slope. The vertical white line across the panels marks the maximum length of progradation attained in panel D.


A
00:00:00
B
00:18:20
Shoreline
C
00:36:40
D
00:55:00
E
01:13:20
F
01:31:40
G
01:50:00
H
Final Stratigraphy of the experiment at t=1h50min
B
C
D
E
F
G

Fig 4.7

Figure 4.7: Series of time-lapse photographs taken during run qHσL. In this experiment, due to the high qs to σH ratio, the system can maintain shoreline progradation during the whole experimental run and is able to prograde the entire length of the basin. Panel H is a line drawing of the internal architecture of the sediment pile, featuring, as labeled, the same intervals shown in panels A through G. The pink arrow points to the position of the shoreline at each step.

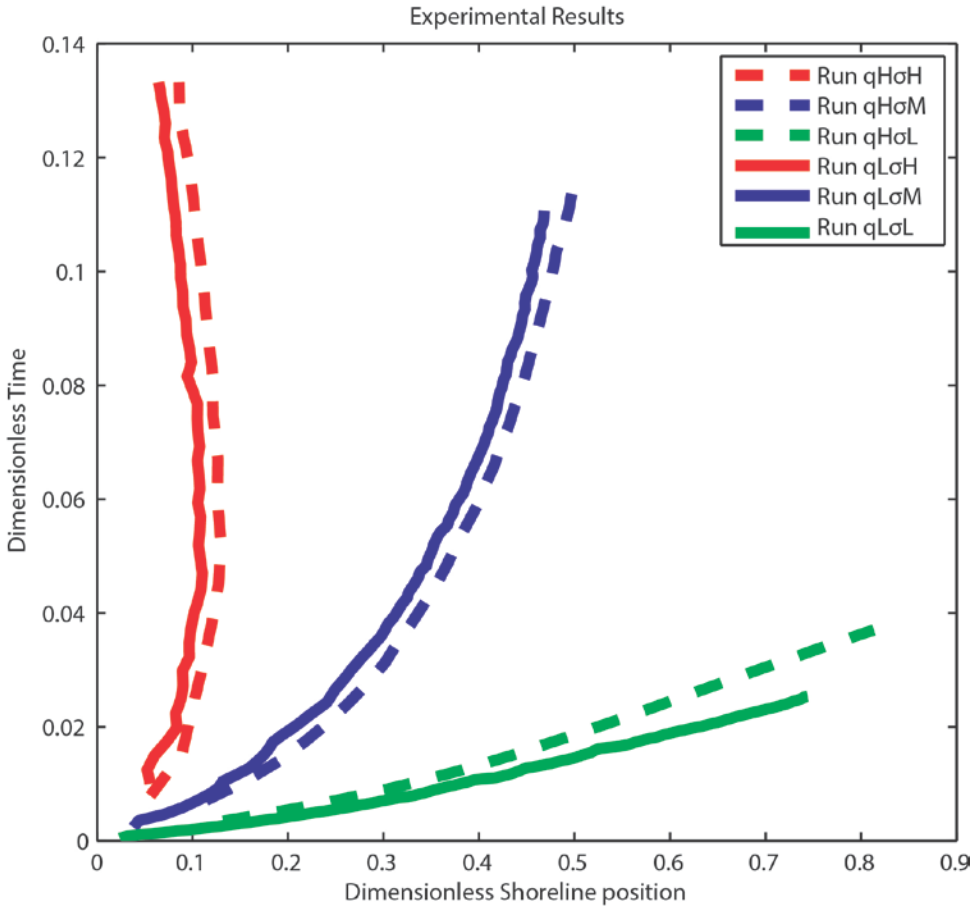

Figure 4.8: Shoreline position through time for all the experimental runs conducted. Runs qHσH and qLσH present autoretreat due to their low ratio of q_s to σ_H. In runs qHσM and qLσM it is unclear what behavior will develop, though a stationary shoreline seems likely. The high ratio of q_s to σ_H allows runs qHσL and qLσL to attain the autoaccelerated regression state.

Figure 4.7 shows photographs taken from the experimental run qHσL and illustrates a case of autoaccelerated shoreline evolution. During the time interval between t =0 min (Fig. 4.7A) and t=18 min (Fig. 4.7B) the shoreline advanced about 33% of the total basin length in 15% of the total run time, similar to the initial progradation of the qHσH case. In the period between t=18 min (Fig. 4.7B) and t=37 min (Fig. 4.7C),

progradation was maintained but at a highly reduced rate. Finally between t =55 min (Fig. 4.7D) and the end of the run (Fig. 4.7G) the progradation rate showed a slight increase.

There were major differences between the two experiments (qHσH and qHσL) in terms of the overall trend in system aggradation and change in foreset length. Delta top aggradation in qHσL, including the fluvial distributary deposits, was highly reduced due to slower subsidence. In qHσH, the foreset length increased with time, and therefore the volume of sediment deposited on the foreset, which was required to maintain progradation of the shoreline at a constant rate, also continuously increased. In qHσL, in contrast, the advancing sediment wedge moved closer to the distant hinge of the basin and so extended into shallower water, thus permitting no foreset-surface lengthening. The rapid shoreline regression gave rise to relatively thin topset deposits due to decreasing accommodation and distribution of sediment across the delta length.

DISCUSSION

Comparison of physical and analytical models

To validate the results of the mathematical model against the experimental results, we applied the input parameters used in the flume experiments to the geometrical model.

As shown in Fig. 4.9, modeling predictions have good correlation with the results of the experimental runs. The shoreline trajectories observed in the experimental runs and associated analytical solutions present the same overall behavior, but in most cases the model results over-estimate the magnitude of shoreline migration rates and the progradation lengths of the clastic wedge. The discrepancies are, in general, greater in the low sediment supply runs and in the runs with higher subsidence rates. The comparison

of runs with the same sediment flux but different tilting rates shows that the analytical model over-predicts migration rate especially in the high subsidence runs. The qLσH condition was thus the case where there was largest disparity between the results of the physical model and mathematical solution, whereas the qHσL run produced an almost perfect match between both sets of results.

The source of error in the modeling prediction is related in part to the differences between the setup of the physical and mathematical models. Specifically, the rotation of the upstream wall in the flume (in contrast to the constant vertical wall of the geometrical model) decreased the rate and magnitude of shoreline progradation and eventually promoted the shoreline retreat. The rotation of the wall also explains why experiments with high subsidence and low sediment supply showed the largest difference between the mathematical model results and experimental results, since the magnitude of rotation was greater with higher subsidence rates and the longer run times of low sediment supply runs.

Model limitations

The physical and geometrical models presented here are 2D models, where the whole deltaic surface is represented as a laterally-averaged, single, dip-oriented line. This integration eliminates the autogenic effects of lobe switching as well as sediment storage and release cycles (Kim & Jerolmack, 2008; Powell *et al.*, 2012), which would be averaged out over long-term scales. The current 2D models are most appropriate for indicating the long-term trend in the stratigraphic signal.

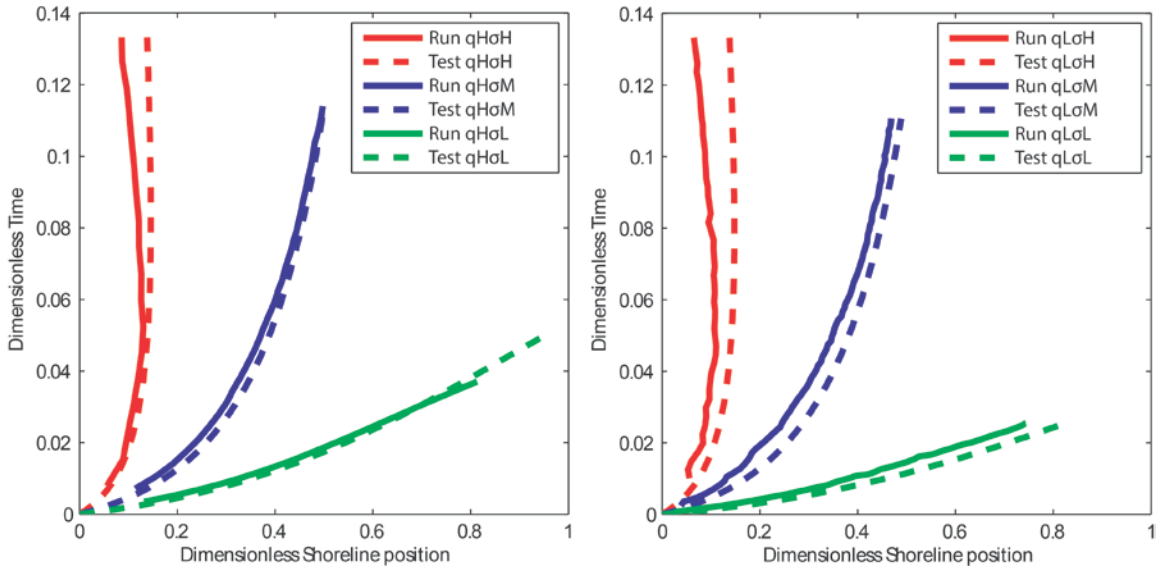

Figure 4.9: Plots of shoreline position through time comparing the experimental runs with the geometrical model tests using the same parameters. Each pair of experimental and geometrical runs shows a good correlation.

Retro-arc foreland basins present a curvilinear basement profile resulting from the elastic flexure of the lithosphere, but our models use a linear tilted profile for the basement. However, the flexural profile approximates a linear hinge-like subsidence over a long distance from the orogen. The geometrical model presented here does not capture these dynamic changes.

Model limitations

The physical and geometrical models presented here are 2D models, where the whole deltaic surface is represented as a laterally-averaged, single, dip-oriented line. This integration eliminates the autogenic effects of lobe switching as well as sediment storage and release cycles (Kim & Jerolmack, 2008; Powell *et al.*, 2012), which would be

averaged out over long-term scales. The current 2D models are most appropriate for indicating the long-term trend in the stratigraphic signal.

Retro-arc foreland basins present a curvilinear basement profile resulting from the elastic flexure of the lithosphere, but our models use a linear tilted profile for the basement. However, the flexural profile approximates a linear hinge-like subsidence over a long distance from the orogen. The geometrical model presented here does not capture these dynamic changes.

We isolated only a few key parameters in the experiments in order to clearly identify the stratigraphic responses that were direct products of these input controls. It is often difficult to decouple the interactions and feedback between different external controls producing the sedimentary record. Although sediment supply, subsidence, tectonic movement and base level rates are far from steady in nature, the steady forcing applied here can approximate averaged forcing over the time scales for the three types of stratal stacking in the clastic wedges studied here. Our experimental results provide a basis to assess the autogenic behavior of the shoreline system in this type of back-tilted setting, but they cannot be taken as a direct and complete parallel of natural systems, even though the processes that appear in the model are also present in natural systems (Paola *et al.*, 2001).

Application to field conditions

Chronostratigraphic models, and in particular sequence stratigraphic models (Van Wagoner *et al.*, 1988; Allen & Posamentier, 1993) are based on the concept that stratal stacking patterns are the key to stratigraphic history (Jervey, 1988; Posamentier & Vail, 1988), where changes in these stacking patterns have generally been interpreted in terms

of unsteady forcing by sediment supply, tectonics, climate and sea level. Recent studies, however, have called this into question. Autostratigraphy (Muto *et al.*, 2007) was developed to persuade researchers that stratigraphic breaks and changes in stacking patterns should be explained with autogenic responses before using allogenic explanations. Autostratigraphy describes how steady forcing of the above large-scale drivers can produce non-uniform, non-steady, autogenic stratigraphic responses in the rock record, reflecting self-organization within sedimentary systems at surprisingly long time-scales (Kim *et al.*, 2006; Muto *et al.*, 2007). Although the above concept has been promoted mainly from an experimental and theoretical point of view (Muto & Steel, 1992; 1997; 2002b; Muto & Swenson, 2006; Kim & Muto, 2007; Muto *et al.*, 2007; Swenson & Muto, 2007; Petter & Muto, 2008) it is now also being applied in field studies (Kertznus & Kneller, 2009; Ryan *et al.*, 2009; Enge *et al.*, 2010; Hampson, 2010; Petter *et al.*, 2011). Even with these recent advancements in autostratigraphy, however, autostratigraphic modeling has not yet paid attention to stratigraphic responses due to spatially non-uniform subsidence patterns. Stratigraphic patterns are ultimately linked to the geometry of the sediment-receiving basin (mainly shaped by tectonics) and the geometry of the sediment pile (mainly due to the sediment transport processes). Therefore a proper characterization of the effects of spatially varying subsidence is of paramount importance for accurate interpretation of the basin-fill history.

In addition, previous models of foreland basins have not identified the sustained and accelerated shoreline progradation highlighted by this study, believed here to typify supply-dominated systems in foreland basins. Sustained and accelerated shoreline progradation appears to be possible in the more proximal parts of foreland basins even during maximum shortening in the orogenic belt, when the amount of flexural subsidence is maximum due to the increased load. Therefore if the sediment flux entering the basin is

large enough, the coarse-grained sediment need not be entirely trapped in the foredeep of the basin but can regress across much of the basin toward the shallow distal region, without either increase in the sediment flux or decrease in the subsidence rate. Consequently, in the debate between the two-phase model of (Heller *et al.*, 1988) and the sediment driven examples (Burbank *et al.*, 1992; Marzo & Steel, 2000; Horton *et al.*, 2004), both models are possible at different sediment flux and subsidence rate scenarios. The key criteria to distinguish between the stratal patterns of these two models are (1) the flat shoreline trajectories and shortening of the deltaic foresets towards the distal side of the basin in the sediment-driven cases, and (2) the presence of a regional erosional surface separating the syn-orogenic and post-orogenic phases in the two-phase model.

The model in the present study suggests a flux threshold condition between the autoacceleration and autoretreat scenarios of $q \cong {L\sigma_H}/{2}$. The cases of accelerated shoreline migration in the test model and experiment had $q > {L\sigma_H}/{2}$; for example, the ratio $\frac{2q}{L\sigma_H}$ is 0.96 in Test-A, 1.04 in Test-C, 0.47 in qLσH and 2.92 in qLσL (Fig. 4.4). Two very different kinds of basin evolution are defined by this threshold; sedimentary systems in autoaccelerated basins will completely fill the accommodation space created, whereas basins experiencing shoreline autoretreat will never be completely infilled. This categorization is similar to the concept of underfilled and overfilled basins; however, this latter concept has been variously proposed, defined, and used, and it is now usually applied to different temporal stages in the evolution of a basin (Covey, 1986; Tankard, 1986; Flemings, P.B. & Jordan, 1989; Gawthorpe & Leeder, 2000; Yang & Miall, 2010; Yang, 2011).

The mathematical model presented here can be applied to field datasets in order to explore and roughly estimate the timing of orogenic pulses with respect to deposition of clastic wedges, subsidence history, and the clastic wedge migration pattern in a basin.

The model is not able to capture three-dimensional aspects of basin filling history, but it is able to provide a first-order understanding of stratigraphic development averaged across the basin width. Varying relative sea level and sediment supply, which are often required to investigate field data, can be numerically simulated using the current mathematical model but that is beyond the scope of this study. In the following paragraph, an example is provided to demonstrate scaling of a field tectonic condition using the mathematical model and quantifying the minimum sediment supply into the basin associated with recorded stratigraphic architecture.

The Albian Torok and Nanushuk formations (Mull *et al.*, 2003) of the North Slope of Alaska inside the National Petroleum Reserve-Alaska are used to calculate a first order approximation of the sediment flux. The Torok and Nanushuk formations form a clastic wedge that prograded into the Colville Foreland Basin with sediments supplied mainly from the Ancestral Brooks Range. Interpreted seismic sections and well-log correlations (Decker, 2007; Houseknecht *et al.*, 2009) clearly show strong progradational, continental slope clinoforms that overcame the imposed active subsidence, with foreset slope segments that became shorter as the clastic wedge climbed the ramp of the foreland basin. The clastic wedge almost reaches the end of the back-tilted basement (Fig. 4.10) with no internal unconformity; a setting analogous to that discussed previously where the shoreline autoaccelerates across the basin, therefore the condition $q > \frac{L\sigma_H}{2}$ seems to be met.

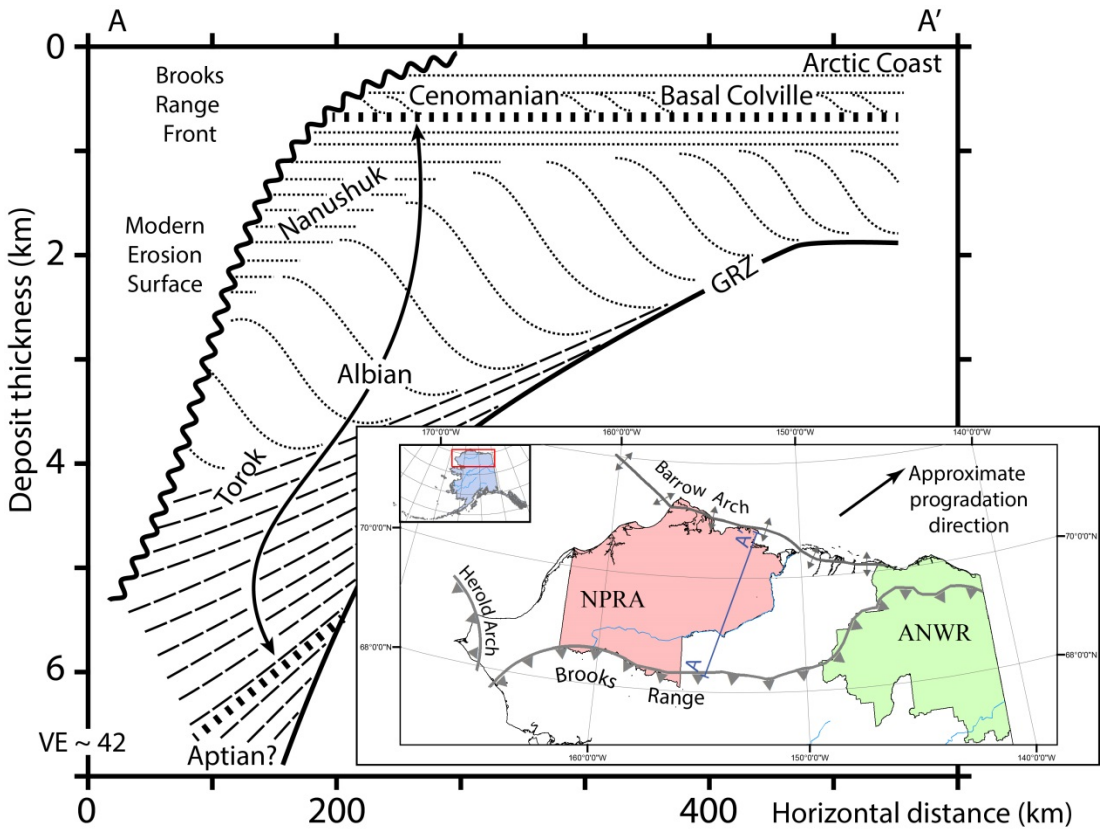

Figure 4.10: Schematic stratigraphic correlation chart of the Brookian sequence that fills the Colville basin, including the Torok and Nanushuk formations. The reduction in clinoform height of the clastic wedge as it prograded can be seen, as well as its advance far into the basin. Modified from Houseknecht and Schenk (2001). The blue line on the map shows the approximate position of this correlation chart. (NPRA. National Petroleum Reserve – Alaska; ANWR Arctic National Wildlife Reserve)

From published data (Houseknecht & Schenk, 2001; Decker, 2007; 2010), the following variables were collected and/or estimated: 1) basin length is about 280 km; 2) the subsidence measured near the foredeep, which is equivalent to the upstream boundary

of the model, is 4.6 km; 3) the duration of clastic wedge sedimentation is some 13My, which gives an average subsidence rate of 0.35 km/My; 4) the width of the protruding delta lobe (*sensu* Muto and Steel (2002a)), which is the approximate lateral extent of deposition, is 220 km. Applying these values into the condition of autoacceleration provides a minimum sediment-supply of 0.049 km^2/kyr. This rate is similar to the two-dimensional sediment supply of the smallest deltas calculated by Muto and Steel (2002a) for similar shelf margins. Multiplying this two-dimensional sediment supply by the width of the protruding delta lobe results in a minimum required sediment supply into the Colville Basin during Albian times of 10.8 km^3/ky, which is similar to modern mountain rivers in America and Europe (Milliman & Syvitski, 1992). This is the time-averaged, minimum sediment supply rate that would result in an autoaccelerated shelf-edge trajectory under constant tectonic back tilting without changes in sediment supply over time. The Albian Torok and Nanushuk formations show a progradational pattern, but this does not show a strong acceleration toward the distal end of the basin. There are two likely causes for the lack of acceleration based on the mathematical model: (1) reduction in sediment supply, but remaining greater than the minimum calculated to maintain progradation, (2) a greater rate of tectonic tilting in the early stages of basin formation.

The above estimate is a first-order approximation of the minimum sediment supply delivered by the river systems into the basin with very conservative values taken from published data. This type of estimation, though rough, might in some cases be the only way to estimate the sediment supply delivered to a basin.

CONCLUSIONS

Three different autostratigraphic shoreline trajectory responses are described for an experimental foreland basin developed under different conditions of back-tilting subsidence rate: autoretreat, stationary, and autoaccelerated. *Autoretreat* occurs as the delta topset and foreset lengthen during progradation, such that maintenance of deposition over the whole deltaic surface requires more and more sediment through time. The shoreline trajectory in this case shows a change from progradation and aggradation to retrogradation under steady external forcing. *Autoacceleration* occurs where the rate of foreset slope shortening (due to shoreline migration into shallower water of the distal side of the foreland basin) is greater than the rate of lengthening of the delta topset. The shoreline trajectory for autoacceleration indicates continuous progradation through time, but also a change of the migration rate from initial deceleration to marked acceleration. A *stationary* shoreline trajectory occurs at the boundary between the previous two states, and is an unlikely case because of the perfect equilibrium required between the allogenic controls. Thus, even with constant external forcing the shoreline trajectory displays autogenic changes in forward migration rate that are recorded in the basin-fill stratigraphy.

The states of autoretreat and autoacceleration are defined by a threshold value in the ratio between the rate of hinged subsidence across the length of the basin and the rate of sediment supply, $2q_s/L\sigma_H = 1$. Autoretreat occurs for values of this ratio smaller than 1, whereas autoacceleration occurs for values larger than 1.

This improved understanding of sediment wedge progradation in foreland-basin type subsidence complements the two-phase (Heller *et al.*, 1988) and the supply-dominated (Marzo & Steel, 2000) conceptual models for foreland basin evolution, and show that both models are possible in scenarios with different sediment flux and subsidence rates.

REFERENCES

ALLEN, G.P. & POSAMENTIER, H.W. (1993) Sequence Stratigraphy and Facies Model of an Incised Valley Fill - the Gironde Estuary, France. *Journal of Sedimentary Petrology*, **63,** 378-391.

ASCHOFF, J. & STEEL, R. (2011) Anomalous Clastic Wedge Development During the Sevier-Laramide Transition, North American Cordilleran Foreland Basin, USA. *Geological Society of America Bulletin*, **123,** 1822-1835.

BLAIR, T.C. & BILODEAU, W.L. (1988) Development of Tectonic Cyclothems in Rift, Pull-Apart, and Foreland Basins: Sedimentary Response to Episodic Tectonism. *Geology*, **16,** 517-520.

BURBANK, D.W., PUIGDEFABREGAS, C. & MUÑOZ, J.A. (1992) The Chronology of the Eocene Tectonic and Stratigraphic Development of the Eastern Pyrenean Foreland Basin, Northeast Spain. *Geological Society of America Bulletin*, **104,** 1101-1120.

CATUNEANU, O., HANCOX, P.J. & RUBIDGE, B.S. (1998) Reciprocal Flexural Behaviour and Contrasting Stratigraphies: A New Basin Development Model for the Karoo Retroarc Foreland System, South Africa. *Basin Research*, **10,** 417-439.

CATUNEANU, O. (2004) Retroarc Foreland Systems - Evolution through Time. *Journal of African Earth Sciences*, **38,** 225-242.

CLEVIS, Q., DE BOER, P. & WACHTER, M. (2003) Numerical Modelling of Drainage Basin Evolution and Three-Dimensional Alluvial Fan Stratigraphy. *Sedimentary Geology*, **163,** 85-110.

CLEVIS, Q., DE BOER, P.L. & NIJMAN, W. (2004) Differentiating the Effect of Episodic Tectonism and Eustatic Sea-Level Fluctuations in Foreland Basins Filled by Alluvial Fans and Axial Deltaic Systems: Insights from a Three-Dimensional Stratigraphic Forward Model. *Sedimentology*, **51,** 809-835.

COVEY, M. (1986) The Evolution of Foreland Basins to Steady State: Evidence from the Western Taiwan Foreland Basin. In: *Foreland Basins* (Ed. by P. A. Allen & P. Homewood), *Spec. Publ. Int. Ass. Sediment.*, **8**, 77-90. Blackwell Publishing Ltd.

CRABAUGH, J.P. (2001) Nature and Growth of Nonmarine-to-Marine Clastic Wedges: Examples from the Upper Cretaceous Iles Formation, Western Interior (Colorado) and the Lower Paleogene Wilcox Group of the Gulf of Mexico Basin (Texas). Ph. D. Dissertation Thesis, University of Wyoming, Laramie.

CROSS, T.A. & PILGER, R.H. (1978) Tectonic Controls of Late Cretaceous Sedimentation, Western Interior, USA. *Nature*, **274,** 653-657.

DECELLES, P.G., LAWTON, T.F. & MITRA, G. (1995) Thrust Timing, Growth of Structural Culminations, and Synorogenic Sedimentation in the Type Sevier Orogenic Belt, Western United-States. *Geology*, **23,** 699-702.

DECELLES, P.G. & GILES, K.A. (1996) Foreland Basin Systems. *Basin Research*, **8,** 105-123.

DECKER, P.L. (2007) Brookian Sequence Stratigraphic Correlations, Umait Field to Milne Point Field, West-Central North Slope, Alaska, Alaska Division of Geological & Geophysical Surveys. **Preliminary Interpretative Report 2007-2,** 19p., 11 sheet.

DECKER, P.L. (2010) Brookian Sequence Stratigraphic Framework of the Northern Colville Foreland Basin, Central North Slope, Alaska (Poster and Presentation): Dnr Spring Technical Review Meeting, Anchorage, April 21-22, 2010, Alaska Division of Geological & Geophysical Surveys**,** 30 p., 31 sheet.

DEVLIN, W.J., RUDOLPH, K.W., SHAW, C.A. & EHMAN, K.D. (1993) The Effect of Tectonic and Eustatic Cycles on Accommodation and Sequence-Stratigraphic Framework in the Upper Cretaceous Foreland Basin of Southwestern Wyoming. In: *Sequence Stratigraphy and Facies Associations* (Ed. by H. W. Posamentier, C. P. Summerhayes, B. U. Haq & G. P. Allen), *Spec. Publ. Int. Ass. Of Sediment.*, **18**, 501-520. Blackwell Publishing Ltd., Boston.

DICKINSON, W.R. (1974) Plate Tectonics and Sedimentation. In: *Tectonics and Sedimentation* (Ed. by W. R. Dickinson), **22**, 1-27. SEPM (Society for Sedimentary Geology), Tulsa, OK.

ENGE, H.D., HOWELL, J.A. & BUCKLEY, S.J. (2010) The Geometry and Internal Architecture of Stream Bars in the Panther Tongue and the Ferron Sandstone Members, Utah, U.S.A. *Journal of Sedimentary Research*, **80,** 1018-1031.

FLEMINGS, P.B. & JORDAN, T.E. (1989) A Synthetic Stratigraphic Model of Foreland Basin Development. *Journal of Geophysical Research-Solid Earth and Planets*, **94,** 3851-3866.

FLEMINGS, P.B. & JORDAN, T.E. (1990) Stratigraphic Modelling of Foreland Basins - Interpreting Thrust Deformation and Lithosphere Rheology. *Geology*, **18,** 430-434.

FLEMINGS, P.B. & GROTZINGER, J.P. (1996) Strata: Freeware for Analyzing Classic Stratigraphic Problems. *GSA Today*, **6,** 1-7.

GALLOWAY, W.E. (1989) Genetic Stratigraphic Sequences in Basin Analysis. 1. Architecture and Genesis of Flooding-Surface Bounded Depositional Units. *Aapg Bulletin-American Association of Petroleum Geologists*, **73,** 125-142.

GARCIA-CASTELLANOS, D. (2002) Interplay between Lithospheric Flexure and River Transport in Foreland Basins. *Basin Research*, **14,** 89-104.

GARCIA-CASTELLANOS, D., VERGES, J., GASPAR-ESCRIBANO, J. & CLOETINGH, S. (2003) Interplay between Tectonics, Climate, and Fluvial Transport During the Cenozoic Evolution of the Ebro Basin (Ne Iberia). *Journal of Geophysical Research-Solid Earth*, **108**.

GAWTHORPE, R.L., FRASER, A.J. & COLLIER, R.E.L. (1994) Sequence Stratigraphy in Active Extensional Basins: Implications for the Interpretation of Ancient Basin-Fills. *Marine and Petroleum Geology*, **11,** 642-658.

GAWTHORPE, R.L. & LEEDER, M.R. (2000) Tectono-Sedimentary Evolution of Active Extensional Basins. *Basin Research*, **12,** 195-218.

HAMPSON, G.J. (2010) Sediment Dispersal and Quantitative Stratigraphic Architecture across an Ancient Shelf. *Sedimentology*, **57,** 96-141.

HELLAND-HANSEN, W. & GJELBERG, J.G. (1994) Conceptual Basis and Variability in Sequence Stratigraphy - a Different Perspective. *Sedimentary Geology*, **92,** 31-52.

HELLER, P.L., BOWDLER, S.S., CHAMBERS, H.P., COOGAN, J.C., HAGEN, E.S., SHUSTER, M.W., WINSLOW, N.S. & LAWTON, T.F. (1986) Time of Initial Thrusting in the Sevier Orogenic Belt, Idaho-Wyoming and Utah. *Geology*, **14,** 388-391.

HELLER, P.L., ANGEVINE, C.L., WINSLOW, N.S. & PAOLA, C. (1988) Two-Phase Stratigraphic Model of Foreland-Basin Sequences. *Geology*, **16,** 501-504.

HELLER, P.L. & PAOLA, C. (1992) The Large-Scale Dynamics of Grain-Size Variation in Alluvial Basins, 2: Application to Syntectonic Conglomerate. *Basin Research*, **4,** 91-102.

HENRIKSEN, S., HAMPSON, G.J., HELLAND-HANSEN, W., JOHANNESSEN, E.P. & STEEL, R.J. (2009) Shelf Edge and Shoreline Trajectories, a Dynamic Approach to Stratigraphic Analysis. *Basin Research*, **21,** 445-453.

HORTON, B.K., CONSTENIUS, K.N. & DECELLES, P.G. (2004) Tectonic Control on Coarse-Grained Foreland-Basin Sequences: An Example from the Cordilleran Foreland Basin, Utah. *Geology*, **32,** 637-640.

HOUSEKNECHT, D.W. & SCHENK, C.J. (2001) Depositional Sequences and Facies in the Torok Formation, National Petroleum Reserve - Alaska (Npra). In: *Npra Core Workshop Petroleum Plays and Systems in the National Petroleum Reserve-Alaska* (Ed. by D. W. Houseknecht), 179-200. SEPM (Society for Sedimentary Geology), Tulsa.

HOUSEKNECHT, D.W., BIRD, K.J. & SCHENK, C.J. (2009) Seismic Analysis of Clinoform Depositional Sequences and Shelf-Margin Trajectories in Lower Cretaceous (Albian) Strata, Alaska North Slope. *Basin Research*, **21,** 644-654.

INGERSOLL, R.V. (1988) Tectonics of Sedimentary Basins. *Geological Society of America Bulletin*, **100,** 1704-1719.

JERVEY, M.T. (1988) Quantitative Geological Modeling of Siliciclastic Rock Sequences and Their Seismic Expression. In: *Sea-Level Changes: An Integrated Approach* (Ed. by C. K. Wilgus, B. S. Hastings, H. W. Posamentier, J. C. Van Wagoner, A. C. Ross & C. G. S. C. Kendall), *Sepm Special Publication*, **42**, 47-69. SEPM - Soc. Sedimentary Geology, Tusla, OK.

JORDAN, T.E. (1981) Thrust Loads and Foreland Basin Evolution, Cretaceous, Western United-States. *Aapg Bulletin-American Association of Petroleum Geologists*, **65,** 2506-2520.

JORDAN, T.E. (1995) Retroarc Foreland and Related Basins. In: *Tectonics of Sedimentary Basins* (Ed. by C. J. Busby & R. V. Ingersoll), 331-362. Blackwell Science, Cambridge, MA.

KERTZNUS, V. & KNELLER, B. (2009) Clinoform Quantification for Assessing the Effects of External Forcing on Continental Margin Development. *Basin Research*, **21,** 738-758.

KIM, W., PAOLA, C., SWENSON, J.B. & VOLLER, V.R. (2006) Shoreline Response to Autogenic Processes of Sediment Storage and Release in the Fluvial System. *J. Geophys. Res.*, **111,** F04013.

KIM, W. & MUTO, T. (2007) Autogenic Response of Alluvial-Bedrock Transition to Base-Level Variation: Experiment and Theory. *Journal of Geophysical Research-Earth Surface*, **112,** F3S14.

KIM, W. & JEROLMACK, D.J. (2008) The Pulse of Calm Fan Deltas. *Journal of Geology*, **116,** 315-330.

KING, P.B. (1959) *The Evolution of North America*. Princeton University Press, Princeton.

MARSHALL, K. (1951) *North American Geosynclines*. The Geological Society of America, New York.

MARZO, M. & STEEL, R.J. (2000) Unusual Features of Sediment Supply-Dominated, Transgressive-Regressive Sequences: Paleogene Elastic Wedges, Se Pyrenean Foreland Basin, Spain. *Sedimentary Geology,* **138,** 3-15.

MILLIMAN, J.D. & SYVITSKI, J.P.M. (1992) Geomorphic Tectonic Control of Sediment Discharge to the Ocean - the Importance of Small Mountainous Rivers. *Journal of Geology*, **100,** 525-544.

MULL, C.G., HOUSEKNECHT, D.W. & BIRD, K.J. (2003) Revised Cretaceous and Tertiary Stratigraphic Nomenclature in the Colville Basin, Northern Alaska. *Professional Paper*, U.S. Geological Survey. **1673,** 59.

MUTO, T. & STEEL, R.J. (1992) Retreat of the Front in a Prograding Delta. *Geology*, **20,** 967-970.

MUTO, T. & STEEL, R.J. (1997) Principles of Regression and Transgression: The Nature of the Interplay between Accommodation and Sediment Supply. *Journal of Sedimentary Research,* **67,** 994-1000.

MUTO, T. & STEEL, R.J. (2002a) In Defense of Shelf-Edge Delta Development During Falling and Lowstand of Relative Sea Level. *Journal of Geology*, **110,** 421-436.

MUTO, T. & STEEL, R.J. (2002b) Role of Autoretreat and a/S Changes in the Understanding of Deltaic Shoreline Trajectory: A Semi-Quantitative Approach. *Basin Research,* **14,** 303-318.

MUTO, T. & STEEL, R.J. (2004) Autogenic Response of Fluvial Deltas to Steady Sea-Level Fall: Implications from Flume-Tank Experiments. *Geology*, **32,** 401-404.

MUTO, T. & SWENSON, J.B. (2006) Autogenic Attainment of Large-Scale Alluvial Grade with Steady Sea-Level Fall: An Analog Tank-Flume Experiment. *Geology,* **34,** 161-164.

MUTO, T., STEEL, R.J. & SWENSON, J.B. (2007) Autostratigraphy: A Framework Norm for Genetic Stratigraphy. *Journal of Sedimentary Research,* **77,** 2-12.

NAYLOR, M. & SINCLAIR, H.D. (2008) Pro- Vs. Retro-Foreland Basins. *Basin Research*, **20,** 285-303.

PANG, M. & NUMMENDAL, D. (1995) Flexural Subsidence and Basement Tectonics of the Cretaceous Western Interior Basin, United-States. *Geology*, **23,** 173-176.

PAOLA, C., HELLER, P.L. & ANGEVINE, C.L. (1992) The Large-Scale Dynamics of Grain-Size Variation in Alluvial Basins, 1: Theory. *Basin Research*, **4,** 73-90.

PETTER, A.L. & MUTO, T. (2008) Sustained Alluvial Aggradation and Autogenic Detachment of the Alluvial River from the Shoreline in Response to Steady Fall of Relative Sea Level. *Journal of Sedimentary Research*, **78,** 98-111.

PETTER, A.L., KIM, W., MUTO, T. & STEEL, R.J. (2011) Comment on 'Clinoform Quantification for Assessing the Effects of External Forcing on Continental Margin Development'. *Basin Research*, **23,** 118-121.

POSAMENTIER, H.W. & VAIL, P.R. (1988) Sequences, System Tracts and Eustatic Cycles. *Aapg Bulletin-American Association of Petroleum Geologists*, **72,** 237-237.

POWELL, E.J., KIM, W. & MUTO, T. (2012) Varying Discharge Controls on Timescales of Autogenic Storage and Release Processes in Fluvio-Deltaic Environments: Tank Experiments. *Journal of Geophysical Research: Earth Surface*, **117,** F02011.

RYAN, M.C., HELLAND-HANSEN, W., JOHANNESSEN, E.P. & STEEL, R.J. (2009) Erosional Vs. Accretionary Shelf Margins: The Influence of Margin Type on Deepwater Sedimentation: An Example from the Porcupine Basin, Offshore Western Ireland. *Basin Research*, **21,** 676-703.

SCHLAGER, W. (1993) Accommodation and Supply—a Dual Control on Stratigraphic Sequences. *Sedimentary Geology*, **86,** 111-136.

SINCLAIR, H.D., COAKLEY, B.J., ALLEN, P.A. & WATTS, A.B. (1991) Simulation of Foreland Basin Stratigraphy Using a Diffusion-Model of Mountain Belt Uplift and Erosion - an Example from the Central Apls, Switzerland. *Tectonics*, **10,** 599-620.

STEEL, R.J. (1988) Coarsening-Upward and Skewed Fan Bodies: Symtoms of Strike-Slip and Transfer Fault Movement in Sedimentary Basins. In: *Fan Deltas: Sedimentology and Tectonic Settings* (Ed. by W. Nemec & R. J. Steel), 75-83. Blackie and Son Ltd., Glasgow.

SWENSON, J.B. & MUTO, T. (2007) Response of Coastal Plain Rivers to Falling Relative Sea-Level: Allogenic Controls on the Aggradational Phase. *Sedimentology*, **54,** 207-221.

TANKARD, A.J. (1986) On the Depositional Response to Thrusting and Lithospheric Flexure: Examples from the Appalachian and Rocky Mountain Basins. In: *Foreland Basins* (Ed. by P. A. Allen & P. Homewood), *Ias Special Publication*, **8**, 369-392. Blackwell Publishing Ltd.

TOMER, A., MUTO, T. & KIM, W. (2011) Autogenic Hiatus in Fluviodeltaic Successions: Geometrical Modeling and Physical Experiments. *Journal of Sedimentary Research*, **81,** 207-217.

VAN HOUTEN, F.B. (1974) Northern Alpine Molasse and Similar Cenozoic Sequences of Southern Europe. In: *Modern and Ancient Geosynclinal Sedimentation* (Ed. by R. H. Dott Jr. & R. H. Shaver), *Sepm Special Publication*, **No.19**, 14. SEPM, Tulsa.

VAN WAGONER, J.C., POSAMENTIER, H.W., MITCHUM, R.M., JR., VAIL, P.R., SARG, J.F., LOUTIT, T.S. & HARDENBOL, J. (1988) An Overview of the Fundamentals of Sequence Stratigraphy and Key Definitions. *Special Publication - Society of Economic Paleontologists and Mineralogists*, **42,** 39-45.

YANG, Y. & MIALL, A.D. (2010) Migration and Stratigraphic Fill of an Underfilled Foreland Basin: Middle–Late Cenomanian Belle Fourche Formation in Southern Alberta, Canada. *Sedimentary Geology*, **227,** 51-64.

YANG, Y. (2011) Tectonically-Driven Underfilled–Overfilled Cycles, the Middle Cretaceous in the Northern Cordilleran Foreland Basin. *Sedimentary Geology*, **233,** 15-27.

Chapter Five: Conclusions

The broad results of the research presented in this dissertation focus on the effect that subsidence has in the stratigraphy of foreland basins, and how this stratigraphy changes as dynamic subsidence becomes more important and as Laramide structures initiate. Early stages of foreland basin back-tilt impact on this stratigraphy are examined by geometric and flume-tank modeling. Late stages in the transition to Laramide tectonics are captured in a study of the Late Campanian Williams Fork Clastic Wedge. A re-examination of the character of the very youngest segments on the transgressive limb of the wedge provides a new interpretation of these uppermost sandbodies as storm to tidal transgressive shelf ridges, the third description of this type of ancient reservoir in the literature. The major contributions of this work are:

1. The core of the studied clastic wedge, the Canyon Creek Member, shows a general trend of thickening and decreasing net-to-gross from proximal to distal, and a transition from braided to meandering fluvial style in the same direction; not the trends that would be expected in a foreland basin. These trends rather indicate a period of quiescence in the orogenic belt during which the subsidence pattern in the foreland basin was reversed by denudation of the orogen and, importantly, eastward migration of the broader dynamic subsidence across the region.
2. The general proximal-to-distal trends found in the Canyon Creek member are visibly and markedly disturbed around the borders and crests of Rock Springs Uplift, the Sierra Madre Uplift, the Rawlins Uplift, the Moxa Arch and the Uinta Mountains. This is a clear indication that these Laramide-style structures were

already active during the time of deposition of the Canyon Creek Member. In the cases of the Rock Springs, Sierra Madre and Rawlins uplifts the impact was expressed as areas of increased thickness (subsidence) along the down-warped sides, but markedly reduced thickness (reduced subsidence but no marked surface relief) on the crestal areas. Along the northern edge of the Uinta Mountains, and probably along the Wind River Range (though not mapped in this work) it is very likely that there was marked topographic expression with erosion and sediment delivery into the Canyon Creek system.

3. Two sandstone bodies of the Almond formation are reinterpreted as transgressive shelf ridges. The lower body was generated by tidal currents that reworked the older shoreline substrate. The second body is also a shelf ridge but shows a change of process domination from being initially storm reworked, but then becoming strongly tidally dominated prior to the final, major Lewis transgression.
4. The sandstone bodies interpreted as transgressive shelf ridges demonstrate how, during a major transgression with great shelf widening, the process domination can change markedly, probably due to predictable tidal resonance as shelf width exceeds 200km (Dalrymple, 2012).
5. Transgressive tidal shelf ridges typically have the following characteristics: (1) Sandstone body dominated by stacked cross strata (though not so if body is storm created) and encased in marine mudstones; (2) erosive surface at the base of the body (transgressive ravinement); (3) non-erosive, likely intensely bioturbated upper boundary (abandonment surface); (4) clean well sorted cross-stratified sandstones with little or no mud; (5) mixture of shallow marine macrofauna, fully marine microfauna, and fully marine stressed ichnofauna; and (6) common

internal laterally accreting surfaces as such bodies migrate obliquely to their length.

6. Three different autostratigraphic shoreline trajectory responses are described for an experimental foreland basin developed under different conditions of back-tilting subsidence rate: autoretreat, stationary, and autoaccelerated.

7. *Autoretreat* describes the driving mechanism of the trajectory of a shoreline that shows a change from progradation and aggradation to retrogradation under steady external forcing. The shoreline trajectory for *autoacceleration* shows continuous progradation through time, but with a change of the migration rate from initial deceleration to marked acceleration.

8. The states of autoretreat and autoacceleration are defined by a threshold value in the ratio between the rate of hinged subsidence across the length of the basin and the rate of sediment supply, $2qs/L\sigma H = 1$. Autoretreat occurs for values of this ratio smaller than 1, whereas autoacceleration occurs for values larger than 1.

9. This improved understanding of sediment-wedge progradation in foreland-basin type subsidence complements the two-phase (Heller et al., 1988) and the supply-dominated (Marzo & Steel, 2000) conceptual models for foreland basin.

Appendix A: Well database detail

The well logs used in this study correspond to the wells listed in Table A.1 and are distributed as shown in Figure A.1.

Table A.1: List of wells used in this study

Well ID #	API #	Longitude	Latitude	Well Name
1	0508105321	-107.435486	40.452255	Voloshin #1
2	0508105345	-107.621292	40.497665	Yost #1
3	0508105354	-107.642197	40.558044	Government #1
4	0508105357	-107.707504	40.581421	Thomas G Dorough - G
5	0508105381	-107.679153	40.635666	Clara Sturman Estate
6	0508106174	-107.483707	40.473969	Levkulich #1
7	0508106200	-107.627301	40.493818	Billing 1
8	0508106242	-107.900284	40.831085	Government #13-1
9	0508106260	-108.49763	40.96585	Shell Creek 44-27 (1
10	0508106317	-107.712124	40.489957	Robertson 10-1
11	0508106413	-107.921951	40.817474	FLB Unit #23-2
12	0508106433	-107.444895	40.459649	1 Paulovich
13	0508106556	-107.679783	40.483418	Silver 9-11
14	0508106590	-107.490447	40.48239	2-16 State
15	0508106600	-107.76947	40.636246	Peroulis #2-19
16	0508106603	-107.530685	40.437576	Trapper Mine #1-31
17	0508106622	-108.315857	40.971786	Powder Wash Deep Uni
18	0508106668	-107.6082	40.502747	Zimmerman/Chamberlin
19	0508106669	-107.910901	40.574935	Federal #11-1
20	0508106670	-107.746275	40.527087	Kleitz 23-29 #1
21	0508106672	-107.5932	40.475338	State 15-2
22	0508106689	-107.70723	40.585098	Peroulis Federal #3-
23	0508106719	-107.640772	40.497238	FEE 691-701
24	0508106726	-107.612231	40.493668	FEE 691-0906
25	0508106816	-107.606201	40.493618	Aetna 1
26	0508106842	-107.607571	40.497358	Young 1
27	0510706033	-107.358003	40.48245	State #1-15
28	0510706039	-107.097534	40.348183	Fish Creek 6-36
29	0510706055	-107.312701	40.44307	Breshears #14-30
30	0510706079	-107.159978	40.624669	Cottonwood Creek Fed

Table A.1 (Continued)

Well ID #	API #	Longitude	Latitude	Well Name
31	0510706080	-107.2663	40.443381	Dry Creek Unit 0-28-
32	0510706080	-107.2663	40.443381	Dry 0-28-6-88
33	0510706081	-107.133816	40.450601	Grace 1-27
34	0510706087	-107.155618	40.632349	Cottonwood Creek #2
35	0510706098	-107.134188	40.675179	Hayden Public Librar
36	0510706109	-107.117745	40.378172	Roche 23-5
37	0510706127	-107.387404	40.481959	CO ST 1-16
38	0510706137	-107.257689	40.440571	Dry Creek Unit #34-4
39	0510706137	-107.257689	40.440571	Dry Creek 34-4
40	0510706144	-107.360093	40.46029	Temple 1-22
41	0510706144	-107.360093	40.46029	Temple 1-22
42	0510706164	-107.310542	40.524439	Colorado State #1-31
43	0510706196	-107.21241	40.605249	State of Colorado 36
44	0510706197	-107.203099	40.606709	State of Colorado 36
45	0510706201	-107.395444	40.46887	Breeze #44-17
46	0510706207	-107.381624	40.47017	Breeze #34-16
47	4900705122	-107.64845	41.50827	Hollr Springs 1
48	4900705209	-107.72586	41.59256	Creston Unit A-1
49	4900720133	-107.7015	41.55581	Creston Unit #1
50	4900720214	-107.44428	41.69222	Mesa Federal 1
51	4900721029	-107.76691	41.54978	Creston Nose #1
52	4900721091	-107.69221	41.45121	Muddy Creek #18-1
53	4900721227	-107.74136	41.02159	South Baggs Federal
54	4900721249	-107.88686	41.51941	Echo Springs Deep No
55	4900721377	-107.666346	41.157639	Robbers Que 2-29
56	4900721407	-107.76602	41.12798	Blue Goose Unit 8-5-
57	4900721584	-107.79896	41.510937	Creston Nose No. 1-3
58	4900721984	-107.562156	41.56037	Ar Fee 1890-SW5
59	4900722194	-107.767778	41.13917	Robbers Gulch 9-32-1
60	4900722238	-107.816106	41.35635	Barrel Springs Unit
61	4900722621	-107.825506	41.239688	Flat Top 10-26-15-93
62	4900722662	-107.704088	41.251667	Mexican Flats #13-24
63	4900722809	-107.63506	41.10202	Fivemile Point State
64	4900722863	-107.76921	41.35536	Nalsmith Shale 1
65	4900723297	-107.88623	41.29291	Flat Top 2-8-15-93
66	4900723445	-107.818356	41.320885	Barrel Springs 4-36-
67	4902320042	-110.21883	41.68853	Ziegler 1

Table A.1 (Continued)

Well ID #	API #	Longitude	Latitude	Well Name
68	4902320105	-110.29612	41.72252	Dry Muddy Creek UN 1
69	4902320217	-110.38076	41.73555	Champlin 422 Amoco A
70	4902321002	-110.11035	41.63164	Altrogge 3-18
71	4902321005	-110.08422	41.70558	Miller 2
72	4902321205	-110.08457	41.91571	Cow Hollow #68
73	4902321216	-110.06944	41.88062	Cow Hollow #50
74	4902321373	-110.14671	41.91656	Shute Creek Unit #40
75	4902321554	-110.1776	41.8975	Blackjack Federal 30
76	4902321593	-110.19694	41.89778	Blackjack #30-11
77	4902321635	-110.225	41.9125	Mariposa Federal #3
78	4902321648	-110.10725	41.91769	Beard Federal 1-3
79	4903520447	-109.0883	42.27261	Fed-Pacific Creek 1-
80	4903705054	-109.59129	41.02209	Linwood Unit #1
81	4903705088	-108.59684	41.04271	Govt Unit 1-6
82	4903705162	-109.423977	41.141443	Current Creek 4
83	4903705173	-108.73662	41.17237	58-24 Unit 1
84	4903705188	-109.36835	41.20276	Govt 4-9V
85	4903705211	-108.76883	41.23481	Screggs Draw 1
86	4903705280	-109.29944	41.37701	Firehole Unit # 1
87	4903705351	-109.8	41.50991	Spider Creek Unit B-
88	4903705370	-108.67732	41.52786	Kelly 1
89	4903705634	-108.52962	41.63656	UPRR Forrest Arch 55
90	4903705798	-108.58413	41.71535	UPRR Rock Spgs Graze
91	4903705844	-108.87046	41.79166	U.P.R.R. No. 23-17 Z
92	4903705865	-108.533272	41.856505	F-22-98-30-D-1
93	4903705867	-108.67711	41.86049	#2 Black Rock
94	4903705870	-108.48891	41.87131	Yovit Coyce #1
95	4903705906	-109.6425	41.95431	Govt #23-22
96	4903720030	-109.922075	41.087726	Meadow Springs Draw
97	4903720060	-109.07341	41.96944	Nitchie Gulch 9-16
98	4903720240	-108.74988	41.83883	No. 1-Z Garfield Fed
99	4903720241	-108.83519	41.24542	Wanner - GOVT 1
100	4903720243	-108.94034	41.24927	Neithig - GOVT 1
101	4903720285	-109.30282	41.61693	White Mountain Unit
102	4903720286	-108.90922	41.86428	102 GOVT 23-24-22-10
103	4903720299	-109.71319	41.53879	Spider Creek #1
104	4903720303	-109.60545	41.69766	Champlin 97 Amoco 1

Table A.1 (Continued)

Well ID #	API #	Longitude	Latitude	Well Name
105	4903720330	-107.97258	41.70643	Tierney Unit 1
106	4903720344	-109.85806	41.49849	Federal Short #22-32
107	4903720352	-109.14254	41.14832	US-Miller Mountain 1
108	4903720377	-109.32917	41.91509	Husky Federal No. 7-
109	4903720379	-109.806	41.57849	Champlin 157 Amoco 1
110	4903720427	-109.42742	41.53011	Green River 1
111	4903720429	-109.38411	41.56306	West Rock Springs #1
112	4903720431	-109.38451	41.63167	West White Mountain
113	4903720433	-109.95521	41.26152	Leo Unit 1
114	4903720456	-108.60216	41.1053	Kinney Unit W-14726
115	4903720466	-109.854896	41.290261	Wildcat #1X-3
116	4903720525	-108.80286	41.78809	True-Bluewater Reser
117	4903720557	-108.85034	41.20616	Champlin Fed 1-12
118	4903720559	-109.60639	41.18139	Currant Creek 1
119	4903720584	-109.28192	41.89626	Federal - Eden Unit
120	4903720602	-109.854896	41.290261	Henry Unit #1
121	4903720632	-108.37501	41.50243	#1 Delaney Rim Unit
122	4903720650	-109.61351	41.96509	Sandy Bend #1
123	4903720655	-108.727559	41.396406	Brady Deep Unit #23W
124	4903720707	-108.9653	41.18466	Natural Res-Fed 1-24
125	4903720720	-109.61387	42.09944	Simpson Gulch 1
126	4903720724	-108.83087	41.19869	Kent Ranch Unit II2
127	4903720731	-108.85034	41.22396	Four-Thirty-Federal
128	4903720744	-108.03235	41.46207	Champlin #237 Amoco
129	4903720755	-109.77661	41.72741	Tripp Ranch Unit 1-A
130	4903720763	-108.21073	41.47681	Camplin 256 Amoco A
131	4903720764	-107.99881	41.49118	Champlin 261 - A1
132	4903720790	-108.30602	41.44616	#1 North Fork Federal
133	4903720794	-107.53841	41.80222	Champlin 272 – Amoco
134	4903720799	-108.1912	41.62481	Tipton II Unit 1
135	4903720806	-108.18625	41.88269	Red Desert 1
136	4903720810	-107.63879	41.67589	Champlin 252 Amoco
137	4903720832	-108.53575	41.45222	Higgins Unit 6 22-14
138	4903720850	-108.35356	41.97969	Hay Reservoir 15689A
139	4903720853	-108.02107	41.81808	Siberia Ridge Unit 5
140	4903720864	-109.95739	41.50149	Champlin 355 Amoco
141	4903720893	-108.47201	41.49518	Higgins #4 32-32

Table A.1 (Continued)

Well ID #	API #	Longitude	Latitude	Well Name
142	4903720970	-108.85429	41.47571	# 2-1 Amoco - Champl
143	4903720990	-109.40409	41.90649	Big Wind Unit #1
144	4903721015	-108.28332	41.90419	Champlin 438 Amoco A
145	4903721066	-109.57119	41.42959	3-26 Federal Massacr
146	4903721092	-109.51411	41.47899	Massacre Hills - Cha
147	4903721157	-109.20154	41.2915	Silver Dollar 1
148	4903721219	-108.48521	42.14203	Five Fingers Unit 1
149	4903721316	-108.8159	41.4833	3 Government Bluewat
150	4903721319	-109.75073	42.24267	Parrish Mark Unit 1
151	4903721337	-109.99472	41.53056	Champlin 358 Amoco C
152	4903721425	-109.05164	42.12453	Packsaddle Unit 1
153	4903721434	-109.09152	42.26093	Pacific Creek Federa
154	4903721449	-109.17211	41.96385	Boars Tusk W-19510 1
155	4903721547	-108.66463	42.12564	Lost Valley Unit 3
156	4903721671	-108.37092	41.62191	Table Rock Unit 44
157	4903721703	-109.13153	42.03474	Federal 44-24
158	4903721721	-109.1552	42.00944	Goodstein 1
159	4903721735	-110.01	41.91611	46 Whiskey Buttes Un
160	4903721752	-109.04952	42.20036	Rock Cabin Federal 1
161	4903721853	-108.9204	42.11434	Pirate Unit 1
162	4903721927	-109.71611	42.14741	W-62492 1
163	4903721958	-109.45161	41.65963	Dagger Unit 1
164	4903722011	-107.5506	41.67367	1-A Separation Creek
165	4903722059	-109.47222	41.85591	Blue Rim Federal 1-3
166	4903722344	-108.68667	41.47229	Brady Unit 37N
167	4903722661	-109.96497	41.89626	Uprr No. 34-11
168	4903722688	-109.77257	42.00401	Raintree Federal No.
169	4903722702	-109.92894	41.89677	Lombraro Butte Feder
170	4903722920	-108.35117	41.52122	#1 Glasnost Federal
171	4903723066	-109.9759	41.60232	Champlin 206 G 1
172	4903723135	-107.87611	41.68444	Blackbird Federal #2
173	4903723194	-108.66264	41.7975	Twelve Mile Gulch Un
174	4903723259	-109.97429	41.65932	Champlin 285 L 2
175	4903723453	-109.969	41.71384	Champlin 326 Amoco G
176	4903723494	-109.38428	41.7452	Mountaineer No. 1-35
177	4903723539	-109.48137	41.86112	Stratos Federal Unit
178	4903723631	-109.8763	41.97424	Horseshoe Unit #10-1

Table A.1 (Continued)

Well ID #	API #	Longitude	Latitude	Well Name
179	4903723639	-108.04856	41.47342	Champlin Unit 293 #B
180	4903723702	-108.60352	41.99731	Charlotte 3 Fede
181	4903723720	-108.58693	41.47292	Sand Butte 3-5
182	4903723845	-108.24481	41.77428	Wild Thing #322
183	4903723886	-108.36944	41.76777	Sage Flat #6
184	4903724234	-108.27253	41.67704	Sidewinder Unit #2-H
185	4903724248	-108.70694	41.15639	Chicken Springs 33-3
186	4903724261	-108.44861	41.7975	Sage Flat Unit #7H
187	4903724308	-109.54783	41.93163	Stagecoach Draw Unit
188	4903724316	-108.17694	41.74472	Peg Federal #1
189	4903724400	-108.760882	41.39207	Brady Deep #47F
190	4903724404	-110.041428	41.918536	Rainbow Federal 1-6
191	4903724557	-110.02694	41.45444	Church Buttes Unit #
192	4903724948	-108.748072	41.43498	Churchill Federal Un
193	4903725125	-108.74491	41.37869	Brady Deep 56W
194	4903725518	-108.83826	41.24081	Prstate 15102 NE 36
195	4903725850	-108.647328	41.153919	Rhode Island Red Fed
196	4903726359	-108.76276	41.04627	Canyon Creek Unit 44
197	4904105223	-110.196517	41.357356	Target Federal #A1-1
198	4904105236	-110.41409	41.39444	F-43-6-G Gov't. Blan
199	4904120003	-110.48583	41.14341	Blacks Fork Unit #1
200	4904120019	-110.0649	41.25429	Butcher Knife Spring
201	4904120025	-110.05526	41.18911	Big Hollow 16-1
202	4904120038	-110.28028	41.20556	Leavitt Creek Unit #
203	4904120103	-110.17729	41.40789	Champlin 415 Amoco
204	4904120106	-110.41881	41.44472	Amoco Champlin 413
205	4904120200	-110.16876	41.26767	Hank Unit 1
206	4904120263	-110.293497	41.066743	Hiller Federal #1-32
207	4904120367	-110.34181	40.99959	Big Spring Unit #15-
208	4904120454	-110.339533	41.101415	Ausa Federal #1-14
209	4904120556	-110.46681	41.48181	Champlin 549 Amoco B
210	4904120647	-110.235783	41.05861	Taylor Federal #35-1
211	4904120665	-110.379334	41.123219	Lyman #9-7
212	4904120686	-110.116119	41.232369	Allen Federal #1-35
213	4904120724	-110.2575	41.01039	Luckey Ditch Federal
214	4904120732	-110.465605	41.057112	Thunderbolt Mountain
215	4904120740	-110.26611	41.04489	Whiskey Springs Federal

Table A.1 (Continued)

Well ID #	API #	Longitude	Latitude	Well Name
216	4904120759	-110.26511	41.03739	Lucky Ditch Federal
217	4904120774	-110.29944	41.04549	Whiskey Springs #2
218	4904120778	-110.39661	41.54806	WECO-UPRC-WWRC 21-15
219	4904120782	-110.08449	41.05011	Wadsworth Fee #1
220	4904120783	-110.23529	41.136725	Mountain View Unit #
221	4904120786	-110.29815	41.136442	West Reed Unit #1-6
222	4904120793	-110.110374	41.182279	8819 JV-P Dog Spring
223	4904120808	-110.25836	41.0741	Taylor Ranch Federal
224	4904120810	-110.34164	41.04431	Whiskey Springs #6
225	4904120932	-110.198392	41.080196	Longtree #12-30 #12-
226	4904120975	-110.176917	41.110601	Henry #10-17
227	4904120988	-110.0815	41.40536	Church Buttes #135
228	4904121027	-110.142513	41.297477	Cinderella #20-9
229	4904121045	-110.14645	41.48735	Thompson Federal #2-
230	4904121066	-110.35694	41.01444	Wasatch National For
231	4904121077	-110.25443	41.47298	Austin Reservoir #10
232	4904121084	-110.292222	41.53083	Hampton #10-21
233	4904121088	-110.12833	41.49472	State of Wyoming #4
234	4904121106	-110.1025	41.51	Grace USA 1-30 #5

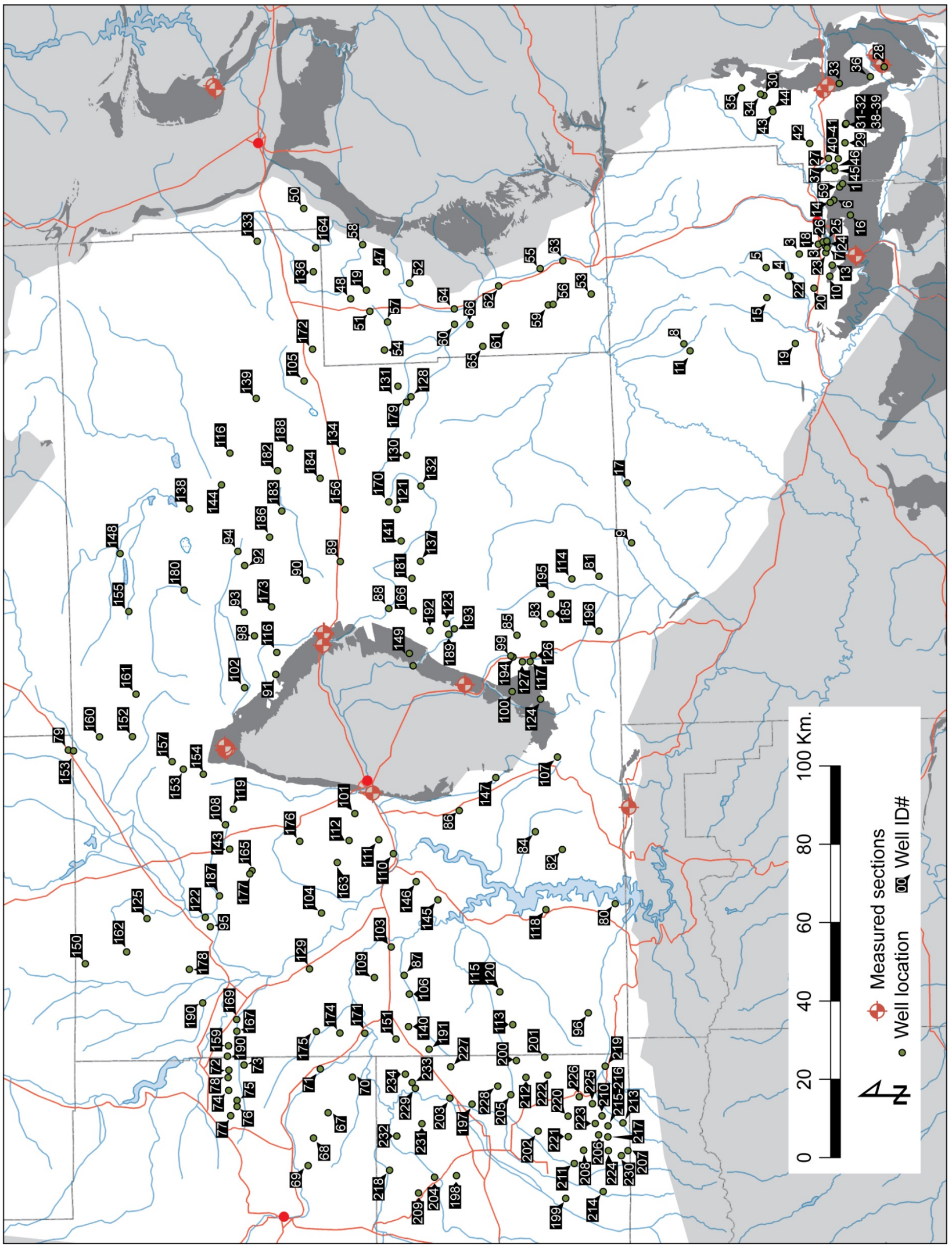

Figure A.1: Map of the study area and location of each well in the dataset. Well ID number is provided for cross-reference with table A.1

Appendix B: Stratigraphic measured section collected

Stratigraphic sections were measured through the Canyon Creek Member, Almond Formation, Twentymile sandstone, Holderness Member, and Pine Ridge sandstone in the Washakie, Hanna, Sand Wash, and Middle Park basins. The location of each measure section can be found in Figure B.1. The UTM coordinates and units measured can be found in Table B.1. Thickness is always measured in meters and the symbols used can be found in Figure B.2.

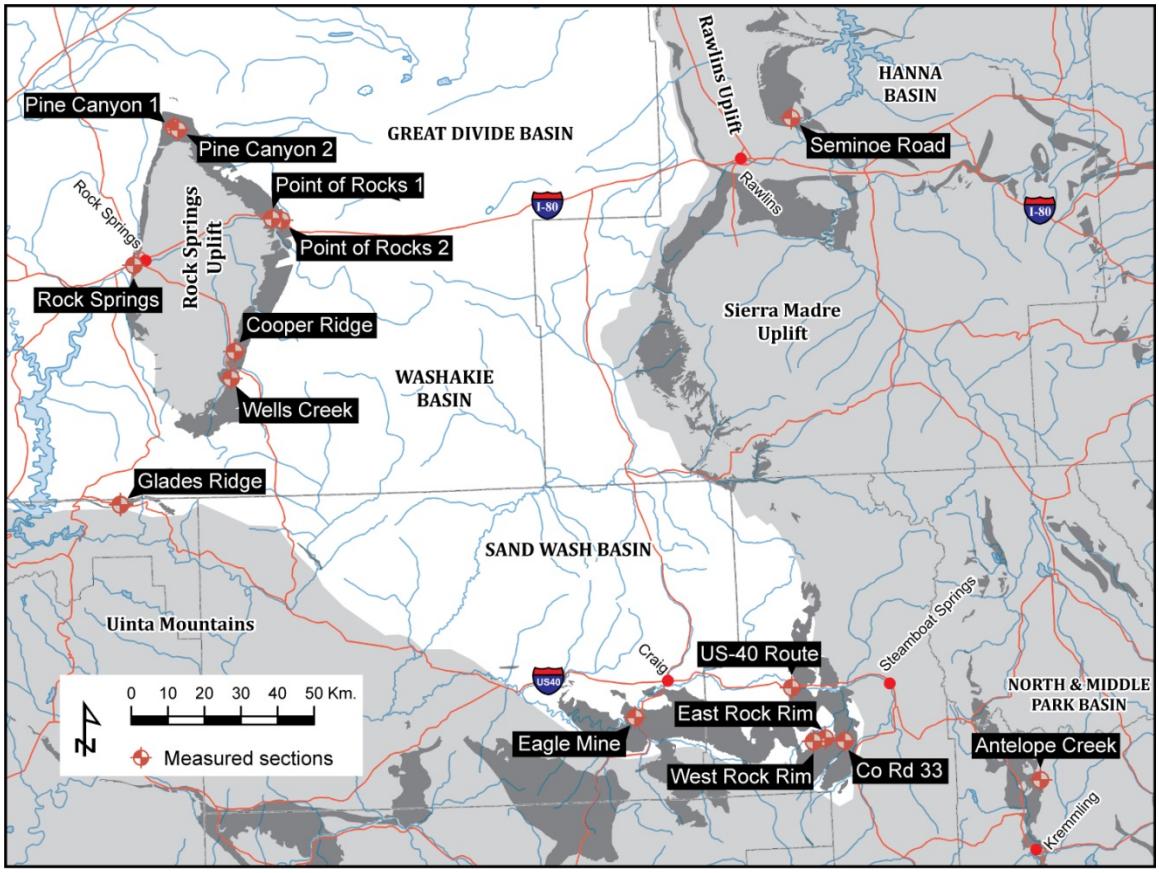

Figure B.1: Map of the study area and location of each stratigraphic measured section in the dataset.

Table B.1: List of the stratigraphic sections measured for this study.

Measured Section	UTM Coordinates Base		UTM Coordinates Top		Lithostratigraphic Units
	Easting	Northing	Easting	Northing	
Pine Canyon 1	12T 657505	4641895	12T 657560	4641980	Almond Fm.
Pine Canyon 2	12T 658010	4641245	12T 658030	4641250	Canyon Creek Mb.
Point of Rocks 1	12T 684275	4616960	12T 684255	4616995	Canyon Creek Mb.
Point of Rocks 2	12T 687025	4616505	12T 687585	4616735	Almond Fm.
Rock Springs	12T 646640	4604170	12T 646625	4604190	Canyon Creek Mb.
Cooper Ridge	12T 674150	4580565	12T 674390	4580670	Canyon Creek Mb.
Wells Creek	12T 673645	4573440	12T 674345	4573200	Almond Fm.
Glades Ridge	12T 642920	4538740	12T 642900	4538795	Canyon Creek Mb.
Seminoe Road	13T 328380	4638655	13T 329470	4639425	Pine Ridge Ssnt., Almond Fm.
Eagle Mine	13T 274695	4478630	13T 275050	4478935	Sub-Twentymile Sstn., Mount Harris Mb.
US-40 Route	13T 317685	4483980	13T 317730	4484070	Twentymile Sstn., Holderness Mb.
East Rock Rim	13T 325570	4470170	13T 325570	4470200	Twentymile Sstn.
West Rock Rim	13T 322860	4468755	13T 322900	4468760	Twentymile Sstn.
Co Rd 33	13T 330580	4473060	13T 330525	4473180	Twentymile Sstn.
Antelope Creek	13T 384020	4454095	13T 384015	4454140	Gunsight Pass Sstn.

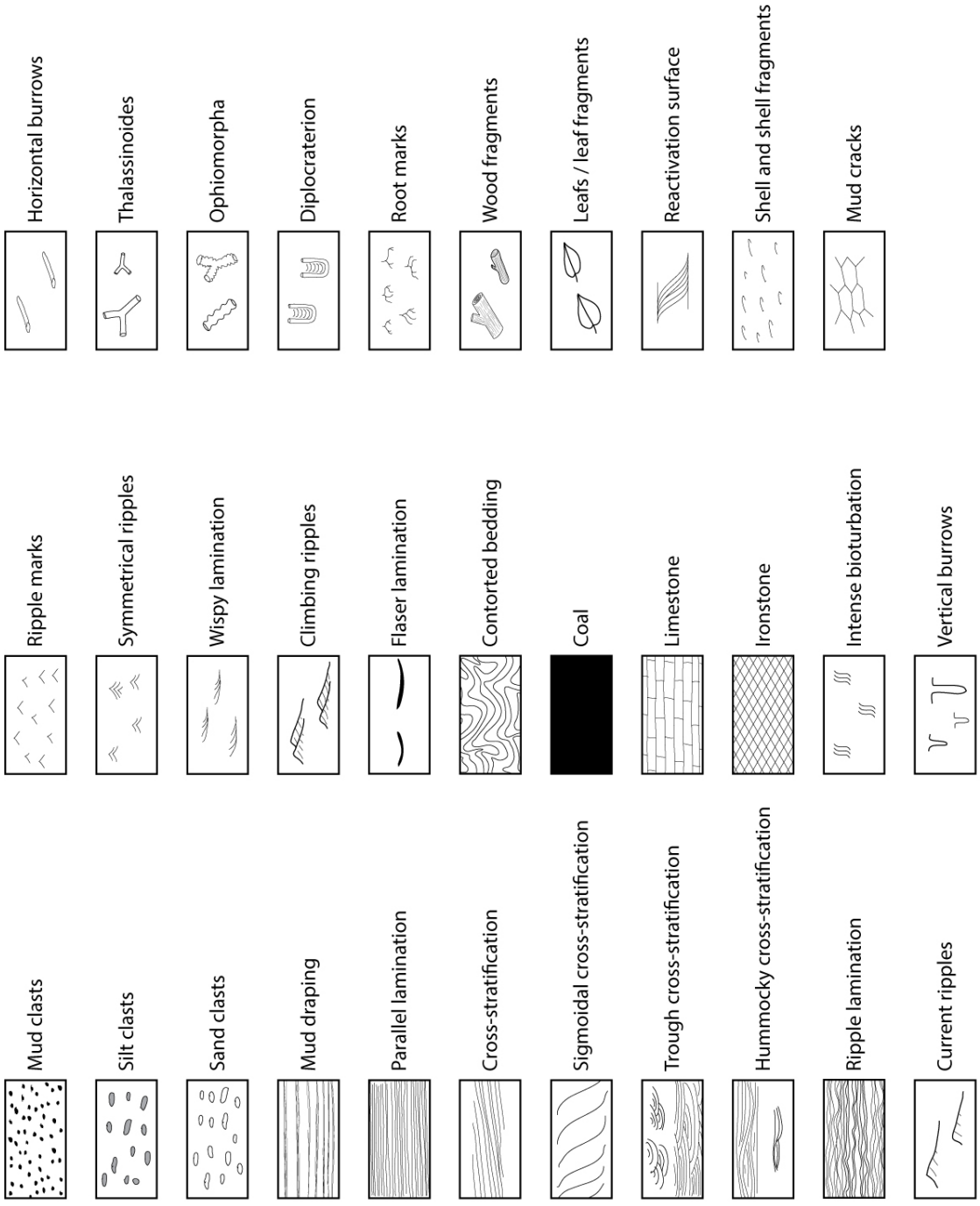

Figure B.2: Legend for the stratigraphic measured sections in figures B.3 through B.50.

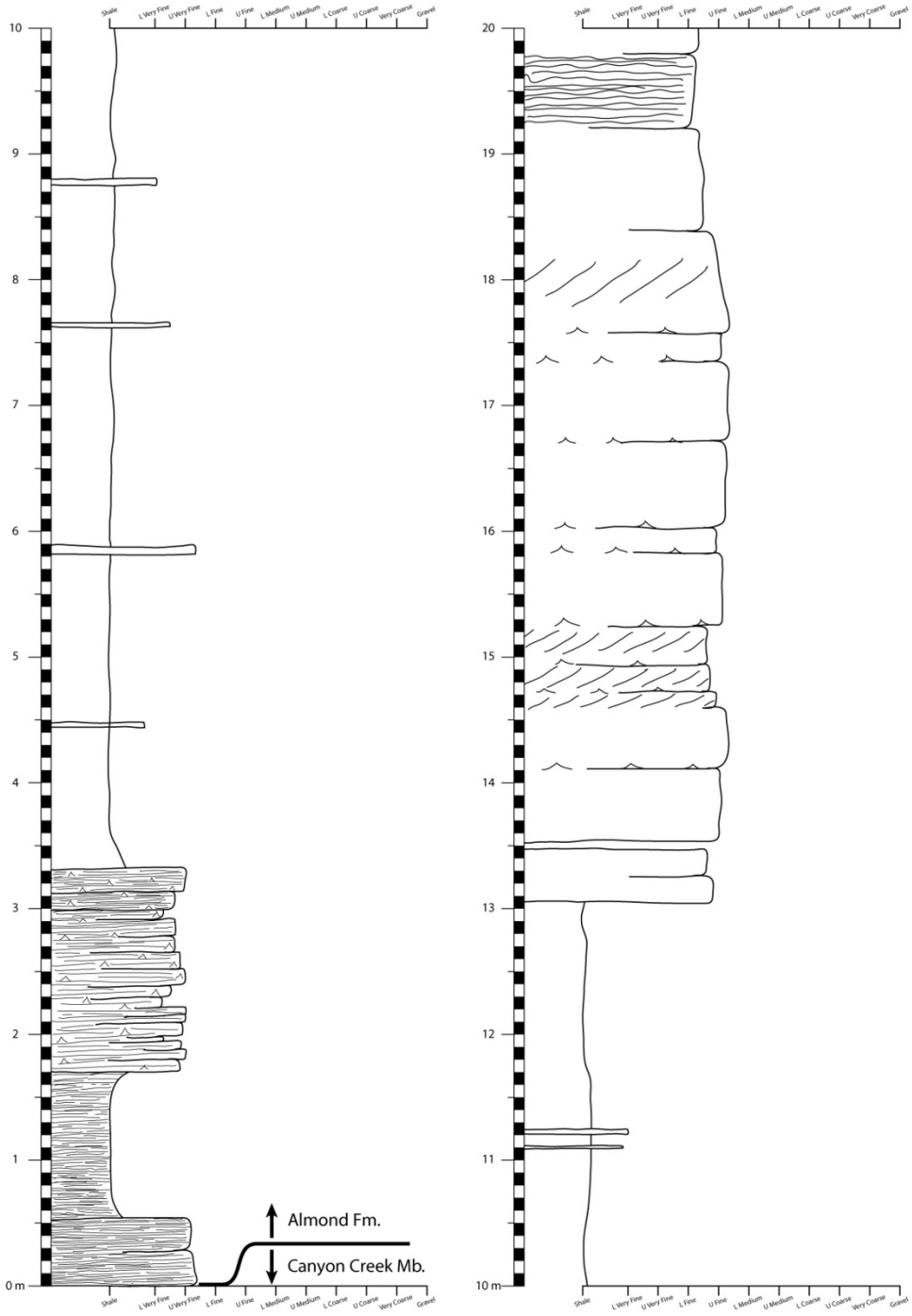

Figure B.3: Pine Canyon 1 section, part 1.

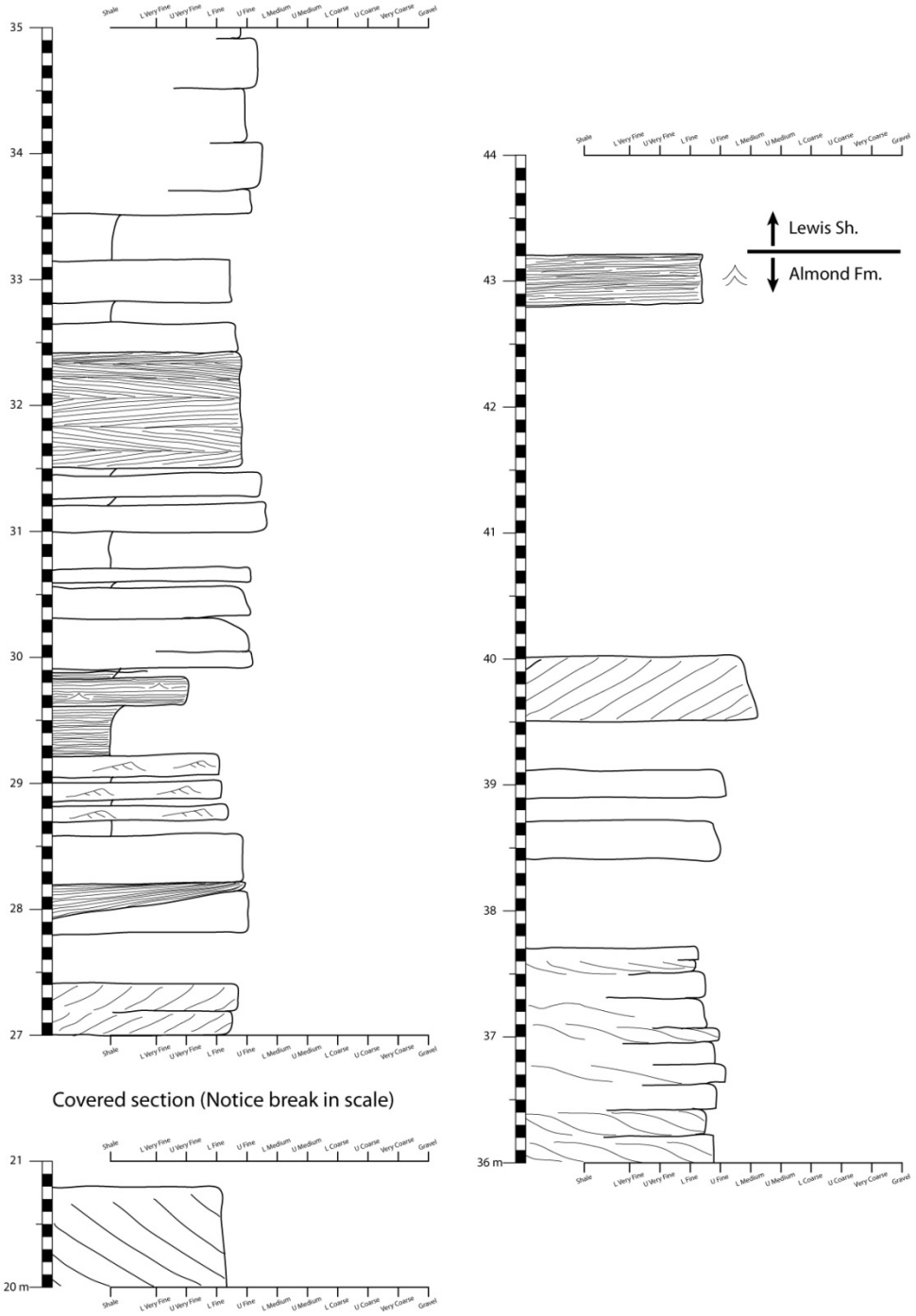

Figure B.4: Pine Canyon 1 section, part 2.

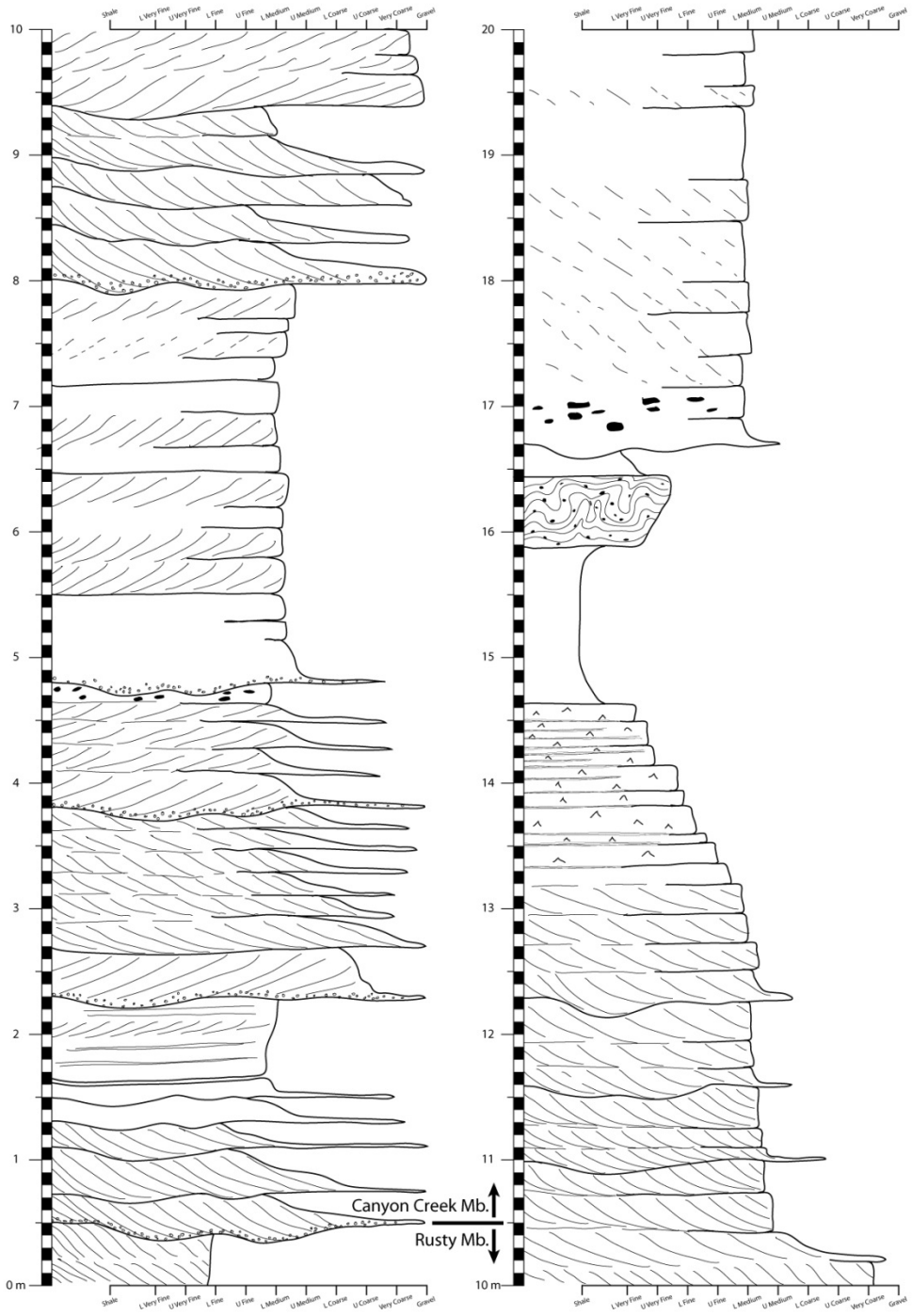

Figure B.5: Pine Canyon 2 section, part 1.

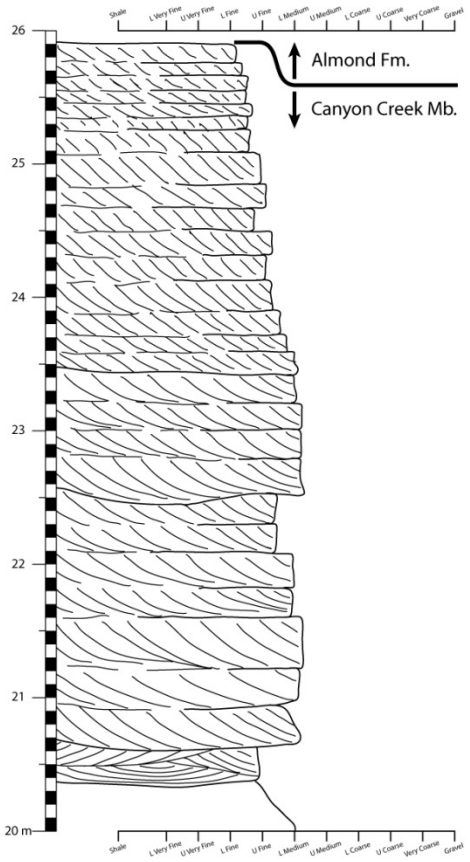

Figure B.6: Pine Canyon 2 section, part 2.

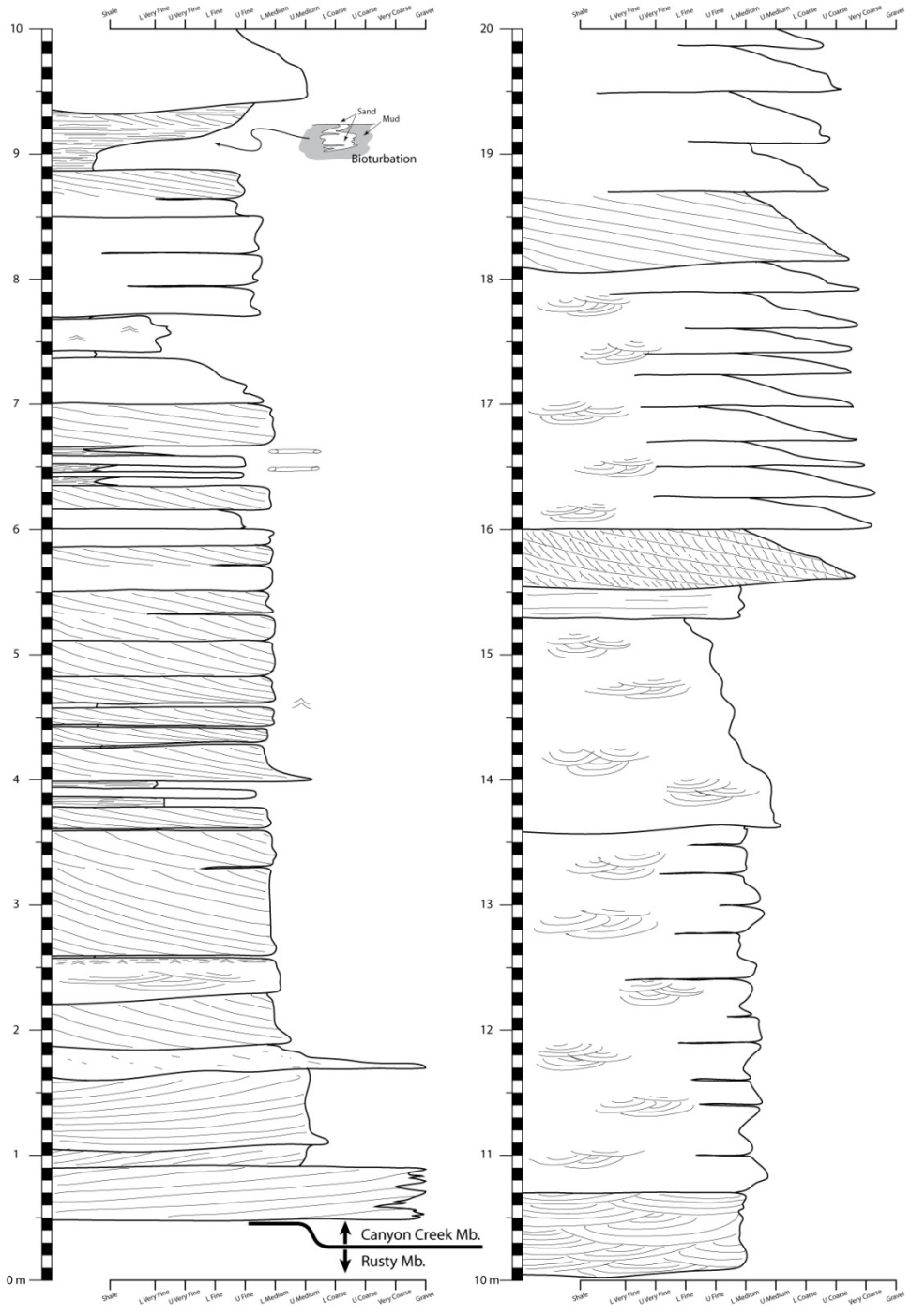

Figure B.7: Point of Rocks 1 section, part 1.

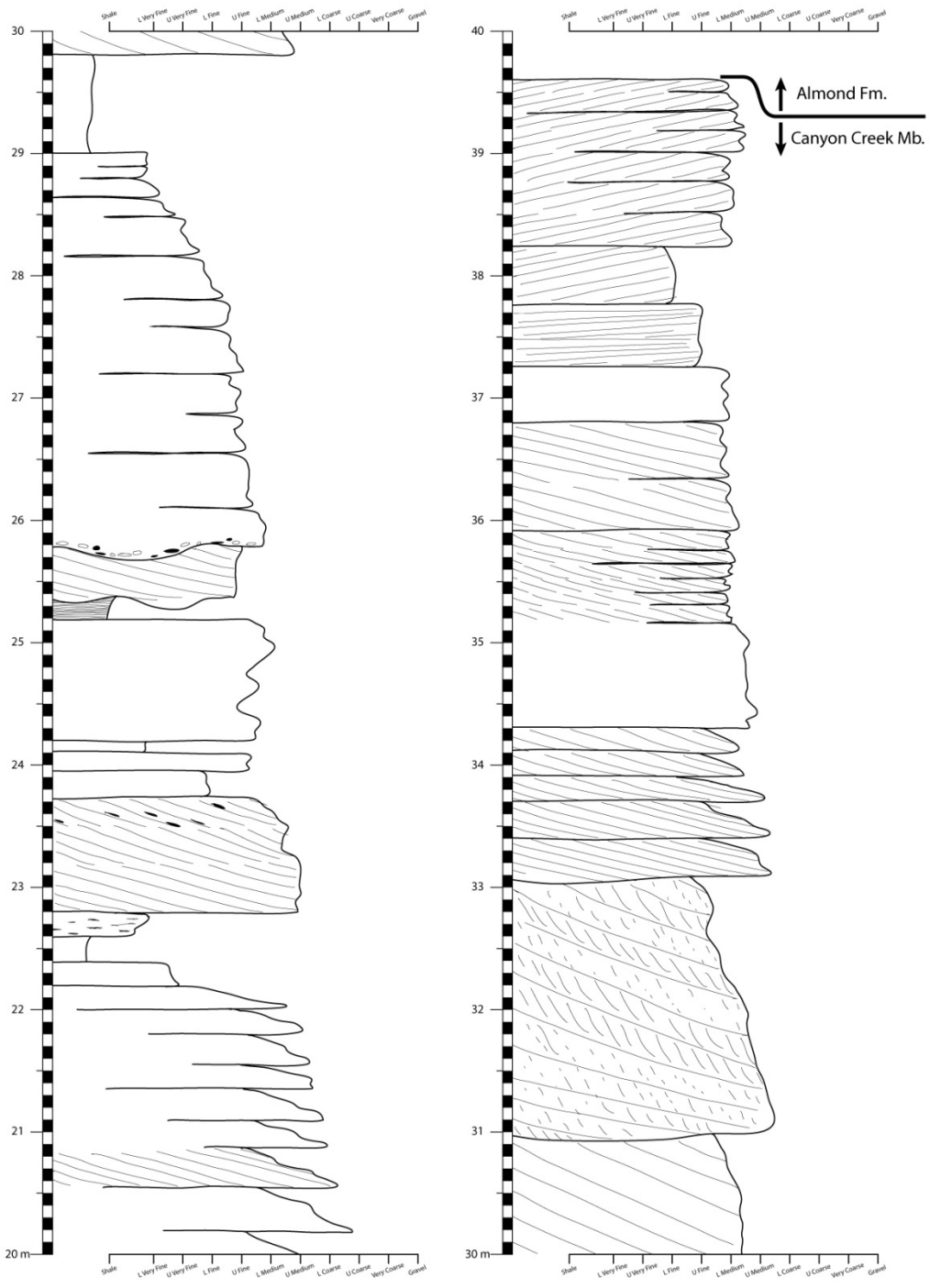

Figure B.8: Point of Rocks 1 section, part 2.

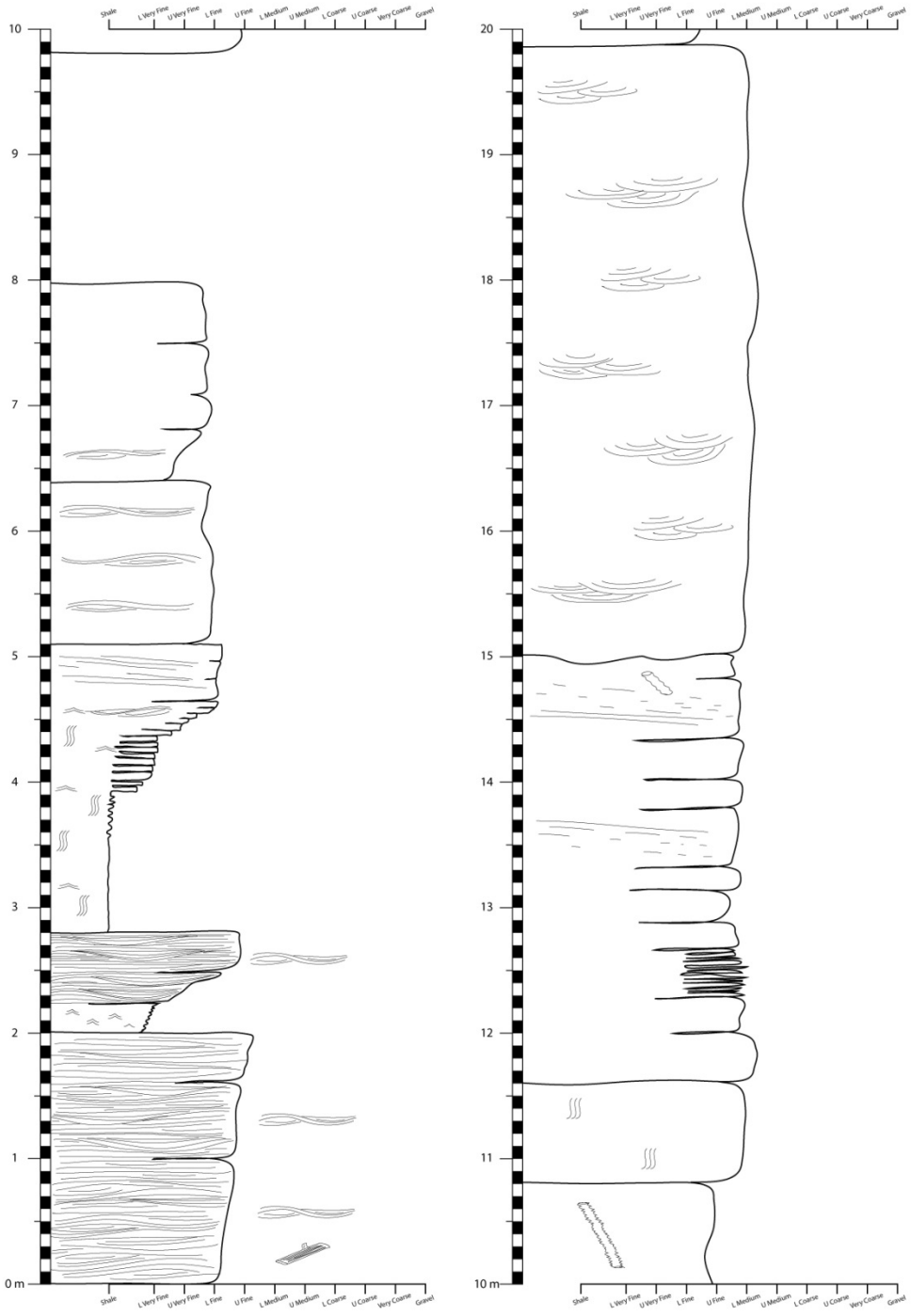

Figure B.9: Point of Rocks 2, part 1.

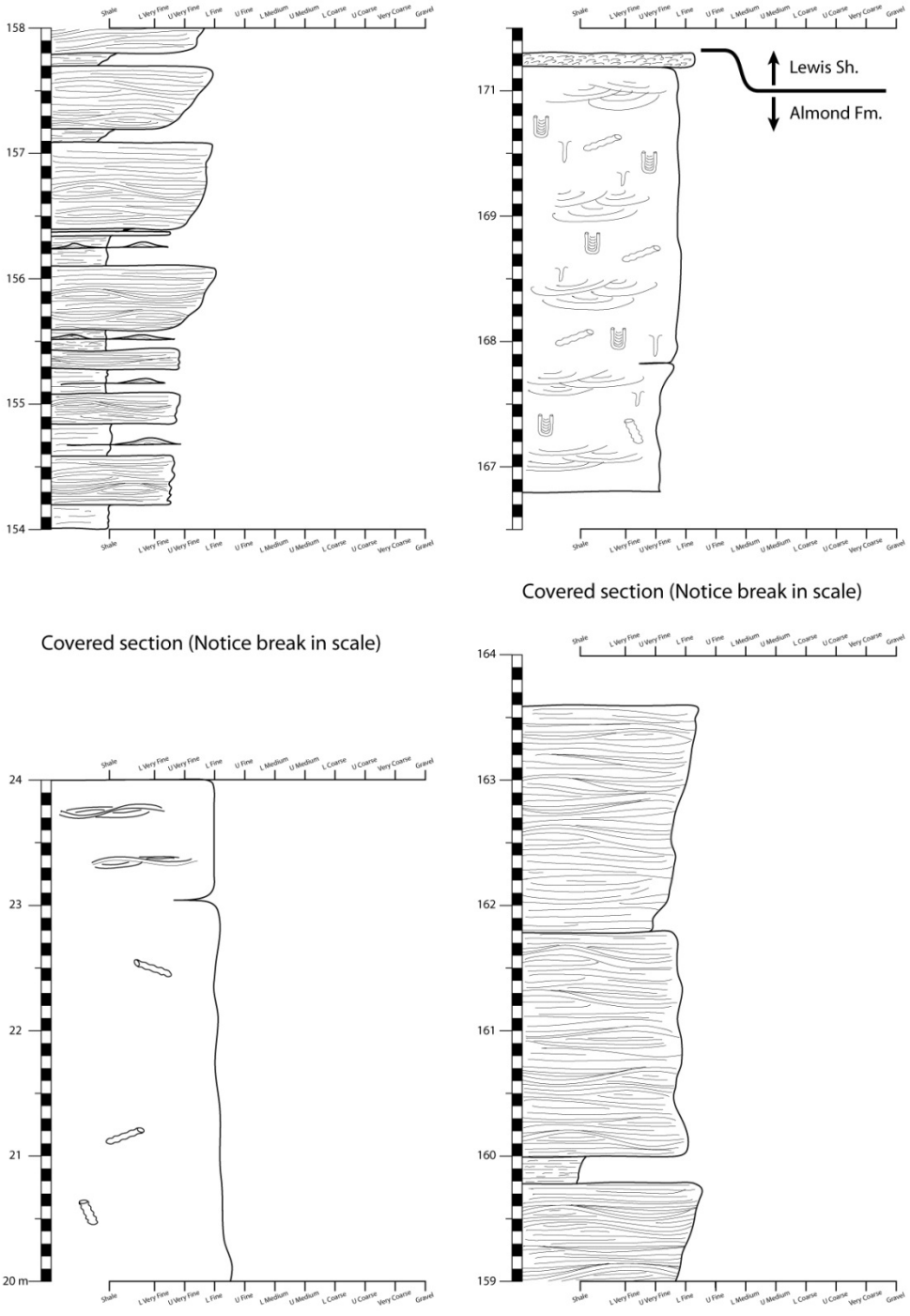

Figure B.10: Point of Rocks 2 section, part 2.

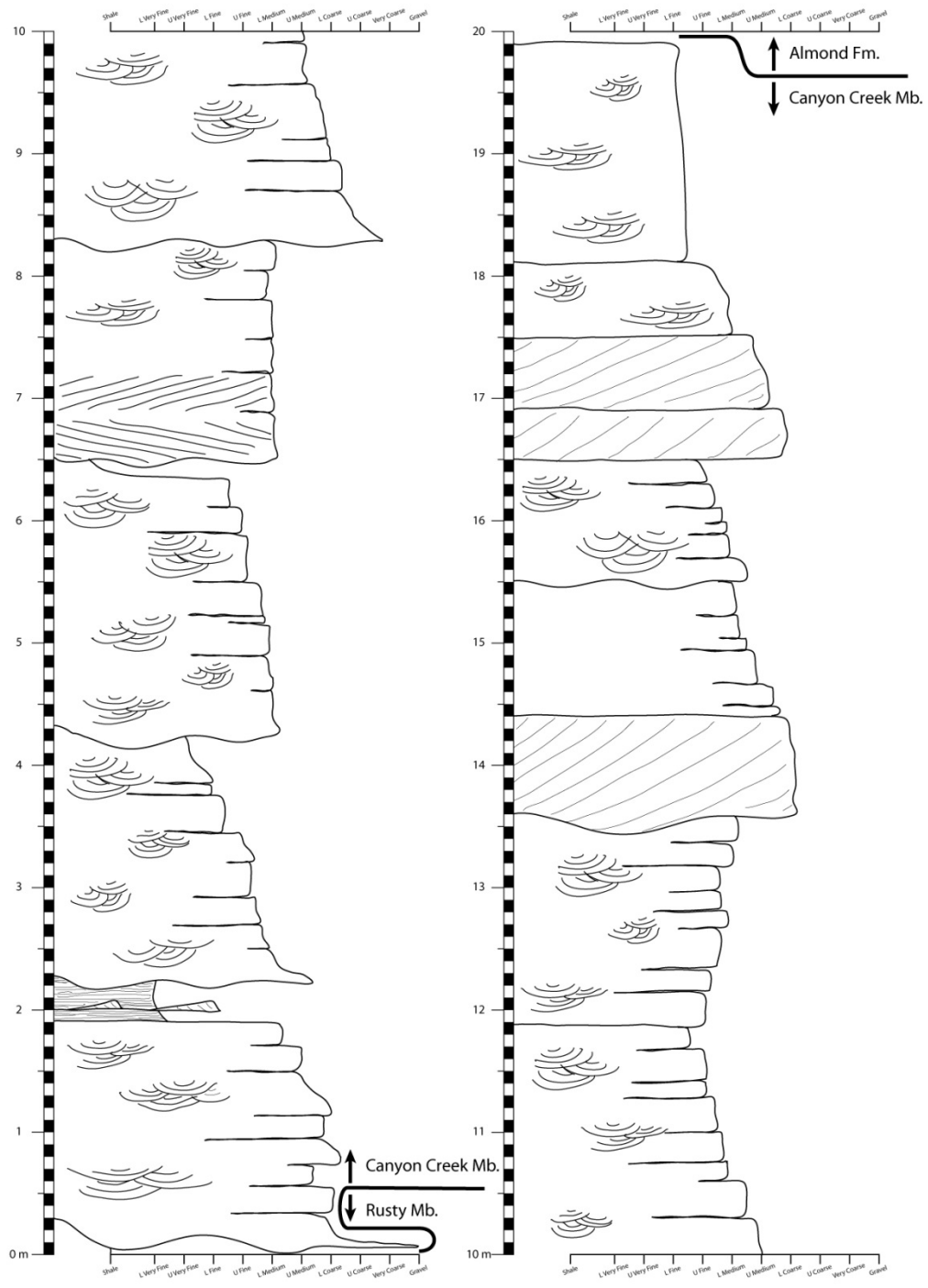

Figure B.11: Rock Springs section.

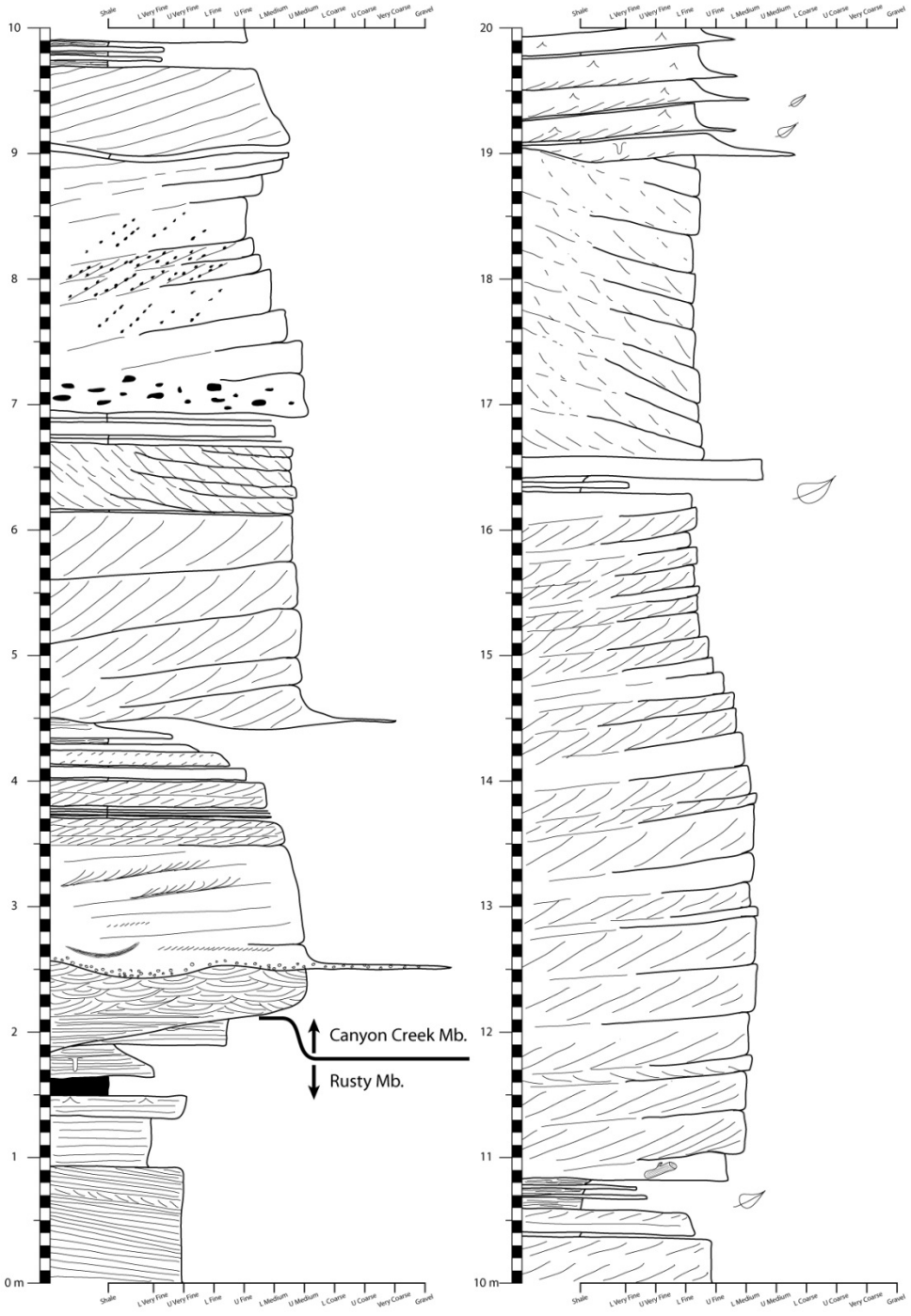

Figure B.12: Cooper Ridge section, part 1.

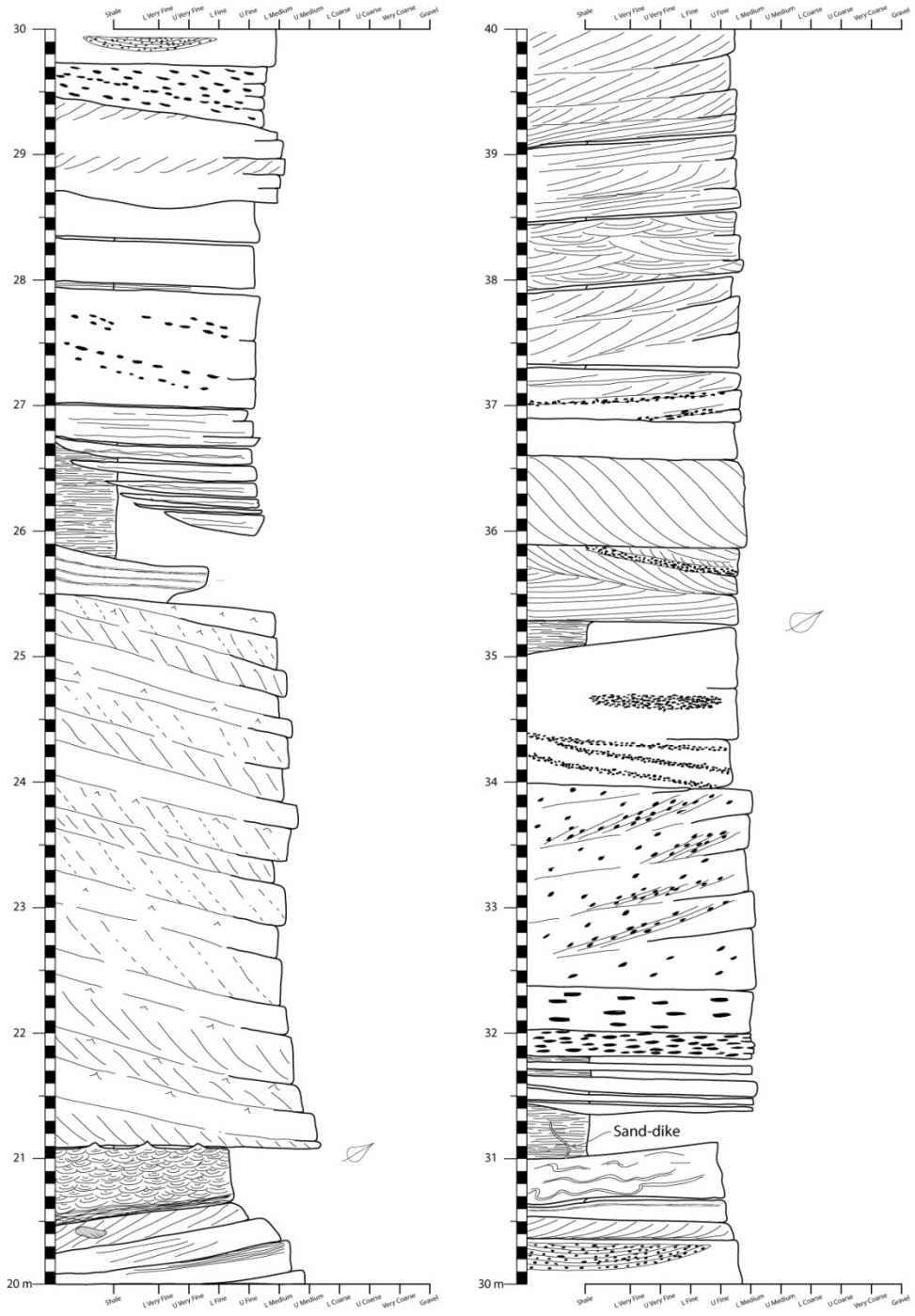

Figure B.13: Cooper Ridge section, part 2.

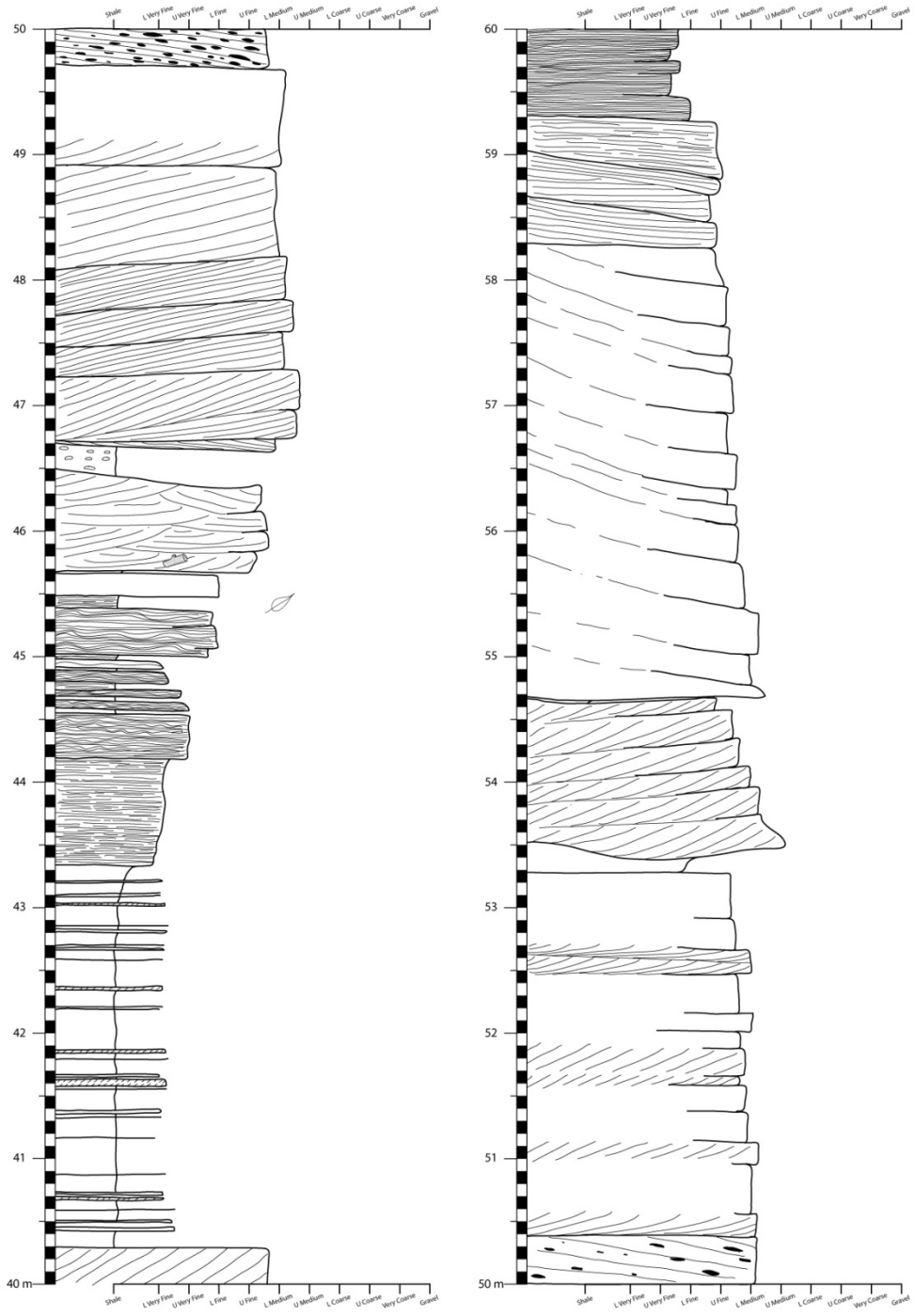

Figure B.14: Cooper Ridge section, part 3.

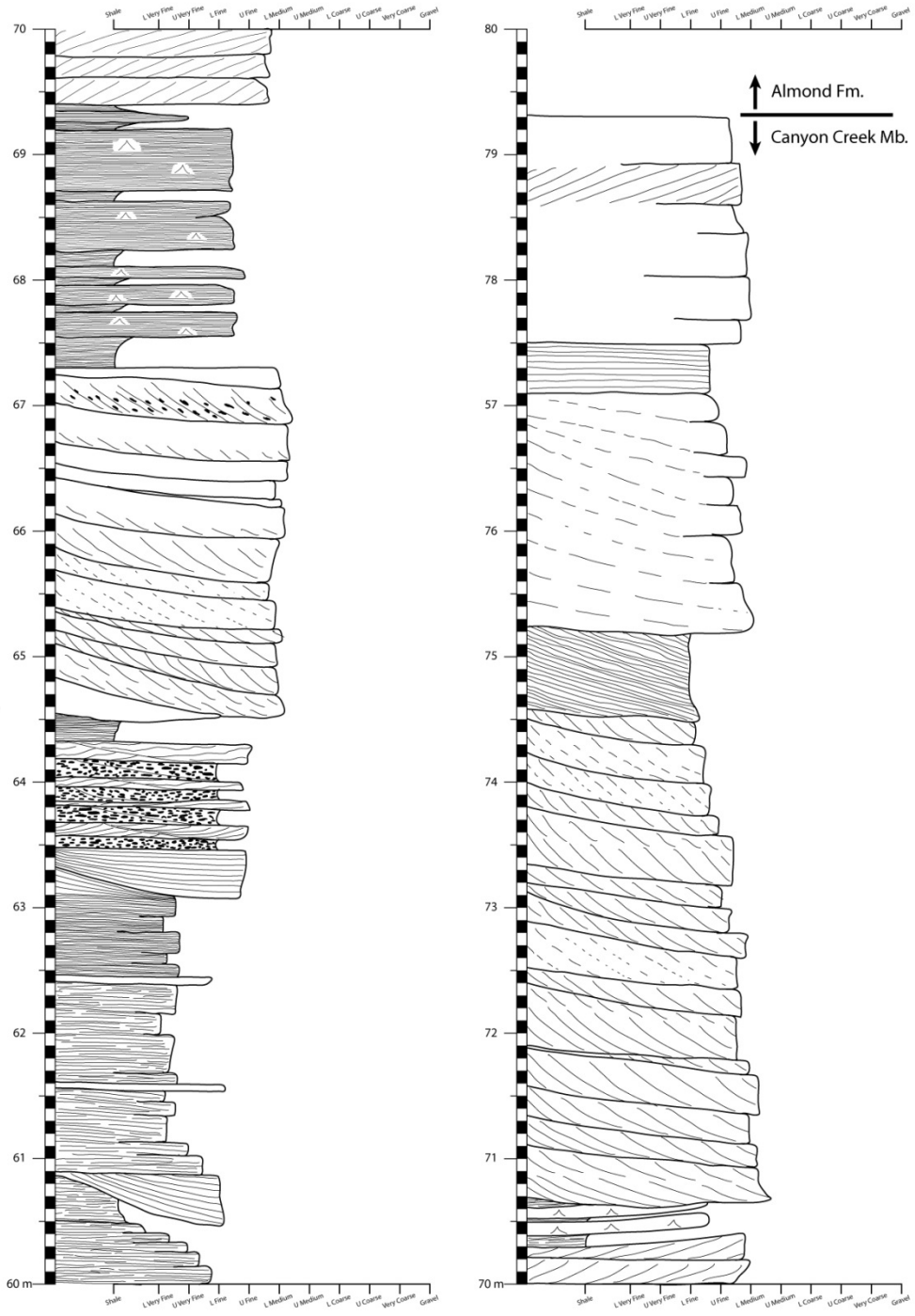

Figure B.15: Cooper Ridge section, part 4.

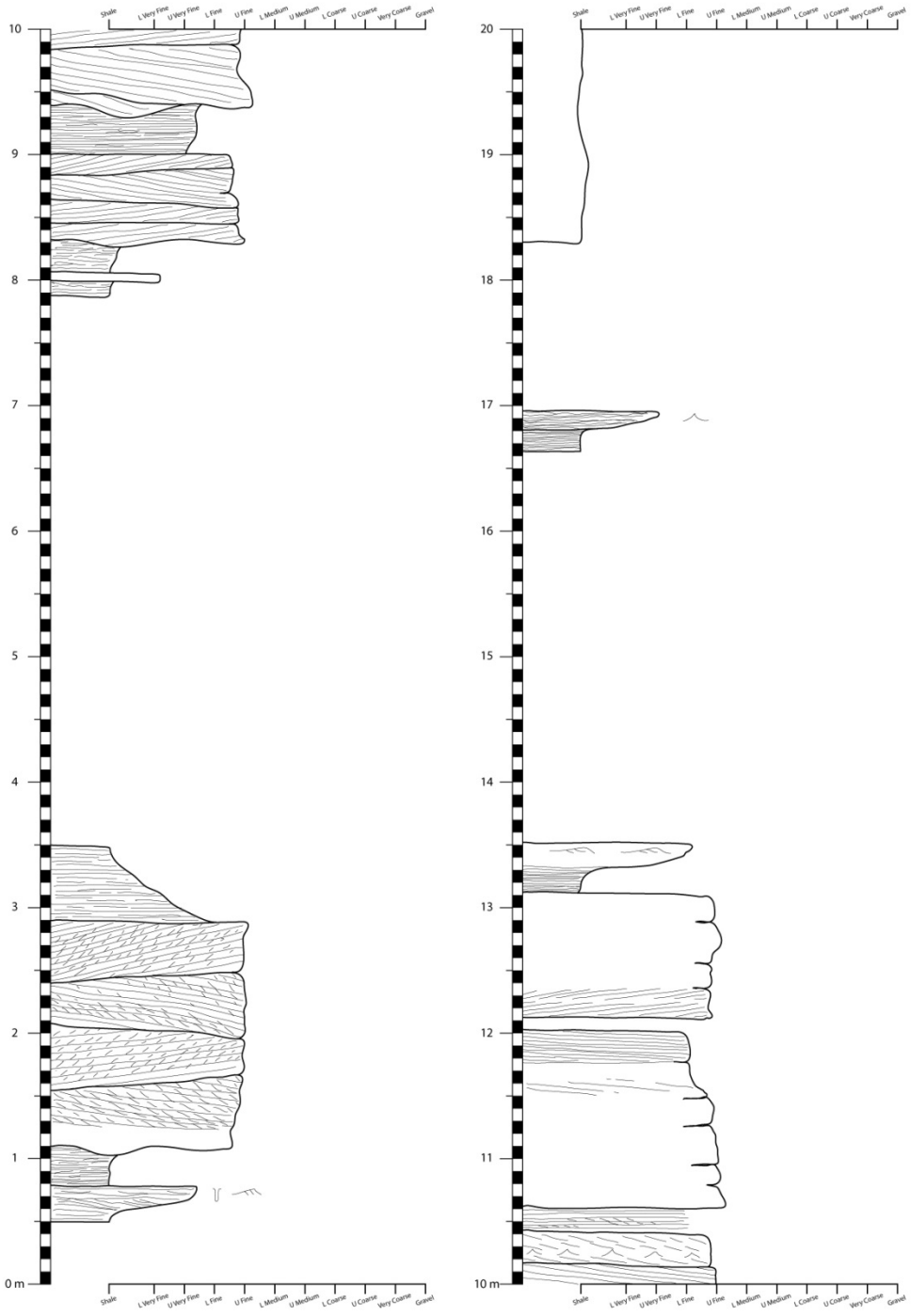

Figure B.16: Wells Creek section, part 1.

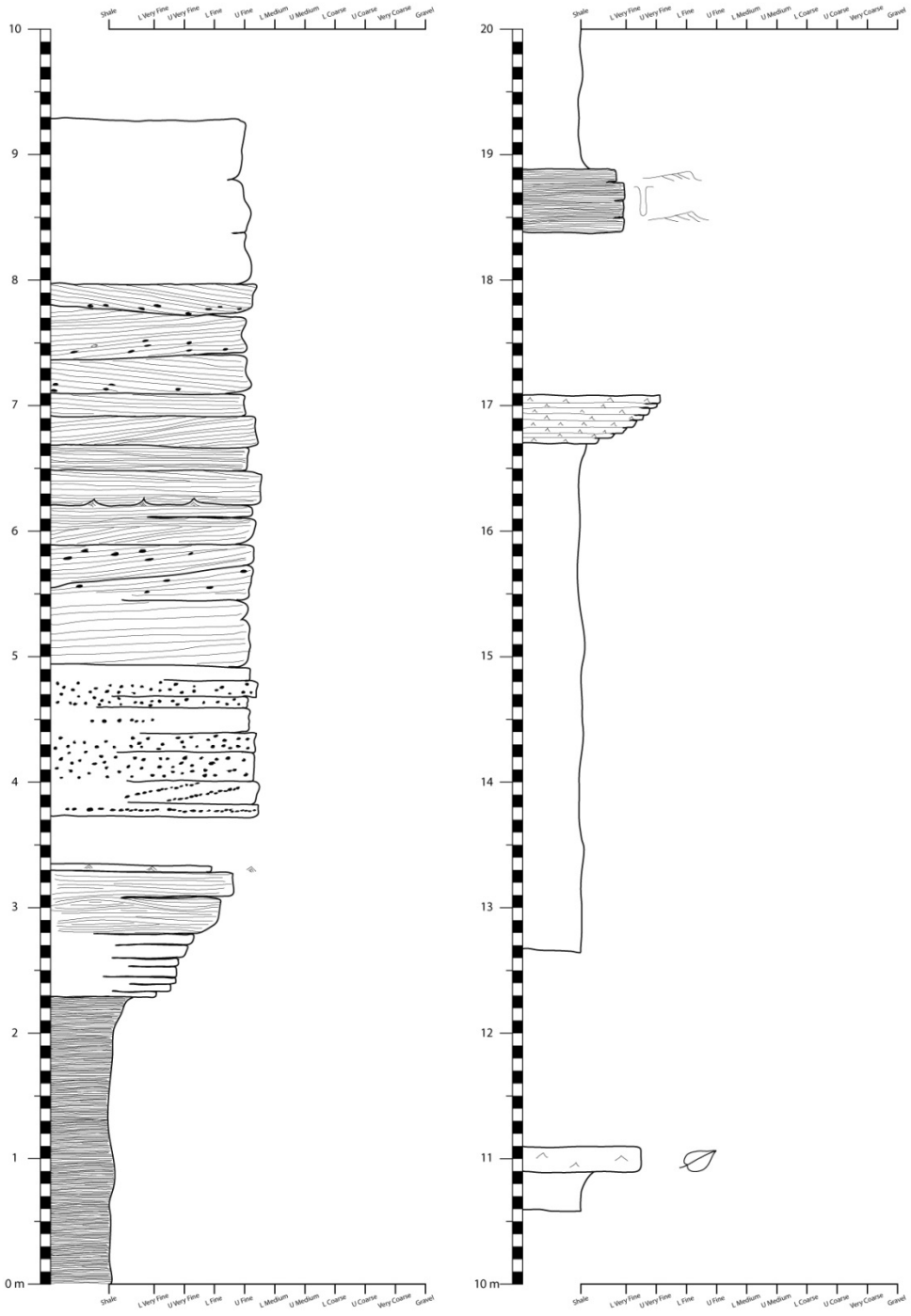

Figure B.17: Wells Creek section, part 2.

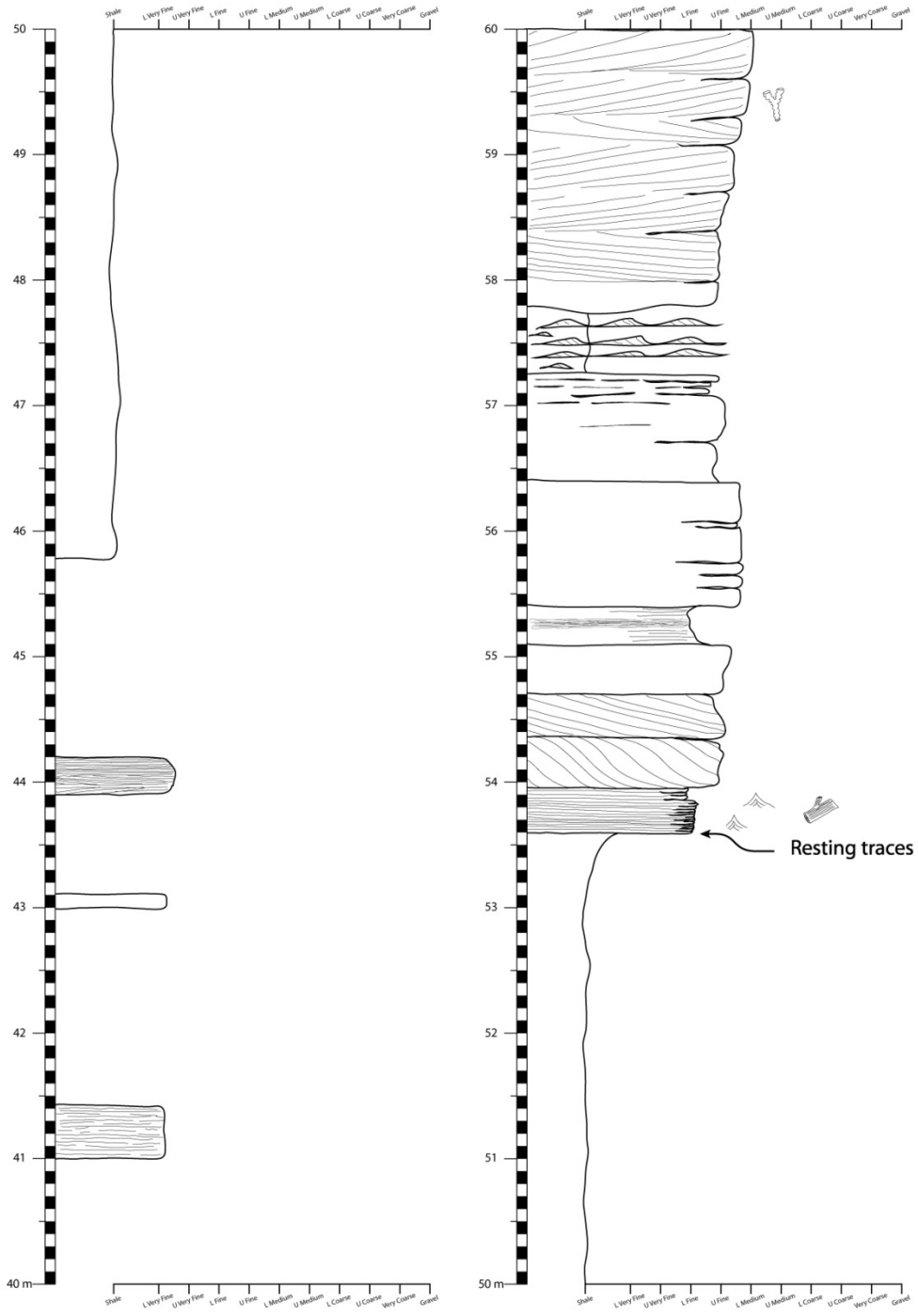

Figure B.18: Wells Creek section, part 3.

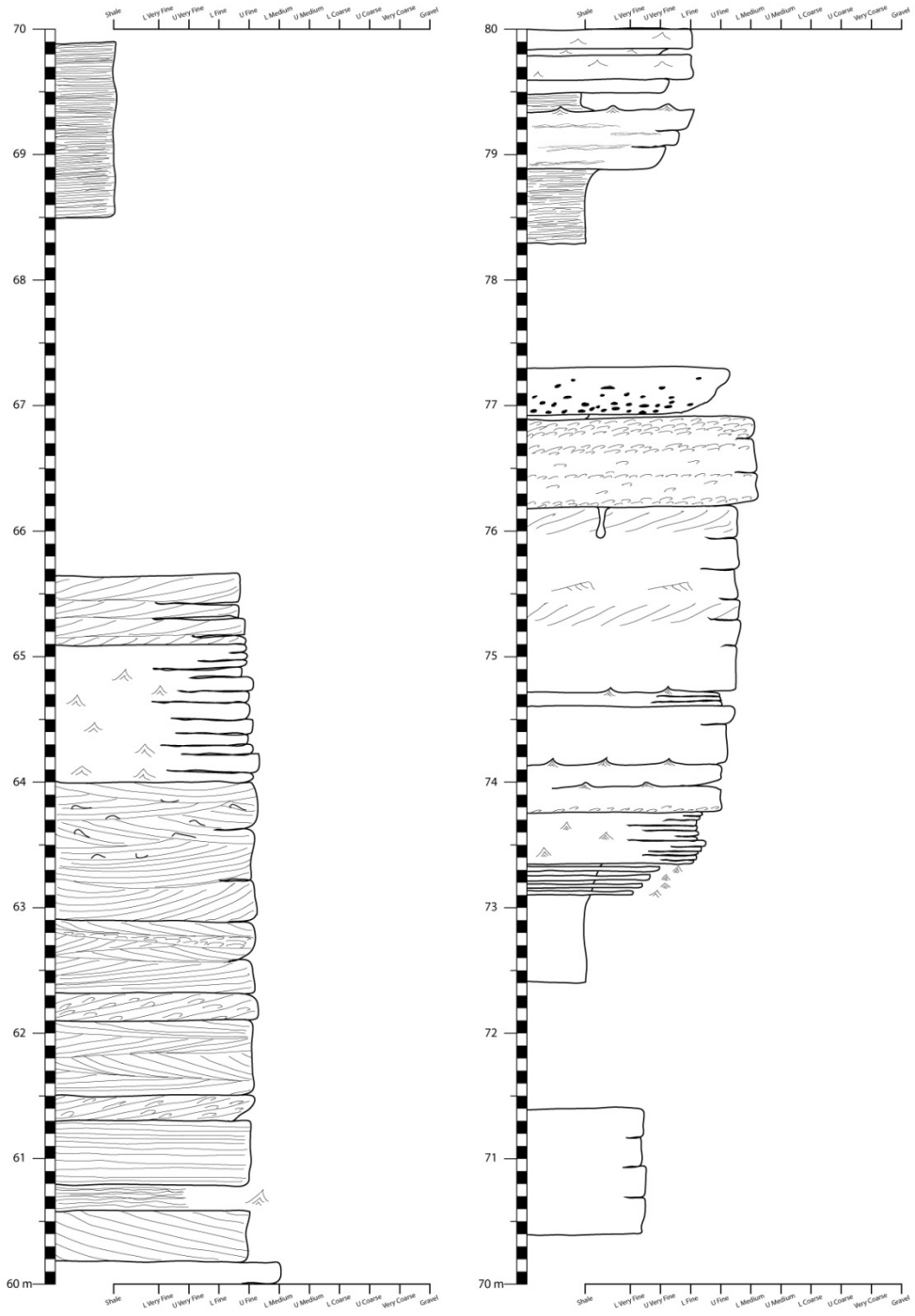

Figure B.19: Wells Creek section, part 4.

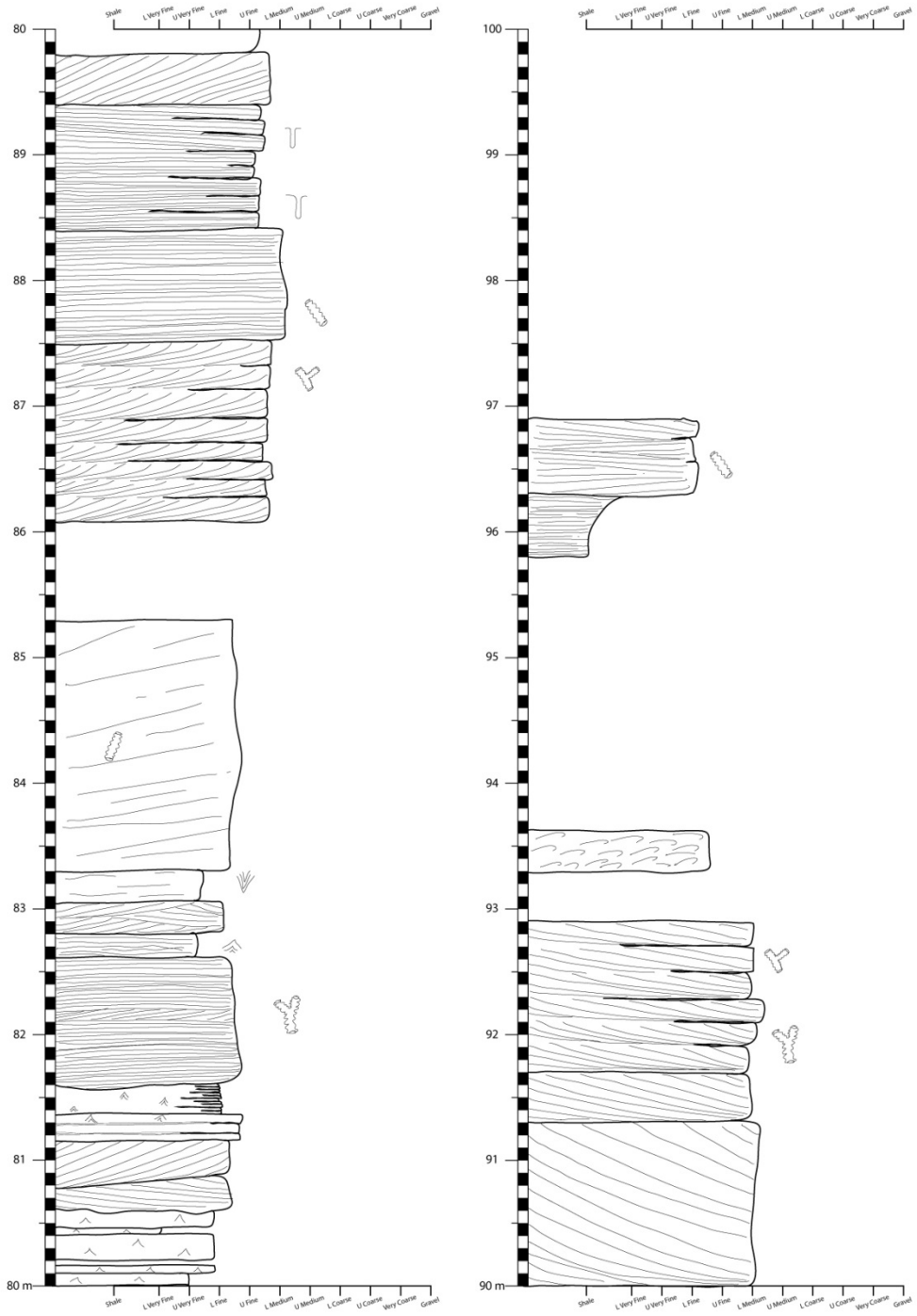

Figure B.20: Wells Creek section, part 5.

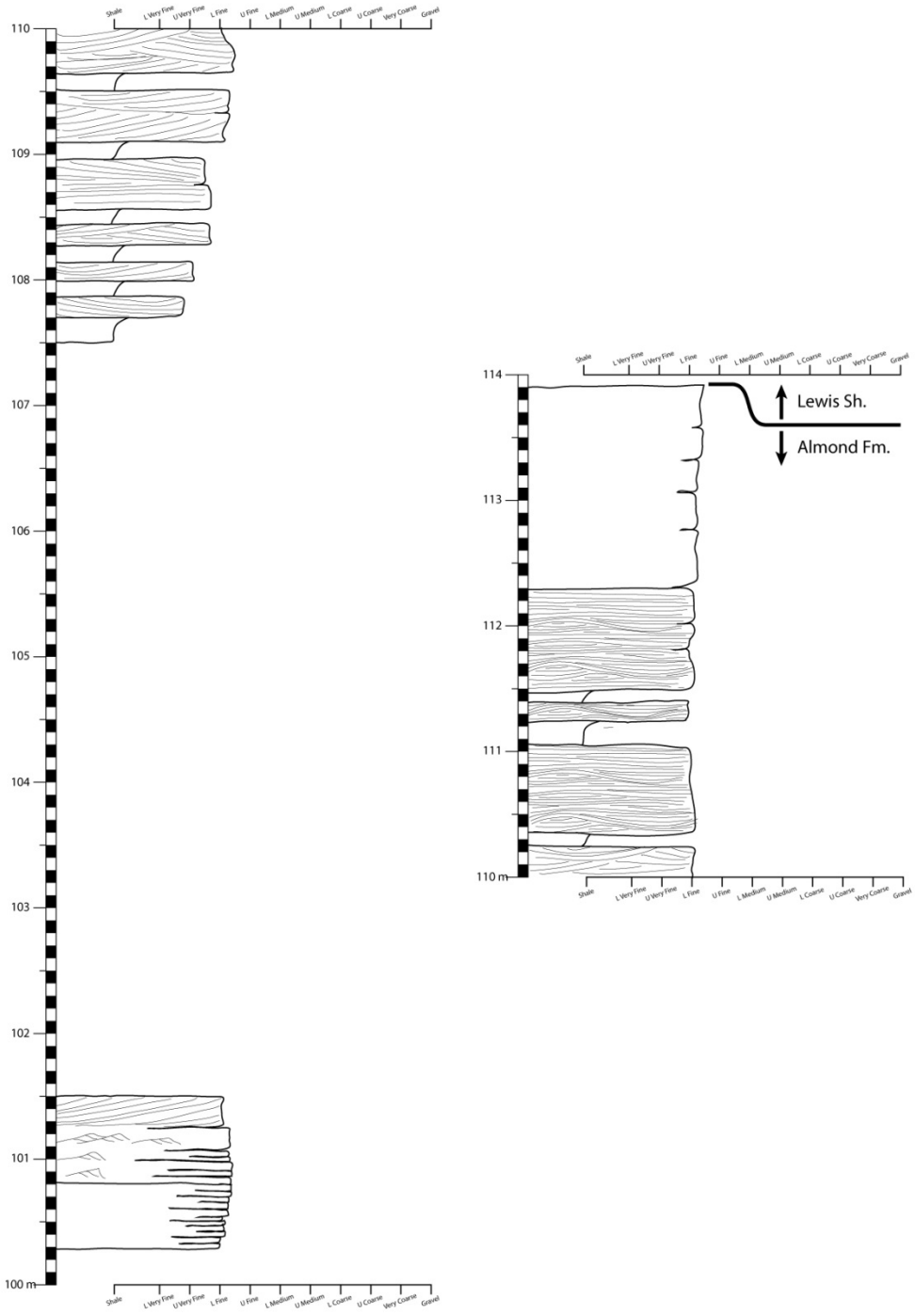

Figure B.21: Wells Creek section, part 6.

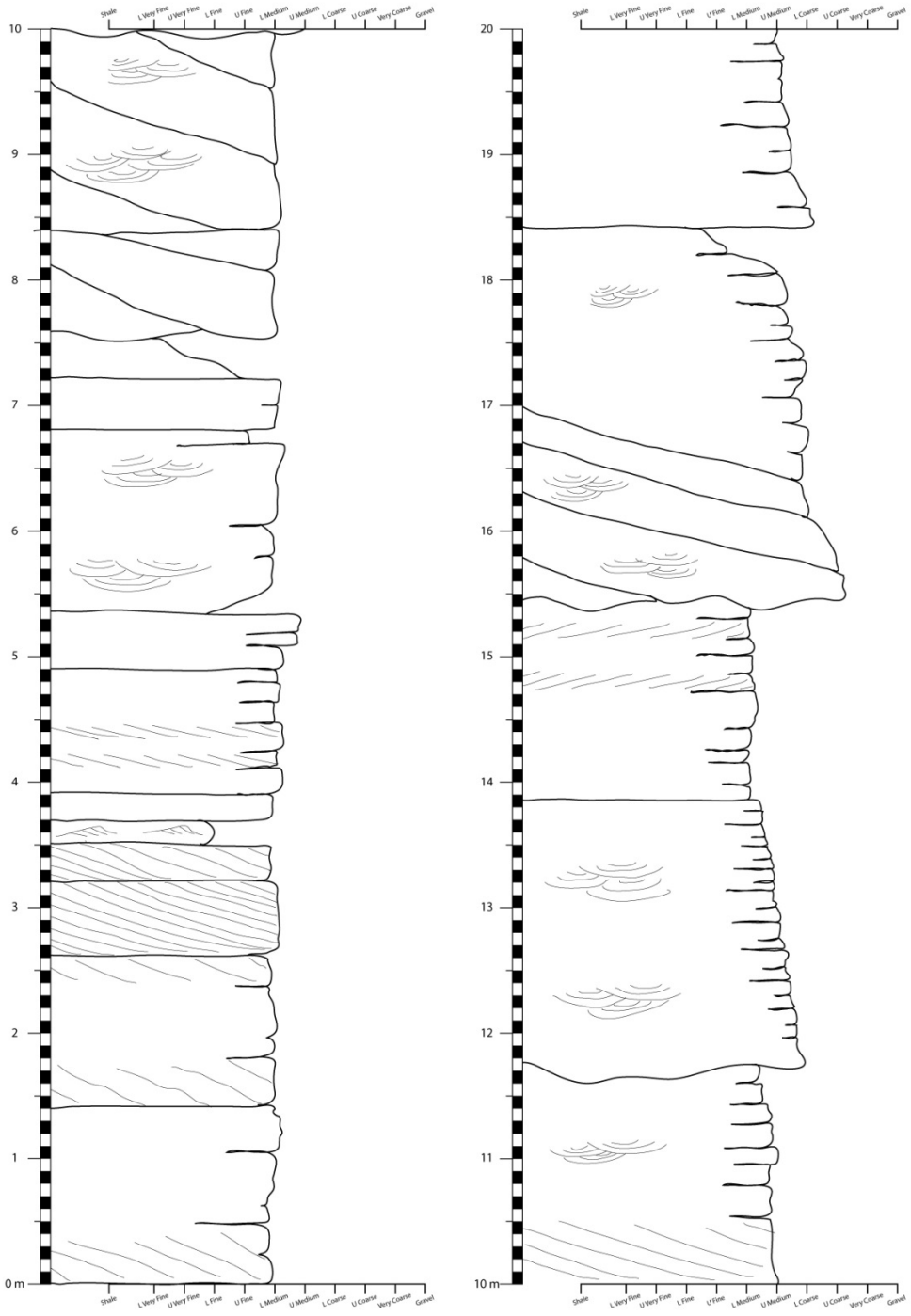

Figure B.22: Glades Ridge section, part 1.

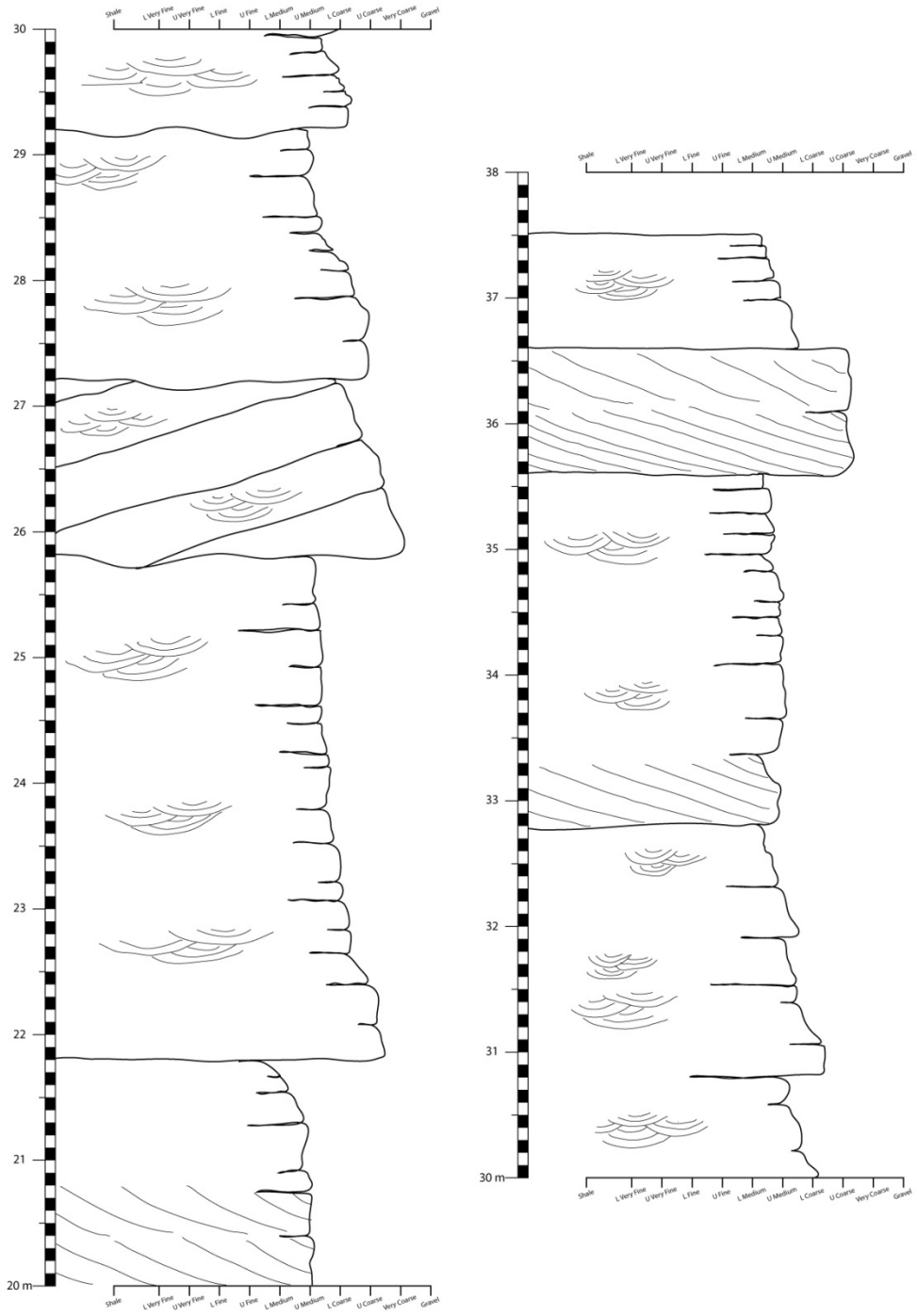

Figure B.23: Glades Ridge section, part 2.

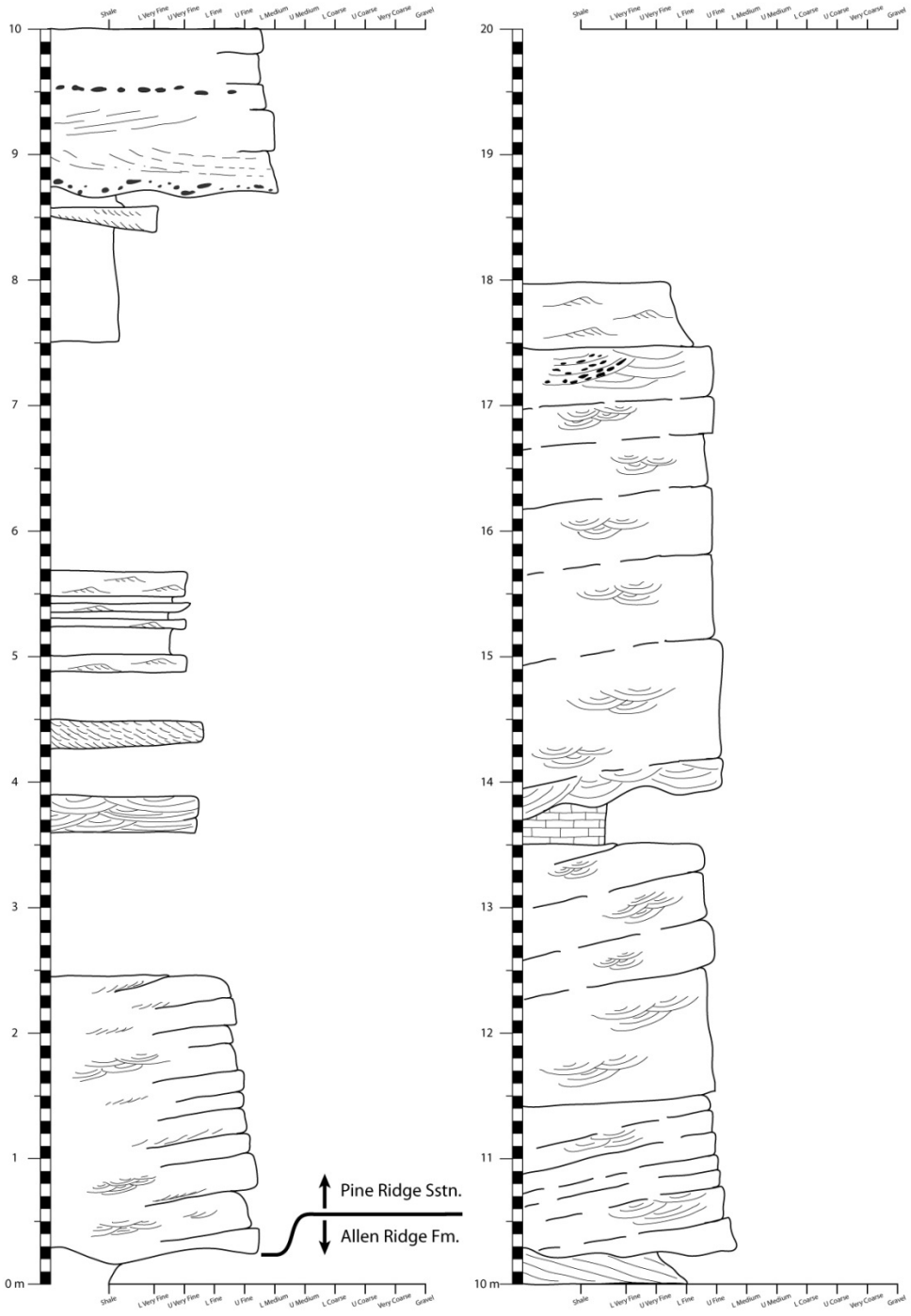

Figure B.24: Seminoe Road section, part 1.

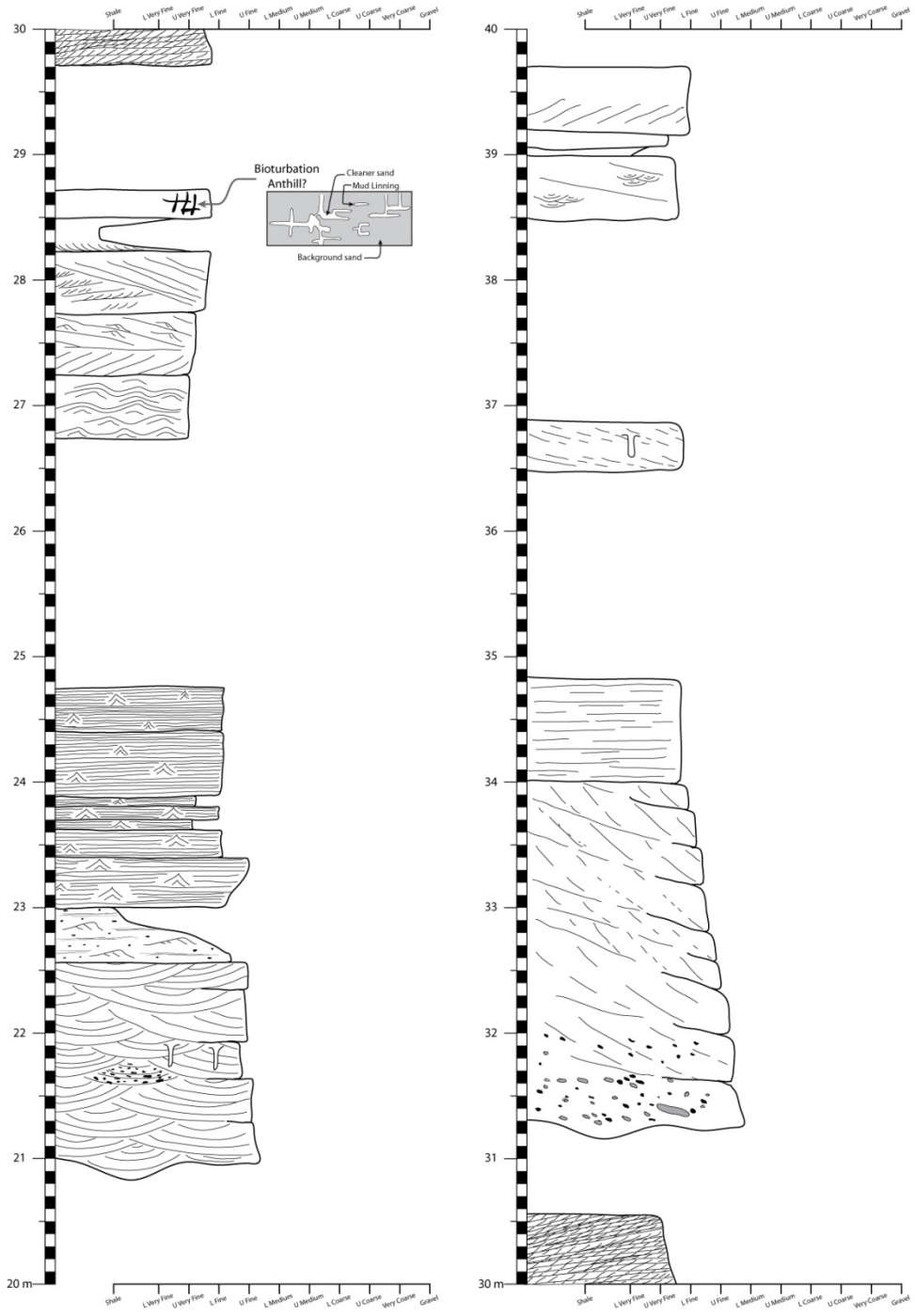

Figure B.25: Seminoe Road section, part 2.

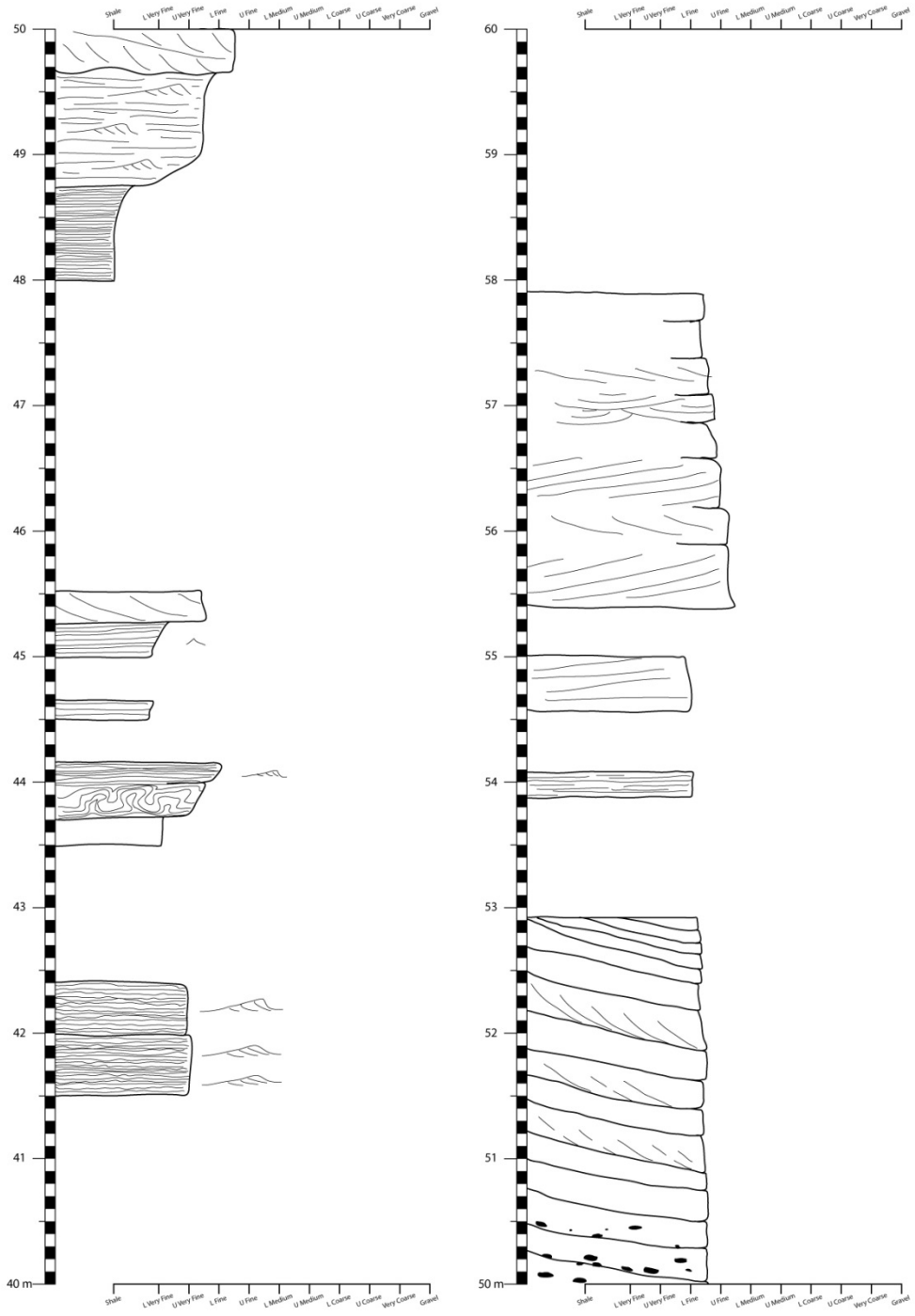

Figure B.26: Seminoe Road section, part 3.

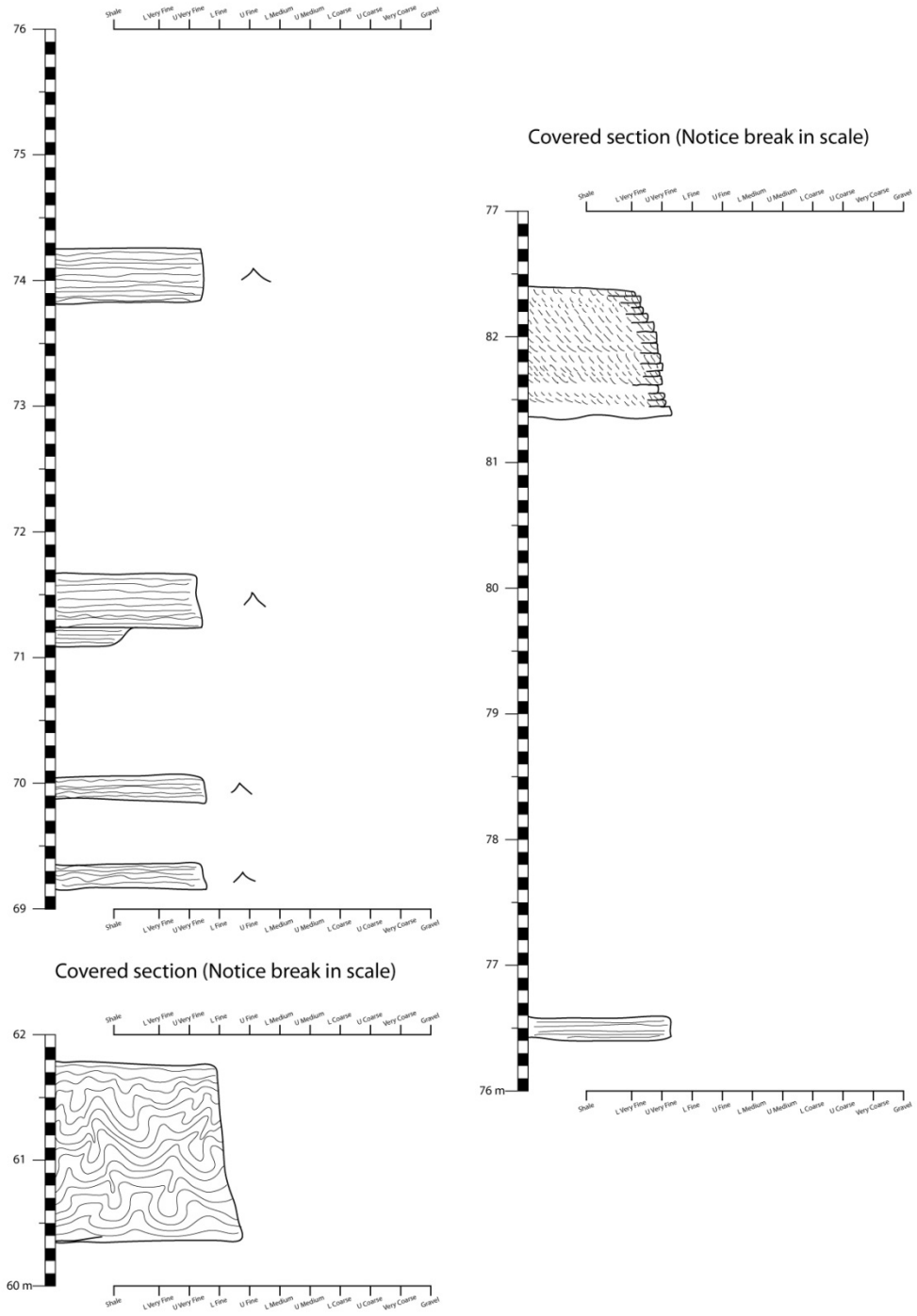

Figure B.27: Seminoe Road section, part 4.

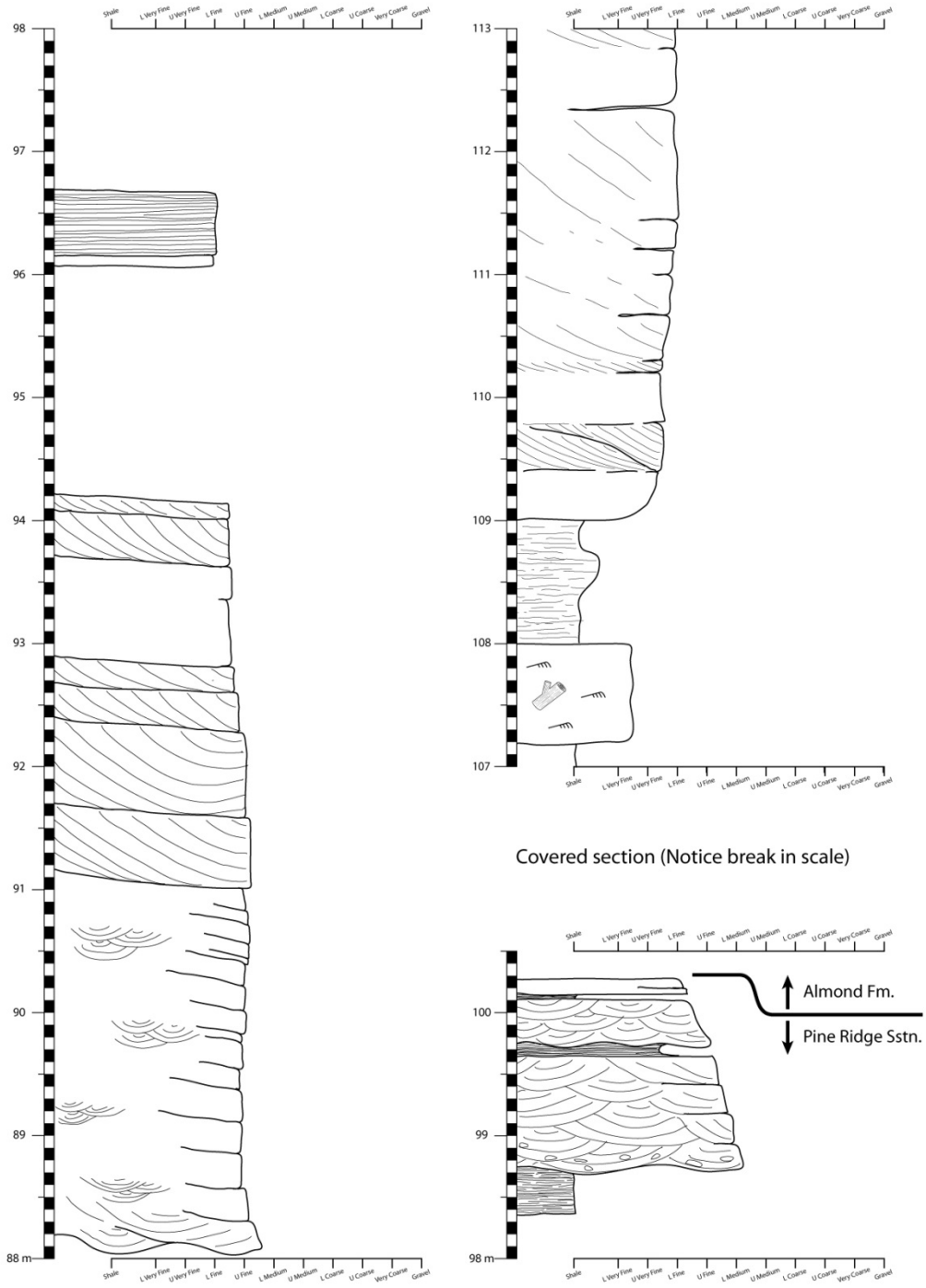

Figure B.28: Seminoe Road section, part 5.

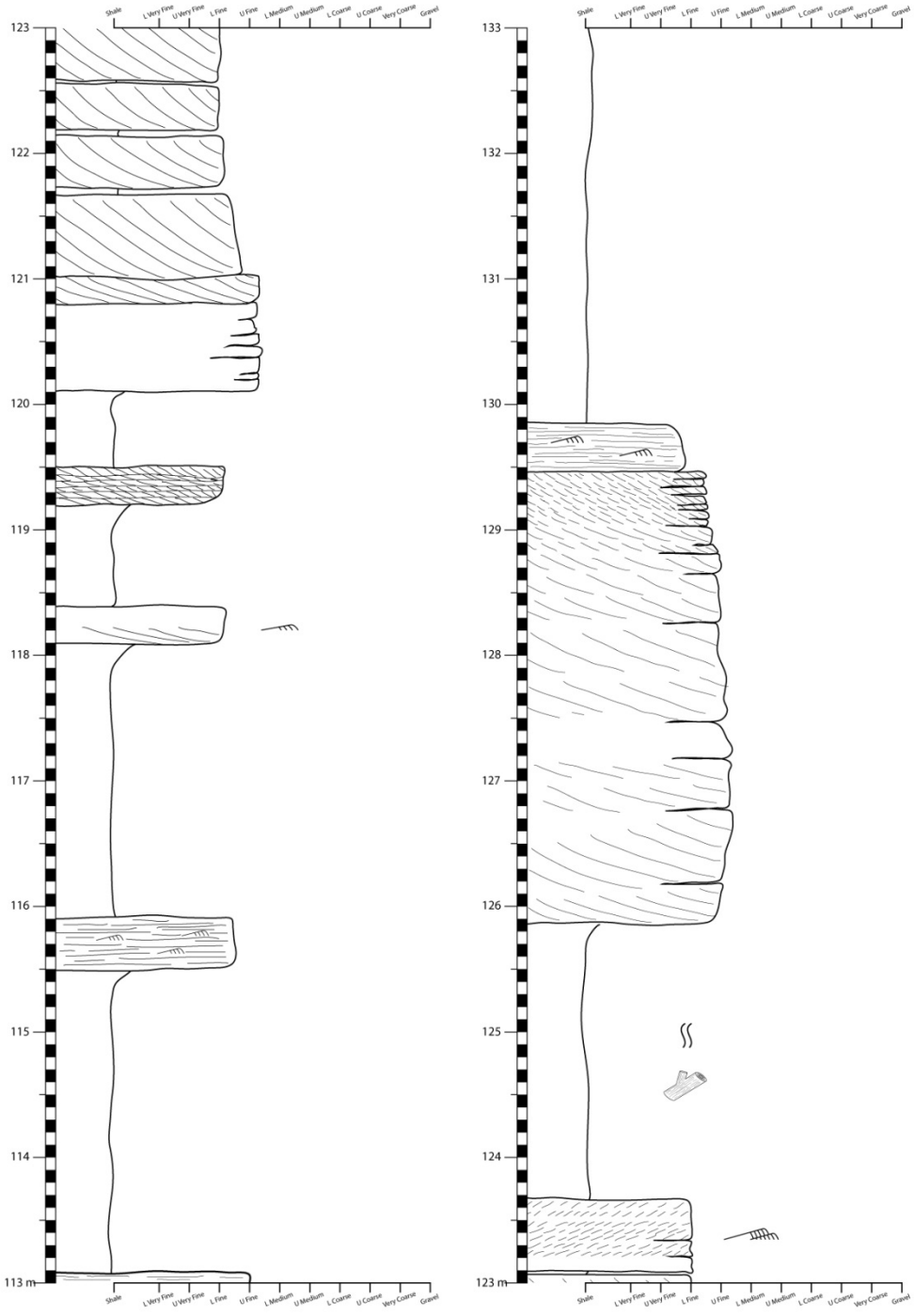

Figure B.29: Seminoe Road section, part 6.

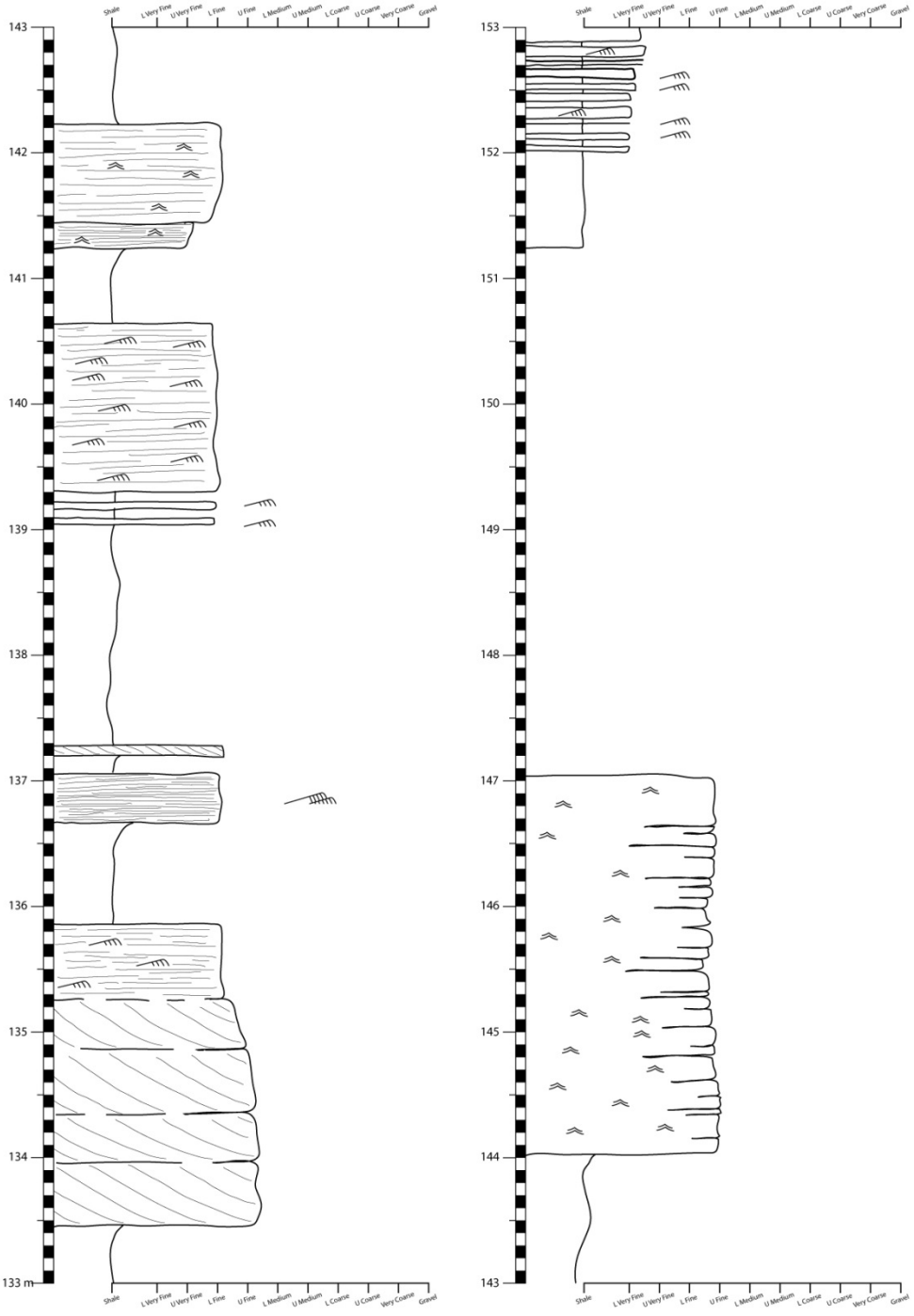

Figure B.30: Seminoe Road section, part 7.

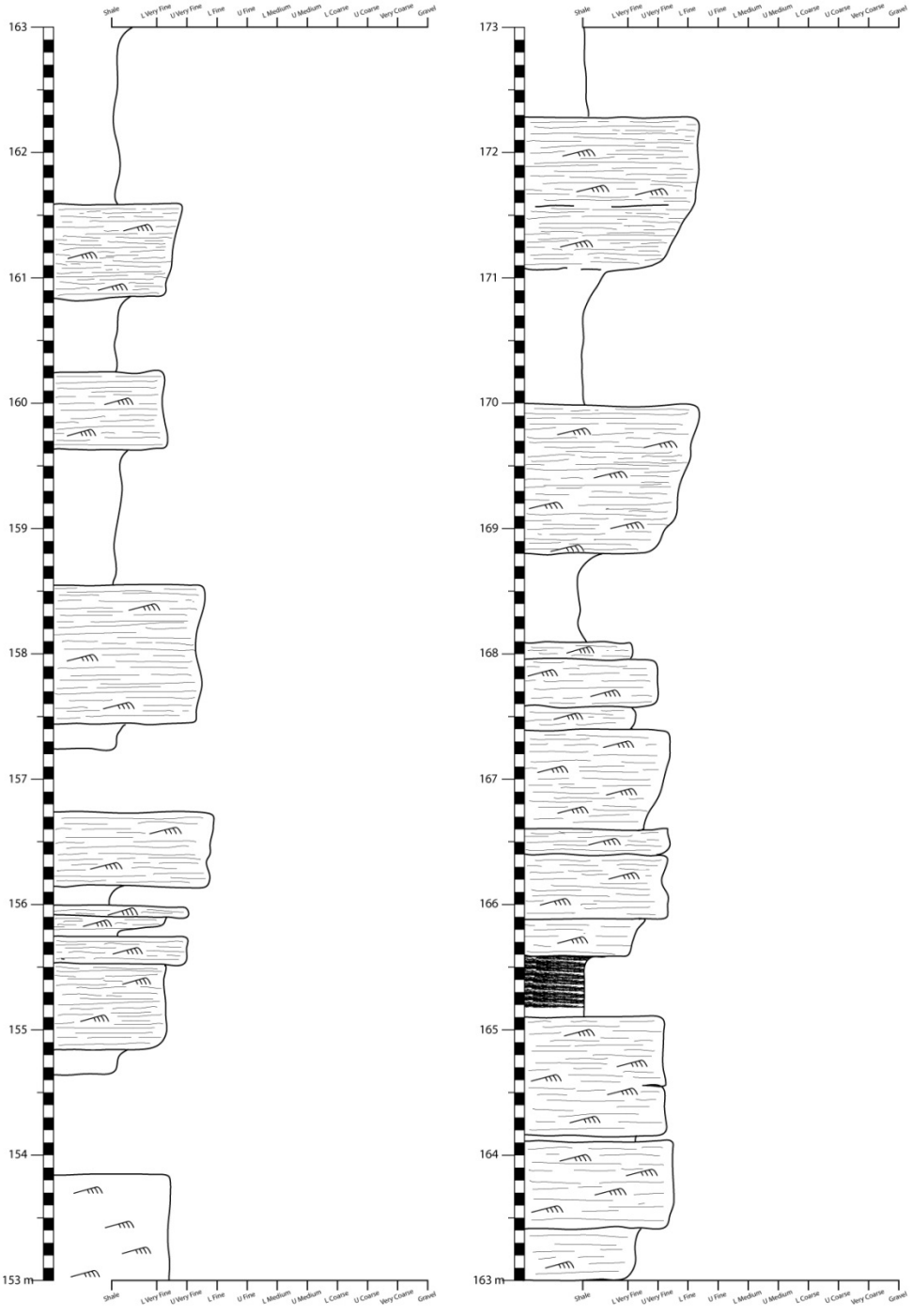

Figure B.31: Seminoe Road section, part 8.

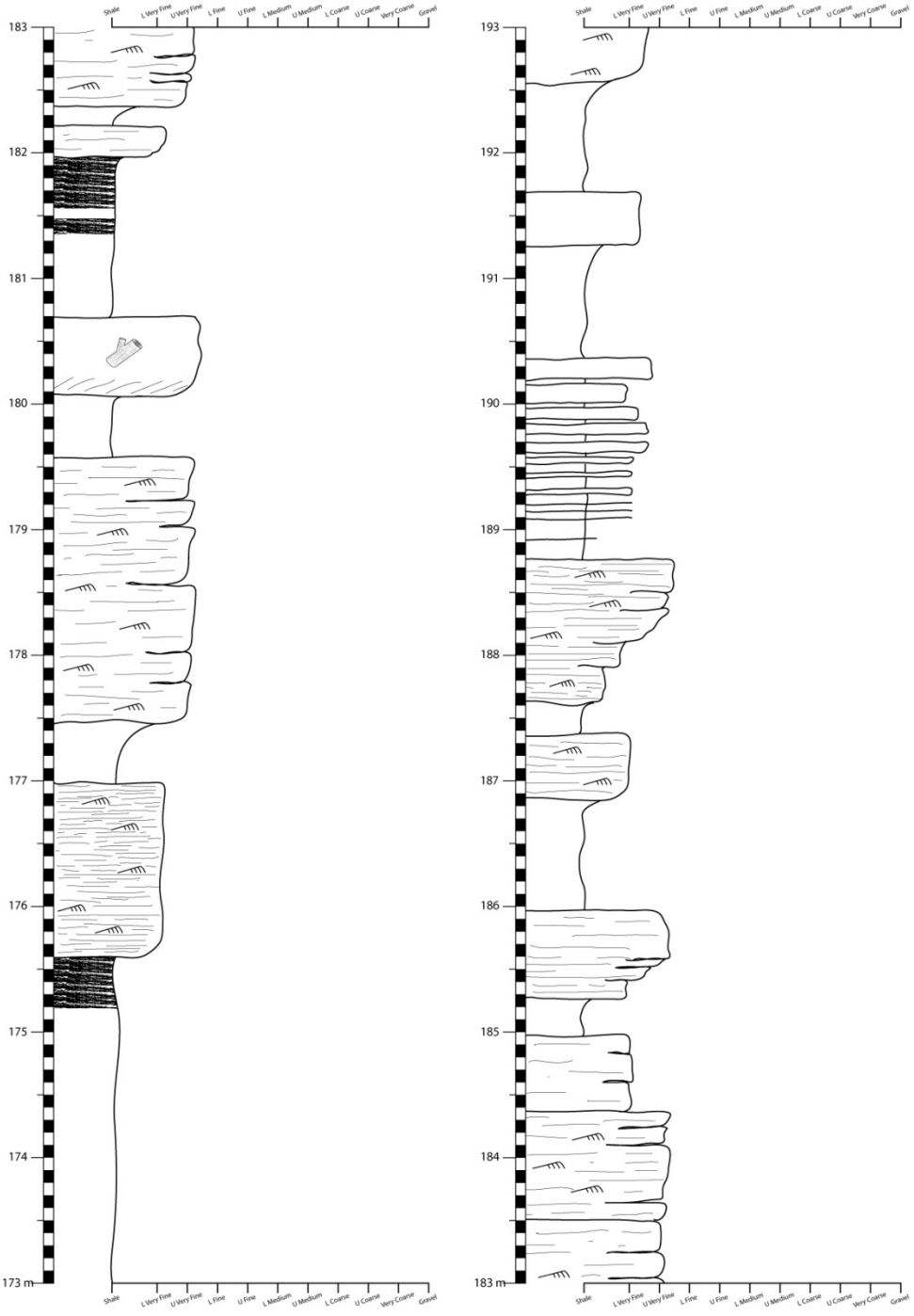

Figure B.32: Seminoe Road section, part 9.

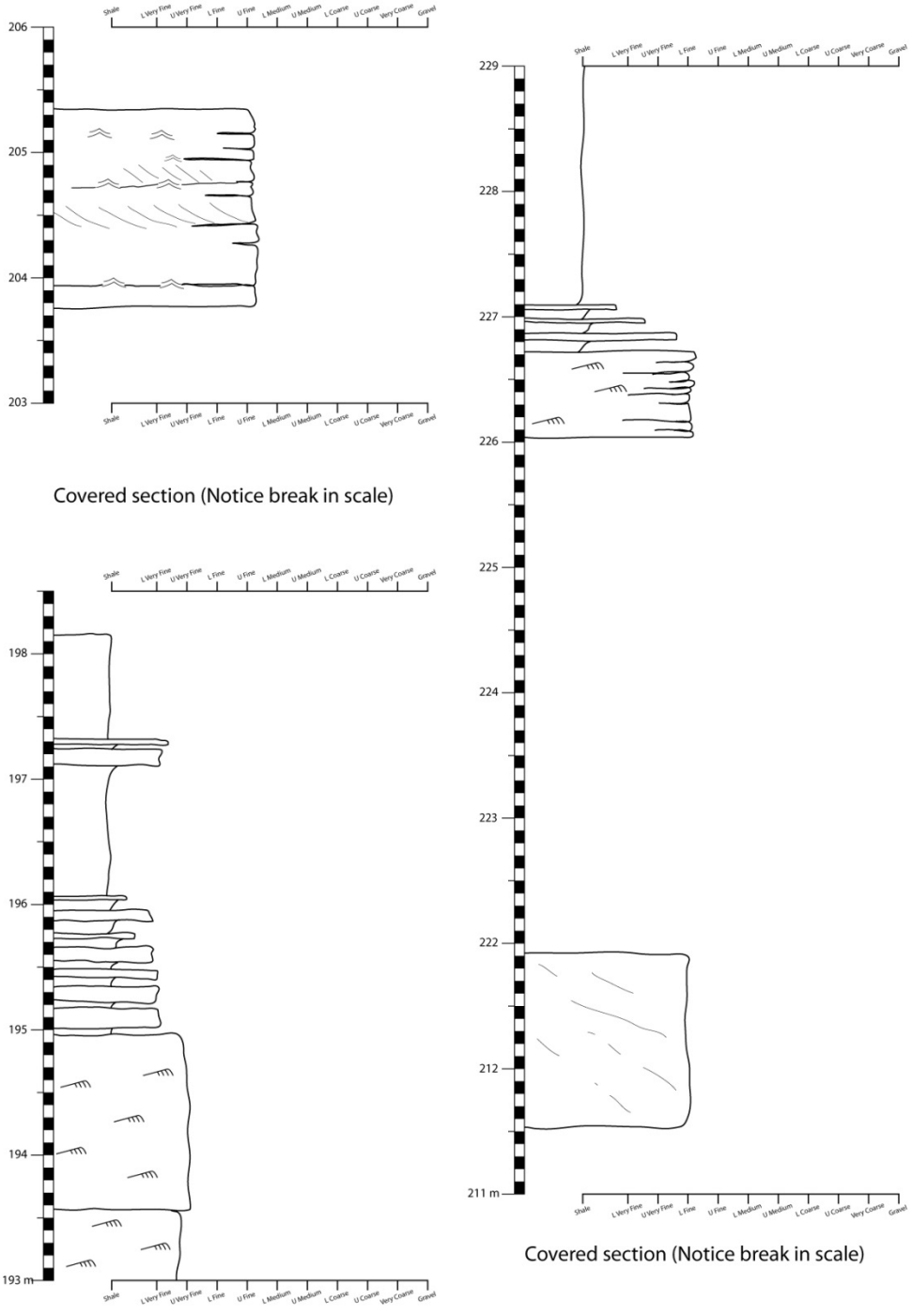

Figure B.33: Seminoe Road section, part 10.

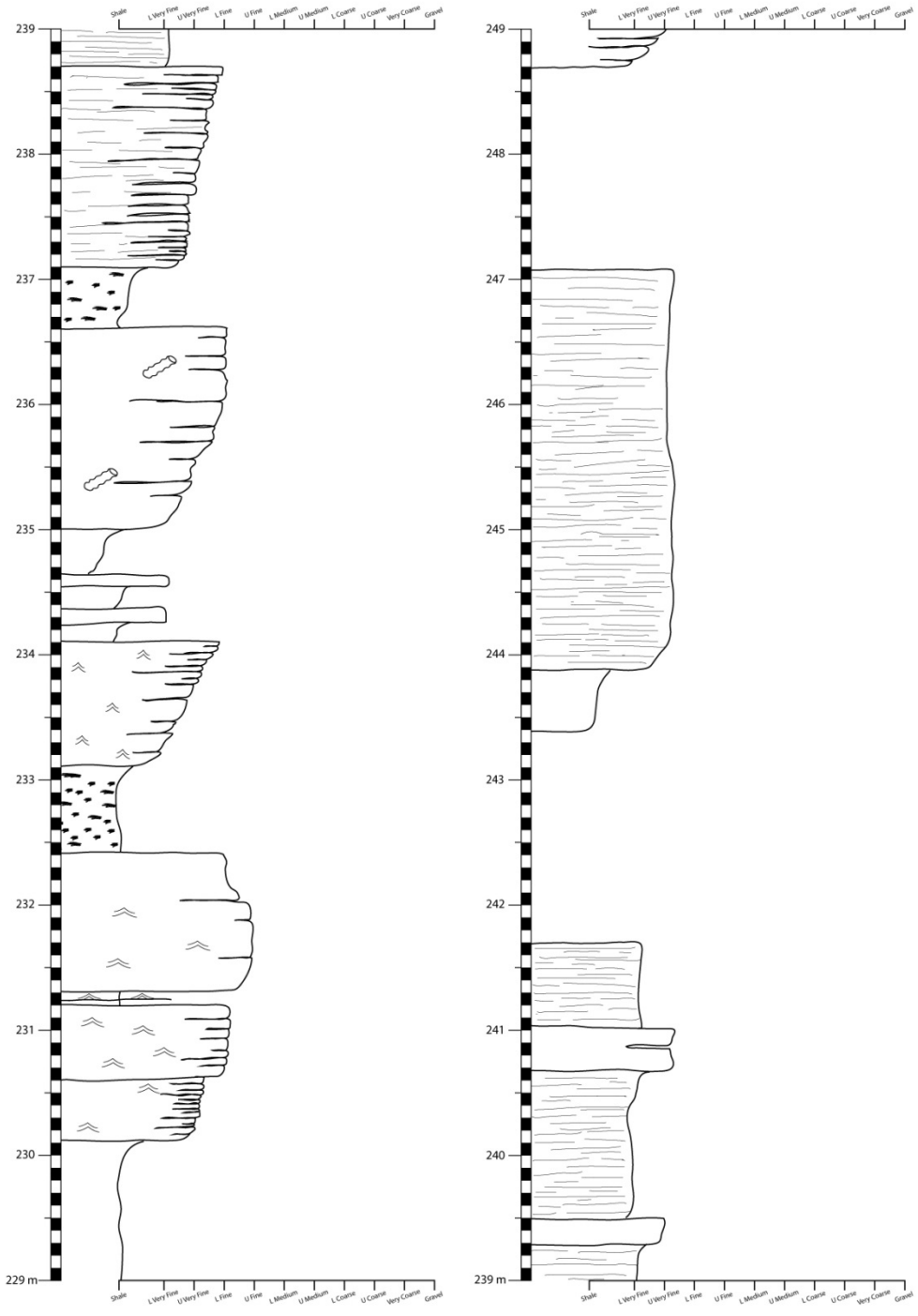

Figure B.34: Seminoe Road section, part 11.

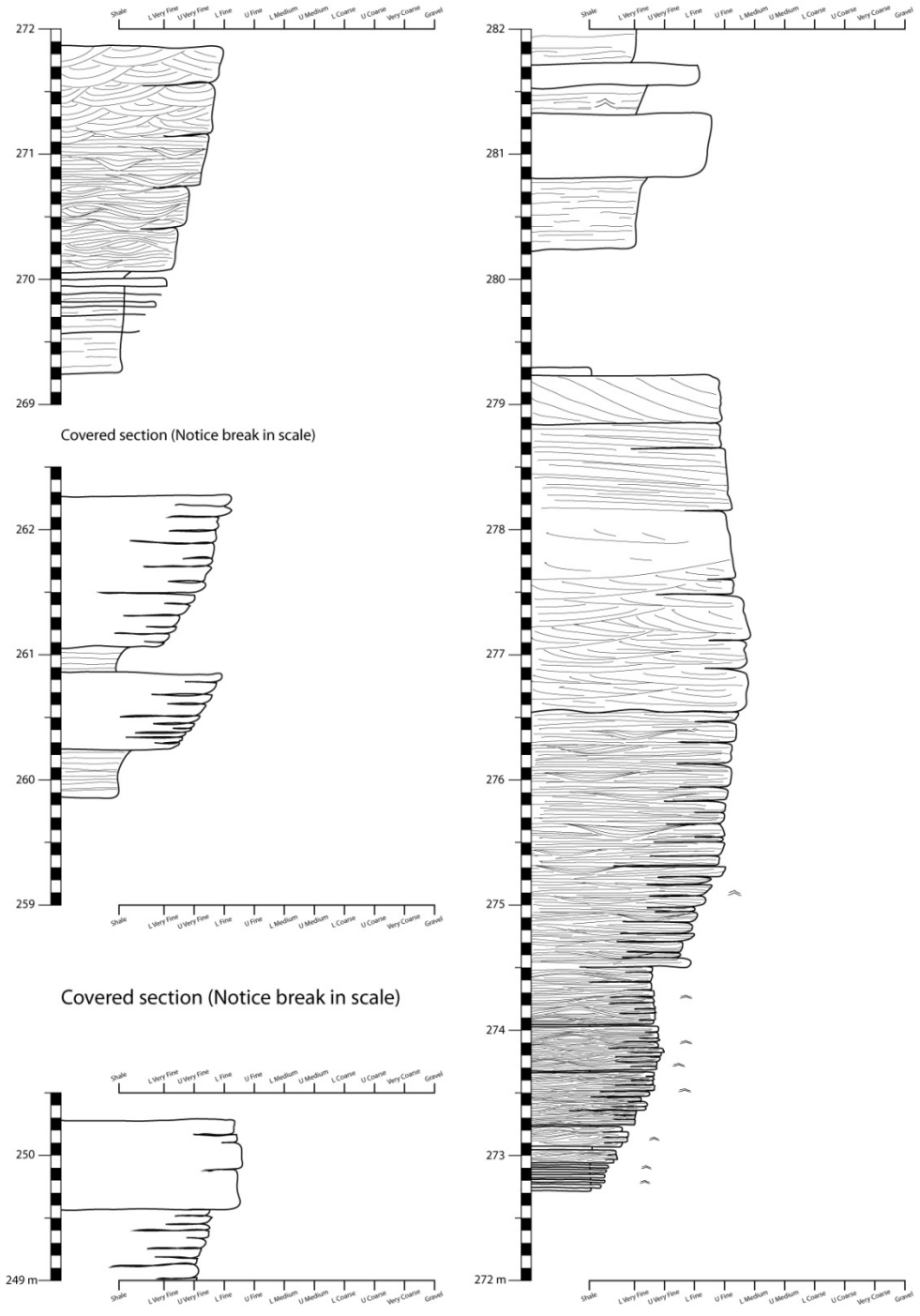

Figure B.35: Seminoe Road section, part 12.

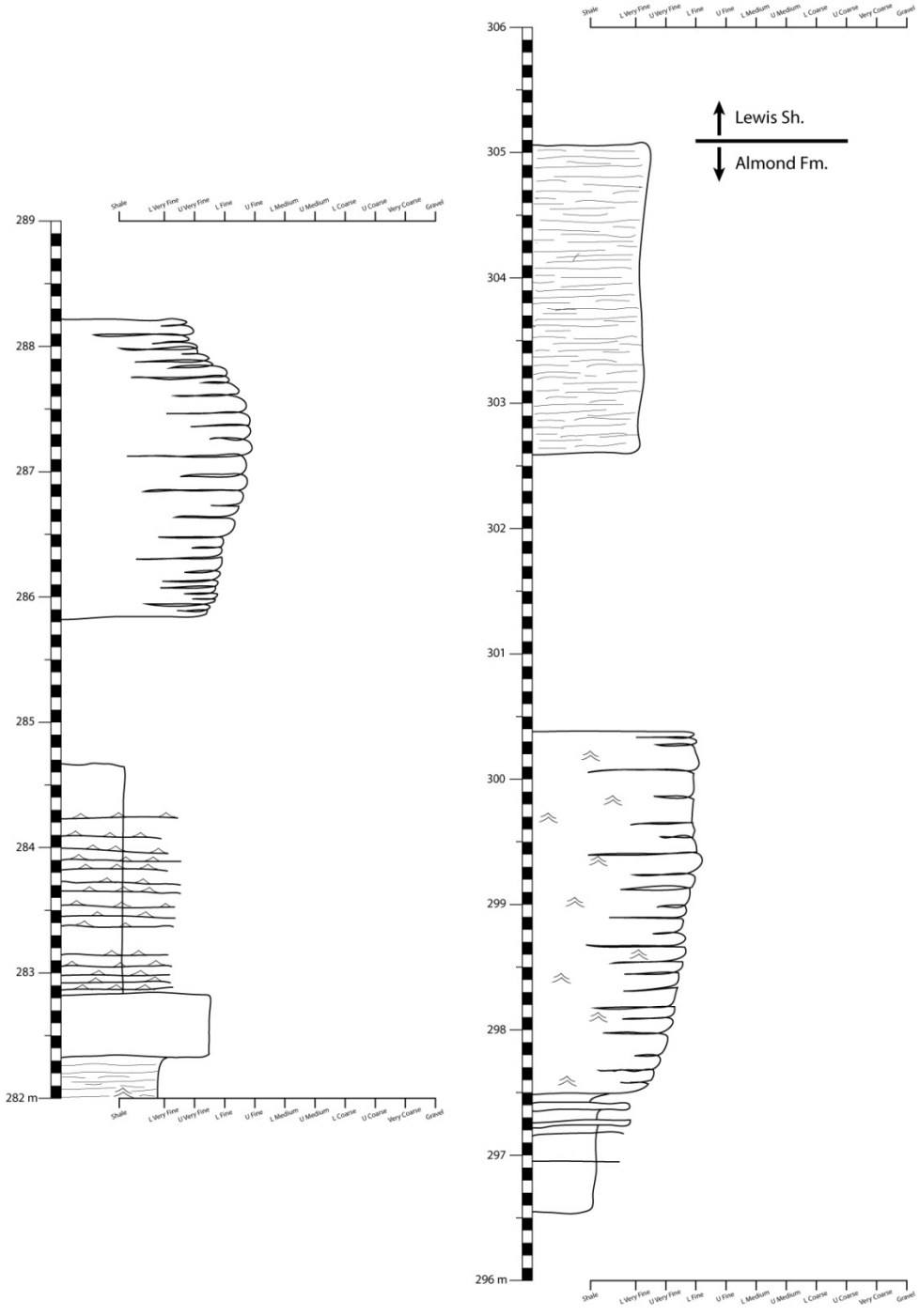

Figure B.36: Seminoe Road section, part 13.

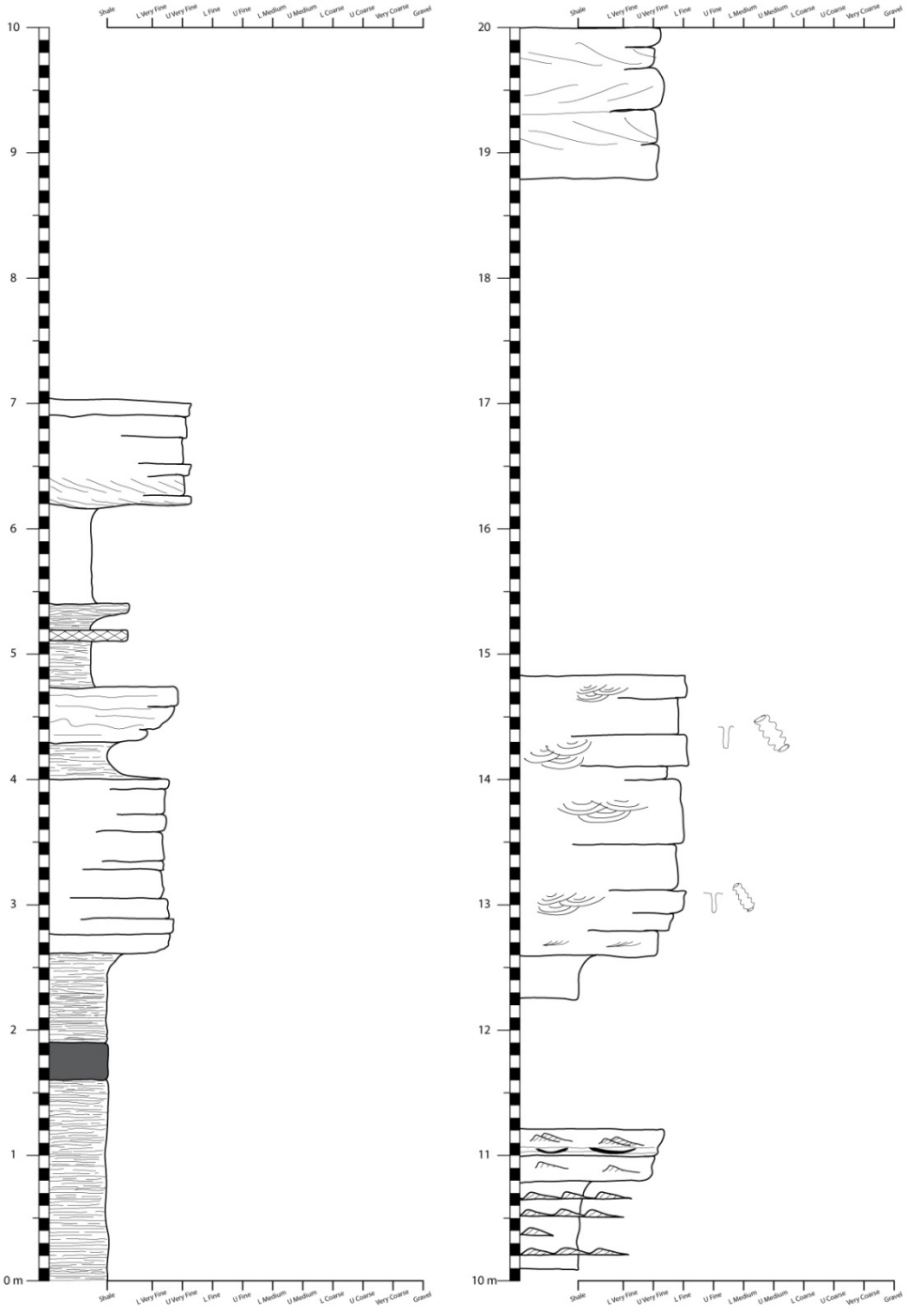

Figure B.37: Eagle Mine section, part 1.

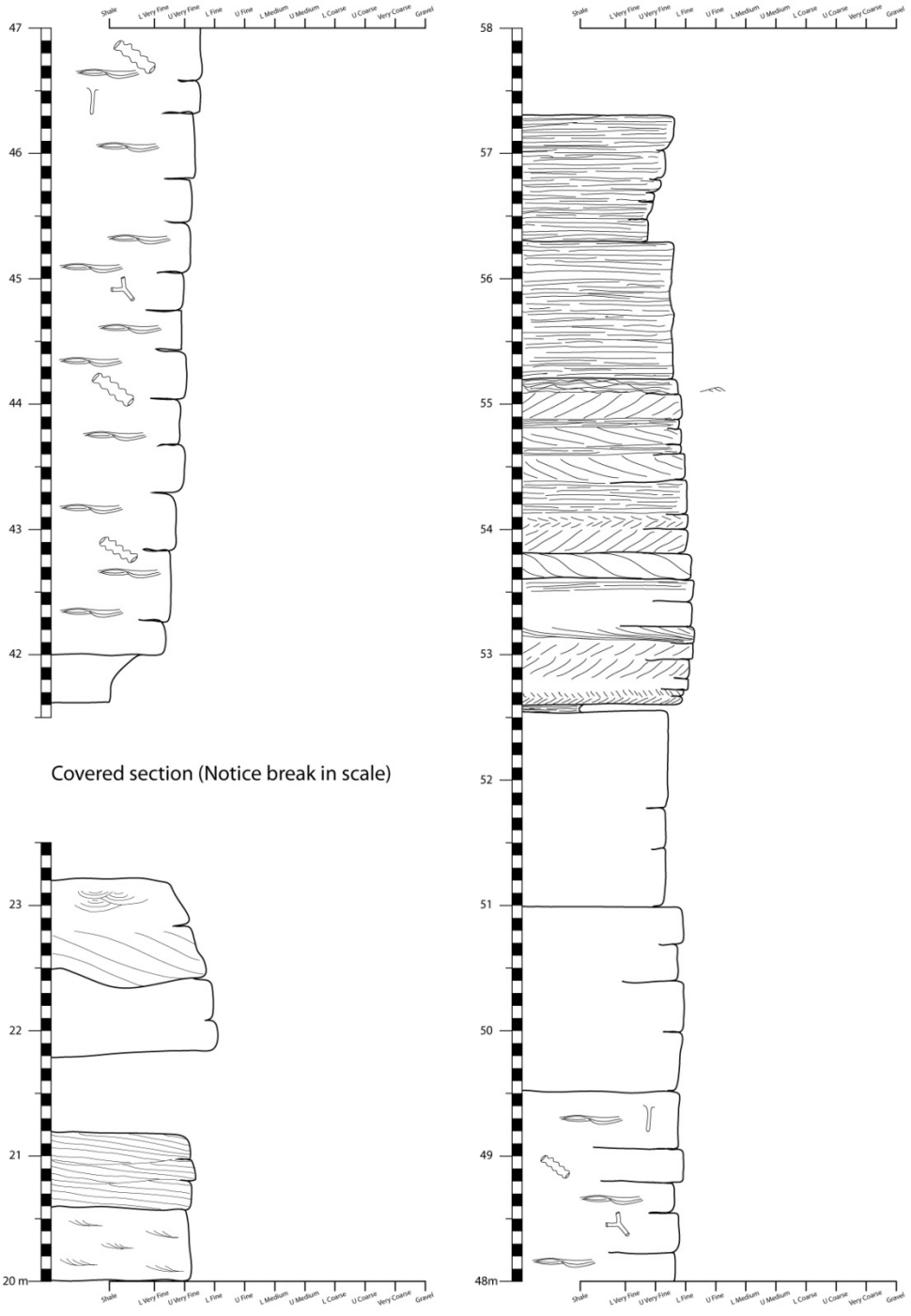

Figure B.38: Eagle Mine section, part 2.

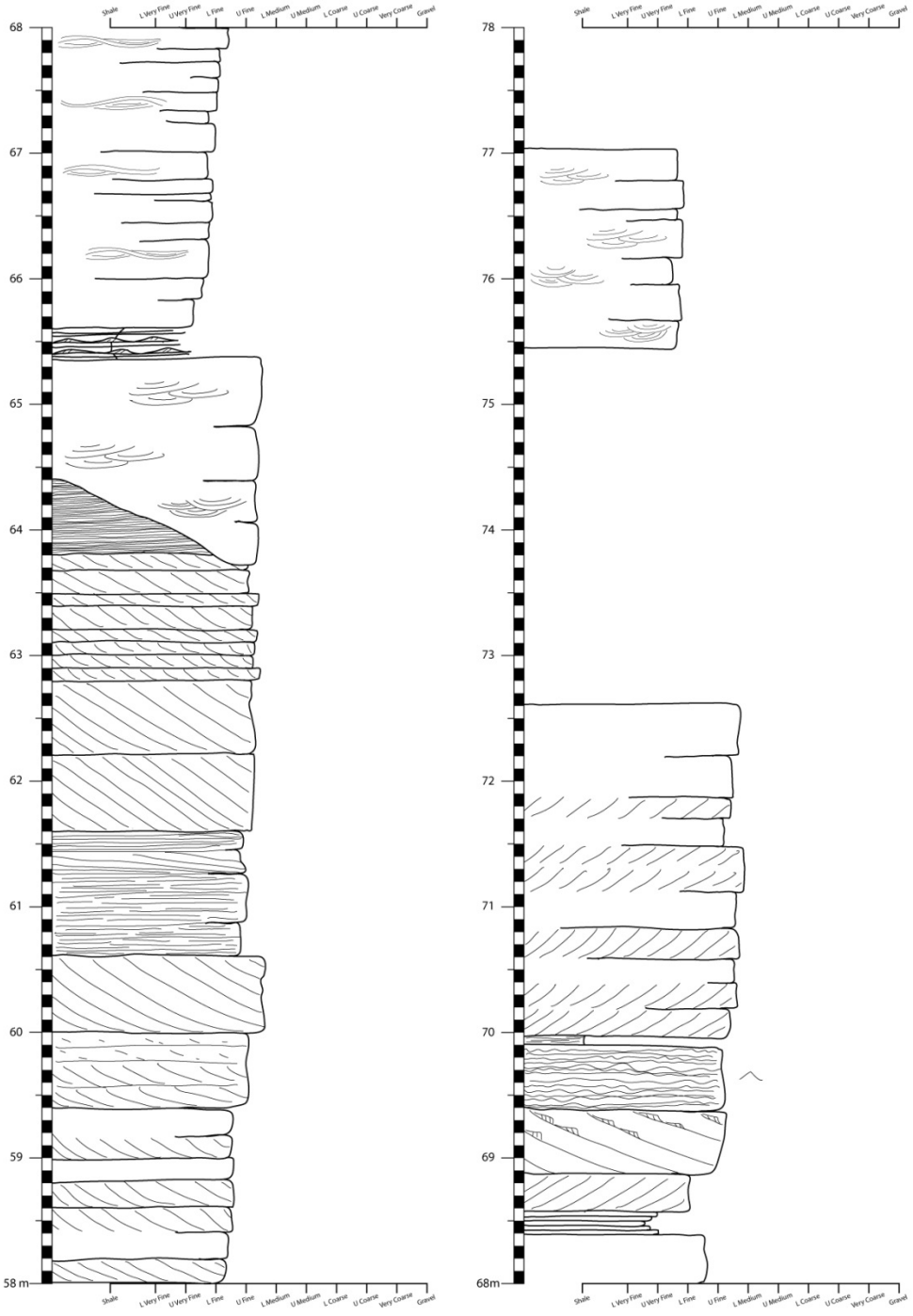

Figure B.39: Eagle Mine section, part 3.

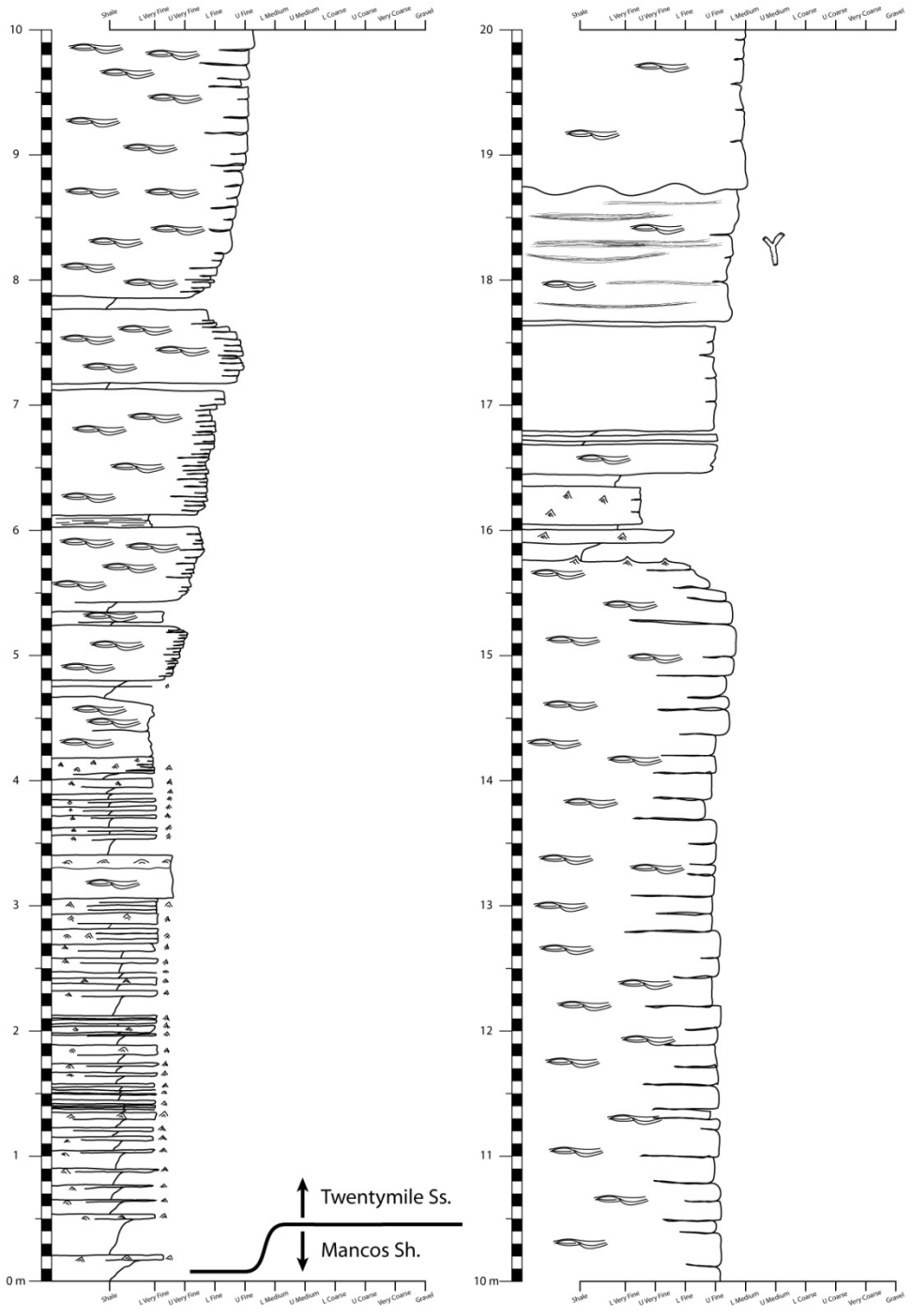

Figure B.40: US-40 Route section, part 1.

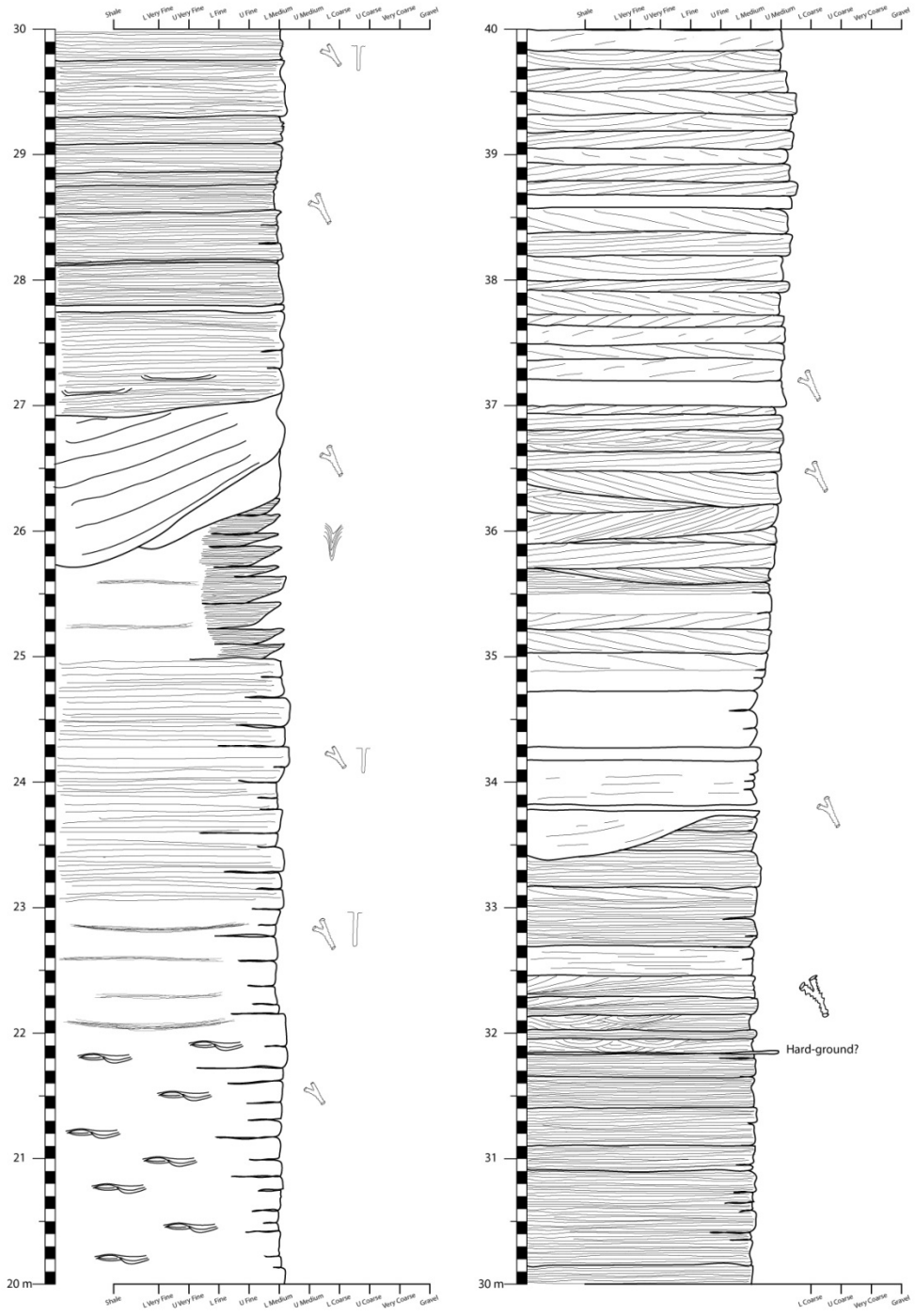

Figure B.41: US-40 Route section, part 2.

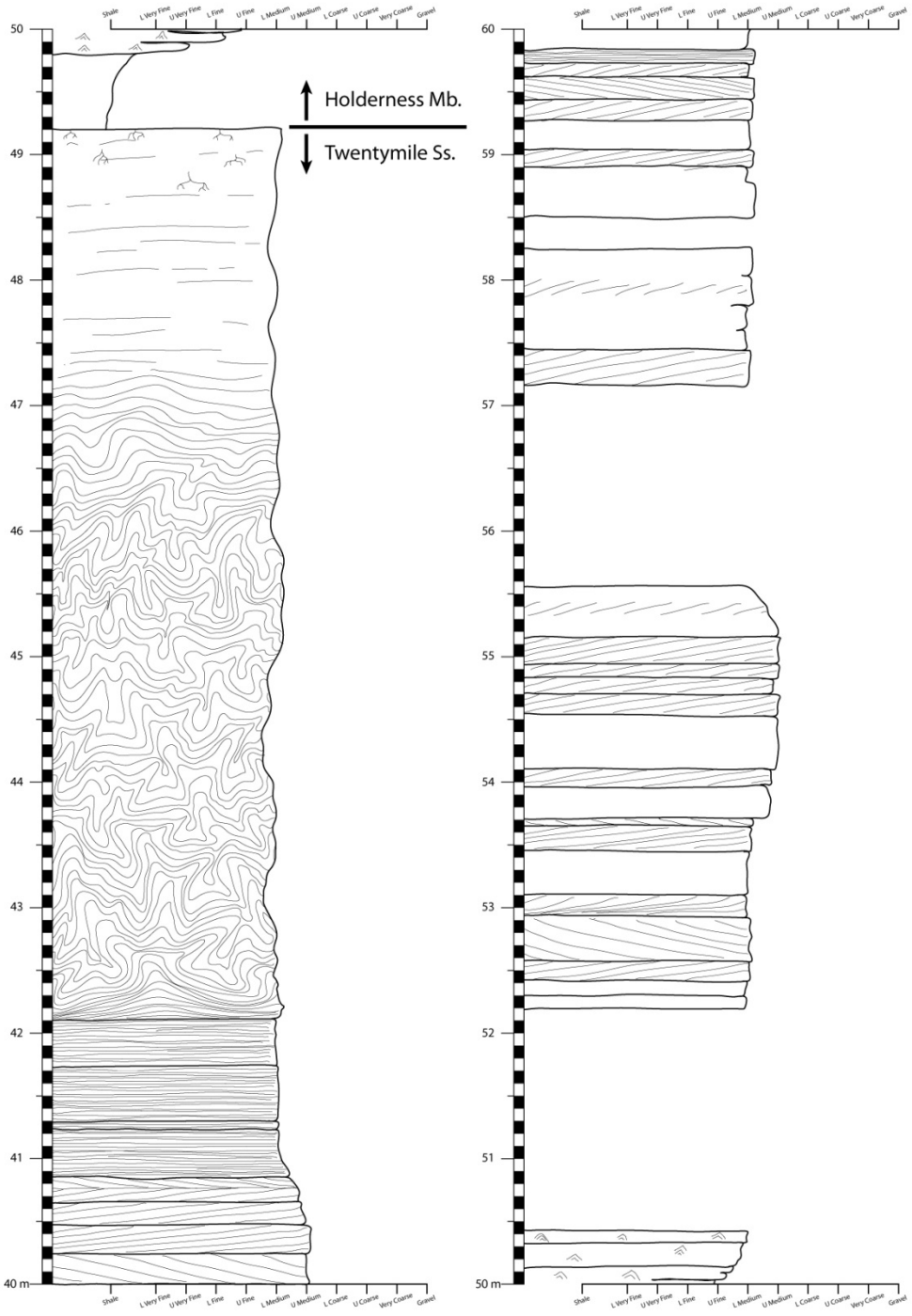

Figure B.42: US-40 Route section, part 3.

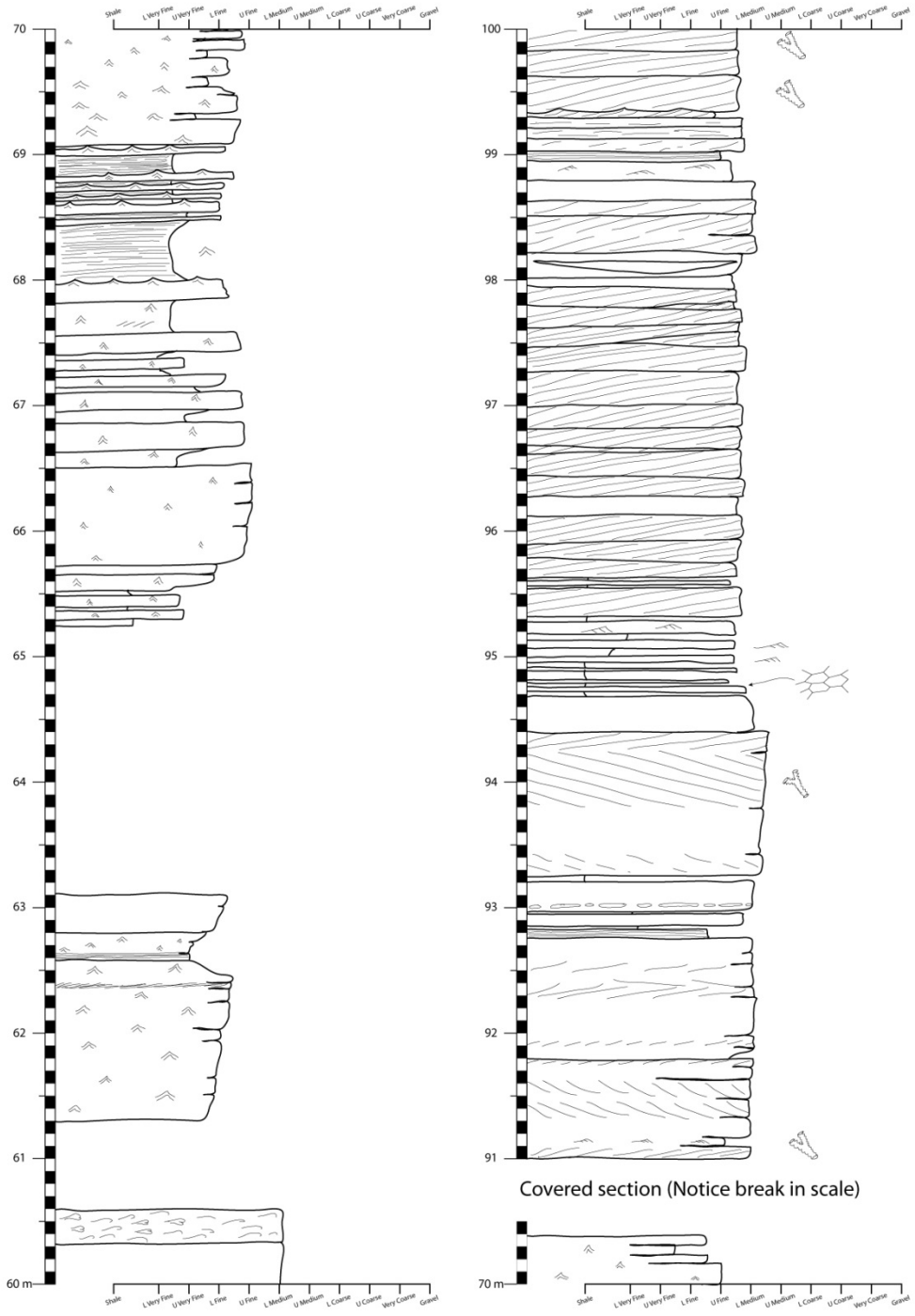

Figure B.43: US-40 Route section, part 4.

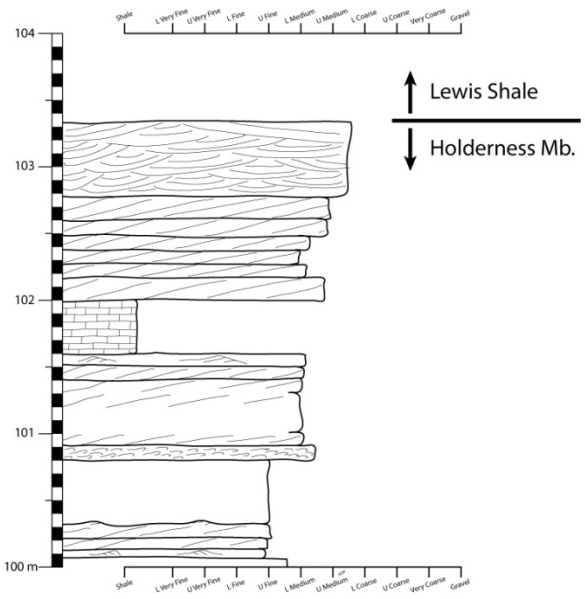

Figure B.44: US-40 Route section, part 5.

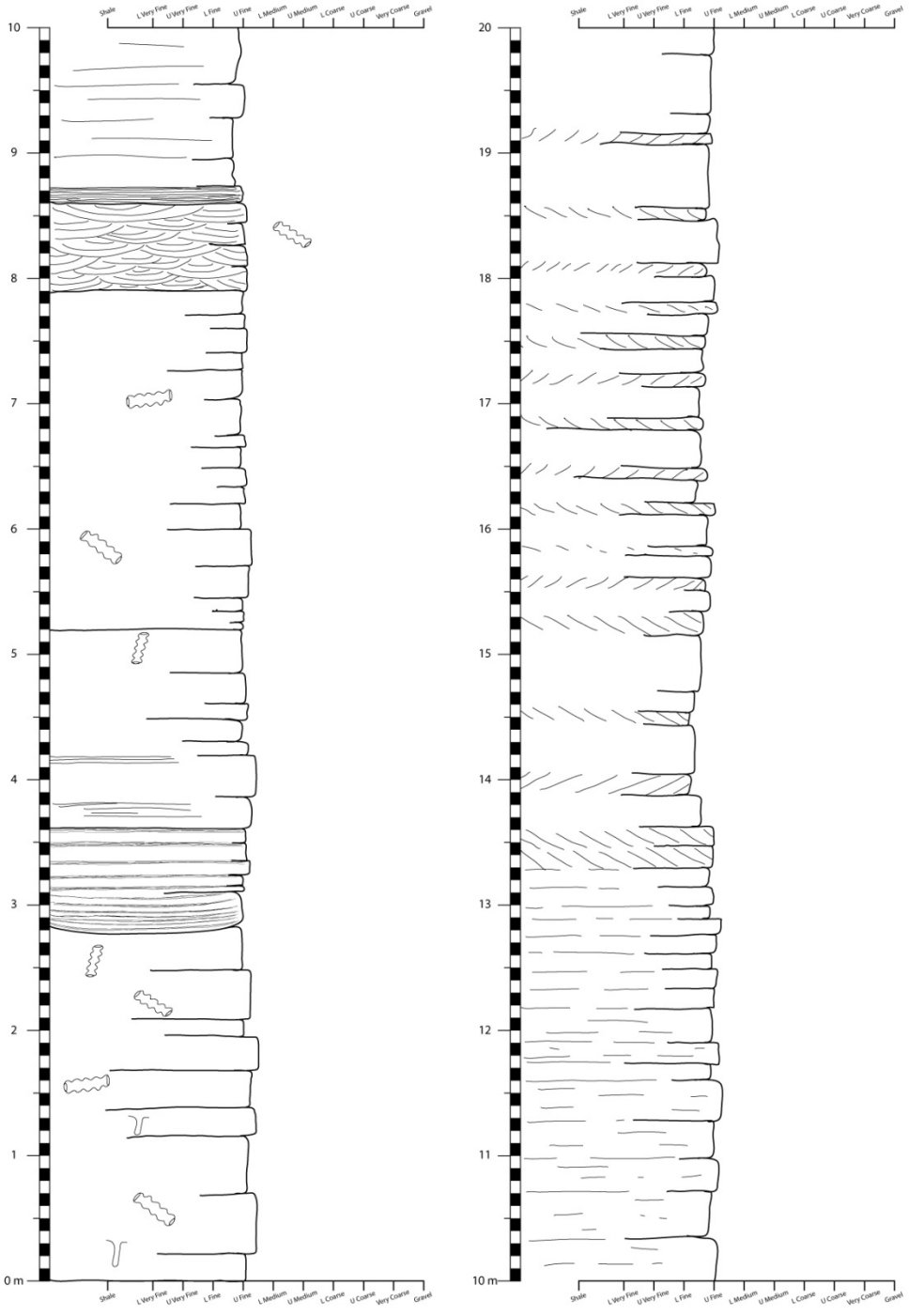

Figure B.45: East Rock Rim section, part 1.

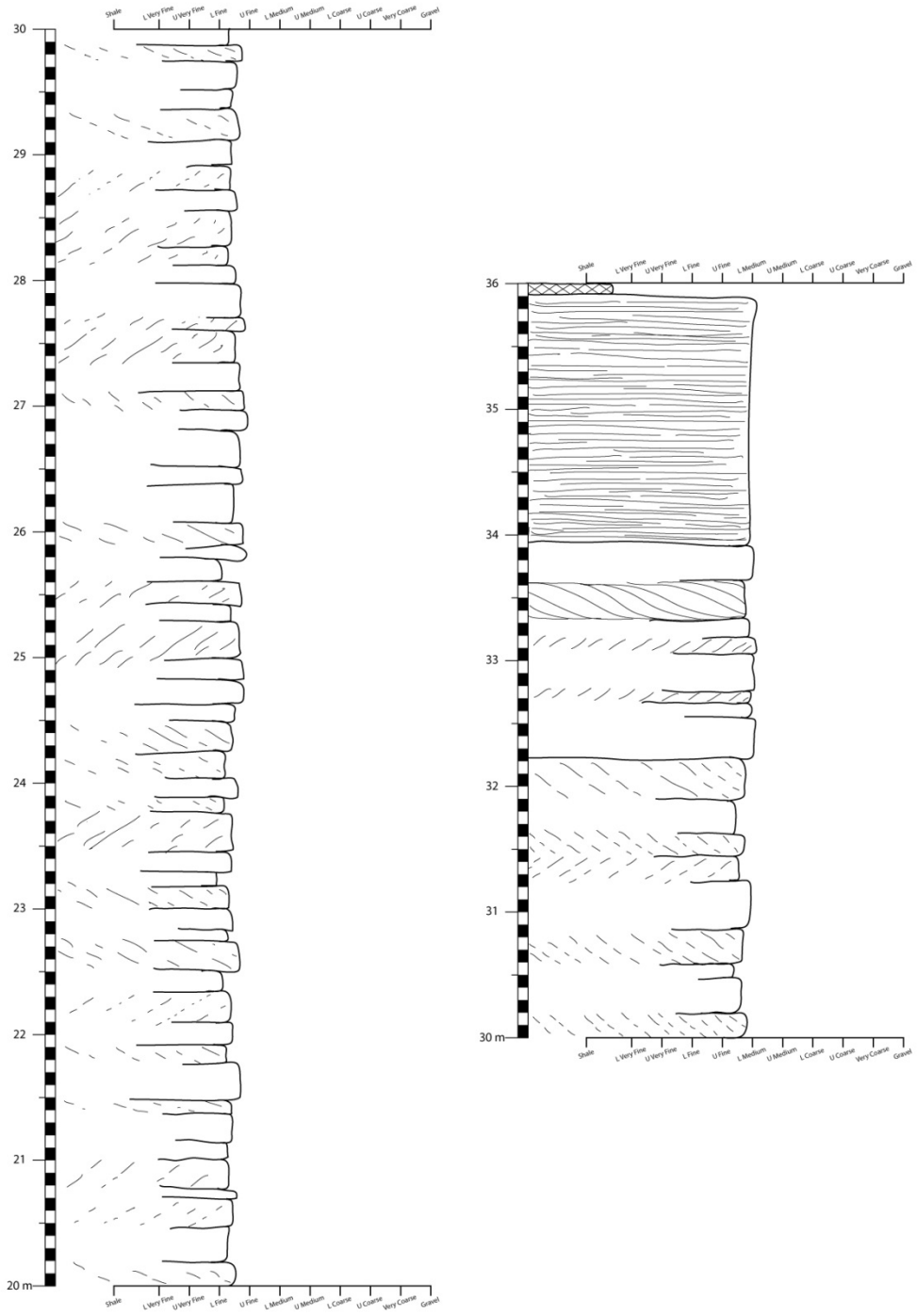

Figure B.46: East Rock Rim section, part 2.

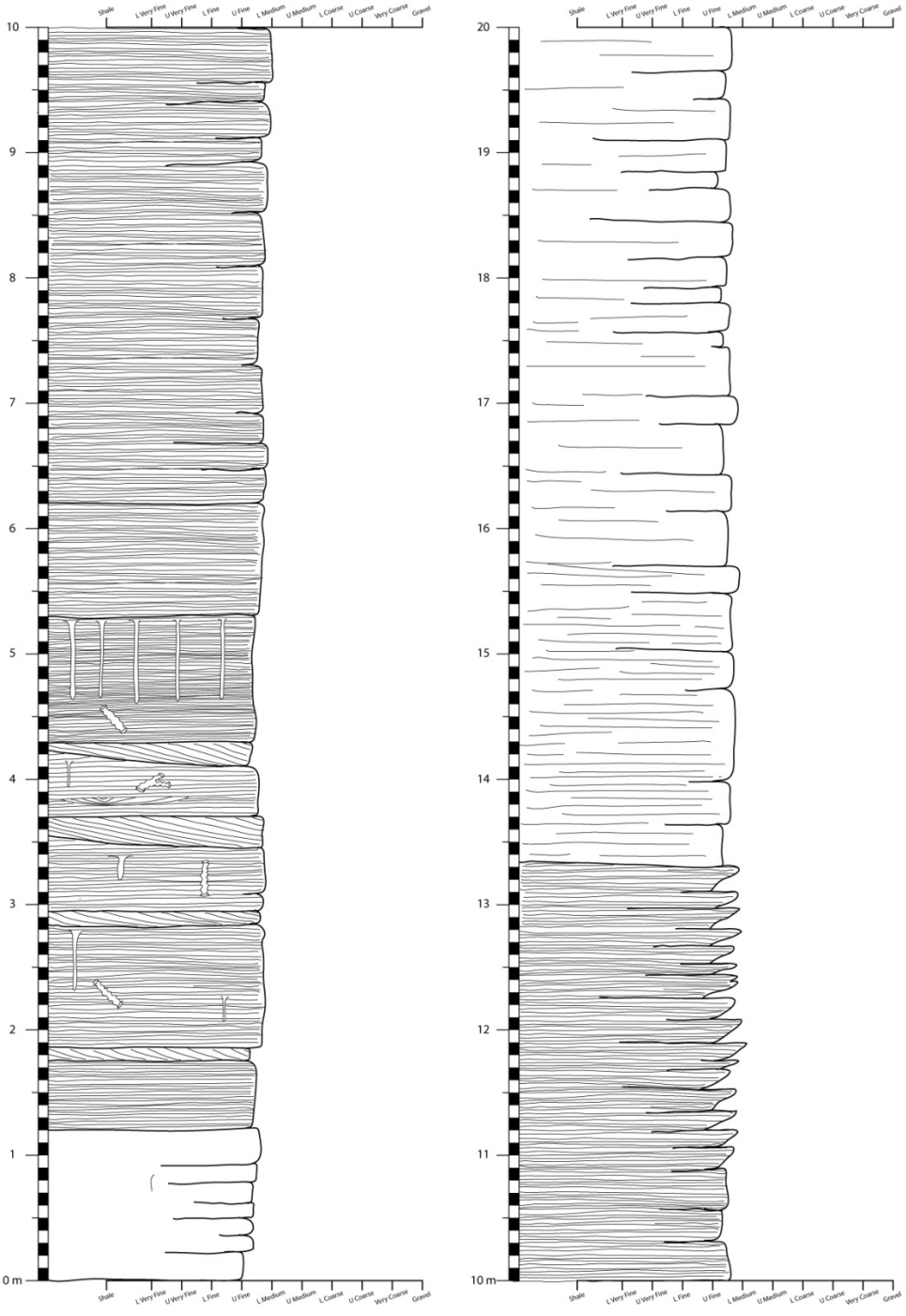

Figure B.47: West Rock Rim section, part 1.

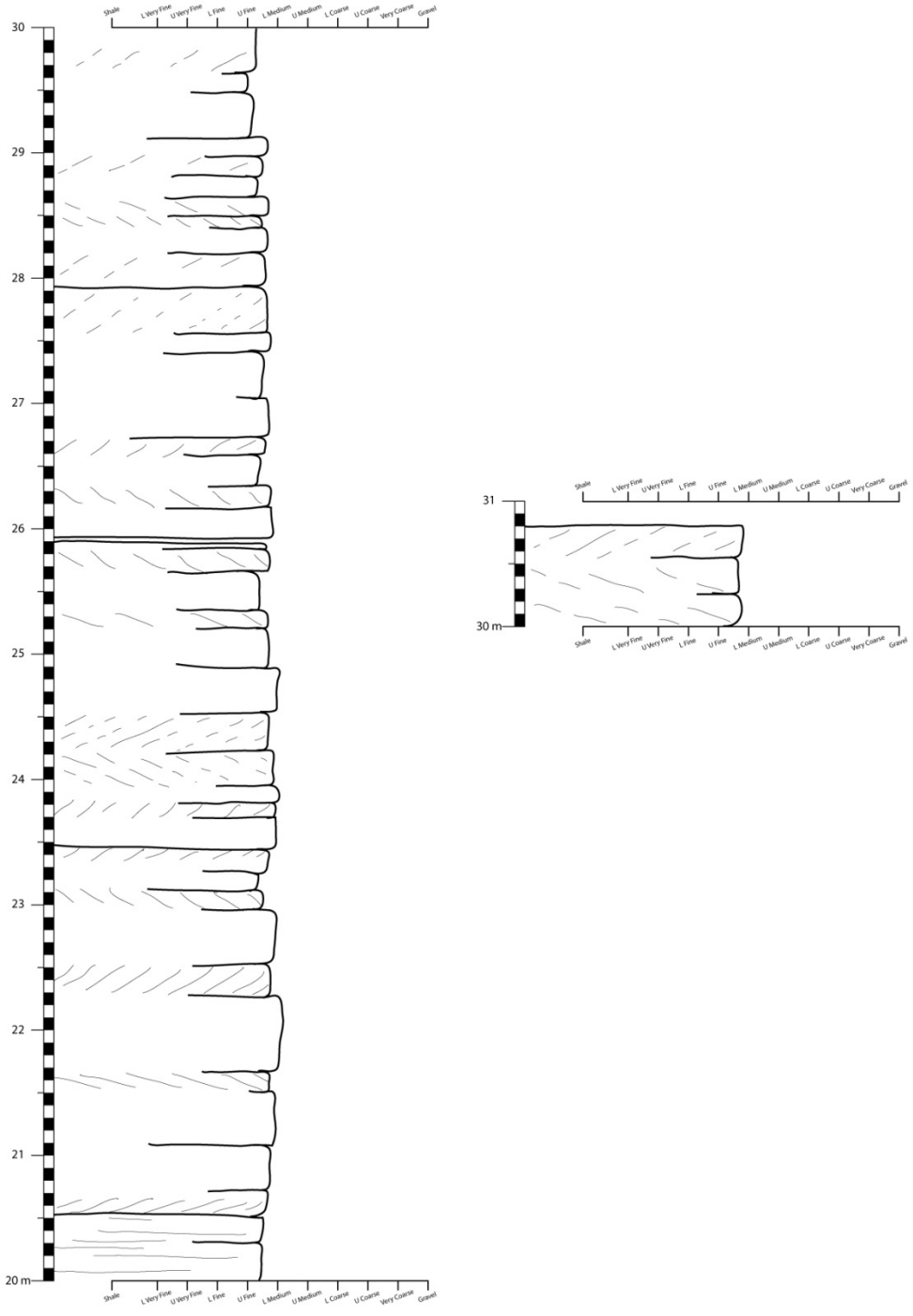

Figure B.48: West Rock Rim, part 2.

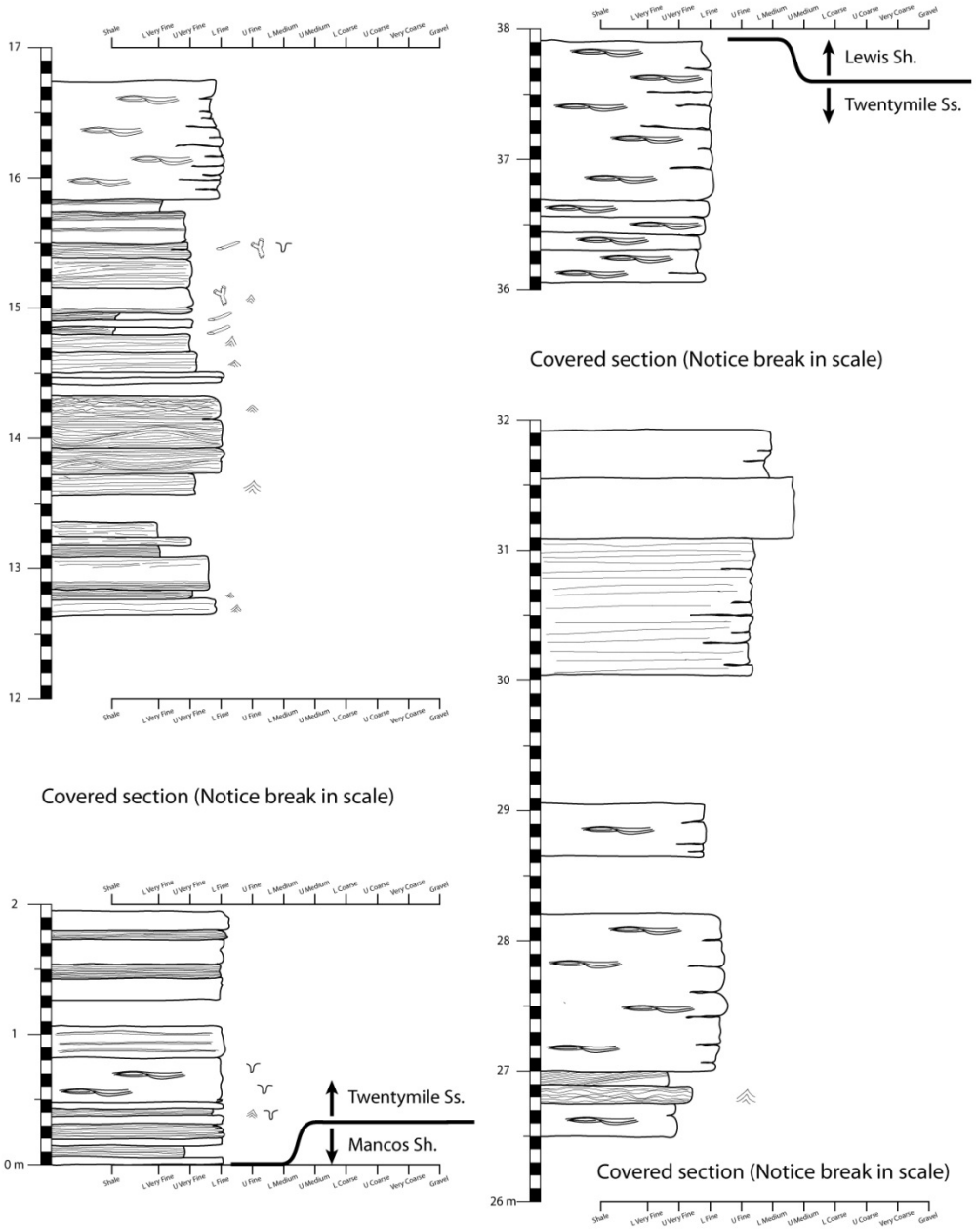

Figure B.49: Co Rd 33 section.

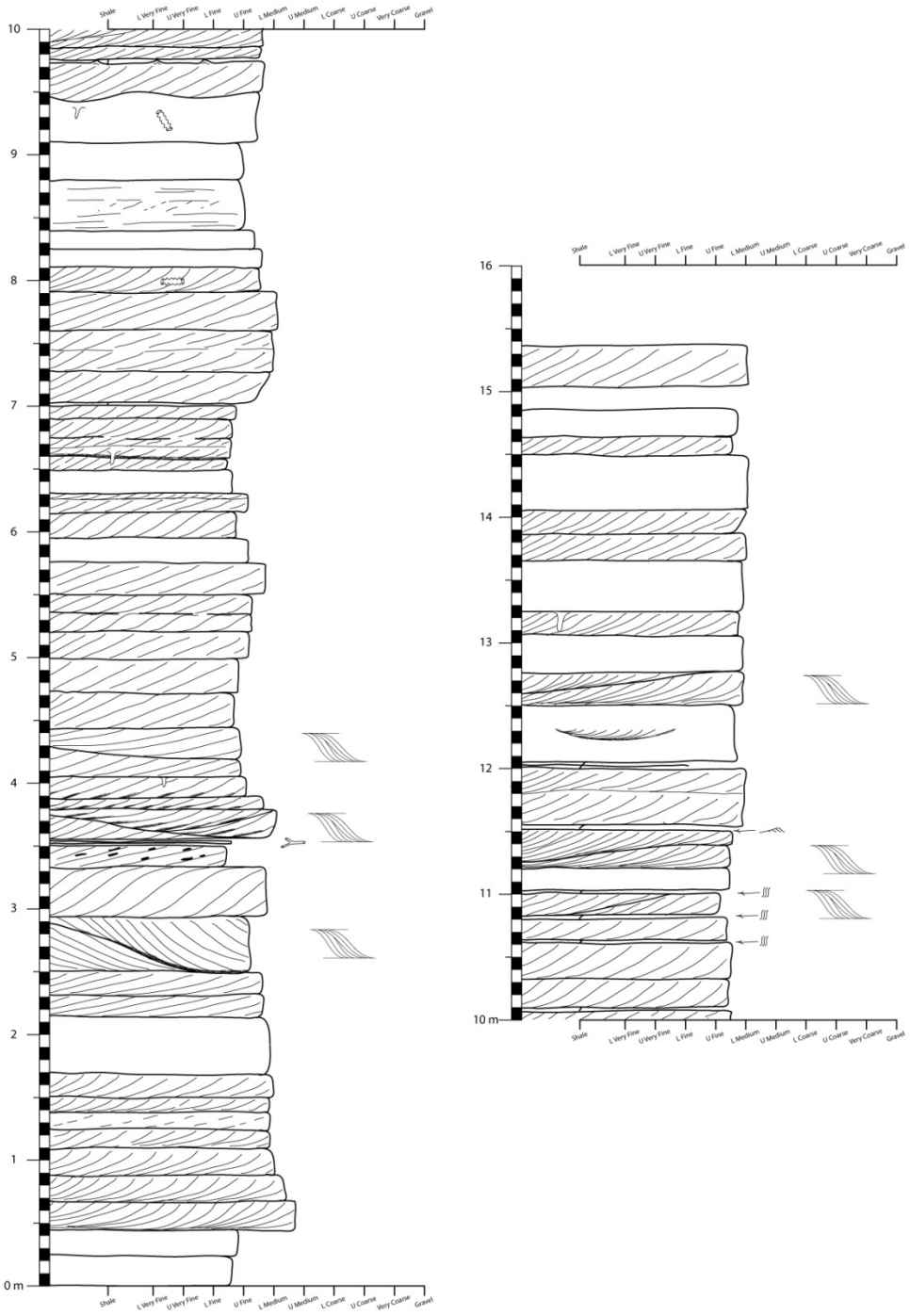

Figure B.50: Antelope Creek section.

Appendix C: Explanation of the governing equation and its derivation

To calculate the area of the modeled sediment pile, the total area is subdivided into three triangles as shown in Figure C.1. The area of triangle A can be calculated as:

(1) $$A = \frac{1}{2}(\eta_r - z)s,$$

the area of triangle B as:

(2) $$B = \frac{1}{2}(z - \eta_u)s,$$

and the area of triangle C as:

(3) $$C = \frac{1}{2}(z - \eta_b)u.$$

The governing equation is a mass-balance equation, which balances the total area of the sediment pile, corrected for deposit porosity (φ), with the sediment supply (q_s) over a given time (t) and the initial coastal prism (A_i), and takes the following form:

(4) $$q_s t + A_i = \left[\frac{1}{2}(\eta_r - z)s + \frac{1}{2}(z - \eta_u)s + \frac{1}{2}(z - \eta_b)u\right](1 - \varphi)$$

The constant foreset slope (S_f), the topset slope (S_t) and the basement slope (S_b) are defined as

(5) $$S_t = \frac{(z-\eta_r)}{s},$$

(6) $$S_f = \frac{(\eta_u - z)}{u - s},$$

(7) $$S_b = \frac{(\eta_u - \eta_b)}{u}.$$

Equations (5, 6, and 7) can be rearranged as

(8) $$\eta_r - z = -S_t s,$$

(9) $$z - \eta_u = S_f(s - u),$$

(10) $$\eta_u = uS_b + \eta_b.$$

Combining equations (6) and (10) results in

(11) $$u = \alpha\left(S_f s - z + \eta_b\right),$$

where

(12) $$\alpha = \left(S_f - S_b\right)^{-1}.$$

Equations (9) and (11) produces the following relationship:

(13) $$z - \eta_u = S_f s - \alpha S_f^2 s + \alpha S_f z - \alpha S_f \eta_b.$$

The three terms in the square bracket on the right-hand side of equation (4) can be substituted with equations (8), (11), and (13), respectively and equation (4) turns into the following form:

(14) $$\frac{2(q_s t + A_i)}{1-\varphi} = \left(S_f - \alpha S_f^2 - S_t\right)s^2 + 2\alpha S_f z s - 2\alpha S_f \eta_b s - \alpha\left(z^2 + \eta_b^2 - 2z\eta_b\right).$$

This can be also rearranged to

(15) $$0 = \left(S_f - \alpha S_f^2 - S_t\right)s^2 + 2\alpha S_f (z - \eta_b)s - \alpha(z - \eta_b)^2 - \frac{2(q_s t + A_i)}{1-\varphi}.$$

Using equation (15), the shoreline position (s) can be solved by applying a quadratic equation as follows:

(16) $$s = \frac{-2\alpha S_f (z-\eta_b) + \sqrt{\left[2\alpha S_f (z-\eta_b)\right]^2 + 4\left(S_f - \alpha S_f^2 - S_t\right)\left[\alpha(z-\eta_b)^2 + \frac{2(q_s t + A_i)}{1-\varphi}\right]}}{2\left(S_f - \alpha S_f^2 - S_t\right)}$$

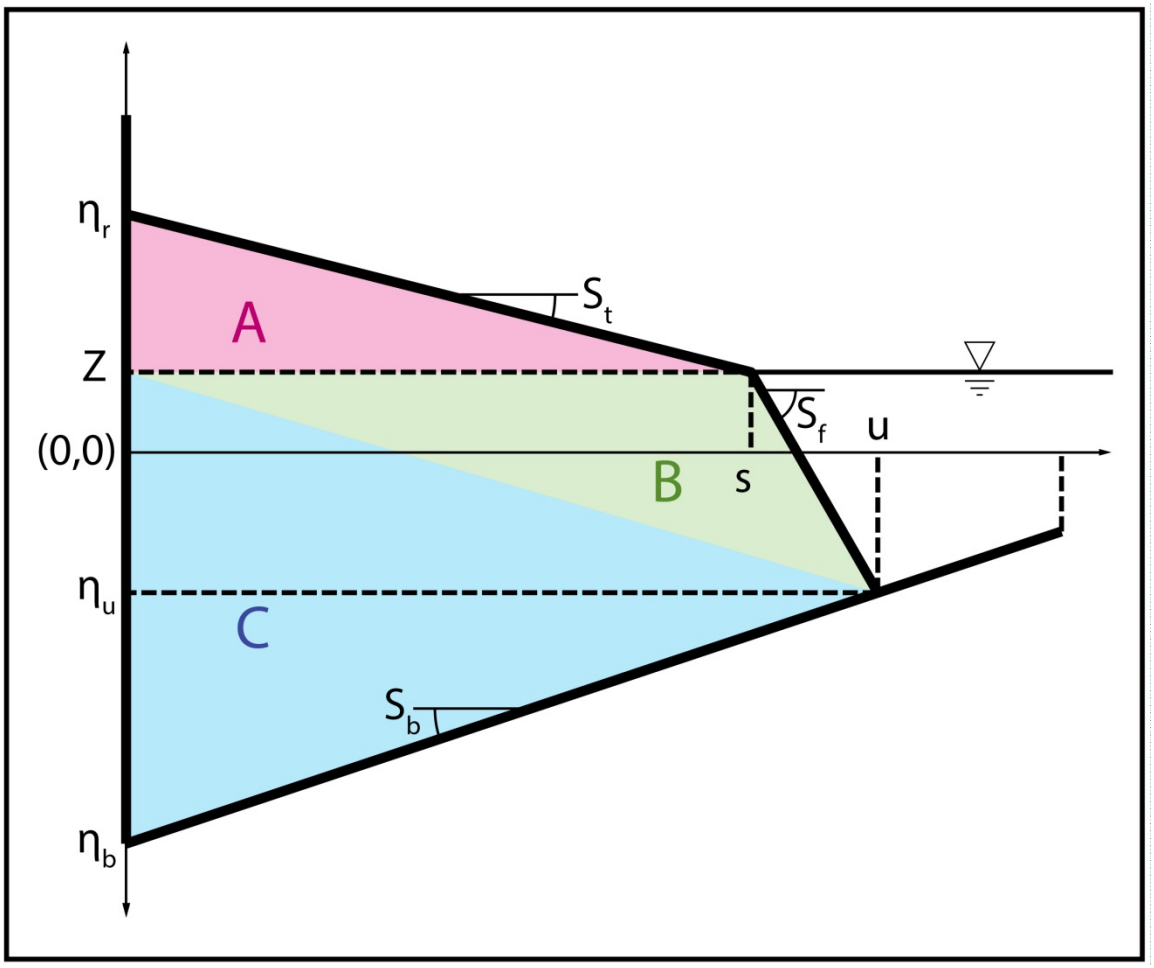

Figure C.1: Modeled deltaic body showing the main variables and the three triangles used to calculate its area.

References

ALLEN, G.P. & POSAMENTIER, H.W. (1993) Sequence Stratigraphy and Facies Model of an Incised Valley Fill - the Gironde Estuary, France. *Journal of Sedimentary Petrology*, **63,** 378-391.

ALLEN, J.R.L. (1982) *Sedimentary Structures, Their Character and Physical Basis, Volume 2*. Elsevier, Amsterdam, Netherlands.

ASCHOFF, J. & STEEL, R. (2011a) Anomalous Clastic Wedge Development During the Sevier-Laramide Transition, North American Cordilleran Foreland Basin, USA. *Geological Society of America Bulletin*, **123,** 1822-1835.

ASCHOFF, J.L. & STEEL, R.J. (2011b) Anatomy and Development of a Low-Accommodation Clastic Wedge, Upper Cretaceous, Cordilleran Foreland Basin, USA. *Sedimentary Geology*, **236,** 1-24.

ASHBY, J.M., GEISSMAN, J.W. & WEIL, A.B. (2005) Has the Eastern End of the Uinta Mountains Been Bent? Paleomagnetic and Fault Kinematic Assessment. In: *Uinta Mountain Geology* (Ed. by C. M. Dehler, J. L. Pederson, D. A. Sprinkel & B. J. Kowallis), **33**, 285-. Utah Geological Association, Salt Lake City, UT.

BADER, J.W., GILL, J.R., COBBAN, W.A. & LAW, B.E. (1983) Biostratigraphic Correlation Chart of Some Upper Cretaceous Rocks from the Lost Soldier Area, Wyoming to West of Craig, Colorado, U.S. Geological Survey. Denver, CO.

BARLOW JR, J.A. (1955) Structure of the Rawlins Uplift, Carbon County, Wyoming.

BASSETTI, M.A., JOUET, G., DUFOIS, F., BERNÉ, S., RABINEAU, M. & TAVIANI, M. (2006) Sand Bodies at the Shelf Edge in the Gulf of Lions (Western Mediterranean): Deglacial History and Modern Processes. *Marine Geology*, **234,** 93-109.

BENDA, T.L. (2000) Facies, Architecture, and Sequence Stratigraphy of a Fourth-Order Clastic Wedge: Upper Cretaceous Twentymile Sandstone, (Mesaverde Group) Northwest Colorado, University of Wyoming, Laramie.

BERNE, S., LERICOLAIS, G., MARSSET, T., BOURILLET, J.F. & DE BATIST, M. (1998) Erosional Offshore Sand Ridges and Lowstand Shorefaces; Examples from Tide- and Wave-Dominated Environments of France. *Journal of Sedimentary Research*, **68,** 540-555.

BLAIR, T.C. & BILODEAU, W.L. (1988) Development of Tectonic Cyclothems in Rift, Pull-Apart, and Foreland Basins: Sedimentary Response to Episodic Tectonism. *Geology*, **16,** 517-520.

BLAKEY, R. (2011) Colorado Plateau Geosystems, Inc., from http://cpgeosystems.com/index.html.

BOGGS JR., S. (2012) Marginal Marine Environments. In: *Principles of Sedimentology and Stratigraphy* (Ed. by S. Boggs Jr.), 246-227. Pearson Education, Upper Saddle River, NJ.

BULLIMORE, S.A., HELLAND-HANSEN, W., HENRIKSEN, S. & STEEL, R.J. (2008) Shoreline Trajectory and Its Impact on Coastal Depositional Environments: An Example from the Upper Cretaceous Mesaverde Group, Northwestern Colorado, USA. In: *Recent Advances in Models of Siliciclastic Shallow-Marine Stratigraphy* (Ed. by G. J. Hampson, R. J. Steel & P. M. Burgess), *Sepm Special Publication*, **90**, 209-236. SEPM - Soc. Sedimentary Geology, Tulsa.

BURBANK, D.W., PUIGDEFABREGAS, C. & MUÑOZ, J.A. (1992) The Chronology of the Eocene Tectonic and Stratigraphic Development of the Eastern Pyrenean Foreland Basin, Northeast Spain. *Geological Society of America Bulletin*, **104,** 1101-1120.

CARVAJAL, C. & STEEL, R. (2009) Shelf-Edge Architecture and Bypass of Sand to Deep Water: Influence of Shelf-Edge Processes, Sea Level, and Sediment Supply. *Journal of Sedimentary Research*, **79,** 652-672.

CARVAJAL, C. & STEEL, R. (2012) Source-to-Sink Sediment Volumes within a Tectono-Stratigraphic Model for a Laramide Shelf-to-Deep-Water Basin: Methods and Results. *Tectonics of Sedimentary Basins: Recent Advances***,** 131-151.

CATTANEO, A. & STEEL, R.J. (2003) Transgressive Deposits: A Review of Their Variability. *Earth-Science Reviews*, **62,** 187-228.

CATUNEANU, O., HANCOX, P.J. & RUBIDGE, B.S. (1998) Reciprocal Flexural Behaviour and Contrasting Stratigraphies: A New Basin Development Model for the Karoo Retroarc Foreland System, South Africa. *Basin Research*, **10,** 417-439.

CATUNEANU, O. (2004) Retroarc Foreland Systems - Evolution through Time. *Journal of African Earth Sciences*, **38,** 225-242.

CLEVIS, Q., DE BOER, P. & WACHTER, M. (2003) Numerical Modelling of Drainage Basin Evolution and Three-Dimensional Alluvial Fan Stratigraphy. *Sedimentary Geology*, **163,** 85-110.

CLEVIS, Q., DE BOER, P.L. & NIJMAN, W. (2004) Differentiating the Effect of Episodic Tectonism and Eustatic Sea-Level Fluctuations in Foreland Basins Filled by Alluvial Fans and Axial Deltaic Systems: Insights from a Three-Dimensional Stratigraphic Forward Model. *Sedimentology,* **51,** 809-835.

COBBAN, W.A., WALASZCZYK, I., OBRADOVICH, J.D. & MCKINNEY, K.C. (2006) A Usgs Zonal Table for the Upper Cretaceous Middle Cenomanian--Maastrichtian of the Western Interior of the United States Based on Ammonites, Inoceramids, and Radiometric Ages. *USGS Open Report,* USGS. Denver**,** 45.

CONSTENIUS, K.N., ESSER, R.P. & LAYER, P.W. (2003) Extensional Collapse of the Charleston-Nebo Salient and Its Relationship to Space-Time Variations in Cordilleran Orogenic Belt Tectonism and Continental Stratigraphy. In: *Cenozoic Systems of the Rocky Mountain Region* (Ed. by R. G. Raynolds & R. M. Flores), 303-354. Rocky Mountain Section (SEPM), Denver, CO.

COVEY, M. (1986) The Evolution of Foreland Basins to Steady State: Evidence from the Western Taiwan Foreland Basin. In: *Foreland Basins* (Ed. by P. A. Allen & P. Homewood), *Spec. Publ. Int. Ass. Sediment.*, **8**, 77-90. Blackwell Publishing Ltd.

CRABAUGH, J.P. (2001) Nature and Growth of Nonmarine-to-Marine Clastic Wedges: Examples from the Upper Cretaceous Iles Formation, Western Interior (Colorado) and the Lower Paleogene Wilcox Group of the Gulf of Mexico Basin (Texas). Ph. D. Dissertation Thesis, University of Wyoming, Laramie.

CROSS, T.A. & PILGER, R.H. (1978) Tectonic Controls of Late Cretaceous Sedimentation, Western Interior, USA. *Nature,* **274,** 653-657.

CROSS, T.A. (1986) Tectonic Controls of Foreland Basin Subsidence and Laramide Style Deformation, Western United States. *Special Publications International Association of Sedimentologists,* **8,** 453.

DALRYMPLE, R.W. (1984) Morphology and Internal Structure of Sandwaves in the Bay of Fundy. *Sedimentology,* **31,** 365-382.

DALRYMPLE, R.W. (2012) Tidal Depositional Systems. In: *Facies Model 4* (Ed. by N. P. James & R. W. Dalrymple), 201-231. Geological Association of Canada, St. John's, Canada.

DAVIS, R.A. & BALSON, P.S. (1992) Stratigraphy of a North Sea Tidal Sand Ridge. *Journal of Sedimentary Research,* **62,** 116-121.

DAVIS, R.A., KLAY, J. & JEWELL, P. (1993) Sedimentology and Stratigraphy of Tidal Sand Ridges Southwest Florida Inner Shelf. *Journal of Sedimentary Research,* **63,** 91-104.

DAVIS, W.M. (1898) *The Triassic Formations of Connecticut.* U.S.G.S. Annual report, No. 18, part 2.

DECELLES, P.G. (1994) Late Cretaceous-Paleocene Synorogenic Sedimentation and Kinematic History of the Sevier Thrust Belt, Northeast Utah and Southwest Wyoming. *Geological Society of America Bulletin,* **106,** 32-56.

DECELLES, P.G., LAWTON, T.F. & MITRA, G. (1995) Thrust Timing, Growth of Structural Culminations, and Synorogenic Sedimentation in the Type Sevier Orogenic Belt, Western United-States. *Geology,* **23,** 699-702.

DECELLES, P.G. & MITRA, G. (1995) History of the Sevier Orogenic Wedge in Terms of Critical Taper Models, Northeast Utah and Southwest Wyoming. *Geological Society of America Bulletin,* **107,** 454-462.

DECELLES, P.G. & GILES, K.A. (1996) Foreland Basin Systems. *Basin Research,* **8,** 105-123.

DECELLES, P.G. (2004) Late Jurassic to Eocene Evolution of the Cordilleran Thrust Belt and Foreland Basin System, Western USA. *American Journal of Science,* **304,** 105-168.

DECELLES, P.G. & COOGAN, J.C. (2006) Regional Structure and Kinematic History of the Sevier Fold-and-Thrust Belt, Central Utah. *Geological Society of America Bulletin,* **118,** 841-864.

DECKER, P.L. (2007) Brookian Sequence Stratigraphic Correlations, Umait Field to Milne Point Field, West-Central North Slope, Alaska, Alaska Division of Geological & Geophysical Surveys. **Preliminary Interpretative Report 2007-2,** 19p., 11 sheet.

DECKER, P.L. (2010) Brookian Sequence Stratigraphic Framework of the Northern Colville Foreland Basin, Central North Slope, Alaska (Poster and Presentation): Dnr Spring Technical Review Meeting, Anchorage, April 21-22, 2010, Alaska Division of Geological & Geophysical Surveys**,** 30 p., 31 sheet.

DEVLIN, W.J., RUDOLPH, K.W., SHAW, C.A. & EHMAN, K.D. (1993) The Effect of Tectonic and Eustatic Cycles on Accommodation and Sequence-Stratigraphic Framework in the Upper Cretaceous Foreland Basin of Southwestern Wyoming. In: *Sequence Stratigraphy and Facies Associations* (Ed. by H. W. Posamentier, C.

P. Summerhayes, B. U. Haq & G. P. Allen), *Spec. Publ. Int. Ass. Of Sediment.*, **18**, 501-520. Blackwell Publishing Ltd., Boston.

DICKINSON, W.R. (1974) Plate Tectonics and Sedimentation. In: *Tectonics and Sedimentation* (Ed. by W. R. Dickinson), **22**, 1-27. SEPM (Society for Sedimentary Geology), Tulsa, OK.

DICKINSON, W.R. & SNYDER, W.S. (1978) Plate Tectonics of the Laramide Orogeny. In: *Laramide Folding Associated with Basement Block Faulting in the Western United States* (Ed. by V. Mattheus), **Memoir no.121**, 355-366. Geological Society of America, Boulder, CO.

DICKINSON, W.R., KLUTE, M.A., HAYES, M.J., JANECKE, S.U., LUNDIN, E.R., MCKITTRICK, M.A. & OLIVARES, M.D. (1988) Paleogeographic and Paleotectonic Setting of the Laramide Sedimentary Basins in Central Rocky-Mountain Region. *Geological Society of America Bulletin*, **100,** 1023-1039.

DOTT, R.H. & BOURGEOIS, J. (1982) Hummocky Stratification - Significance of Its Variable Bedding Sequences. *Geological Society of America Bulletin*, **93,** 663-680.

ENGE, H.D., HOWELL, J.A. & BUCKLEY, S.J. (2010) The Geometry and Internal Architecture of Stream Bars in the Panther Tongue and the Ferron Sandstone Members, Utah, U.S.A. *Journal of Sedimentary Research*, **80,** 1018-1031.

FLEMINGS, P.B. & JORDAN, T.E. (1989) A Synthetic Stratigraphic Model of Foreland Basin Development. *Journal of Geophysical Research-Solid Earth and Planets*, **94,** 3851-3866.

FLEMINGS, P.B. & JORDAN, T.E. (1990) Stratigraphic Modelling of Foreland Basins - Interpreting Thrust Deformation and Lithosphere Rheology. *Geology*, **18,** 430-434.

FLEMINGS, P.B. & GROTZINGER, J.P. (1996) Strata: Freeware for Analyzing Classic Stratigraphic Problems. *GSA Today*, **6,** 1-7.

FLORES, R.M. (1978) Barrier and Back-Barrier Environments of Deposition of the Upper Cretaceous Almond Formation, Rock Springs Uplift, Wyoming. *Mountain Geologist*, **15,** 57-65.

GALLOWAY, W.E. (1989) Genetic Stratigraphic Sequences in Basin Analysis. 1. Architecture and Genesis of Flooding-Surface Bounded Depositional Units. *Aapg Bulletin-American Association of Petroleum Geologists*, **73,** 125-142.

GARCIA-CASTELLANOS, D. (2002) Interplay between Lithospheric Flexure and River Transport in Foreland Basins. *Basin Research*, **14,** 89-104.

GARCIA-CASTELLANOS, D., VERGES, J., GASPAR-ESCRIBANO, J. & CLOETINGH, S. (2003) Interplay between Tectonics, Climate, and Fluvial Transport During the Cenozoic Evolution of the Ebro Basin (Ne Iberia). *Journal of Geophysical Research-Solid Earth*, **108**.

GAWTHORPE, R.L., FRASER, A.J. & COLLIER, R.E.L. (1994) Sequence Stratigraphy in Active Extensional Basins: Implications for the Interpretation of Ancient Basin-Fills. *Marine and Petroleum Geology*, **11,** 642-658.

GAWTHORPE, R.L. & LEEDER, M.R. (2000) Tectono-Sedimentary Evolution of Active Extensional Basins. *Basin Research*, **12,** 195-218.

GILL, J.R., MEREWETHER, E.A. & COBBAN, W.A. (1970) *Stratigraphy and Nomenclature of Some Upper Cretaceous and Lower Tertiary Rocks in South-Central Wyoming*. U.S. Geological Survey, Denver, CO.

GOMEZ-VEROIZA, C.A. & STEEL, R.J. (2010) Iles Clastic Wedge Development and Sediment Partitioning within a 300-Km Fluvial to Marine Campanian Transect (3 M.Y.), Western Interior Seaway, Southwestern Wyoming and Northern Colorado. *AAPG Bulletin*, **94,** 1349-1377.

GOMEZ, C.A. (2009) Clastic Wedge Development and Sediment Budget in a Source-to-Sink Transect (Late Campanian Western Interior Basin, Sw Wyoming and N Colorado). Ph.D. Dissertation Thesis, University of Texas at Austin, Austin.

GREEN, G.N. (1992) The Digital Geologic Map of Colorado in Arc/Info Format: U.S. Geological Survey, Open-File Report of-92-507, Scale 1:500000.

GREEN, G.N. & DROUILLARD, P.H. (1994) The Digital Geologic Map of Wyoming in Arc/Info Format: U.S. Geological Survey, Open-File Report of-94-425, Scale 1:500000.

GURNIS, M. (1993) Phanerozoic Marine Inundation of Continents Driven by Dynamic Topography above Subducting Slabs. *Nature*, **364,** 589-593.

HAMPSON, G.J. & STORMS, J.E.A. (2003) Geomorphological and Sequence Stratigraphic Variability in Wave-Dominated, Shoreface-Shelf Parasequences. *Sedimentology*, **50,** 667-701.

HAMPSON, G.J. (2010) Sediment Dispersal and Quantitative Stratigraphic Architecture across an Ancient Shelf. *Sedimentology*, **57,** 96-141.

HANSEN, W.R. (1986) *Neogene Tectonics and Geomorphology of the Eastern Uinta Mountains in Utah, Colorado, and Wyoming*. U.S. Geological Survey, Denver, CO.

HAQ, B.U., HARDENBOL, J. & VAIL, P.R. (1987) Chronology of Fluctuating Sea Levels since the Triassic. *Science*, **235,** 1156-1167.

HARMS, J.C., SOUTHARD, J.B., SPEARING, D.R. & WALKER, R.G. (1975) Stratification Produced by Migrating Bed Forms. In: *Depositional Environments as Interpreted from Primary Sedimentary and Stratigraphic Sequences* (Ed. by J. C. Harms, J. B. Southard, D. R. Spearing & R. G. Walker), *Sepm Short Course Notes*, **2**, 45-61. SEPM (Society for Sedimentary Geology).

HARTLEY, A.J., WEISSMANN, G.S., NICHOLS, G.J. & WARWICK, G.L. (2010) Large Distributive Fluvial Systems: Characteristics, Distribution, and Controls on Development. *Journal of Sedimentary Research*, **80,** 167-183.

HELLAND-HANSEN, W. & GJELBERG, J.G. (1994) Conceptual Basis and Variability in Sequence Stratigraphy - a Different Perspective. *Sedimentary Geology*, **92,** 31-52.

HELLER, P.L., BOWDLER, S.S., CHAMBERS, H.P., COOGAN, J.C., HAGEN, E.S., SHUSTER, M.W., WINSLOW, N.S. & LAWTON, T.F. (1986) Time of Initial Thrusting in the Sevier Orogenic Belt, Idaho-Wyoming and Utah. *Geology*, **14,** 388-391.

HELLER, P.L., ANGEVINE, C.L., WINSLOW, N.S. & PAOLA, C. (1988) Two-Phase Stratigraphic Model of Foreland-Basin Sequences. *Geology*, **16,** 501-504.

HELLER, P.L. & PAOLA, C. (1992) The Large-Scale Dynamics of Grain-Size Variation in Alluvial Basins, 2: Application to Syntectonic Conglomerate. *Basin Research*, **4,** 91-102.

HENRIKSEN, S., HAMPSON, G.J., HELLAND-HANSEN, W., JOHANNESSEN, E.P. & STEEL, R.J. (2009) Shelf Edge and Shoreline Trajectories, a Dynamic Approach to Stratigraphic Analysis. *Basin Research*, **21,** 445-453.

HINTZE, L.F., WILLIS, G.C., LAES, D.Y.M., SPRINKEL, D.A. & BROWN, K.D. (2000) Digital Geologic Map of Utah: Utah Geological Survey, Map 179dm, Scale 1:500000.

HORTON, B.K. & DECELLES, P.G. (2001) Modern and Ancient Fluvial Megafans in the Foreland Basin System of the Central Andes, Southern Bolivia: Implications for Drainage Network Evolution in Fold-Thrust Belts. *Basin Research*, **13,** 43-63.

HORTON, B.K., CONSTENIUS, K.N. & DECELLES, P.G. (2004) Tectonic Control on Coarse-Grained Foreland-Basin Sequences: An Example from the Cordilleran Foreland Basin, Utah. *Geology*, **32,** 637-640.

HOUBOLT, J.J.H.C. (1968) Recent Sediments in the Southern Bight of the North Sea. *Geologie en Mijnbouw*, **47,** 245-273.

HOUSEKNECHT, D.W. & SCHENK, C.J. (2001) Depositional Sequences and Facies in the Torok Formation, National Petroleum Reserve - Alaska (Npra). In: *Npra Core Workshop Petroleum Plays and Systems in the National Petroleum Reserve-Alaska* (Ed. by D. W. Houseknecht), 179-200. SEPM (Society for Sedimentary Geology), Tulsa.

HOUSEKNECHT, D.W., BIRD, K.J. & SCHENK, C.J. (2009) Seismic Analysis of Clinoform Depositional Sequences and Shelf-Margin Trajectories in Lower Cretaceous (Albian) Strata, Alaska North Slope. *Basin Research*, **21,** 644-654.

INGERSOLL, R.V. (1988) Tectonics of Sedimentary Basins. *Geological Society of America Bulletin*, **100,** 1704-1719.

IZZET, G.A., COBBAN, W.A. & GILL, J.R. (1971) The Pierre Shale near Kremmling, Colorado, and Its Correlation to the East and the West. *Geological Survey Professional Paper*. U. S. G. Survey. **684-A**.

JERVEY, M.T. (1988) Quantitative Geological Modeling of Siliciclastic Rock Sequences and Their Seismic Expression. In: *Sea-Level Changes: An Integrated Approach* (Ed. by C. K. Wilgus, B. S. Hastings, H. W. Posamentier, J. C. Van Wagoner, A. C. Ross & C. G. S. C. Kendall), *Sepm Special Publication*, **42**, 47-69. SEPM - Soc. Sedimentary Geology, Tusla, OK.

JONES, C.H., FARMER, G.L., SAGEMAN, B. & ZHONG, S. (2011) Hydrodynamic Mechanism for the Laramide Orogeny. *Geosphere*, **7,** 183-201.

JORDAN, T.E. (1981) Thrust Loads and Foreland Basin Evolution, Cretaceous, Western United-States. *Aapg Bulletin-American Association of Petroleum Geologists*, **65,** 2506-2520.

JORDAN, T.E. (1995) Retroarc Foreland and Related Basins. In: *Tectonics of Sedimentary Basins* (Ed. by C. J. Busby & R. V. Ingersoll), 331-362. Blackwell Science, Cambridge, MA.

KERTZNUS, V. & KNELLER, B. (2009) Clinoform Quantification for Assessing the Effects of External Forcing on Continental Margin Development. *Basin Research*, **21,** 738-758.

KIEFT, R.L., HAMPSON, G.J., JACKSON, C.A.-L. & LARSEN, E. (2011) Stratigraphic Architecture of a Net-Transgressive Marginal- to Shallow-Marine Succession:

Upper Almond Formation, Rock Springs Uplift, Wyoming, U.S.A. *Journal of Sedimentary Research*, **81,** 513-533.

KIM, W., PAOLA, C., SWENSON, J.B. & VOLLER, V.R. (2006) Shoreline Response to Autogenic Processes of Sediment Storage and Release in the Fluvial System. *J. Geophys. Res.*, **111,** F04013.

KIM, W. & MUTO, T. (2007) Autogenic Response of Alluvial-Bedrock Transition to Base-Level Variation: Experiment and Theory. *Journal of Geophysical Research-Earth Surface*, **112,** F3S14.

KIM, W. & JEROLMACK, D.J. (2008) The Pulse of Calm Fan Deltas. *Journal of Geology*, **116,** 315-330.

KING, P.B. (1959) *The Evolution of North America*. Princeton University Press, Princeton.

KIRSCHBAUM, M.A. & ROBERTS, L.N. (2005) Stratigraphic Framework of the Cretaceous Mowry Shale, Frontier Formation and Adjacent Units, Southwestern Wyoming Province, Wyoming, Colorado, and Utah. *US Geological Survey Southwestern Wyoming Province Assessment Team, Petroleum systems and geologic assessment of oil and gas in the southwestern Wyoming province, Wyoming, Colorado, and Utah: US Geological Survey digital data series DDS*, **69**.

KRYSTINIK, L. & DEJARNETT, B.B. (1995) Lateral Variability of Sequence Stratigraphic Framework in the Campanian and Lower Maastrichtian of the Western Interior Seaway. In: *Sequence Stratigraphy of Foreland Basin Deposits* (Ed. by J. C. Van Wagoner & G. T. Bertram), *Aapg Memoir*, **64**, 11-26. The American Association of Petroleum Geologists, Tulsa, OK.

LEARY, R., DECELLES, P., GEHRELS, G. & MORRISS, M. (2014) Fluvial Deposition During Transition from Flexural to Dynamic Subsidence in the Cordilleran Foreland Basin: Ericson Formation, Western Wyoming, U.S.A. *Basin Research***,** n/a-n/a.

LECKIE, D.A. & WALKER, R.G. (1982) Storm- and Tide-Dominated Shorelines in Cretaceous Moosebar-Lower Gates Interval; Outcrop Equivalents of Deep Basin Gas Trap in Western Canada. *AAPG Bulletin*, **66,** 138-157.

LECLAIR, S.F. & BRIDGE, J.S. (2001) Quantitative Interpretation of Sedimentary Structures Formed by River Dunes. *Journal of Sedimentary Research*, **71,** 713-716.

LEFEBRE, G.B. (1988) Tectonic Evolution of Hanna Basin, Wyoming: Laramide Block Rotation in the Rocky Mountain Foreland. Ph.D. Dissertation Thesis, University of Wyoming, Laramie, WY.

LEIER, A.L., DECELLES, P.G. & PELLETIER, J.D. (2005) Mountains, Monsoons, and Megafans. *Geology*, **33,** 289-292.

LEVA LÓPEZ, J., KIM, W. & STEEL, R.J. (2014) Autoacceleration of Clinoform Progradation in Foreland Basins: Theory and Experiments. *Basin Research,* 1365-2117.

LEVA LÓPEZ, J. & STEEL, R.J. (In preparation) Campanian Laramide Signals and Architecture of a Widespread Fluvial Sheetsand: Canyon Creek Sandstone, Southern Wyoming.

LI, W.G., BHATTACHARYA, J. & ZHU, Y.J. (2011) Architecture of a Forced Regressive Systems Tract in the Turonian Ferron "Notom Delta", Southern Utah, USA. *Marine and Petroleum Geology*, **28,** 1517-1529.

LIU, L. & GURNIS, M. (2010) Dynamic Subsidence and Uplift of the Colorado Plateau. *Geology*, **38,** 663-666.

LIU, S.F. & NUMMEDAL, D. (2004) Late Cretaceous Subsidence in Wyoming: Quantifying the Dynamic Component. *Geology*, **32,** 397-400.

LIU, S.F., NUMMEDAL, D., YIN, P.G. & LUO, H.J. (2005) Linkage of Sevier Thrusting Episodes and Late Cretaceous Foreland Basin Megasequences across Southern Wyoming (USA). *Basin Research,* **17,** 487-506.

LIU, S.F., NUMMEDAL, D. & LIU, L. (2011) Migration of Dynamic Subsidence across the Late Cretaceous United States Western Interior Basin in Response to Farallon Plate Subduction. *Geology,* **39,** 555-558.

LOVE, J.D. (1961) Definition of Green River, Great Divide, and Washakie Basins, Southwestern Wyoming. *AAPG Bulletin*, **45,** 1749-1755.

MARSHAK, S., KARLSTROM, K. & TIMMONS, J.M. (2000) Inversion of Proterozoic Extensional Faults: An Explanation for the Pattern of Laramide and Ancestral Rockies Intracratonic Deformation, United States. *Geology,* **28,** 735-738.

MARSHALL, K. (1951) *North American Geosynclines*. The Geological Society of America, New York.

MARTINSEN, O.J., MARTINSEN, R.S. & STEIDTMANN, J.R. (1993) Mesaverde Group (Upper Cretaceous), Southeastern Wyoming - Allostratigraphy Versus Sequence Stratigraphy in a Tectonically Active Area. *Aapg Bulletin-American Association of Petroleum Geologists*, **77,** 1351-1373.

MARTINSEN, O.J., ALF RYSETH, A., HELLAND-HANSEN, W., FLESCHE, H., TORKILDSEN, G. & IDIL, S. (1999) Stratigraphic Base Level and Fluvial Architecture: Ericson

Sandstone (Campanian), Rock Springs Uplift, Sw Wyoming, USA. *Sedimentology*, **46,** 235-263.

MARTINSEN, R.S. & CHRISTIANSEN, G.E. (1992) A Stratigraphic and Environmental Study of the Almond Formation, Mesaverde Group, Greater Green River Basin, Wyoming. In: *Rediscover the Rockies; 43rd Annual Field Conference Guidebook* (Ed. by C. E. Mullen), 171-190. Wyoming Geological Association, Casper, WY.

MARTINSEN, R.S. (1995) Stratigraphy and Lithofacies of the Almond Formation, Washakie and Great Divide Basins, Wyoming. *Guidebook - Wyoming Geological Association*. G. E. Christiansen, M. A. Olson & R. C. Surdam, Wyoming Geological Association : Casper, WY, United States. United States. **1995,** 297-310.

MARTINSEN, R.S. (1998) Compartmentalization of Sandstone Reservoirs Due to Syndepositional Faulting, Almond Formation, Washakie Basin, Wyoming. In: *Compartmentalized Reservoirs in Rocky Mountain Basins* (Ed. by R. M. Slatt), *Rmag Symposium*, 71-98. The Rocky Mountain Association of Geologists, Denver, CO.

MARTINSEN, R.S. (2003A) Depositional Remnants, Part 2: Examples from the Western Interior Cretaceous Basin of North America. *Aapg Bulletin*, **87,** 1883-1909.

MARTINSEN, R.S. (2003B) Depositional Remnants, Part 1: Common Components of the Stratigraphic Record with Important Implications for Hydrocarbon Exploration and Production. *Aapg Bulletin*, **87,** 1869-1882.

MARZO, M. & STEEL, R.J. (2000) Unusual Features of Sediment Supply-Dominated, Transgressive-Regressive Sequences: Paleogene Elastic Wedges, Se Pyrenean Foreland Basin, Spain. *Sedimentary Geology*, **138,** 3-15.

MASTERS, C.D. (1966) Sedimentology of the Mesaverde Group and of the Upper Part of the Mancos Formation, Northwestern Colorado, Yale University, New Haven.

MELLERE, D. & STEEL, R.J. (1995) Variability of Lowstand Wedges and Their Distinction from Forced-Regressive Wedges in the Mesaverde Group, Southeast Wyoming. *Geology*, **23,** 803-806.

MELLERE, D. & STEEL, R.J. (2000) Style Contrast between Forced Regressive and Lowstand/Transgressive Wedges in the Campanian of South-Central Wyoming (Hatfield Member of the Haystack Mountains Formation). *Geological Society, London, Special Publications*, **172,** 141-162.

MILLER, K.G., WRIGHT, J.D. & BROWNING, J.V. (2005) Visions of Ice Sheets in a Greenhouse World. *Marine Geology*, **217,** 215-231.

MILLIMAN, J.D. & SYVITSKI, J.P.M. (1992) Geomorphic Tectonic Control of Sediment Discharge to the Ocean - the Importance of Small Mountainous Rivers. *Journal of Geology,* **100,** 525-544.

MULL, C.G., HOUSEKNECHT, D.W. & BIRD, K.J. (2003) Revised Cretaceous and Tertiary Stratigraphic Nomenclature in the Colville Basin, Northern Alaska. *Professional Paper,* U.S. Geological Survey. **1673,** 59.

MUTO, T. & STEEL, R.J. (1992) Retreat of the Front in a Prograding Delta. *Geology,* **20,** 967-970.

MUTO, T. & STEEL, R.J. (1997) Principles of Regression and Transgression: The Nature of the Interplay between Accommodation and Sediment Supply. *Journal of Sedimentary Research,* **67,** 994-1000.

MUTO, T. & STEEL, R.J. (2002A) Role of Autoretreat and a/S Changes in the Understanding of Deltaic Shoreline Trajectory: A Semi-Quantitative Approach. *Basin Research*, **14,** 303-318.

MUTO, T. & STEEL, R.J. (2002B) In Defense of Shelf-Edge Delta Development During Falling and Lowstand of Relative Sea Level. *Journal of Geology,* **110,** 421-436.

MUTO, T. & STEEL, R.J. (2004) Autogenic Response of Fluvial Deltas to Steady Sea-Level Fall: Implications from Flume-Tank Experiments. *Geology*, **32,** 401-404.

MUTO, T. & SWENSON, J.B. (2006) Autogenic Attainment of Large-Scale Alluvial Grade with Steady Sea-Level Fall: An Analog Tank-Flume Experiment. *Geology,* **34,** 161-164.

MUTO, T., STEEL, R.J. & SWENSON, J.B. (2007) Autostratigraphy: A Framework Norm for Genetic Stratigraphy. *Journal of Sedimentary Research,* **77,** 2-12.

NARA, M. (1995) Rosselia Socialis - a Dwelling Structure of a Probably Terebellid Polychaete. *Lethaia,* **28,** 171-178.

NARA, M. (1997) High-Resolution Analytical Method for Event Sedimentation Using Rosselia Socialis. *Palaios,* **12,** 489-494.

NARA, M. (2002) Crowded Rosselia Socialis in Pleistocene Inner Shelf Deposits: Benthic Paleoecology During Rapid Sea-Level Rise. *Palaios*, **17,** 268-276.

NAYLOR, M. & SINCLAIR, H.D. (2008) Pro- Vs. Retro-Foreland Basins. *Basin Research*, **20,** 285-303.

NICHOLSON, A. (2010) Tectonic Control on Sedimentation: An Example from the Rock Springs Uplift, Sw Wyoming. *Undergraduate Senior Honors Thesis*, University of Texas at Austin. Austin**,** 29.

OBRADOVICH, J.D. (1993) A Cretaceous Time Scale. In: *Evolution of the Western Interior Basin* (Ed. by W. G. E. Caldwell & E. G. Kauffman), **Special Paper**, 379-396. Geological Association of Canada.

OLARIU, C., STEEL, R.J., DALRYMPLE, R.W. & GINGRAS, M.K. (2012A) Tidal Dunes Versus Tidal Bars: The Sedimentological and Architectural Characteristics of Compound Dunes in a Tidal Seaway, the Lower Baronia Sandstone (Lower Eocene), Ager Basin, Spain. *Sedimentary Geology*, **279,** 134-155.

OLARIU, C. (2014) Autogenic Process Change Modern Deltas: Lessons for the Ancient. In: *From Depositional Systems to Sedimentary Successions on the Norwegian Continental Shelf* (Ed. by A. W. Martinius, R. Ravnås, J. A. Howell, R. Steel, . J. & J. P. Wonham), *Int. Assoc. Sedimentol. Spec. Publ.*, **46**, 149-166. John Wiley & Sons, Inc.

OLARIU, M.I., CARVAJAL, C.R., OLARIU, C. & STEEL, R.J. (2012B) Deltaic Process and Architectural Evolution During Cross-Shelf Transits, Maastrichtian Fox Hills Formation, Washakie Basin, Wyoming. *AAPG Bulletin*, **96,** 1931-1956.

OLARIU, M.I., OLARIU, C., STEEL, R.J., DALRYMPLE, R.W. & MARTINIUS, A.W. (2012c) Anatomy of a Laterally Migrating Tidal Bar in Front of a Delta System: Esdolomada Member, Roda Formation, Tremp-Graus Basin, Spain. *Sedimentology*, **59,** 356-378.

PANG, M. & NUMMENDAL, D. (1995) Flexural Subsidence and Basement Tectonics of the Cretaceous Western Interior Basin, United-States. *Geology*, **23,** 173-176.

PAOLA, C., HELLER, P.L. & ANGEVINE, C.L. (1992) The Large-Scale Dynamics of Grain-Size Variation in Alluvial Basins, 1: Theory. *Basin Research*, **4,** 73-90.

PEMBERTON, S.G. & MACEACHERN, J.A. (1995) The Sequence Stratigraphic Significance of Trace Fossils: Examples from the Cretaceous Foreland Basin of Alberta, Canada. In: *Sequence Stratigraphy of Foreland Basin Deposits* (Ed. by J. C. Van Wagoner & G. T. Bertram), *Memoirs*, **64**, 429-475. American Association of Petroleum Geologists, Tulsa, OK.

PETTER, A.L. & MUTO, T. (2008) Sustained Alluvial Aggradation and Autogenic Detachment of the Alluvial River from the Shoreline in Response to Steady Fall of Relative Sea Level. *Journal of Sedimentary Research*, **78,** 98-111.

PETTER, A.L., KIM, W., MUTO, T. & STEEL, R.J. (2011) Comment on 'Clinoform Quantification for Assessing the Effects of External Forcing on Continental Margin Development'. *Basin Research*, **23,** 118-121.

PLINK-BJORKLUND, P. (2008) *Wave-to-Tide Facies Change in a Campanian Shoreline Complex, Chimney Rock Tongue, Wyoming-Utah, USA*. SEPM - Soc Sedimentary Geology, Tulsa.

PLINT, A.G. (1988) Sharp-Based Shoreface Sequences and "Offshore Bars" in the Cardium Formation of Alberta: Their Relationship to Relative Changes in Sea Level. In: *Sea Level Changes: An Integrated Aproach* (Ed. by C. K. Wilgus, B. S. Hastings, H. W. Posamentier, J. C. Van Wagoner, A. C. Ross & C. G. S. C. Kendall), *Sepm Special Publication*, **42**, 357-370. SEPM, Tulsa, OK.

PLINT, A.G. (2010) Wave- and Storm-Dominated Shorelines and Shallow-Marine Systems. In: *Facies Models 4* (Ed. by N. P. James & R. W. Dalrymple), 167-201. Geological Association of Canada, St.John's, Newfoundland & Labrador.

POSAMENTIER, H.W. & VAIL, P.R. (1988) Sequences, System Tracts and Eustatic Cycles. *Aapg Bulletin-American Association of Petroleum Geologists*, **72,** 237-237.

POSAMENTIER, H.W. (2002) Ancient Shelf Ridges—a Potentially Significant Component of the Transgressive Systems Tract: Case Study from Offshore Northwest Java. *AAPG Bulletin*, **86,** 75-106.

POWELL, E.J., KIM, W. & MUTO, T. (2012) Varying Discharge Controls on Timescales of Autogenic Storage and Release Processes in Fluvio-Deltaic Environments: Tank Experiments. *Journal of Geophysical Research: Earth Surface*, **117,** F02011.

PRYOR, W.A. (1961) Petrography of Mesaverde Sandstones in Wyoming.

REYNAUD, J.-Y., TESSIER, B., PROUST, J.-N., DALRYMPLE, R., MARSSET, T., DE BATIST, M., BOURILLET, J.-F. & LERICOLAIS, G. (1999) Eustatic and Hydrodynamic Controls on the Architecture of a Deep Shelf Sand Bank (Celtic Sea). *Sedimentology*, **46,** 703-721.

REYNAUD, J.-Y. & DALRYMPLE, R.W. (2012) Shallow-Marine Tidal Deposits. In: *Principles of Tidal Sedimentology* (Ed. by R. A. Davis Jr & R. W. Dalrymple), 335-369. Springer, Dordrecht.

ROEHLER, H.W. & HANSEN, D.E. (1989) Surface and Subsurface Correlations Showing Depositional Environments of Upper Cretaceous Mesaverde Group and Associated Formations, Lost Soldier Field to Cow Creek, Southwest Wyoming, U.S. Geological Survey. Denver, CO.

ROEHLER, H.W. (1990) *Stratigraphy of the Mesaverde Group in the Central and Eastern Greater Green River Basin, Wyoming, Colorado and Utah* U.S. Geological Survey, Denver, CO.

RYAN, M.C., HELLAND-HANSEN, W., JOHANNESSEN, E.P. & STEEL, R.J. (2009) Erosional Vs. Accretionary Shelf Margins: The Influence of Margin Type on Deepwater Sedimentation: An Example from the Porcupine Basin, Offshore Western Ireland. *Basin Research*, **21,** 676-703.

SCHLAGER, W. (1993) Accommodation and Supply—a Dual Control on Stratigraphic Sequences. *Sedimentary Geology*, **86,** 111-136.

SCHWARZ, E. (2012) Sharp-Based Marine Sandstone Bodies in the Mulichinco Formation (Lower Cretaceous), Neuquen Basin, Argentina: Remnants of Transgressive Offshore Sand Ridges. *Sedimentology*, **59**.

SIEPMAN, B.R. (1986) Facies Relationships in Campanian Wave-Dominated Coastal Deposits in Sand Wash Basin. In: *New Interpretations of Northwest Colorado Geology* (Ed. by D. S. Stone & K. S. Johnson), 157-164. Rocky Mountain Association of Geologists, Denver.

SINCLAIR, H.D., COAKLEY, B.J., ALLEN, P.A. & WATTS, A.B. (1991) Simulation of Foreland Basin Stratigraphy Using a Diffusion-Model of Mountain Belt Uplift and Erosion - an Example from the Central Apls, Switzerland. *Tectonics*, **10,** 599-620.

SNEDDEN, J.W. & DALRYMPLE, R.W. (1999) Modern Shelf Sand Ridges: From Historical Perspective to a Unified Hydrodynamic and Evolutionary Model. In: *Isolated Shallow Marine Sand Bodies : Sequence Stratigraphic Analysis and Sedimentologic Interpretation* (Ed. by K. M. Bergman & J. W. Snedden), *Sepm Special Publication No.64*, **64**, 13-28. SEPM (Society for Sedimentary Geology), Tulsa, OK.

SNEDDEN, J.W., TILLMAN, R.W. & CULVER, S.J. (2011) Genesis and Evolution of a Mid-Shelf, Storm-Built Sand Ridge, New Jersey Continental Shelf, U.S.A. *Journal of Sedimentary Research*, **81,** 534-552.

STEEL, R.J. (1988) Coarsening-Upward and Skewed Fan Bodies: Symtoms of Strike-Slip and Transfer Fault Movement in Sedimentary Basins. In: *Fan Deltas: Sedimentology and Tectonic Settings* (Ed. by W. Nemec & R. J. Steel), 75-83. Blackie and Son Ltd., Glasgow.

STEEL, R.J., PLINK-BJORKLUND, P. & ASCHOFF, J. (2012) Tidal Deposits of the Campanian Western Interior Seaway, Wyoming, Utah and Colorado, USA. In: *Principles of Tidal Sedimentology* (Ed. by R. A. Davis Jr & R. W. Dalrymple), 437-471. Springer Netherlands.

SWENSON, J.B. & MUTO, T. (2007) Response of Coastal Plain Rivers to Falling Relative Sea-Level: Allogenic Controls on the Aggradational Phase. *Sedimentology*, **54,** 207-221.

SWIFT, D.J.P. & FIELD, M.E. (1981) Evolution of a Classic Sand Ridge Field: Maryland Sector, North American Inner Shelf. *Sedimentology*, **28,** 461-482.

SWIFT, D.J.P., SNEDDEN, J.W. & PLINT, A.G. (1995) Tongues, Ridges and Wedges: Highstand Versus Lowstand Architecture in Shallow Marine Basins. *SEPM Field Research Conference*, SEPM. Casper and Thermopolis, Wyoming. **June 24-29, 1995**.

TANKARD, A.J. (1986) On the Depositional Response to Thrusting and Lithospheric Flexure: Examples from the Appalachian and Rocky Mountain Basins. In: *Foreland Basins* (Ed. by P. A. Allen & P. Homewood), *Ias Special Publication*, **8**, 369-392. Blackwell Publishing Ltd.

THOMAS, M.A. & ANDERSON, J.B. (1994) Sea-Level Controls on the Facies Architecture of the Trinity/Sabine Incised-Valley System, Texas Continental Shelf. In: *Incised-Valley Systems* (Ed. by R. W. Dalrymple, R. Boyd & B. A. Zaitlin), *Sepm Special Publication*, **51**, 63-82. SEPM (Society for Sedimentary Geology), Tulsa, OK.

TILLMAN, R.W. & MARTINSEN, R.S. (1984) The Shannon Shelf-Ridge Sandstone Complex, Salt Creek Anticline Area, Powder River Basin, Wyoming. In: *Siliciclastic Shelf Sediments* (Ed. by R. W. Tillman & C. T. Siemers), *Special Publication*, **34**, 85-142. SEPM (Society for Sedimentary Geology), Tulsa, OK.

TOBIN, R.C., MCCLAIN, T., LIEBER, R.B., OZKAN, A., BANFIELD, L.A., MARCHAND, A.M.E. & MCRAE, L.E. (2010) Reservoir Quality Modeling of Tight-Gas Sands in Wamsutter Field: Integration of Diagenesis, Petroleum Systems, and Production Data. *AAPG Bulletin*, **94,** 1229-1266.

TOMER, A., MUTO, T. & KIM, W. (2011) Autogenic Hiatus in Fluviodeltaic Successions: Geometrical Modeling and Physical Experiments. *Journal of Sedimentary Research*, **81,** 207-217.

TRENTESAUX, A., STOLK, A. & BERNÉ, S. (1999) Sedimentology and Stratigraphy of a Tidal Sand Bank in the Southern North Sea. *Marine Geology*, **159,** 253-272.

VAN DE MEENE, J.W.H. & VAN RIJN, L.C. (2000) The Shoreface-Connected Ridges Along the Central Dutch Coast — Part 1: Field Observations. *Continental Shelf Research*, **20,** 2295-2323.

VAN HOUTEN, F.B. (1974) Northern Alpine Molasse and Similar Cenozoic Sequences of Southern Europe. In: *Modern and Ancient Geosynclinal Sedimentation* (Ed. by R. H. Dott Jr. & R. H. Shaver), *Sepm Special Publication*, **No.19**, 14. SEPM, Tulsa.

VAN WAGONER, J.C., POSAMENTIER, H.W., MITCHUM, R.M., JR., VAIL, P.R., SARG, J.F., LOUTIT, T.S. & HARDENBOL, J. (1988) An Overview of the Fundamentals of Sequence Stratigraphy and Key Definitions. *Special Publication - Society of Economic Paleontologists and Mineralogists*, **42,** 39-45.

WALKER, R.G. & BERGMAN, K.M. (1993) Shannon Sandstone in Wyoming; a Shelf-Ridge Complex Reinterpreted as Lowstand Shoreface Deposits. *Journal of Sedimentary Research*, **63,** 839-851.

WEIL, A.B. & YONKEE, W.A. (2012) Layer-Parallel Shortening across the Sevier Fold-Thrust Belt and Laramide Foreland of Wyoming: Spatial and Temporal Evolution of a Complex Geodynamic System. *Earth and Planetary Science Letters*, **357–358,** 405-420.

WOOD, L.J. (2004) Predicting Tidal Sand Reservoir Architecture Using Data from Modern and Ancient Depositional Systems. In: *Integration of Outcrop and Modern Analogs in Reservoir Modeling* (Ed. by G. M. Grammer, P. M. Harris & G. P. Eberli), *Aapg Memoir*, **80**, 45-66. The American Association of Petroleum Geologists, Tulsa, OK.

YANG, Y. & MIALL, A.D. (2010) Migration and Stratigraphic Fill of an Underfilled Foreland Basin: Middle–Late Cenomanian Belle Fourche Formation in Southern Alberta, Canada. *Sedimentary Geology*, **227,** 51-64.

YANG, Y. (2011) Tectonically-Driven Underfilled–Overfilled Cycles, the Middle Cretaceous in the Northern Cordilleran Foreland Basin. *Sedimentary Geology*, **233,** 15-27.

ZHENXIA, L., DONGXING, X., BERNE, S., KUIYANG, W., MARSSET, T., YUXIANG, T. & BOURILLET, J.F. (1998) Tidal Deposition Systems of China's Continental Shelf, with Special Reference to the Eastern Bohai Sea. *Marine Geologyv*, **145,** 225-253.

Vita

Julio Leva López (double surname) was born many years ago in Madrid, Spain. He soon developed an interest for natural sciences that led him to pursue a Licenciatura in geological sciences at the Universidad Complutense de Madrid (UCM).

During his time at the UCM, Julio participated in an experimental edaphology study, in a paleontological excavation of Eocene mammals and mapped mineralizations in a volcanic caldera of an old gold mining site in Almeria; he also worked as an intern for six months in TeleAtlas Iberia SA, a company dedicated to digital cartography. He spent the last year of the Licenciatura as an exchange student at the University of Texas at Austin. He obtained his Licenciatura in Geology in June 2007.

In 2008 he moved to Austin, Texas to start a PhD in geological sciences with a focus on stratigraphy and basin analysis. During his PhD he lecture a session of sedimentary geology, worked as assistant instructor for three sessions of field camp and taught sedimentary rocks labs as well as GIS & GPS labs. He also had an internship with Swift Energy Co. studying possible hydrocarbon leads in the fluvial systems of the Wilcox Formation.

"Someone else always has to carry on the story." – J.R.R. Tolkien, The Lord of the Rings.

Permanent email address: julioleva@gmail.com
This dissertation was typed by Julio Leva López.